Ion-molecule reactions at low temperature with uniform supersonic flows and insights into the chemistry of astrophysical environments

Ahmad Mortada

UNIVERSITÉ DE RENNES 1

THESE DE DOCTORAT DE

L'UNIVERSITE DE RENNES 1

ECOLE DOCTORALE N° 596
Matière, Molécules, Matériaux
Spécialité : Physique

Par

Ahmad MORTADA

Ion-molecule reactions at low temperature with uniform supersonic flows and insights into the chemistry of astrophysical environments

Thèse présentée et soutenue à Rennes, le 5 janvier 2022

Unité de recherche : Institut de physique de Rennes (IPR UMR 6251)

Rapporteurs avant soutenance :

Véronique VUITTON Directrice de Recherche, IPAG - Grenoble
Wolf GEPPERT Professeur, Département de Physique – Université de Stockholm - SUEDE

Composition du Jury :

Examinateurs :	Claire ROMANZIN	Maître de conférences	Université Paris-saclay
	François LIQUE	Professeur	Université de Rennes 1
Dir. de thèse :	Ludovic BIENNIER	Chargé de Recherche	Université de Rennes 1
Co-dir. de thèse :	Sophie CARLES	Maître de conférences	Université de Rennes 1

Dedication

To the unknown on earth, the known in heaven…

Abstract

Understanding the mechanisms governing the formation of complex organic molecules in the interstellar medium and cold planetary atmospheres relies in particular on the exploration of ionic processes under extreme conditions. The CRESU-SIS experimental setup, developed to study ion-neutral reactions in the gas phase at low temperatures, is able to meet this challenge. This unique instrument, which combines a selective ion source (SIS) with the CRESU reactor which generates a uniform supersonic flow at very low temperature, makes it possible to measure the rate coefficients of the reactions between ions and neutral molecules and to determine the branching ratios between the different exit channels. The reactivity of N_2^+, Ar^+, and CH_2CN^+ ions with hydrocarbons (e.g CH_4, C_2H_4 ...) has been studied experimentally and analyzed using quantum calculations. The reaction between N_2^+ and the linear isomers of C_3H_4 (allene and propyne) has been included into a photochemical model for the atmosphere of Titan.

Keywords: CRESU, laboratory astrophysics, reactive collisions, ionic processes, chemistry of the interstellar medium, Titan's atmosphere

---

Résumé

La compréhension des mécanismes régissant la formation des molécules organiques complexes dans le milieu interstellaire et les atmosphères planétaires froides repose notamment sur l'exploration de processus ioniques en conditions extrêmes. Le dispositif expérimental CRESU-SIS, développé pour étudier les réactions ion-neutre en phase gazeuse à basse température, est en mesure de répondre à ce défi. Cet instrument unique, qui combine une source d'ions sélective (SIS) au réacteur CRESU qui génère un écoulement supersonique uniforme de très basse température, permet de mesurer les coefficients de vitesse de réactions entre des ions et des molécules neutres et de déterminer les rapports de branchement entre les différentes voies de sortie. La réactivité des ions N_2^+, Ar^+, et CH_2CN^+ avec des hydrocarbures (e.g CH_4, C_2H_4…) a été étudiée expérimentalement et analysée à l'aide de calculs quantiques. La réaction entre N_2^+ et les isomères linéaires de C_3H_4 (allene et propyne) a été incluse dans un modèle photochimique pour l'atmosphère de Titan.

Mots clés : CRESU, astrophysique de laboratoire, collisions réactives, processus ioniques, chimie du milieu interstellaire, atmosphère de Titan

Acknowledgements

First and foremost, praises and thanks to the God, the Almighty, for His showers of blessings throughout my research work to complete the research successfully.

I wish to express my thanks to Mrs. Véronique Vuitton and Mr. Wolf Geppert for the time that they spend to review the manuscript of the thesis as well to Mrs. Claire Romanzin and Mr. François Lique for accepting to be a part of the jury.

I would like to express my deep and sincere gratitude to my research supervisors, Ludovic Biennier and Sophie Carles, for giving me the opportunity to do research and providing invaluable guidance throughout this research. Their dynamism, vision, sincerity and motivation have deeply inspired me. They have taught me the methodology to carry out the research and to present the research works as clearly as possible. It was a great privilege and honor to work and study under their guidance. I am extremely grateful for what they have offered me. I would also like to thank them for their friendship, empathy, and great sense of humor.

I am extending my thanks to my colleagues in the Laboratory Astrophysics group and other colleagues in the molecular physics department at the IPR. I really liked the scientific discussions we had. I would like to thank Jonathan Courbe for the mechanical design, J. Thiévin for the data acquisition, and Abdessamad Benidar for the simulations. I would like also to thank my Lebanese friends in France, and all my friends in my village.

My parents, all the vocabularies in the world are not enough to express my immense acknowledgment, thanks to you I am here. Your love, your support and encouragement have allowed me to always stand up to overcome any difficulty and continue the path of success with great confidence. You are the origin of all my successes, and I will never forget that. My dear brother Mohamad, my dear sister Malak, a big thank you for your continuous encouragement and support. In the worst times of my life, I have always been able to count on you.

And last but not least, my special thanks go to my fiancee Rayhana, I wanted you to know how much your support has been of great help to me. It is your encouragement and patience that helped me to achieve this point. You are the source of happiness in my life. Thank you for everything done for me. I love you.

Table of Contents:

Chapter 1:
Ion chemistry in space

1.1 Introduction

Astrochemistry, also known as molecular astrophysics, is ‘the study of the formation, destruction and excitation of molecules in astronomical environments and their influence on the structure, dynamics and evolution of astronomical objects’ as stated by the pioneer of this field, Alexander Dalgarno in 2008.[1]

Due to a complex mixture of gravity, turbulence, rotation, radiation, thermodynamics, and magnetic fields, the matter in the universe is not static, but rather in continuous evolution through what is known as the cosmic matter cycle schematically depicted in the figure 1.1. As the star nuclear fuel is depleted, the star becomes unstable and loses its mass by ejecting material into the interstellar medium, which accumulates to form an interstellar cloud of gas and dust at very low density. When the mass of the interstellar cloud becomes sufficient to cause contraction by self-gravitation, a protostellar system is formed. A protostellar system undergoes a contraction, leading to the formation of a central protostar and rotating disk of gas and dust that accretes more material to form more molecules (accretion disk). In the outer region of the accretion disk, planets and comets will form. When the central temperature and the density increase, a thermonuclear reaction is ignited in the central star and a newborn star appears. Planets, comets, and interplanetary material remain in orbit around the star. Three main categories have drawn the

attention of astrochemical studies: the interstellar medium (ISM), the circumstellar environments and planetary atmospheres.

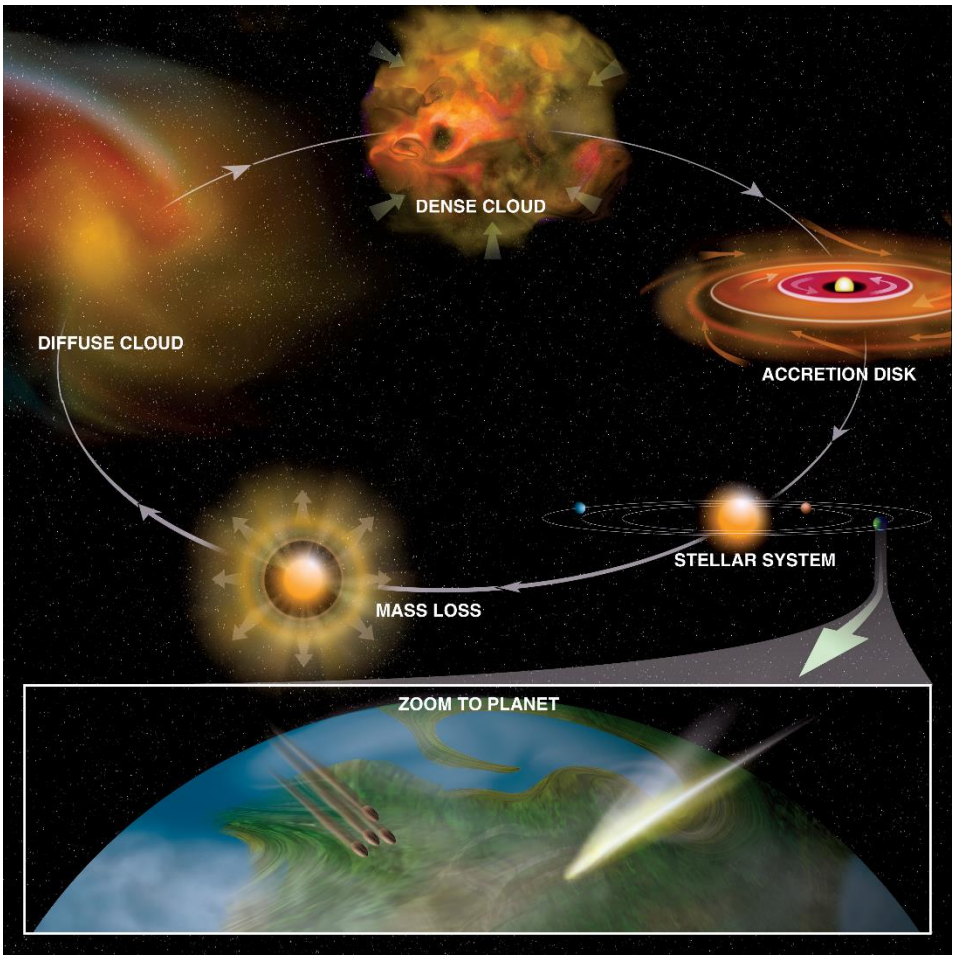

Figure 1.1 : cycle of matter in the universe. (Credit: Bill Saxton, NRAO/AUI/NSF/)

Interstellar medium. The interstellar medium is a very dilute gas that fills the space between stars, it is composed by gas and dust: by mass 99 % of gaseous species which include atoms, molecules, radicals and ions, and 1% of cosmic dust. The temperature in the ISM ranges from more than 10^6 K down to 10 K and densities from as low as 10^{-4} to more than 10^8 molecules cm^{-3}.

Several environments with different physical and chemical characteristics are found in the ISM: the interstellar clouds, the intercloud gas, and the diffuse nebula (H_{II} regions). The interstellar clouds correspond to the colder and denser concentration of the gas. The intercloud gas is divided in two categories based on temperature: the hot coronal gas which is a product of hot gases ejected from stellar explosion and winds, and the warm intercloud medium which is the intergalactic vast region. H_{II} regions are composed by ionic gases due to UV, X-Rays, and cosmic

rays. The H^+ ion is the main compound in these regions (with temperatures around 10000 K). The most famous example of H_{II} regions is the Orion Nebula.

Circumstellar environments. In their late stage of evolution, stars eject considerable amounts of material into space (up to 10^{-5} of the mass of the star per year), generating a huge layer of gas and dust. [2] The temperature and density gradient found in the circumstellar envelope give rise to a complex chemistry in these regions (Figure 1.2) attested by the detection of numerous species. A well-known example is the circumstellar envelope of the carbon-rich star IRC+10216.

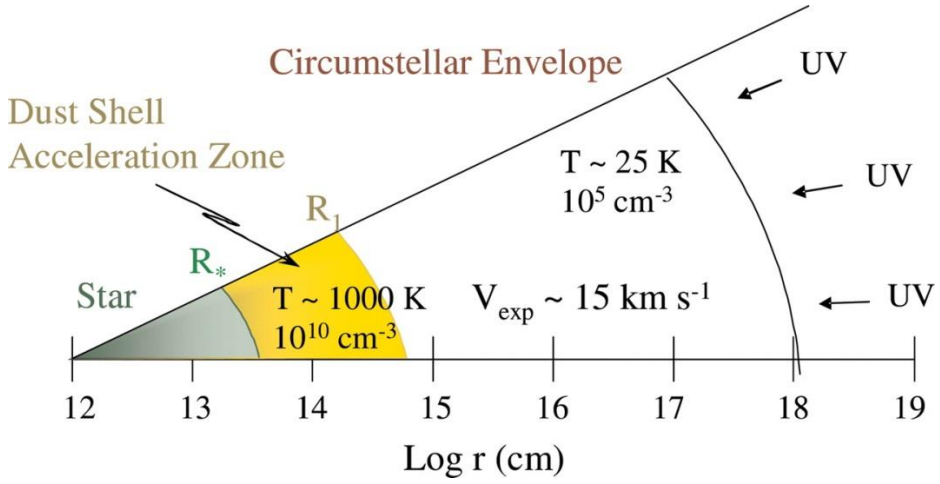

Figure 1.2: Cross section of a circumstellar envelope, plotted in terms of the logarithm of the distance from the central star log(r), Regions of LTE (Local Thermodynamical Equilibrium) chemistry, dust formation, and UV-induced photochemistry are shown. Adapted from Lucy M. Ziurys 2006.[2]

Planetary atmospheres refer to the envelope of gases that surrounds any of the planets within or outside the solar system. In our solar system: Jupiter, Saturn, Uranus, Neptune, Earth, Titan (a Saturn's moon), Venus, Mars, and Triton (a Neptune's moon) have atmospheres.

Similarly to the interstellar medium and the circumstellar envelopes, ions and neutral molecules are observed, and play a crucial role in the chemistry of the atmospheres of rocky planets, gaseous planets and their satellites, for example: Titan's atmosphere.[3] Until recently, the positive species were the only ions detected in space; however, this situation has changed with the discovery of various molecular anions in the interstellar medium and Titan's atmosphere.[4]

1.2 Observation of ions in space environments

Ions in astrophysical environments are sparse, this is a reason that makes their detection not simple and requires methods that are highly sensitive and unambiguous. Radioastronomy has been proved very successful in detecting molecular ions and neutrals in space. Most of emission lines for specific rotational transitions of various simple molecules or molecular ions (~80%) are

detected by radiotelescopes in the MHz or GHz frequency range. These spectral features can be exceptionally sharp, due to the very low temperature and (by terrestrial standards) low pressure of the interstellar clouds containing these molecules. For example, recently, the Yebes 40 m and IRAM radiotelescopes were used in the detection of the rotational emission lines of the CH_3CO^+ ion in the TMC-1.[5] The detection of the HC_3S^+ ion in the TMC-1 was also performed by the Yebes 40 m observatory.[6] Another example is the detection of the presence of the deuterated ammonium ion, NH_3D^+ in Orion and in the cold prestellar core B1-bS using the IRAM 30 m radiotelescope (which is the most sensitive single antenna radiotelescope in the world).[7]

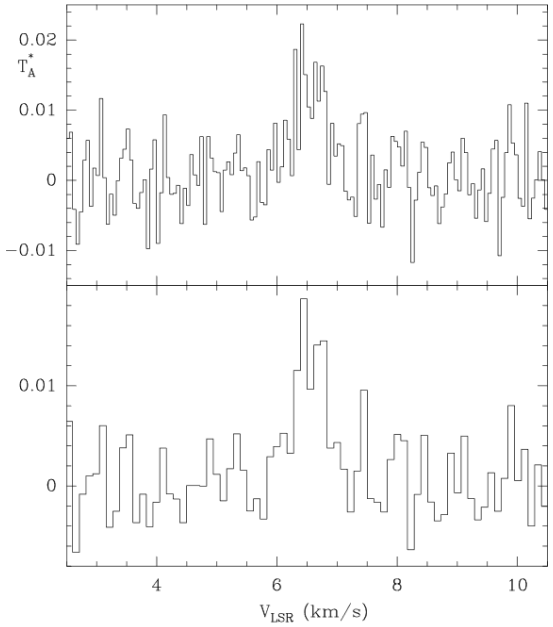

Figure 1.3: Observed spectrum towards B1-bS (α_{2000}=03^h 33^m 21.34^s, δ_{2000}=31^o 07' 26.7") at the expected frequency of NH_3D^+ J_K=1_0-0_0 transition. The upper panel contains the raw data resulting from a total integration time of 51 hours with a spectral resolution of 48.8KHz (0.054 km s^{-1}). The bottom panel shows the same data smoothed to 98 KHz. For a LSR velocity of the source of 6.5 km s^{-1} the derived line frequency for the observed featureis 262816.73±0.1 MHz. Adapted from J. Cernicharo et al. 2016[7]

Infrared spectroscopy is also used to detect molecules in astrophysical environments, particularly those that are highly symmetric or with non-zero permanent dipole moments. This technique is useful for the detection of transitions that occur between vibrational states. For example, T. R. Geballe detected the IR spectrum of the H_3^+ ion in dark and diffuse clouds, and in the Galactic Center source GCS 3-2.[8] This ion play an important role in interstellar chemistry, by initiating a chain of reactions that lead to the production of many of the complex molecular species observed in the interstellar medium. A substantial benefit of IR spectroscopy is the ability to observe molecules condensed into interstellar ices. While condensed-phase molecules cannot undergo free rotation, their vibrational transitions remain accessible.

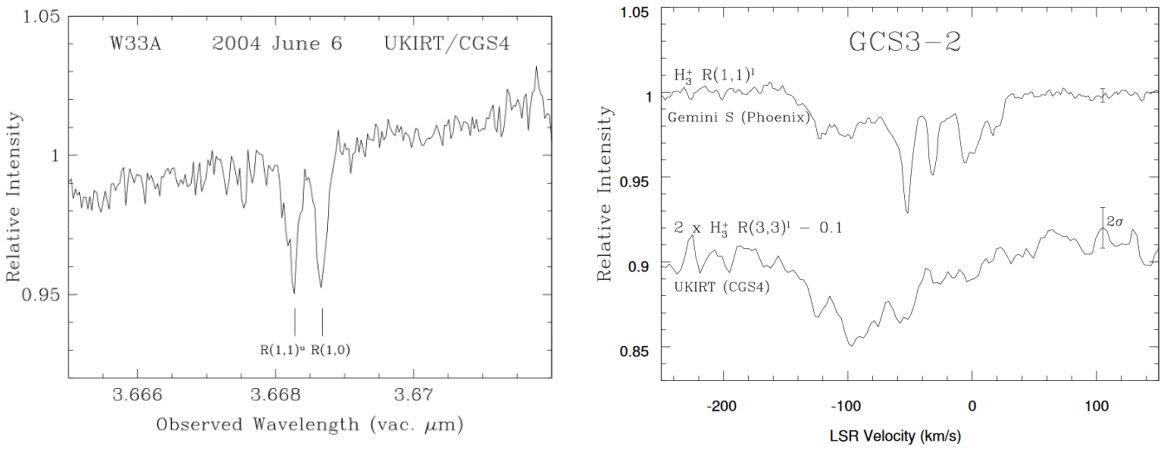

Figure 1.4 : Left: The H_3^+ ortho-para doublet seen towards W 33A IR. **Right**: Two H_3^+ lines observed towards the Galactic Center" Quintuplet" source GCS 3-2. Adapted from T. R. Geballe 2005. [8]

As of September 2021, about 250 molecules from different families have been detected in the interstellar medium or circumstellar shells. The list of these molecules is presented in the tables 1.1 and 1.2. In the interstellar medium, 25 cations and 7 anions were observed, while the first cation, CH^+ was detected over eight decades ago.[9]

2 atoms	3 atoms	4 atoms	5 atoms	6 atoms	7 atoms
H_2	C_3*	c-C_3H	C_5*	C_5H	C_6H
AlF	C_2H	l-C_3H	C_4H	l-H_2C_4	CH_2CHCN
AlCl	C_2O	C_3N	C_4Si	C_2H_4*	CH_3C_2H
C_2**	C_2S	C_3O	l-C_3H_2	CH_3CN	HC_5N
CH	CH_2	C_3S	c-C_3H_2	CH_3NC	CH_3CHO
CH^+	HCN	C_2H_2*	H_2CCN	CH_3OH	CH_3NH_2
CN	HCO	NH_3	CH_4*	CH_3SH	c-C_2H_4O
CO	HCO^+	HCCN	HC_3N	HC_3NH^+	H_2CCHOH
CO^+	HCS^+	$HCNH^+$	HCCNC	HCCCHO	C_6H^-
CP	HOC^+	HNCO	HCOOH	NH_2CHO	CH_3NCO
SiC	H_2O	HNCS	H_2CNH	C_5N	HC_5O
HCl	H_2S	$HOCO^+$	H_2C_2O	l-HC_4H*	$HOCH_2CN$
KCl	HNC	H_2CO	H_2NCN	l-HC_4N	HCCCHNH (2020)
NH	HNO	H_2CN	HNC_3	c-H_2C_3O	HC_4NC (2020)
NO	MgCN	H_2CS	SiH_4*	H_2CCNH (?)	c-C_3HCCH (2021)
NS	MgNC	H_3O^+	H_2COH^+	C_5N^-	l-H_2C_5 (2021)
NaCl	N_2H^+	c-SiC_3	C_4H^-	HNCHCN	MgC_5N (2021)
OH	N_2O	CH_3*	HC(O)CN	SiH_3CN	
PN	NaCN	C_3N^-	HNCNH	C_5S	
SO	OCS	PH_3	CH_3O	MgC_4H	
SO^+	SO_2	HCNO	NH_4^+	CH_3CO^+ (2021)	
SiN	c-SiC_2	HOCN	H_2NCO^+	C_3H_3 (2021)	
SiO	CO_2*	HSCN	$NCCNH^+$	H_2C_3S (2021)	
SiS	NH_2	H_2O_2	CH_3Cl	HCCCHS (2021)	
CS	$H_3^{+(*)}$	C_3H^+	MgC_3N		
HF	SiCN	HMgNC	NH_2OH (2020)		
HD	AlNC	HCCO	HC_3O^+ (2020)		
FeO?	SiNC	CNCN	HC_3S^+ (2021)		

O_2	HCP	HONO	H_2C_2S (2021)
CF^+	CCP	MgC_2H	C_4S (2021)
SiH?	AlOH	HCCS (2021)	HC(O)SH (2021)
PO	H_2O^+	HNCN (2021)	HC(S)CN (2021)
AlO	H_2Cl^+		
OH^+	KCN		
CN^-	FeCN		
SH^+	HO_2		
SH	TiO_2		
HCl^+	C_2N		
TiO	Si_2C		
ArH^+	HS_2		
N_2	HCS		
NO^+?	HSC		
NS^+	NCO		
HeH^+	CaNC		
	NCS (2021)		

Table 1.1 : Molecules in the Interstellar Medium or Circumstellar Shells (source: https://cdms.astro.uni-koeln.de/)

8 atoms	9 atoms	10 atoms	11 atoms	12 atoms	>12 atom
CH_3C_3N	CH_3C_4H	CH_3C_5N	HC_9N	c-C_6H_6*	C_{60}*
$HC(O)OCH_3$	CH_3CH_2CN	$(CH_3)_2CO$	CH_3C_6H	n-C_3H_7CN	C_{70}*
CH_3COOH	$(CH_3)_2O$	$(CH_2OH)_2$	C_2H_5OCHO	i-C_3H_7CN	C_{60}^+*
C_7H	CH_3CH_2OH	CH_3CH_2CHO	$CH_3OC(O)CH_3$	$C_2H_5OCH_3$	c-C_6H_5CN
C_6H_2	HC_7N	CH_3CHCH_2O	$CH_3C(O)CH_2OH$ (2020)	1-c-C_5H_5CN (2021)	$HC_{11}N$
CH_2OHCHO	C_8H	CH_3OCH_2OH	c-C_5H_6 (2021)	2-c-C_5H_5CN (2021)	1-$C_{10}H_7CN$ (2021)
l-HC_6H*	$CH_3C(O)NH_2$	c-C_6H_4 (2021)	$HOCH_2CH_2NH_2$ (2021)		2-$C_{10}H_7CN$ (2021)
CH_2CHCHO	C_8H^-	H_2CCCHC_3N (2021)			c-C_9H_8 (2021
CH_2CCHCN	C_3H_6				
H_2NCH_2CN	CH_3CH_2SH				
CH_3CHNH	CH_3NHCHO				
CH_3SiH_3	HC_7O				
$H_2NC(O)NH_2$	HCCCHCHCN (2021)				
$HCCCH_2CN$ (2020)	H_2CCHC_3N (2021)				
HC_5NH^+ (2020	$H_2CCCHCCH$ (2021)				
CH_2CHCCH (2021)					
MgC_6H (2021					

Table 1.2 : Molecules in the Interstellar Medium or Circumstellar Shells (source: https://cdms.astro.uni-koeln.de/)

In tables 1.1 and 1.2:

* indicates molecules that have been detected by their rotation-vibration spectrum,

** those detected by electronic spectroscopy only.

In addition, ions and neutrals in astrophysical environments can also be discovered by space probes that aim to discover the planets and its systems. The Cassini-Huygens mission -also called Cassini- is an example (Figure 1.5)[10]. This spacecraft was launched on October 15, 1997 by a collaboration between NASA, the European Space Agency (ESA), and the Italian Space Agency (ASI) to explore Saturn, its rings and natural satellites.

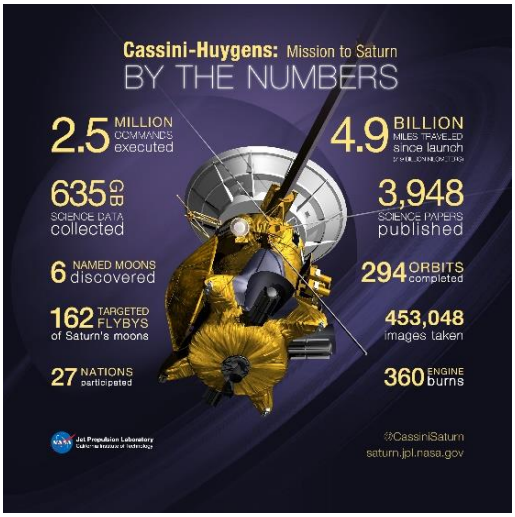

Figure 1.5: Cassini-Huygens by the numbers, credits: NASA

An Ion Neutral Mass Spectrometer INMS recorded mass spectra of species present in the Titan's atmosphere. Thousands of neutral and ionic molecules were detected.[3,11] The analysis of the Cassini orbiter measurements have revealed a surprising abundance of protonated nitriles in Titan's ionosphere (Vuitton et al 2006)[12], suggesting a more evolved nitrogen chemistry than was previously believed to exist.

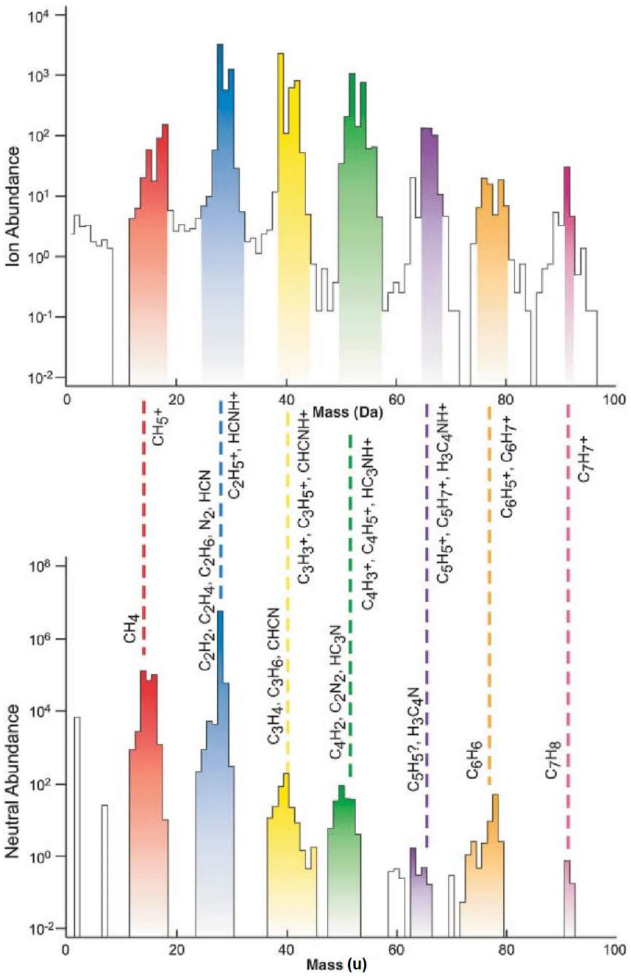

Figure 1.6: Correspondence of ion (upper) and neutral (lower) mass spectra measured by INMS during T19 flyby between 950 and 1000 km. Benzene molecules and their ion counterpart can be identified at 78 and 79 u in the spectra. High-pressure background in the ion source has been subtracted from the neutral spectrum. (Adapted from Waite et al., 2007)[11]

Molecules in the interstellar medium, circumstellar envelops, and planetary atmospheres are formed via several physical-chemical processes. Table 1.3 presents the list of the main chemical processes involving ions of interest for astrophysical environments. These reactions correspond to the main pathways for the formation, growth and destruction of ions in space. They are important for the construction of photochemical models with the goal of reproduction of relative abundances of observed species.

Ion–molecule reactions	Charge transfer	$A^+ + B \rightarrow B^+ + A$
	Dissociative charge transfer	$A^+ + BC \rightarrow A + B^+ + C$
	Radiative transfer	$A^+ + B \rightarrow AB^+ + h\nu$
	Atomic transfer	$AB^+ + C \rightarrow A^+ + BC$
Electron recombination reactions	Radiative	$A^+ + e \rightarrow A + h\nu$
	Dissociative	$AB^+ + e \rightarrow A + B$
	Dissociative excitation	$AB^+ + e \rightarrow A + B^+ + e$
	Ion pair formation	$A^+ + e \rightarrow B^+ + C^-$
	Dissociative ionization	$AB^+ + e \rightarrow A^+ + B^+ + 2e$
Photochemical processes	Photoionization	$AB + h\nu \rightarrow AB^+ + e$
	Photodissociation	$AB^+ + h\nu \rightarrow A^+ + B$
Electron attachment	Electron attachment	$A + e \rightarrow A^-$
	Three body electron attachment	$A + e + M \rightarrow A^- + M$
	Radiative electron attachment	$A + e \rightarrow A^- + h\nu$
	Dissociative electron attachment	$AB + e \rightarrow A^- + B$
Other	Cosmic ray ionization	$A + CR \rightarrow A^+$ $AB + CR \rightarrow A^+ + B$
	Anion – Neutral reactions	$A^- + B \rightarrow AB + e$ $A^- + BC \rightarrow AB^- + C$

Table 1.3 : Non-exhaustive list of the main chemical processes of ions interest in the astrophysical environments.

In the next sections, we will detail the pathways leading to the formation, growth and destruction of cations and anions in astrophysical environments.

1.3 Formation of cations in space environments

Various processes are held responsible for the production of cations in space. Cosmic radiation, UV rays, x-rays, and shock waves all contribute, albeit they are clearly not of equal importance in the various astronomical environments populating the Universe.

1.3.1. Cosmic rays.

The cosmic radiation was discovered in 1912 by the Austrian physicist Hess, who used the ionization chambers to determine the radiative ionization rate at various altitudes during a balloon flight. The cosmic rays (CR) that move in space at nearly the speed of light, are high energy particles composed primarily of protons and atomic nuclei species, electrons and even antiparticles, with an additional contribution of gamma photons, neutrinos and neutrons.[13] Generally, CR constitute an important source of ionization in many astronomical environments and planetary atmospheres.

Stellar flares, coronal mass ejections, explosions of supernovae and active galactic nuclei, acceleration by pulsars and jets from black holes could be the origins of cosmic rays in our galaxy. The energy of these cosmic rays usually ranges from 100 to 10 GeV, the radiation intensity strongly decreasing at energies above 1 GeV.

Similarly, the Sun also acts as a sporadic source of cosmic rays through shockwaves and solar flares. Referring to Mewaldt et al. 1996,[14] the maximum energy of solar cosmic-ray particles lies at approximately 10–100 MeV, but, very rarely, higher energy particles are observed arising from the Sun. In our solar system, in addition to the lower energy solar cosmic rays emitted by the Sun, galactic cosmic rays (GCR) which are high energy particles (energy ~ 10^{17} eV) originating from the extrasolar system, and extragalactic cosmic rays (very-high-energy particles, up to 10^{20} eV) are present. [15,16]

According to Dalgarno et al. 1996,[17] the CR ionization rate in the interstellar gas depends on the relative amount of H, H_2, and He. . In molecular clouds, a large majority of CR–H_2 impacts leads to the formation of H_2^+ with a small amount of H^+ ions.

In star-forming regions, the contribution of the UV radiation in the production of ionized species is much less important than cosmic-rays since UV photons are blocked by a thin layer of gas and dust. Their high penetration power makes cosmic rays as a principal source of ionization in dark clouds and dark cores as well.

We will present some examples showing the role of cosmic rays in the ionization of the atmospheres of planets and their satellites. The first example is in the Venusian atmosphere (below 70 km), where the O_2^+, CO_2^+ and CO^+ ions are mainly produced by the cosmic-ray ionization.[18] The second example is Mars's atmosphere: cosmic rays contribute in the ionization of neutral species especially at altitudes below 80 km. Ar^+, H_2^+, H_2O^+, O_3^+ and NO^+ ions are produced by CR ionization, consequently, their abundance is very low above this altitude. In

addition, in Titan's atmosphere, at altitudes below 100 km, where the moon's haze blocks the UV radiation and the magnetospheric electrons contribute little in the ionization of neutral species, the cosmic-ray ionization is one of the most crucial pathways for ion formation.[19] According to G.J. Molina-Cuberosa et al.,[20] cosmic rays penetrate deeply into the atmosphere of Titan generating an electron density peak around 90 km, similar in magnitude to the ionospheric peak produced by solar radiation in the upper atmosphere.

1.3.2 Photoionization

Photoionization refers to a process in which highly energetic radiation with wavelengths of < 100 nm is absorbed by removing electrons from atoms or molecules, resulting into electrically charged particles. But not every interaction between a photon and an atom, or molecule, will result in photoionization. If the radiation energy is below the ionization threshold, the photoionization cross section is near zero and photodissociation processes take over. In our solar system, the ionization potentials of neutral atmospheric species are close to the UV photons and X-rays energies, [21] making the UV radiation and X-rays the most considerable photoionizing sources.

An example for the contribution of photoionization of molecules in planetary atmospheres is the ionosphere of Mars,[22] in which the UV dissociative ionization of CO_2 , i.e. the main constituent of the atmosphere, is the dominant source of the O^+ and CO^+ fragments.[23] Figure 1.7 illustrates a model of the production ion rate by photoionization in the atmosphere of Mars from 80 to 300 km.

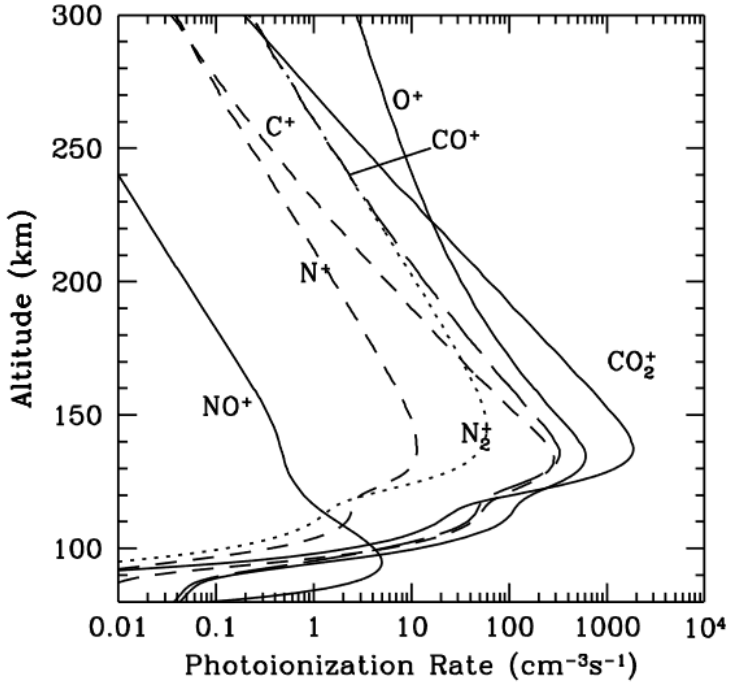

Figure 1.7 : Computed photoionization rate profiles from 80 to 300 km for 7 ions for a high solar activity 60° SZA (Solar Zenith Angle) model of Mars.[21]

1.3.2.1 UV radiation:

When a molecule absorbs UV radiation, to two distinct chemical processes can occur, the photodissociation and the photoionization. UV radiation can also heats molecules present in the H-dominated and less dense part of the PDR (photon dominated region) where the UV radiation drives mainly the chemistry of the medium facing the UV source.[24] In our solar system, the sun is the main source of the UV radiation.

Another example for the contribution of UV radiation in the ionization of molecules in astrophysical environments is the upper layer of Titan's atmosphere primarily constituted of N_2 (>95%) and a few percent of CH_4, especially above an altitude of 700 km, where it is an efficient source in the production of N_2^+ (the main product), N^+, CH_4^+, and CH_3^+ ions.[19] (Figure 1.8).

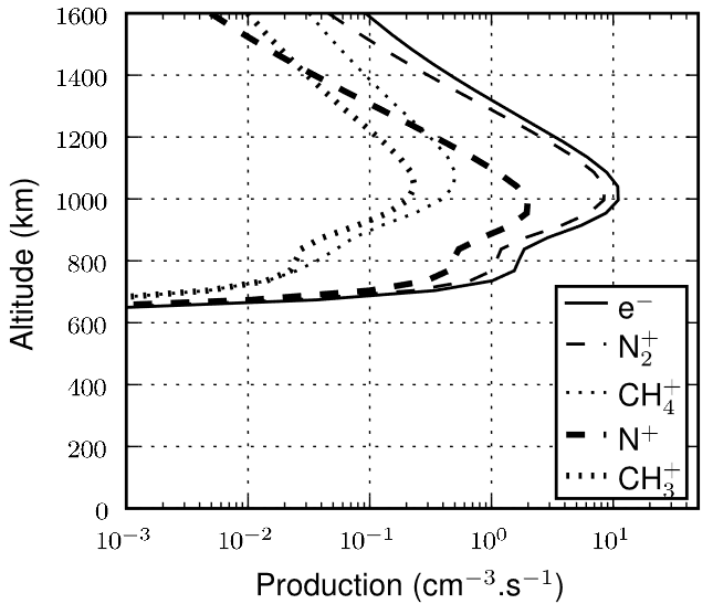

Figure 1.8 : Ionization due to EUV/XUV solar flux in the atmosphere of Titan computed for a solar zenith angle of 40° with a solar flux given by $F_{10.7}$=80. From G. Gronoff et al. 2009 [19]

1.3.2.2 X-rays:

Absorption of X-rays radiation by neutral molecules in astrophysical environments can lead to the their ionization. [25] Unlike FUV photons (6 < hν < 13.6 eV), referring to Stäuber et al,[26] X-rays can also ionize atoms and molecules with an ionization threshold above 13.6 eV (e.g. H, He, N and O) and can even doubly ionize many species. For example, in the AFGL 2591 region (a star forming region), X-rays lead to the formation of many ions (such as H^+, C^+, N^+, O^+, HCO^+, HOC^+, N_2H^+, SO^+…), and SH^+ and HSO^+ are found to be excellent X-ray tracers. They are 100−10 000 times more abundant in models with X-rays than models which consider only far UV ionization.[26]

In addition, the interaction of X-rays with planetary atmospheres could create an ionospheric layer below those created by the UV photons, since they can penetrate further than the UV radiation. According to M. Banaszkiewicz et al.,[27] solar flare X-rays interact with the atmosphere of Titan, leading to the photoionization of some neutral molecules, and so contribute to the increase of the electron and ion density at altitudes of 400-900 km.

1.3.3 Shock waves

When a material moving faster than the speed of sound (supersonic velocity, Mach number is greater than 1) encounters another medium, a hydrodynamic process occurs with a sudden jump in the density, pressure, temperature, and velocity of the gas, what is called the shock wave.[28] When the shock hits, the kinetic energy of the gas in converted into thermal energy, and the medium undergoes a compression and heating at temperatures higher than those encountered in

photoionized ions. In the interstellar medium, the regions ionized by shock waves can be distinguishable to the photoionized regions by using temperature-sensitive lines of ions.[29] Referring to Allen et al.,[30] cloud-cloud collisions, the expansion of H_{II} regions into the surrounding interstellar medium, outflows from young stellar objects, supernova blast waves, outflows from active and starburst galaxies, and collisions between galaxies are the primary sources of shock waves in space. According to Tielens,[31] because of shock particles move at high velocities, the reactions with energy barrier can proceed in this environment, leading to a chemistry different from that occurring in dark clouds.

1.3.4 The Solar wind

The solar wind is a flow of charged particles that are ejected from the sun. The solar wind which is mainly composed of electrons, protons and He_2^+ ions is an important source of the ionization of atmospheric species. The neutrals such as C, O, Ne, Si, S, Ar and Fe, as well as traces of Kr and Xe, can also be minor constituents of the solar wind. The solar wind (then called solar corpuscular radiation) has two components: fast and slow. The fast wind is associated with coronal holes and has the characteristics of being uniform and stable. The slow wind is quite variable in terms of temperature, composition, magnetic field strength…and in contrast with fast wind, is not in equilibrium with the corona and transition layers at its base.[32]

In the upper layers of planetary atmospheres, the solar wind contributes in the ionization of neutral species by electron impact, charge exchange and ion sputtering. The latter is a process by which an energetic ion deposits its energy in a material initiating a cascade of events which eventually leads to the ejection of atoms or molecules from the surface of the material. Ions lose their energy by direct knock-on (momentum transfer) collisions with an atom in the material and by electronically exciting the atoms and molecules. For example, in the Martian atmosphere, a part of the neutral atmosphere is ionized by the solar EUV and the photo-electrons from the sun. These newly ionized particles are ‘picked-up’ by the magnetic field lines initially frozen in the solar wind but distorted near Mars, and they are accelerated along gyroradial trajectories in the Martian tail direction.[33]

In our solar system, according to Roberston and Carvens,[34] the charge exchange reactions between highly energetic solar wind ions and atmospheric neutrals molecules lead to the formation of highly excited ions. Resulting ions cool down by emitting soft X-rays (with energies below 5 KeV) and EUV photons.

1.3.5 Magnetospheric ions and electrons.

The giant planets have extended magnetospheres. The rings and satellites forming the systems of these planets are directly embedded into magnetospheric plasma, which is sustained by the rotating magnetic field of the planet. The bombardment of magnetospheric ions and electrons can be a source of ionization in these regions. [35]

Figure 1.9 shows the contribution of the fluxes of magnetospheric electrons and UV radiation in the ionization of water vapor molecules the H_2O-dominated atmosphere of icy moons of the giant planets. Other primary components such as O_2 and H_2 can be ionized by the same processes. In this scheme, the H^+, H_2^+, O^+, OH^+, and H_2O^+ can then be efficiently converted into the hydroxonium ion H_3O^+ through reaction with molecular hydrogen. [36]

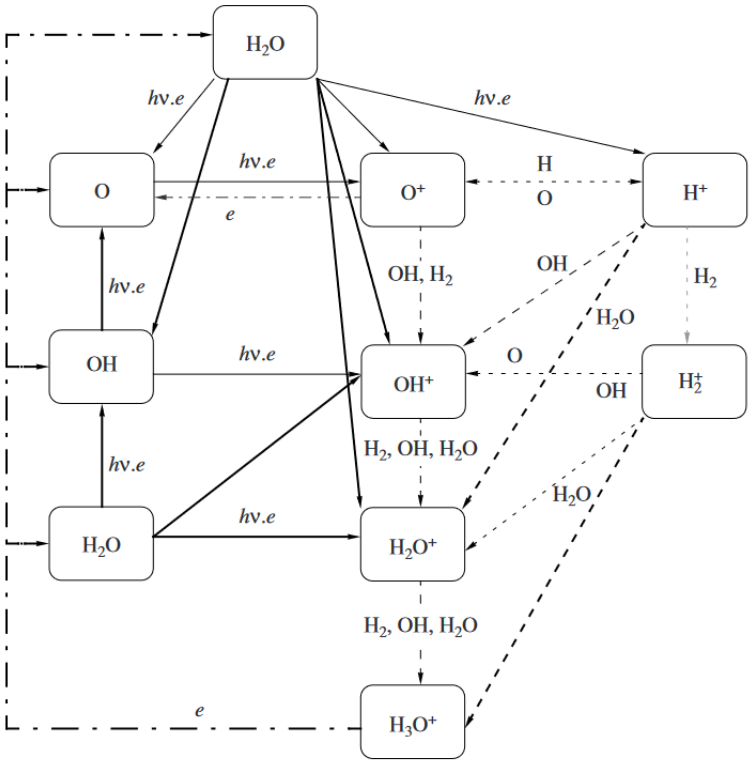

Figure 1.9 : The scheme of the ionization chemistry for water vapor the H_2O-dominated atmosphere of icy moons: The primary photolysis and electron impact processes are shown by the solid lines; the ion–molecular reactions and the reactions of the dissociative recombination are shown by dashed and dash-and-dot lines, respectively. From Shematovich 2008. [36]

In Titan's atmosphere, where the UV and X-rays are the dominant ionization sources, it exists some contribution of the magnetospheric charged particles in the 500 km to 1000 km altitude range (according to the model calculations of Cravens et al 2007).[37]

1.4. Important anion formation processes

For decades, ion chemistry in astrophysical environments was focused almost entirely on positive ions. Recently, the detection of negative ions drew attention to their contribution in astrochemistry. The dissociative attachment and radiative attachment are two major pathways for anions production (Table 1.3). Radiative association and ion-pair (corresponding to production of cation and anion pair species) formation have also a contribution in the formation of anions in space.

The first observed interstellar negative ion in the gas phase was C_6H^- and was discovered in the C-star envelope IRC+10216 by McCarthy et al. in 2006[38]. This observation was rapidly followed by the detection of C_4H^- by Cernicharo et al. 2007.[39] The abundance between the two ions, $[C_4H^-]/[C_6H^-] = 1/6$, is more than two orders of magnitude smaller than that between their neutral counterparts, $[C_4H]/[C_6H] = 45$. After the detection of C_6H^- and C_4H^-, C_8H^- ,[40] C_3N^- ,[41] C_5N^- [42] and CN^- [43] anions were also discovered in IRC+10216 through radio observations.[44] The derived abundances of the C_8H^-, C_6H^-, C_4H^- anions compared to C_8H, C_6H, C_4H neutrals are 5%, 1.6% and 0.014% respectively. [40]

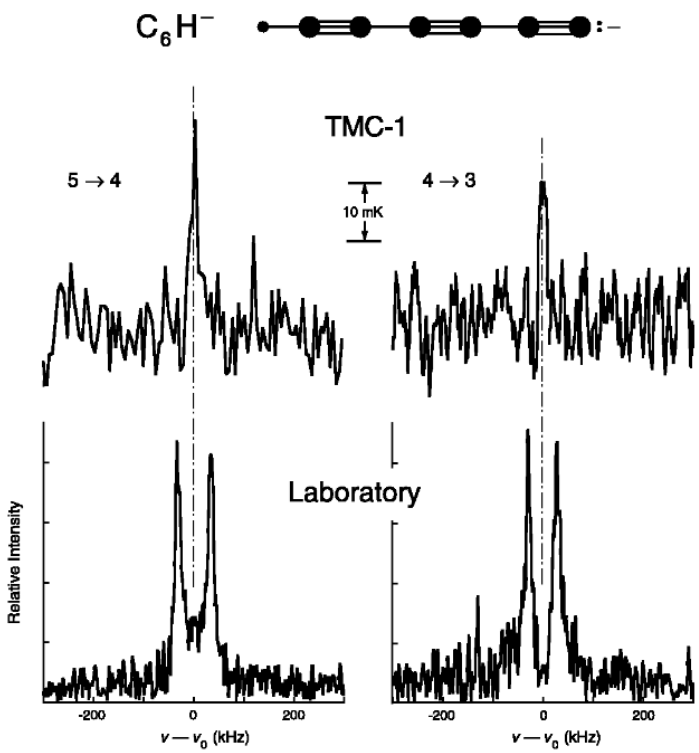

Figure 1.10 : Two rotational transitions of C_6H^- anion in the laboratory and in TMC-1. Frequencies are relative to the laboratory rest frequencies, assuming the standard mean radial velocity of 5.80 km s^{-1} for TMC-1. From M. C. McCarthy et al. 2006. [38]

The presence of numerous negative ions with mass-to-charge ratios of up to∼10 000 has also been revealed in Titan's upper atmosphere by the Electron Spectrometer sensor of the Cassini Plasma Spectrometer (CAPS-ELS) on-board the Cassini spacecraft during high altitude flybys.[11,45] According to Vuitton et al. ,[46] and despite the low resolution of the spectrum (Δm/m ∼ 17%), two negative ion peaks centered at 22 ± 4 and 44 ± 8 u/q were clearly identified and assigned to CN^- and C_3N^- ions. A third small peak at 82±14 u/q may be present as well (Figure 1.11).

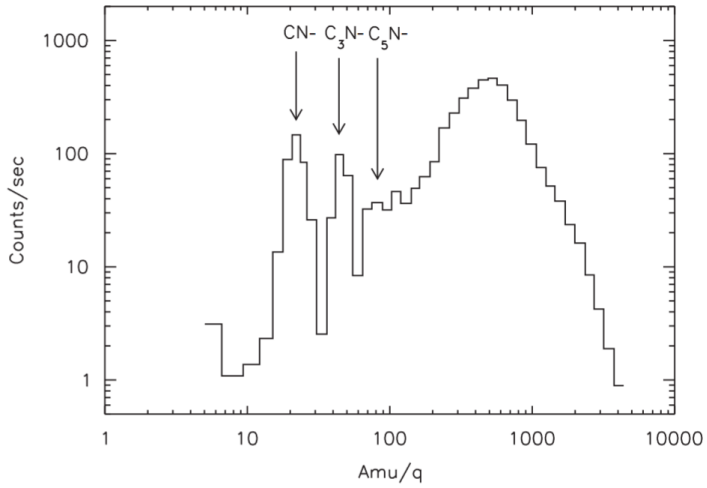

Figure 1.11 : Negative ions measured in each CAPS-ELS energy bin at an altitude of 1015 km during the T40 encounter. The attribution of the peaks is based on the ionospheric chemistry model. From Vuitton et al. 2009[46]

In addition to planetary atmospheres and circumstellar envelopes of dying stars, anions play a role in the chemistry of dark clouds, PDRs, cometary comae, and protostellar envelopes, and they play an important role in the synthesis of very large hydrocarbon species.[4]

1.4.1 Dissociative electron attachment.

Dissociative attachment has been found to be one of the most efficient anion formation processes under laboratory conditions. In this mechanism, a free electron attaches to a neutral molecule forming a highly excited intermediate compound that subsequently fragments into a neutral and an anion:

$$AB + e^- \rightarrow (AB^-)^* \rightarrow A^- + B$$

Referring to Petrie,[47] the CN^- ion can be formed in dense interstellar clouds and circumstellar envelopes by (exothermic) dissociative attachment of free electrons to MgCN and MgNC isomers .

In astrophysical environments where the electrons can be present with more than 1.3 eV energy such as Titan's upper atmosphere, the C_3N^- anion could be formed by dissociative attachment of HC_3N (endoergic pathway). This also applies for the CN^- anion that can be produced by dissociative electron capture on various nitrile species[46]. The presence of HCN, C_2N_2, CH_3CN, C_2H_3CN and HC_3N has been inferred from analysis of INMS spectra with mixing ratios ranging from 2×10^{-4} to 2×10^{-6}. According to Vuitton et al., C_2H^-, C_4H^-, C_6H^- carbonaceous anions can as well be generated in Titan's upper atmosphere by the same mechanism, i.e. electronic dissociative attachment on C_2H_2, C_4H_2, C_6H_2 respectively.

1.4.2 Radiative electron attachment

Radiative attachment of thermal electrons to atoms or radicals is a process that can lead to the formation of negative ions in various astrophysical environments:

$$A + e^- \rightarrow (A^-)^* \rightarrow A^- + h\nu$$

The radiative electronic attachment onto C_2H, C_4H, C_6H and C_3N leads to the formation of the negative ions, C_2H^-, C_4H^-, C_6H^- and C_3N^-, respectively. The H^-, CH_2^-, CH_3^-, OH^- and CN^- anions can be produced by thermal electron capture by the neutral molecules but the rate coefficients have not been determined. Radiative attachment is likely to proceed at a rate only slightly faster than that of an atomic species. According to Chandrasekaran et al.[49] the radiative electron attachment (REA) leading to the formation of C_6^- is estimated to be 3×10^{-7} cm^3 s^{-1} at 300 K.

In planetary ionospheres, where the pressure is low, radiative attachment can be a very efficient process. Together with dissociative attachment of ozone, radiative attachment to O and non-dissociative electron attachment on O_2 (three-body stabilization) ensures that anions out number free electrons in the Martian atmosphere below 30 km.[20]

1.4.3 Radiative association of anions.

According to Senent et al. and Vuitton et al. ,[50,51] anions in astrophysical environments could be formed by radiative association of anions with neutrals. An example of this mechanism is the reaction between C_n^- and H, that yields to the formation of exited C_nH^- anion which then relaxes by emitting a photon.

Using a selected ion flow tube apparatus (see chapter 2), Eichelberger et al. 2007[52] have determined the rate coefficients for the reactions of C_n^- and HC_n^- with H, N, and O atoms in order to characterize their interstellar chemistry. Reactions between the carbon chain anions and H and O occur readily, with rate coefficients ranging from mid to high 10^{-10} cm^3s^{-1}. These studies further

demonstrated that radiative association is only feasible for large C_n^- ions with n > 6, since associative detachment outcompetes the association process for smaller species.

Another example for the radiative association process is the reaction between H^- and H_2, that yields to the formation of H_3^-, this reaction takes place in the interstellar medium, according to M. Ayouz et al (2011).[53]

1.4.4 Radiative ion-pair formation

Photo-ionization can induce the formation of a positive and negative ion pair ($AB + h\nu \rightarrow A^- + B^+$). The cross-section of this process is several orders of magnitude lower than that of the formation of a positive ion and a neutral. Anion formation through this mechanism has been included in models of Titan's ionosphere (Vuitton et al 2009).[46] For example, the photoionization of HCN and of C_2H_2 leads to the formation of CN^-/H^+ C_2H^-/H^+ ions pairs respectively.

1.5 Growth and destruction of ions in space

1.5.1 Cations growth and destruction

Cation-neutral reactions are the most efficient process for the recycling and growth of cations in planetary atmospheres and interstellar medium. According to Beck et al,[54] the abundance of the atomic ions in the CSE, is strongly affected by the charge-transfer reactions (CT) between neutrals and ions. The charge transfer reactions can also occur between molecular ions and neutrals. For example, in Martian atmosphere, the charge transfer reactions between N_2^+, Ar^+, CO^+ and CO_2 is an important ionization pathway, leading to the formation of CO_2^+ ions. The latter undergo a CT reaction with O_2 leading to O_2^+ ions. In addition, through the same process between O_2^+ ions and NO, the NO^+ ions can also be formed.[55] In addition to charge transfer reactions, cation-neutral transfer reactions in which a part of neutral molecule is transferred to the ion is an important ions destruction pathway in space.

Furthermore, three-body ion-molecule clustering reactions (ion clustering) exerts also a broad influence on the physics and chemistry of planetary atmospheres. As an example, cluster ions have been detected in Titan's ionosphere, $HCO^+ \cdot H_2$ and $CH_5^+ \cdot CH_4 \cdot$are especially prevalent at altitudes below 80 km.[56]

Radiative association reactions contribute in the formation of more complex species in the interstellar medium. For example, radiative association of C_3H^+ and H_2 leads to the formation of $C_3H_3^+$, which can exist in two forms, a cyclic (c-C_3H_3+) and a linear one H_2CCCH^+. These two

isomers can undergo dissociative recombination forming neutral unsaturated hydrocarbons, according to D. Smith and N.G. Adams.[57]

UV radiation is not only an important production source of ions but also an efficient destroyer of ions (photodissociation reaction). For example, according to Van Dishoeck et al. ,[58] UV radiation dissociates CH^+ and OH^+ ions into smaller ions in Herbig Ae stars.

Reactions between cations and electrons are considered to be an important cations destruction pathway. It exists different types of these reactions: radiative and electronic recombination, ion-pair formation, dissociative excitation, dissociative ionization, and dissociative recombination (Table 1.3). For example, in Titan's atmosphere, the dissociative recombination of protonated nitriles and the larger hydrocarbon ions is often the only destruction route.[3]

1.5.2 Anions growth and destruction

The main destruction mechanisms for anions under astrophysical conditions are: photodetachment, ion-neutral associative detachment, collisional detachment, electron-impact detachment, and mutual neutralization with cations (ion-ion recombination). A recent experimental work by Zabka et al. showed that in the multiple collision regime, negative ion chemistry could lead to the formation of heavy anions of rapidly growing size.[59,60]

For example, for CN^- and C_3N^- anions, the photodetachment by interstellar UV photons is the most important destruction mechanism for these anions in the circumstellar envelope of the carbon-rich star IRC+1021.[61]

The collisional detachment mechanism is an important destruction pathway for weakly bond anions. For example, for the HCN^- anion, the extra electron is weakly bound in the dipole potential of the HCN molecule by only 1.56 meV, thus making the collisional detachment an efficient destruction pathway.[62]

In the early universe, the associative detachment of between H^- anion and H atoms leads to the formation of neutral H_2 molecule ($H^- + H \rightarrow H_2 + e^-$). This molecule plays a fundamental role in the cooling of molecular clouds during the formation of first generation of stars.[63]

In Earth, and in Mars ionosphere at low altitudes, ion-ion recombination is an efficient pathway for the destruction of the ions, for example, the recombination between $NH_4^+(H_2O)_n$ and $HSO_4^-(H_2O)_n$ leads to their destruction.[29]

Polymerization reactions is an important route leading to anions destruction, in which anions incorporate in neutrals molecules can lead to higher mass anions. For example, referring to

Descheneaux et al. ,[64] the repeated insertion of acetylene molecules results in an anion sequence with anions that peaks at the $C_{2n}H^-$ species. Therefore, C_2H^- anions can trigger a consecutive chain of polymerization ($C_2H^- + C_2H_2 \rightarrow C_4H^- + H_2$; $C_{2n}H^- + C_2H_2 \rightarrow C_{2n+2}H^- + H_2$). The precise rate coefficient of these reactions cannot be found in the literature, but base on ions growth rate in silane discharge the rate coefficient for these reactions is estimated to be around 10^{-12} cm^3s^{-1}.[65, 66]

1.6 Conclusion:

This chapter provided an overview on the observation of ions (cations and anions) in spatial environments. The most important ions formation, growth and destruction processes in space were outlined. Among all these processes, ion-neutral reactions play a crucial role in the chemistry of the astrophysical environments, and they are a possible synthetic route for the formation of prebiotic molecules in space.[67] In contrast with cation-neutrals reactions which are more recognized, there are less than a dozen measurements on the gas-phase kinetics of anions at low temperatures below 200 K. The determination of the temperature-dependent kinetic rate coefficients and the branching between the different exit channels is of outmost importance for feeding the photochemical models of astrophysical environments. In the next chapter we will focus on the capture models for the estimation of the rate coefficient and experimental techniques used to study the ion-neutral reactions.

References:

(1) Dalgarno, A. A Serendipitous Journey. Annu. Rev. Astron. Astrophys. **2008**, 46 (1), 1–20. https://doi.org/10.1146/annurev.astro.46.060407.145216.

(2) Ziurys, L. M. The Chemistry in Circumstellar Envelopes of Evolved Stars: Following the Origin of the Elements to the Origin of Life. Proc. Natl. Acad. Sci. **2006**, 103 (33), 12274–12279. https://doi.org/10.1073/pnas.0602277103.

(3) Vuitton, V.; Yelle, R. V.; McEwan, M. J. Ion Chemistry and N-Containing Molecules in Titan's Upper Atmosphere. Icarus **2007**, 191 (2), 722–742. https://doi.org/10.1016/j.icarus.2007.06.023.

(4) Millar, T. J.; Walsh, C.; Field, T. A. Negative Ions in Space. Chem. Rev. **2017**, 117 (3), 1765–1795. https://doi.org/10.1021/acs.chemrev.6b00480.

(5) Cernicharo, J.; Cabezas, C.; Bailleux, S.; Margulès, L.; Motiyenko, R.; Zou, L.; Endo, Y.; Bermúdez, C.; Agúndez, M.; Marcelino, N.; Lefloch, B.; Tercero, B.; de Vicente, P. Discovery of the Acetyl Cation, CH_3CO^+, in Space and in the Laboratory. Astron. Astrophys. **2021**, 646, L7. https://doi.org/10.1051/0004-6361/202040076.

(6) Cernicharo, J.; Cabezas, C.; Endo, Y.; Marcelino, N.; Agúndez, M.; Tercero, B.; Gallego, J. D.; de Vicente, P. Space and Laboratory Discovery of HC_3S^+. Astron. Astrophys. **2021**, 646, L3. https://doi.org/10.1051/0004-6361/202040013.

(7) Cernicharo, J.; Tercero, B.; Fuente, A.; Domenech, J. L.; Cueto, M.; Carrasco, E.; Herrero, V. J.; Tanarro, I.; Marcelino, N.; Roueff, E.; Gerin, M.; Pearson, J. Detection of the Ammonium Ion in Space. Astrophys. J. **2013**, 771 (1), L10. https://doi.org/10.1088/2041-8205/771/1/L10.

(8) Geballe, T. R. H+3 in Dense and Diffuse Clouds, in Our Galaxy and Beyond. 6.

(9) Douglas, A.; Herzberg, G. Note on CH^{+} in Interstellar Space and in the Laboratory. Astrophys. J. **1941**, 94, 381.

(10) Nixon, C. A.; Lorenz, R. D.; Achterberg, R. K.; Buch, A.; Coll, P.; Clark, R. N.; Courtin, R.; Hayes, A.; Iess, L.; Johnson, R. E.; Lopes, R. M. C.; Mastrogiuseppe, M.; Mandt, K.; Mitchell, D. G.; Raulin, F.; Rymer, A. M.; Todd Smith, H.; Solomonidou, A.; Sotin, C.; Strobel, D.; Turtle, E. P.; Vuitton, V.; West, R. A.; Yelle, R. V. Titan's Cold Case Files - Outstanding Questions after Cassini-Huygens. Planet. Space Sci. **2018**, 155, 50–72. https://doi.org/10.1016/j.pss.2018.02.009.

(11) Waite, J. H.; Young, D. T.; Cravens, T. E.; Coates, A. J.; Crary, F. J.; Magee, B.; Westlake, J. The Process of Tholin Formation in Titan's Upper Atmosphere. Science **2007**, 316 (5826), 870–875. https://doi.org/10.1126/science.1139727.

(12) Vuitton, V.; Yelle, R. V.; Anicich (Retired), V. G. The Nitrogen Chemistry of Titan's Upper Atmosphere Revealed. Astrophys. J. **2006**, 647 (2), L175–L178. https://doi.org/10.1086/507467.

(13) Boezio, M.; Munini, R.; Picozza, P. Cosmic Ray Detection in Space. Prog. Part. Nucl. Phys. **2020**, 112, 103765. https://doi.org/10.1016/j.ppnp.2020.103765.

(14) R. A. Mewaldt. Cosmic Rays. Macmillan Encyclopedia of Physics. 1996.

(15) Reames, D. V. Particle Acceleration at the Sun and in the Heliosphere. Space Sci. Rev. **1999**, 90 (3/4), 413–491. https://doi.org/10.1023/A:1005105831781.

(16) Wibig, T.; Wolfendale, A. W. At What Particle Energy Do Extragalactic Cosmic Rays Start to Predominate? J. Phys. G Nucl. Part. Phys. **2005**, 31 (3), 255–264. https://doi.org/10.1088/0954-3899/31/3/005.

(17) Dalgarno, A.; Yan, M.; Liu, W. Electron Energy Deposition in a Gas Mixture of Atomic and Molecular Hydrogen and Helium. Astrophys. J. Suppl. Ser. **1999**, 125 (1), 237–256. https://doi.org/10.1086/313267.

(18) Michael, M.; Tripathi, S. N.; Borucki, W. J.; Whitten, R. C. Highly Charged Cloud Particles in the Atmosphere of Venus. J. Geophys. Res. **2009**, 114 (E4), E04008. https://doi.org/10.1029/2008JE003258.

(19) Gronoff, G.; Lilensten, J.; Desorgher, L.; Flückiger, E. Ionization Processes in the Atmosphere of Titan: I. Ionization in the Whole Atmosphere. Astron. Astrophys. **2009**, 506 (2), 955–964. https://doi.org/10.1051/0004-6361/200912371.

(20) Molina-Cuberos, G.; López-Moreno, J.; Rodrigo, R.; Lichtenegger, H.; Schwingenschuh, K. A Model of the Martian Ionosphere below 70 Km. Adv. Space Res. **2001**, 27 (11), 1801–1806.

(21) Fox, J. L.; Galand, M. I.; Johnson, R. E. Energy Deposition in Planetary Atmospheres by Charged Particles and Solar Photons. Space Sci. Rev. **2008**, 139 (1–4), 3–62. https://doi.org/10.1007/s11214-008-9403-7.

(22) Haider, S. A.; Batista, I. S.; Abdu, M. A.; Santos, A. M.; Shah, S. Y.; Thirupathaiah, P. Flare X-Ray Photochemistry of the E Region Ionosphere of Mars: X-Ray Aeronomy of Mars. J. Geophys. Res. Space Phys. **2016**, 121 (7), 6870–6888. https://doi.org/10.1002/2016JA022435.

(23) Bougher, S. W.; Pawlowski, D.; Bell, J. M.; Nelli, S.; McDunn, T.; Murphy, J. R.; Chizek, M.; Ridley, A. Mars Global Ionosphere-Thermosphere Model: Solar Cycle, Seasonal, and Diurnal Variations of the Mars Upper Atmosphere: BOUGHER ET AL. J. Geophys. Res. Planets **2015**, 120 (2), 311–342. https://doi.org/10.1002/2014JE004715.

(24) Sternberg, A. Chemistry in Dense Photon Dominated Regions. The Physics and Chemistry of Interstellar Molecular Clouds. 1995, pp 175–177.

(25) Wilms, J.; Allen, A.; McCray, R. On the Absorption of X-Rays in the Interstellar Medium. Astrophys. J. **2000**, 542 (2), 914–924. https://doi.org/10.1086/317016.

(26) Stäuber, P.; Doty, S. D.; van Dishoeck, E. F.; Benz, A. O. X-Ray Chemistry in the Envelopes around Young Stellar Objects. Astron. Astrophys. **2005**, 440 (3), 949–966. https://doi.org/10.1051/0004-6361:20052889.

(27) Banaszkiewicz, M.; Zarnecki, J. C. Interaction of Solar Flare X-Rays with the Atmosphere of Titan. Planet. Space Sci. **1998**, 47 (1), 35–44. https://doi.org/10.1016/S0032-0633(98)00105-6.

(28) McKee, C. F.; Draine, B. T. Interstellar Shock Waves. Science **1991**, 252 (5004), 397–403.

(29) Larsson, M.; Geppert, W. D.; Nyman, G. Ion Chemistry in Space. Rep. Prog. Phys. **2012**, 75 (6), 066901. https://doi.org/10.1088/0034-4885/75/6/066901.

(30) Allen, M. G.; Groves, B. A.; Dopita, M. A.; Sutherland, R. S.; Kewley, L. J. The MAPPINGS III Library of Fast Radiative Shock Models. Astrophys. J. Suppl. Ser. **2008**, 178 (1), 20–55. https://doi.org/10.1086/589652.

(31) Tielens, A. G. G. M. The Physics and Chemistry of the Interstellar Medium, Cambridge University Press.; 2005.

(32) Jack Randolph Jokipii, Charles P. Sonett, Mark S. Giampapa. Cosmic Winds and the Heliosphere; 1997.

(33) Johnson, R. E.; Leblanc, F. The Physics and Chemistry of Sputtering by Energetic Plasma Ions. In Physics of Space: Growth Points and Problems; Meyer-Vernet, N., Moncuquet, M., Pantellini, F., Eds.; Springer Netherlands: Dordrecht, 2001; pp 259–269. https://doi.org/10.1007/978-94-010-0904-1_32.

(34) Robertson, I. P.; Cravens, T. E. X-Ray Emission from the Terrestrial Magnetosheath: MAGNETOSHEATH X-RAY EMISSIONS. Geophys. Res. Lett. **2003**, 30 (8). https://doi.org/10.1029/2002GL016740.

(35) McNutt, R. L. Force Balance in the Magnetospheres of Jupiter and Saturn. Adv. Space Res. **1983**, 3 (3), 55–58. https://doi.org/10.1016/0273-1177(83)90256-9.

(36) Shematovich, V. I. Ionization Chemistry in H2O-Dominated Atmospheres of Icy Moons. Sol. Syst. Res. **2008**, 42 (6), 473–487. https://doi.org/10.1134/S0038094608060026.

(37) Cravens, T. E.; Robertson, I. P.; Ledvina, S. A.; Mitchell, D.; Krimigis, S. M.; Waite, J. H. Energetic Ion Precipitation at Titan. Geophys. Res. Lett. **2008**, 35 (3), L03103. https://doi.org/10.1029/2007GL032451.

(38) McCarthy, M. C.; Gottlieb, C. A.; Gupta, H.; Thaddeus, P. LABORATORY AND ASTRONOMICAL IDENTIFICATION OF THE NEGATIVE MOLECULAR ION C6HX. 652, 4.

(39) Cernicharo, J.; Guélin, M.; Agúndez, M.; Kawaguchi, K.; McCarthy, M.; Thaddeus, P. Astronomical Detection of C4H-, the Second Interstellar Anion. Astron. Astrophys. **2007**, 467 (2), L37–L40. https://doi.org/10.1051/0004-6361:20077415.

(40) Brünken, S.; Gupta, H.; Gottlieb, C.; McCarthy, M.; Thaddeus, P. Detection of the Carbon Chain Negative Ion C8H–in TMC-1. Astrophys. J. Lett. **2007**, 664 (1), L43.

(41) Thaddeus, P.; Gottlieb, C.; Gupta, H.; Brünken, S.; McCarthy, M.; Agúndez, M.; Guélin, M.; Cernicharo, J. Laboratory and Astronomical Detection of the Negative Molecular Ion C3N−. Astrophys. J. **2008**, 677 (2), 1132.

(42) Cernicharo, J.; Guelin, M. DETECTION OF C5N- AND VIBRATIONALLY EXCITED C6H IN IRC +10216. 688, 4.

(43) Agúndez, M.; Cernicharo, J.; Guélin, M.; Kahane, C.; Roueff, E.; Kłos, J.; Aoiz, F. J.; Lique, F.; Marcelino, N.; Goicoechea, J. R.; González García, M.; Gottlieb, C. A.; McCarthy, M. C.; Thaddeus, P. Astronomical Identification of CN- , the Smallest Observed Molecular Anion. Astron. Astrophys. **2010**, 517, L2. https://doi.org/10.1051/0004-6361/201015186.

(44) Cernicharo, J.; Marcelino, N.; Pardo, J. R.; Agúndez, M.; Tercero, B.; de Vicente, P.; Cabezas, C.; Bermúdez, C. Interstellar Nitrile Anions: Detection of C_3N^- and C_5N^- in TMC-1. Astron. Astrophys. **2020**, 641, L9. https://doi.org/10.1051/0004-6361/202039231.

(45) Coates, A. J.; Crary, F. J.; Lewis, G. R.; Young, D. T.; Waite, J. H.; Sittler, E. C. Discovery of Heavy Negative Ions in Titan's Ionosphere. Geophys. Res. Lett. **2007**, 34 (22), L22103. https://doi.org/10.1029/2007GL030978.

(46) Vuitton, V.; Lavvas, P.; Yelle, R. V.; Galand, M.; Wellbrock, A.; Lewis, G. R.; Coates, A. J.; Wahlund, J.-E. Negative Ion Chemistry in Titan's Upper Atmosphere. Planet. Space Sci. **2009**, 57 (13), 1558–1572. https://doi.org/10.1016/j.pss.2009.04.004.

(47) Petrie, S. Novel Pathways to CN− within Interstellar Clouds and Circumstellar Envelopes: Implications for IS and CS Chemistry. Mon. Not. R. Astron. Soc. **1996**, 281 (1), 137–144. https://doi.org/10.1093/mnras/281.1.137.

(48) Graupner, K.; Merrigan, T. L.; Field, T. A.; Youngs, T. G. A.; Marr, P. C. Dissociative Electron Attachment to HCCCN. New J. Phys. **2006**, 8 (7), 117–117. https://doi.org/10.1088/1367-2630/8/7/117.

(49) Chandrasekaran, V.; Prabhakaran, A.; Kafle, B.; Rubinstein, H.; Heber, O.; Rappaport, M.; Toker, Y.; Zajfman, D. Formation and Stabilization of C6− by Radiative Electron Attachment. J. Chem. Phys. **2017**, 146 (9), 094302. https://doi.org/10.1063/1.4977059.

(50) Senent, M. L.; Hochlaf, M. AB INITIO CHARACTERIZATION OF C_4^-, C_4H, AND C_4H^-. Astrophys. J. **2010**, 708 (2), 1452–1458. https://doi.org/10.1088/0004-637X/708/2/1452.

(51) Vuitton, V.; Yelle, R. V.; Lavvas, P.; Klippenstein, S. J. RAPID ASSOCIATION REACTIONS AT LOW PRESSURE: IMPACT ON THE FORMATION OF HYDROCARBONS ON TITAN. Astrophys. J. **2012**, 744 (1), 11. https://doi.org/10.1088/0004-637X/744/1/11.

(52) Eichelberger, B.; Snow, T. P.; Barckholtz, C.; Bierbaum, V. M. Reactions of H, N, and O Atoms with Carbon Chain Anions of Interstellar Interest: An Experimental Study. Astrophys. J. **2007**, 667 (2), 1283–1289. https://doi.org/10.1086/520953.

(53) Ayouz, M.; Lopes, R.; Raoult, M.; Dulieu, O.; Kokoouline, V. Formation of H$_3^-$ by Radiative Association of H$_2$ and H$^-$ in the Interstellar Medium. Phys. Rev. A **2011**, 83 (5), 052712. https://doi.org/10.1103/PhysRevA.83.052712.

(54) Beck, H.; Gail, H.-P.; Henkel, R.; Sedlmayr, E. Chemistry in Circumsellar Shells. I-Chromospheric Radiation Fields and Dust Formation in Optically Thin Shells of M-Giants. Astron. Astrophys. **1992**, 265, 626–642.

(55) Haider, S. A.; Abdu, M. A.; Batista, I. S.; Sobral, J. H. A.; Sheel, V.; Molina-Cuberos, G. J.; Maguire, W. C.; Verigin, M. I. Zonal Wave Structures in the Nighttime Tropospheric Density and Temperature and in the D Region Ionosphere over Mars: Modeling and Observations: WAVE STRUCTURES IN THE D REGION OF MARS. J. Geophys. Res. Space Phys. **2009**, 114 (A12), n/a-n/a. https://doi.org/10.1029/2009JA014231.

(56) Borucki, W. J.; Whitten, R. C.; Bakes, E. L. O.; Barth, E.; Tripathi, S. Predictions of the Electrical Conductivity and Charging of the Aerosols in Titan's Atmosphere. Icarus **2006**, 181 (2), 527–544. https://doi.org/10.1016/j.icarus.2005.10.030.

(57) Smith, D.; Adams, N. G. Cyclic and Linear Isomers of C3H2+ and C3H3+: The C3H+ + H2 Reaction. Int. J. Mass Spectrom. Ion Process. **1987**, 76 (3), 307–317. https://doi.org/10.1016/0168-1176(87)83035-5.

(58) van Dishoeck, E. F.; Jonkheid, B.; van Hemert, M. C. Photoprocesses in Protoplanetary Disks. Faraday Discuss. **2006**, 133, 231. https://doi.org/10.1039/b517564j.

(59) Žabka, J.; Romanzin, C.; Alcaraz, C.; Polášek, M. Anion Chemistry on Titan: A Possible Route to Large N-Bearing Hydrocarbons. Icarus **2012**, 219 (1), 161–167. https://doi.org/10.1016/j.icarus.2012.02.031.

(60) Žabka, J.; Ndiaye, I.; Alcaraz, C.; Romanzin, C.; Polášek, M. Experimental and Theoretical Study of the Mechanism of Formation of Astrochemically Important C2n+1N− Anions via Ion/Molecule Reactions. Int. J. Mass Spectrom. **2014**, 367, 1–9. https://doi.org/10.1016/j.ijms.2014.04.008.

(61) Kumar, S. S.; Hauser, D.; Jindra, R.; Best, T.; Roučka, Š.; Geppert, W. D.; Millar, T. J.; Wester, R. PHOTODETACHMENT AS A DESTRUCTION MECHANISM FOR CN^- AND C_3N^- ANIONS IN CIRCUMSTELLAR ENVELOPES. Astrophys. J. **2013**, 776 (1), 25. https://doi.org/10.1088/0004-637X/776/1/25.

(62) Ard, S.; Garrett, W. R.; Compton, R. N.; Adamowicz, L.; Stepanian, S. G. Rotational States of Dipole-Bound Anions of Hydrogen Cyanide. Chem. Phys. Lett. **2009**, 473 (4–6), 223–226. https://doi.org/10.1016/j.cplett.2009.04.007.

(63) Kreckel, H.; Bruhns, H.; Cizek, M.; Glover, S. C. O.; Miller, K. A.; Urbain, X.; Savin, D. W. Experimental Results for H2 Formation from H- and H and Implications for First Star Formation. Science **2010**, 329 (5987), 69–71. https://doi.org/10.1126/science.1187191.

(64) Deschenaux, C.; Affolter, A.; Magni, D.; Hollenstein, C.; Fayet, P. Investigations of CH_4, C_2H_2 and C_2H_4 Dusty RF Plasmas by Means of FTIR Absorption Spectroscopy and Mass Spectrometry. J. Phys. Appl. Phys. **1999**, 32 (15), 1876–1886. https://doi.org/10.1088/0022-3727/32/15/316.

(65) Howling, A. A.; Sansonnens, L.; Dorier, J. -L.; Hollenstein, Ch. Time-resolved Measurements of Highly Polymerized Negative Ions in Radio Frequency Silane Plasma Deposition Experiments. J. Appl. Phys. **1994**, 75 (3), 1340–1353. https://doi.org/10.1063/1.356413.

(66) Perrin, J.; Bohm, C.; Etemadi, R.; Lloret, A. Possible Routes for Cluster Growth and Particle Formation in RF Silane Discharges. Plasma Sources Sci. Technol. **1994**, 3 (3), 252–261. https://doi.org/10.1088/0963-0252/3/3/003.

(67) Spezia, R.; Jeanvoine, Y.; Scuderi, D. Ion–Molecule Reactions as a Possible Synthetic Route for the Formation of Prebiotic Molecules in Space. In Origin and Evolution of Biodiversity; Springer, 2018; pp 277–292.

Chapter 2: Studying Ion-neutral reactions in the laboratory

2.1 Theoretical aspects

Theoretical approaches are required for a better understanding of ion-neutral reactive collisions. Collisions between species can be classified as elastic (only kinetic energy is exchanged between the partners), inelastic (kinetic and internal energy is exchanged) and reactive (the chemical structure of the collision partners is varied). This section is dedicated to the theoretical treatment of ion-neutral reactions employing a selection of models that are based on the long-range capture theory. In this section, we will recall first some basic chemical kinetics before moving to capture theories that can reasonably well model, usually barrierless, ion-molecule reactions.

The well-known capture models which are the Langevin model, the Locked dipole model (LD), the average dipole orientation model (ADO), and the Su and Chesnavich model (SC) have been employed to predict the rate coefficient of ion-neutral reactions, and to understand experimental results that will be presented in next chapters.

2.1.1 Chemical reaction rate

We distinguish different types of elementary reactions, depending on the molecularity, which refers to the number of the reactant particles involved in the reaction. Molecularity can be described as unimolecular (when a molecule rearranges itself producing one or more products), bimolecular (involves the collision of two particles), or termolecular (where two reactants form an initial complex that reacts with the third reactant to form products).

Consider the standard alphabetical reaction between a moles of species A and b moles of species B going to c moles of C and d moles of D given in Equation (2.1):

$$aA + bB \rightarrow cC + dD \qquad \text{Eq. (2.1)}$$

The rate of the reaction is related to the density of the species multiplied by a rate coefficient written generally as:

$$\nu = k[A]^{\alpha}[B]^{\beta} \qquad \text{Eq. (2.2)}$$

where ν is the rate of the chemical reaction, k is the rate coefficient, α and β are the partial orders for A and B respectively (α + β is equal to the global order of the reaction), [A] and [B] are the densities of the reactants. The parameters a and b can be any number (including non-integer numbers) and for simple reactions represent the stoichiometry of the reaction.

A chemical reaction could have zero, first, second or even a third order for astrophysical interest. The first-order rate equation for the removal of a reactant may be written in terms of the rate of change of [A] with time as:

$$\text{Rate} = \frac{d[A]}{dt} = -k[A] \qquad \text{Eq. (2.3)}$$

By integration of the last equation, we obtain the density of species A after a reaction time t:

$$[A]_t = [A]_0 \exp(-kt) \qquad \text{Eq. (2.4)}$$

Where $[A]_0$ is the initial density of species A.

For the second and third order reactions, the rate coefficient is expressed respectively as follows:

$$\text{Rate} = k[A][B] \qquad \text{Eq. (2.5)}$$

$$\text{Rate} = k[A][B][C] \qquad \text{Eq. (2.6)}$$

The pseudo-first-order conditions is obtained when one of the reactants is introduced in excess with respect to the other one (for example [A]>>[B]): its density doesn't change significantly during the reaction, and the second order reaction behaves as a first order reaction.

Eq. (2.4) thus becomes:

$$\text{Rate} = k[A][B] = k_{1st}[B] \qquad \text{Eq.(2. 4)}$$

Where k_{1st} is defined as pseudo-first-order rate coefficient of the reaction, $k_{1st} = k[A]$. Using this method, the second-order/bimolecular ion-neutral reactions that we are interested in studying, are simplified to the pseudo-first-order reaction.

In the pseudo-first-order conditions, the density of reactant B as a function of time is simply given by:

$$[B]_t = [B]_0 \exp(-k_{1st}t) \qquad \text{Eq.(2.7)}$$

Where $[B]_0$ is the initial density of species B.

The unit of the rate coefficient k is $cm^3\ s^{-1}$ (or cm^3 molecule^{-1} s^{-1}), and $cm^6\ s^{-1}$ (or cm^6 molecule^{-2} s^{-1}, due to the contribution of the density of the third neutral partner) for bimolecular and termolecular reactions respectively.

2.1.2 Temperature dependence

Laboratory measurements of gas-phase reactions show that many follow an empirical temperature dependence of the rate coefficient described by the Arrhenius equation:

$$k(T) = A \exp\left[\frac{-E_a(T)}{RT}\right] \qquad \text{Eq. (2.8)}$$

Where:

- A ($cm^3\ s^{-1}$) is the pre-exponential factor which represents the frequency of reactants collision
- R is the perfect gas constant (8.314 J mol^{-1} K^{-1}),
- E_a is the activation energy for the reaction (J mol^{-1}) which is defined as the minimum energy that must be provided into compounds to initiate the reaction.

According to this equation, the rate coefficient increases with the temperature, and the reaction proceed faster. This is due to the increase of the internal energy of molecules, the kinetic energy, and the number of collisions between species. However not all the chemical reactions follow this law (e.g. some gas phase reactions involving ions and radicals). In other cases, the rate coefficient and the temperature are inversely proportional due to quantum effects (e.g. quantum tunneling effect) that is more important at low temperatures. This is known as non-Arrhenius temperature dependence. The Arrhenius equation was updated to Arrhenius-Kooij expression[1] (or the modified Arrhenius equation) and expressed as:

$$k(T) = \alpha \left(\frac{T}{T_0}\right)^{\beta} . e^{-\gamma/T} \qquad \text{Eq.(2. 9)}$$

with β a temperature exponent, which is zero in the original equation. In Eq. (2.9), α replaces A, γ replaces E_a/R, and T_0 is the temperature reference (usually 300 K).

Collision theory states that for a chemical reaction to occur, the reacting particles must collide with one another with sufficient energy (activation energy), and with the proper orientation. The rate of the reaction depends on the frequency of collisions. As stated earlier, collision between two reactants can result in the two molecules bouncing off one another and if no energy is exchanged this is called an elastic collision but if some kinetic, rotational or vibrational energy is exchanged it is called non-elastic. The third option is called reactive scatter and this leads to breaking of bonds and possibly the formation of new bonds. From kinetic theory, the collision rate Z_{AB} between two molecules A and B, assuming that they are hard spheres, is given by:

$$Z_{AB} = N_A N_B \sigma_{AB} \left[\frac{8k_B T}{\pi\mu}\right]^{1/2} \qquad \text{Eq. (2.10)}$$

where N_i are the number density of molecules, σ_{AB} (m^2) is the collision cross-section πr^2 (where r is the radius of the molecule, considering the spherical approximation), k_B is the Boltzmann constant (J K^{-1}), T is the temperature and μ is the reduced mass. The SI unit of Z is $cm^3\ s^{-1}$.

By adding the steric factor, P, which is the ratio between the frequency factor (the pre-exponential factor) and the collision frequency, the rate coefficient k ($cm^3\ s^{-1}$) is expressed by:

$$k(T) = P\ N_A N_B\ \sigma_{AB} \left[\frac{8k_B T}{\pi\mu}\right]^{1/2} \exp\left[-\frac{E_a}{RT}\right] \qquad \text{Eq.(2.11)}$$

The collision theory gives relatively accurate values for pre-exponential factors of reactions between monatomic species, but often fails for reactions between molecules with more complicated structures by several orders of magnitude. The reason for this is that the reacting molecules are able to react in all directions, because they have been considered to be spherical.

2.1.3 Capture models

For ion-neutral reactions, collision theory has evolved into capture models by considering the polarizability, the dipole moment, and the orientation of dipole moment of neutral reactant. Capture models assume that the reaction rate is governed by long-range interactions leading to the capture of the collision partners, while the short-range reaction probability is unity.

2.1.3.1 Langevin model

The Langevin model is the simplest theoretical approach to estimate the rate coefficient between an ion and polarizable neutral colliders.[2] This method has been used extensively to calculate the

collision rate coefficient in many environments, including the interstellar medium, where atomic hydrogen, molecular hydrogen, and atomic oxygen and nitrogen are the most abundant species.

We consider the collision of a point ion with a neutral (sphere) interacting via the charge-induced dipole potential. The total energy of the system in the center of mass frame of reference E_{rel} can be expressed as:

$$E_{rel} = \frac{P_r^2}{2\mu} + V_{eff}(r,L) \qquad \text{Eq. (2.12)}$$

where $\frac{P_r^2}{2\mu}$ is the translational energy, P_r is the radial momentum of the collision partners at separation r, μ is their reduced mass, and the effective potential, V_{eff}, is given by the following expression:

$$V_{eff}(r,L) = \frac{L^2}{2\mu r^2} - \frac{\alpha q^2}{2r^4} = \frac{\mu v^2}{2} \times \frac{b^2}{r^2} - \frac{\alpha q^2}{2r^4} \qquad \text{Eq. (2.13)}$$

where:

- L is the orbital angular momentum of the system (L= μ.v.b, MKS unit kg m^2 s^{-1})
- $\frac{L^2}{2\mu r^2}$ is the orbital rotational energy E_{rot}
- α is the polarizability of neutral molecule ($Å^3$)
- b is the impact parameter
- q is the ion charge.
- $\frac{\mu v^2}{2}$ is the relative impact (translational) energy E_r
- (- $\frac{\alpha q^2}{2r^4}$) is the classical electrostatic attractive potential.

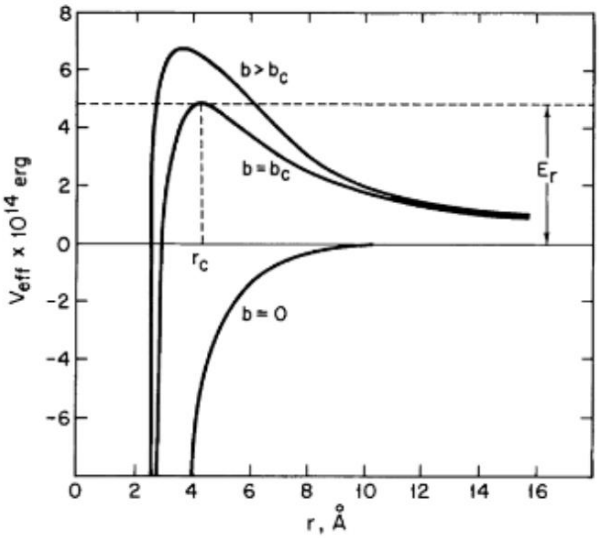

Figure 2.1: Variation of V_{eff} with the relative distance between the ion and neutral (r)[3]

The Langevin potential has a maximum along the reaction coordinate, it is equal to:

$$V_{max}= \frac{E_r^2 b^4}{2\alpha q^2} \qquad \text{Eq. (2.14)}$$

The critical impact parameter corresponding to this potential is:

$$b_{max}= \left(\frac{2\alpha q^2}{E_r}\right)^{1/4} \qquad \text{Eq. (2.15)}$$

When b = 0, the ion is attracted directly and reacts. When $b < b_{max}$ the capture collision probability is 1, and when When $b > b_{max}$ the capture collision probability is 0.

In this case, the cross-section is derived as:

$$\sigma_L = \pi b_{max}^2 = \pi \left(\frac{2\alpha q^2}{E_r}\right)^{1/2} \qquad \text{Eq. (2.16)}$$

By taking into consideration that molecules follow a Maxwell-Boltzmann velocity distribution, the Langevin rate coefficient which is independent of temperature is expressed by:

$$k_L= \sigma_L\, v= 2\pi q\, (\alpha/\mu)^{1/2} \qquad \text{Eq. (2.17)}$$

This model therefore gives a temperature independent rate coefficient, which is a lower limit in the case of dipole molecules. One of studied reactions in our work is the reaction between N_2^+ ion and allene CH_2CCH_2, which is a nonpolar molecule, the rate coefficient dependence with temperature of this reaction follows the Langevin model, and it will be described in detail in chapter 4.

2.1.3.2 Locked dipole model

The Locked dipole model was determined early by Moran and Hamil 1963,[4] it states that the contribution of ion dipole potential to the collision cross section cannot be ignored for target molecules with significant permanent dipole moment. It describes the interaction between an ion (charged point) and a neutral molecule (sphere) with a permanent dipole μ_D. In this model, the rotation is considered as frozen and the dipole orientation is locked toward the ion direction.

The effective potential V_{eff} between an ion and polarizable molecule having a dipole moment μ_D which is oriented in the position of minimum energy is:

$$V_{eff} = \frac{L^2}{2\mu r^2} - \frac{\alpha q^2}{2r^4} - \frac{q\mu_D}{r^2} \qquad \text{Eq. (2.18)}$$

If no alignment of the dipole with the incoming charge, the interaction averages to zero and Langevin theory is applied, If the molecule dipole "locks-in" as the ion approaches, then the ion-dipole interaction is taken into consideration.

The rate coefficient for thermal ions is expressed by:

$$k_{LD} = k_L + 2\pi q \frac{\mu_D \sqrt{2}}{\sqrt{\mu \pi k_B T}} \qquad \text{Eq. (2.19)}$$

Where k_B is Boltzmann's constant = 1.380610^{-16} erg.K^{-1} (cgs), and T is the temperature (K). In this model, the ion field doesn't completely quench the rotational angular momentum of the polar molecule, then the dipole effect (therefore the rate coefficient value) is overestimated in this model.

2.1.3.3 Average Dipole Orientation model ADO

Developed by Su and Bowers in 1973.[5] This theory is formulated in terms of an r-dependent average orientation angle $\overline{\theta}$ (r) between the dipole and the line of centers of collision. The ADO model predicts the dipole dependence in proton transfer, charge transfer, and momentum transfer collisions. The ADO model considers that no net angular momentum between the rotating molecule and the ion-molecule orbital motion (not conserved, oscillations) when the dipole moment of neutral μ_D is increasing, the locking of the dipole increases. The potential energy is expressed by:

$$V(r) = V_L - q\mu_D \cos(\overline{\theta}\,(r))/r^2 \qquad \text{Eq. (2.20)}$$

The average dipole orientation capture rate coefficient is given by:

$$k_{\text{ADO}} = k_L + \frac{2\pi q \mu_D C\sqrt{2}}{\sqrt{\mu \pi k_B T}} \qquad \text{Eq. (2.21)}$$

Where C is the effectiveness of locking the dipole or the locking dipole constant, it is given a value between 0 and 1, qualitatively considered as cos<θ> where <θ> is the average orientation angle of the dipole. In Eq. (2.21), one can say that when C=1, the expression is reduced to locked dipole limit, and when μ=0, the expression returns to Langevin model.

The locking dipole constant is in function of the polarizability and the dipole moment: C=(μ/$\sqrt{\alpha}$). In order to calculate the Average dipole orientation rate coefficient, it is necessary to know the value of (μ/$\sqrt{\alpha}$) for the polar molecule of interest, which then allows the determination of the value of the constant C, as shown in figure 2.2.

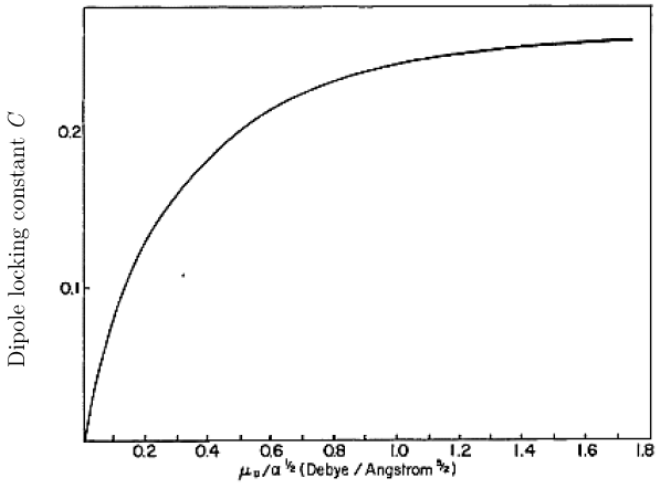

Figure 2.2: Locking dipole constant as a function of (μ/$\sqrt{\alpha}$). Adapted from Su et al. 1978. [6]

By comparing the experimental measurements of the rate coefficient with Langevin, ADO and LD models, we can see that, in some cases, the Langevin model underestimates the rate coefficient, the LD model overestimates it, and the ADO approximation predicts the rate coefficient with a reasonable accuracy.[7] This result is reasonable because the conservation of angular momentum results in smaller values of the effective potential and hence enhances the possibility for capture.

2.1.3.4 Su and Chesnavich model

Previous models (Langevin, LD, and ADO) are informative, they are unable to give information about the classical dynamics of the ion-dipole capture, and on the motion in non-central field.[8] For this reason, Su and Chesnavich developed a theory which is the combined variational state theory (also known as the classical trajectory study). [9] In this framework, the angular momentum

is conserved, the ion in considered as a point charge, and the neutral molecule is considered as two-dimensional rigid rotor. It couples rotational angular momentum of the dipole (J) to orbital angular momentum of the system (L): $\vec{L}$ and $\vec{J}$ are collinear.

The rate coefficient $k_{SC} = K_{cap} \times k_L$ is temperature dependent, where:

- $k_{cap} = 0.4767x + 0.6200$ when $x = \frac{\mu_D}{\sqrt{2\alpha T k_B}} \geq 2$,
- $k_{cap} = (x + 0.5090)^2/10.526 + 0.9754$ when $x < 2$.

One of studied reactions in our work is the reaction between N_2^+ ion and propyne (also known as methylacetylene CH_3CCH), which is a polar molecule ($\mu = 0.78\ Debye$),[10] we have observed that the rate coefficient increases when the temperature decreases, following the Su and Chesnavich model, that will be presented in details in chapter 4.

2.2 Experimental techniques

Over the last decades, a notable development of laboratory instruments has been realized in the studies of ion-neutral reactions at room and low temperatures. Laboratory experiments on elementary reaction processes seek to provide two types of information: the first is the measurement of the rate coefficient k, and the second is the determination of the nature of reaction products. If more than one set of products is energetically accessible, the experimental determination of the branching ratios is necessary. For cold gas-phase reactions, reactants are typically produced either through collisions with cryogenically cooled walls of a reaction cell, or by the expansion of gas from high to low pressure. In this section, we present a range of experimental techniques for application in reaction studies between ionic and neutral atoms/molecules.

2.2.1 Flowing Tubes

2.2.1.1 Flowing Afterglow

A major advance in the afterglow method came with the development of the Flowing Afterglow Langmuir Probe (FALP) apparatus by Smith and Adams.[11] The FALP apparatus is equipped with two main measurement tools, the Langmuir probe (LP) and the Quadrupole Mass Spectrometer (QMS), both movable along the axis of the main chamber.

The FALP apparatus present in Rennes is composed by three main zones: the ion source, the main chamber, and the detection chamber. It uses a helium buffer gas flow (15 slm) through a glass tube (4 cm in diameter), which is weakly ionized in the ion source by a microwave discharge operating at 2.45 GHz (power can be varied between 20 and 200 W). The flow is maintained by a roots blower (4000 m^3 h^{-1}), with a pressure ≈ 0.5 mbar in the reaction zone. A turbomolecular pump is employed to maintain a vacuum of ≈ 10^{-7} mbar in the detection chamber. Generated helium afterglow plasma is formed by ground state helium, electrons, He^+, He_2^+ and metastable helium atoms He^M. Latter species can be a source of ionization. In order to solve this problem, the stainless-steel tube (8 cm in diameter and 100 cm long) has an entry port used for the injection of argon gas Ar that play a role of a quencher to destroy the metastable helium atoms.

The movable mass spectrometer is used to identify ions present in the measurement region of the afterglow and to measure the ratios of the ion signals as a function of distance along the flow and of the electron number density, and so to determine the rate coefficient. A Langmuir probe is attached to the mass spectrometer entrance cone in order to obtain the electron density, simultaneously with the measurement of the relative ion populations.

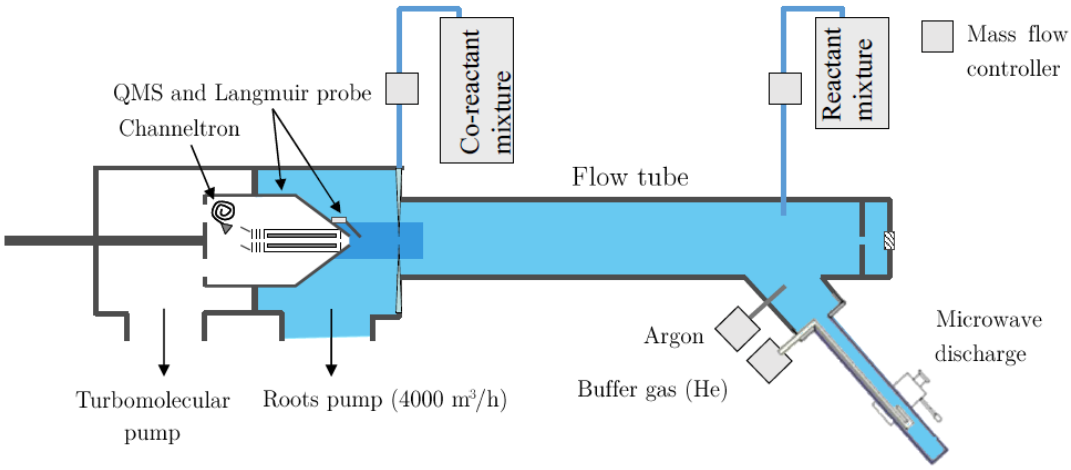

Figure 2.3: flowing afterglow apparatus at the University of Rennes.

An example of reaction studied recently by FALP apparatus, is the reaction between cyanide anion CN^- with cyanoacetylene (HC_3N) at room temperature performed by S.Carles et al. .[12] In that work, the CN^- anions were generated from dissociative electron attachment on a cyanogen bromide (BrCN) precursor. The rate coefficient for the $CN^- + HC_3N$ reaction is measured k= 4.8 (0.3) $\times 10^{-9}$ cm^3/s, this experimental value is in good agreement with the Su and Chesnavich coefficient (k_{SC}= 4.32×10^{-9} cm^3/s).

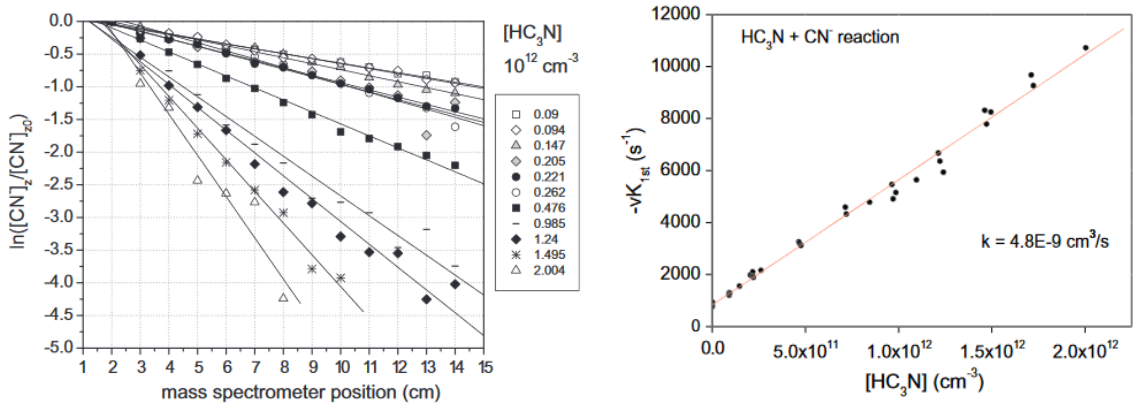

Figure 2.4: Left: examples of $\ln([CN]^-/[CN^-_0]$ according to the mass spectrometer position z and for different $[HC_3N]$ densities up to 2×10^{12} cm^{-3}. **Right**: Graph of $-vk_{first}$ as a function of $[HC_3N]$. The slope is k= 4.8×10^{-9} cm^3/s, considering the measured constant flow velocity of 1.7×10^4 cm/s. The data points are the results of many repetitive runs performed with different flow meters. [12]

The m= 26,50, 79, 81 u masses have been observed and respectively attributed to the CN^-, C_3N^- anions and the two natural bromine isotopes anions. The C_3N^- anion is generated from the proton transfer reaction. These observations confirm the possible pathway of C_3N^- formation from the CN^-/HC_3N reaction which was suggested and taken into account in the Titan's atmosphere model.

By cooling the flow tube and the carrier gas with liquid nitrogen, the FALP technique was updated into cryo-FALP, enabling one to study the ion chemistry at low temperatures down to 80 K.[13,14]

2.2.1.2 SIFT: Selected Ion Flow Tube

In order to study ion-neutral reactions with selection of a single ionic species, and therefore to reduce the side reactions which complicate the ion spectrum, FA technique was extended by N. G Admas and D. Smith in 1975 to the Selected Ion Flow Tube technique (SIFT).[15] Under this scheme, ions are created in the microwave discharge ion source (low- and high-pressure electron impact sources were also previously commonly used). A quadrupole mass filter can be used to pass ions of a given mass-to-charge ratio. These mass-selected ions are injected at energy about 20 eV (in the laboratory frame E_{lab}) via a small aperture into a flow tube, and after they are entrained by a fast-flowing carrier gas (pressure of typically 0.5 Torr). In the FALP and SIFT experiments, for molecular ions, the centre of mass interaction energy with the carrier gas, E_{cm}, should be less than the dissociation energy of the ion. In this regard, because of their small masses, helium or hydrogen are the favored carrier gases, since $E_{cm} = E_{lab} \times [Mc/ (M_i + M_c)]$ where M_c, and M_i are the masses of the carrier gas and the injected ion, respectively. The main

difference between FA and SIFT, is that in the SIFT the ions are created in a remote ion source and not in the carrier gas-reactant-gas mixture. This method was invented to measure kinetic rate coefficients and product branching ratios for the gas phase reactions at room temperature. To work at different temperatures (down to 80 K), the SIFT technique has been extended into a new version: The Variable Temperature Selected Ion Flow Tube (VT-SIFT).[16]

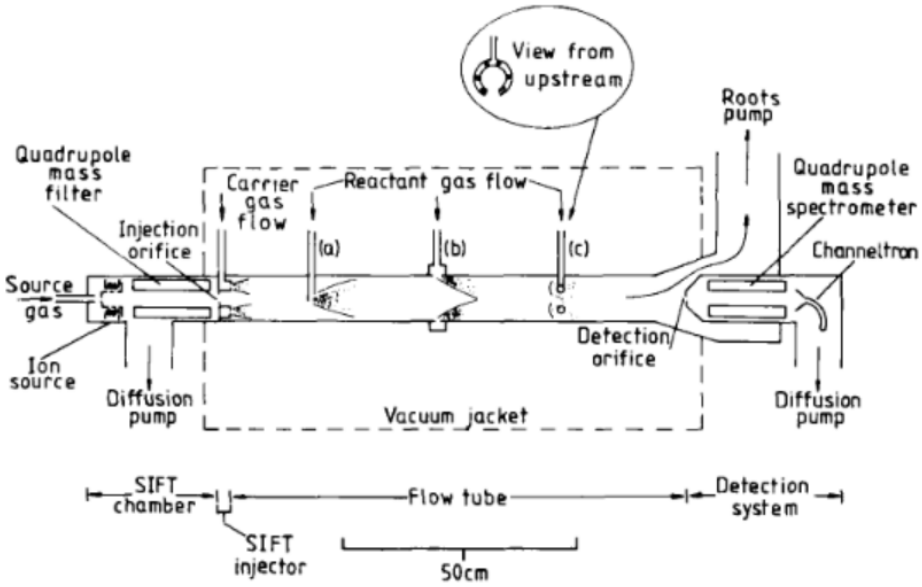

Figure 2.5: A schematic diagram of a typical SIFT apparatus illustrating its major features. From D. Smith and N. G. Adams [16]

The neutral reactant and the ions are injected in lower quantity than the buffer gas. A thermodynamical equilibrium is ensured due to the collisions with the walls of the reactor, which is cryogenically cooled with liquid nitrogen through two loops going in opposite directions along the flow tube. But this technique is limited by the condensation on the wall, and then an increase of the density's uncertainty.

For example, Illia Zymak et al. 2021[17] studied the reactivity of O^- ions with CO_2 molecules with different ternary gases (He and N_2) over the 230–340 K temperature range. This termolecular reaction is considered to be the main production channel of CO_3^- anions in martian atmosphere. The ternary rate coefficient of the reaction was measured equal to $(1.24 \pm 0.06) \times 10^{-28}$ $(300/T)^{2.86\pm0.28}$ and $(2.29 \pm 0.05) \times 10^{-28}$ $(300/T)^{2.06\pm0.13}$ cm^6 s^{-1} for He and N_2 carrier gas, respectively. The results of this VT-SIFT study are in a good agreement with previous measurements obtained using helium carrier gas in flowing afterglow instruments and those obtained using oxygen carrier gas. These experiments have some interest in the study on the effect of the nature of the carrier gas on the rate coefficient for termolecular reactions.

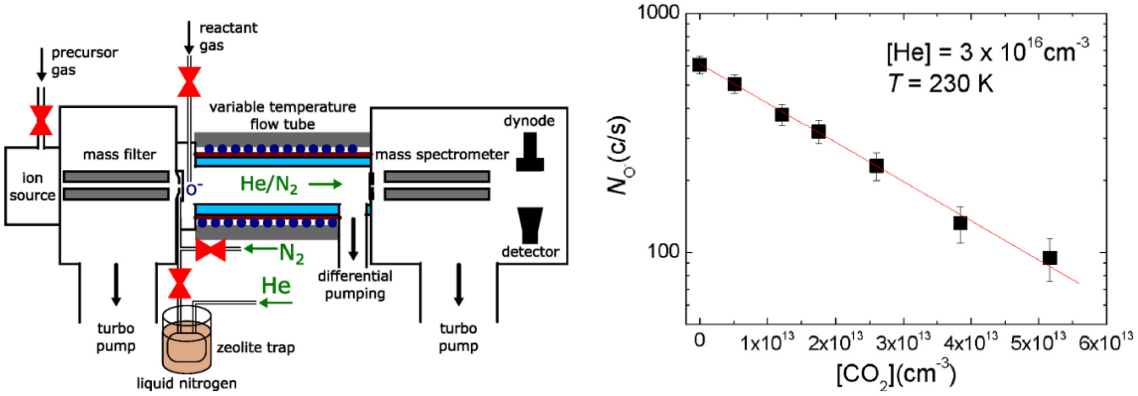

Figure 2.6: Left: Schematic view of the VT-SIFT instrument. **Right**: The count rate of O^- ions (black squares, counts-per-second, c/s) measured at different concentrations of the CO_2 reactant gas and for a constant flow of the helium carrier gas in the flow tube cooled down to 230 K. The exponential decay fit (the mean square roots method) is shown by the red line. Each point represents a value averaged over 20 measurements of c/s, standard measurement deviations is given with error bars. From Zymak et al. 2021. [17]

By addition of a static but variable E-field along the axis of the flow tube reactor in which the ion−molecule reaction takes place, Spesyvyi et al. (2015)[18] updated the SIFT technique into SIFDT (Selected Ion Flow Drift Tube). Its general structure is similar to the familiar SIFT-MS instruments. A voltage between the ends of the flow-drift tube is applied in order to establish a uniform electric field, E, along its axis. The variation of E and the carrier gas number density, n, allows the reduced field strength E/n to be varied at will. This technique allows one to change the kinetic and the internal energies of the reagent ions and also their residence times in the flow-drift tube. In addition to study the kinetics and the products distribution of the ion-neutral reactions, this technique can be employed to investigate the ion mobility, the determination of the collisional cross section, the collisional dissociation.[18,19] …

The optimal working parameters for SIFDT-MS are summarized in Table 2.1 and compared with the corresponding parameters used in SIFT-MS technique. This reveals the enhanced and attractive features of the SIFDT analytical method.

Feature	SIFDT-MS	SIFT-MS
E/N	7 – 14 Td	0
flow/drift tube pressure	2 mbar	1.3 mbar
He flow rate	< 100 mL/min	500 mL/min
sample flow rate	< 4 mL/min	20-30 mL/min
pumping speed	< 1 L/s	7 L/s
reaction time	variable (accurately measured)	fixed
regent ion count rate	up to 1000000 c/s	up to 1000000 c/s
limit od detection	< 1 ppbv	< 1 ppbv
reaction time	variable (accurately measured)	fixed
ion hydration	variable by *E/N* for a given sample flow rate	constant for a given sample flow rate

Table 2.1: Comparison of the optimal operating parameters for the SIFDT-MS instrument and the SIFT-MS instrument. From Anatolii Spesyvyi et al. [18]

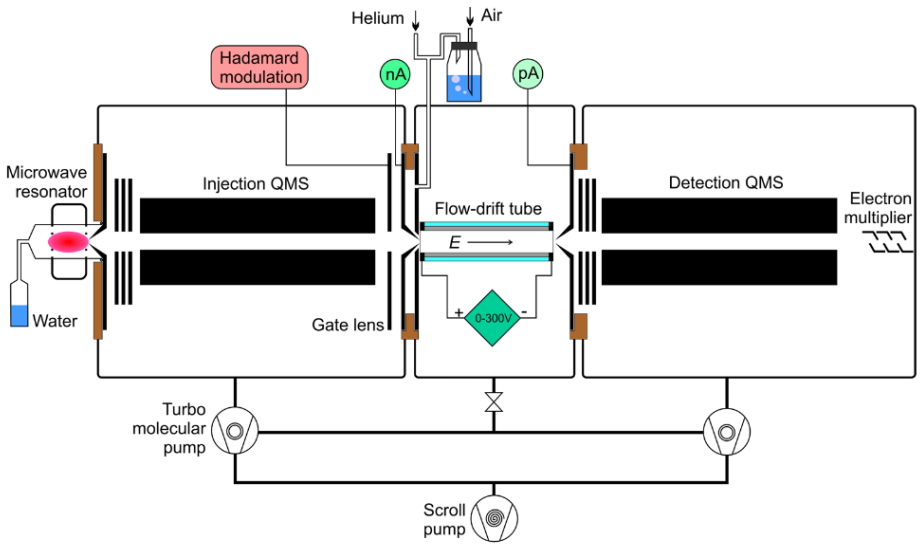

Figure 2.7: Schematic drawing of the selected ion flow-drift tube, SIFDT, apparatus. From A. Spesyvyi et al. [18]

The SIFDT tube is extended by the use of different forms of collision-induced dissociation, CID. The in-tube CID was implemented by applying electrostatic potential difference between the resistive glass flow-drift tube downstream end and the nose cone of a quadrupole mass spectrometer. This method allows, basing on the structural differences and corresponding changes in fragmentation patterns with CID energy, a real-time identification of isomeric products of ion-molecule reactions.[20]

2.2.2 Guided ion beam GIB

The guided ion beam mass spectrometer (GIB-MS) is a versatile technique that allows one to study the ion-neutral reactions over a wide energy range with high sensitivity, and also determination of the integral cross sections with high accuracy.[21] This technique employs two octupole ion guides (O1, O2) and two quadrupoles (Q1, Q2), connected in the O1, Q1, O2, Q2 sequences. (Figure 2.8) A powerful approach for dealing with low-energy ion beams is based on the use of radio-frequency octopole guides, that confine ions in the transverse direction.

The first octupole is used for cooling the ions produced by electron impact, in which their excitation energy is eliminated by collisions with an inert gas (such as helium or argon). These ions are introduced in the first quadrupole to select the mass of the primary ion. Therefore, the mass-selected ions are transferred into the second octupole ion guide located in a chamber which the neutral reactant is introduced. The beam enters a second quadrupole where the ionic products with low kinetic energy (down to 0.04 eV) are collected, mass analyzed and deflected to reach the deflector.

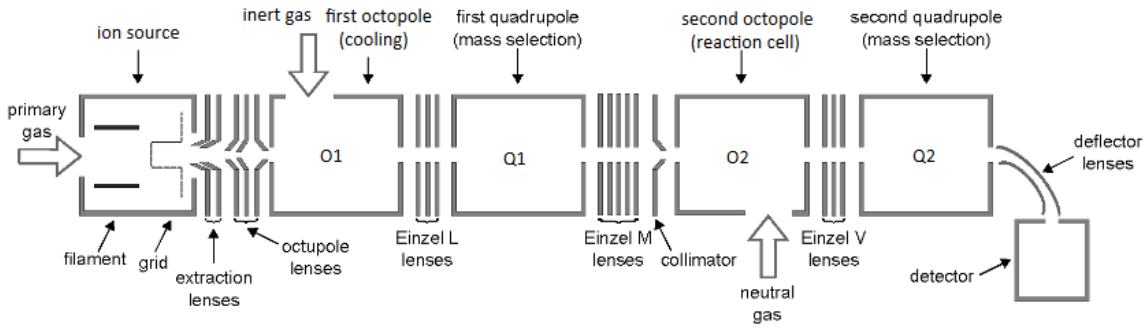

Figure 2.8: schematic representation of guided ion beam mass spectrometer. [22]

An example on the application of GIB-MS technique is the study made by Pantea Fathi et al. in which they studied the reactivity of CH_2CN^+ ion with saturated and unsaturated hydrocarbons i.e acetylene, methane, ethane, and ethylene at different collision energies. These reactions are important in the investigation of molecular growth mechanisms leading to large carbon and nitrogen-bearing species in Titan's ionosphere.[22]

2.2.3 Ion trapping method

Another technique to study ion-neutral reactions at low temperatures (down to 10 K) is the ion trapping method developed by Gerlich D.[23] This cryogenic approach is constituted of 22 pole electrodes on which nonhomogeneous radiofrequency are applied in order to produce an attractive potential to trap the ions.

Ions are generated by electron impact (for example), and after, they are selected by mass by a quadrupole mass filter and are then injected in the trap's interior. The collisions with the trap's cryogenic surface leads to the cooling of reaction zone (employing e.g liquid nitrogen as a cryogenic coolant). The trapping time vary between milliseconds and few minutes. The density of neutral reactant can be varied between 10^9 molecules/cm^3 and 10^{14} molecules/cm^3. By choosing an appropriate combination between these two parameters (the trapping time and the density), this method can be used to measure the rate coefficient of fast and slow bimolecular reactions.

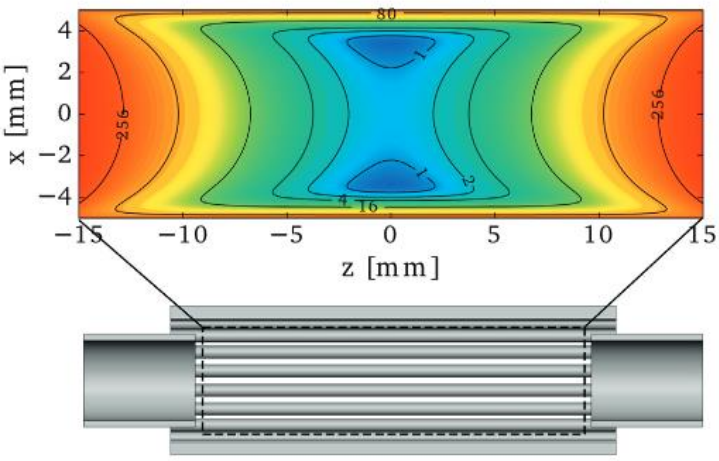

Figure 2.9: Lower part: Cross section of a CAD-model of a 22-pole trap including cylindrical end electrodes. Upper part: Effective potential in the x-z-plane. Equipotential values are given in meV[24]

As an example, Sunil S. Kumar rt al. 2018[25] used the cryogenic ion trapping technique to make the kinetic study for the reactions between OH^+ and H_2O^+ ions with H_2 at low temperatures (21 to 155 K). These reactions contribute in the cycle of formation of water molecules in the diffuse interstellar medium (ISM). Their low-temperature measurements show that both OH^+ and H_2O^+ ions react very fast with molecular hydrogen, with rate coefficients almost approaching the classical Langevin collision limit, $k_L \sim 1.5 \times 10^{-9}$ cm^3 s^{-1}.

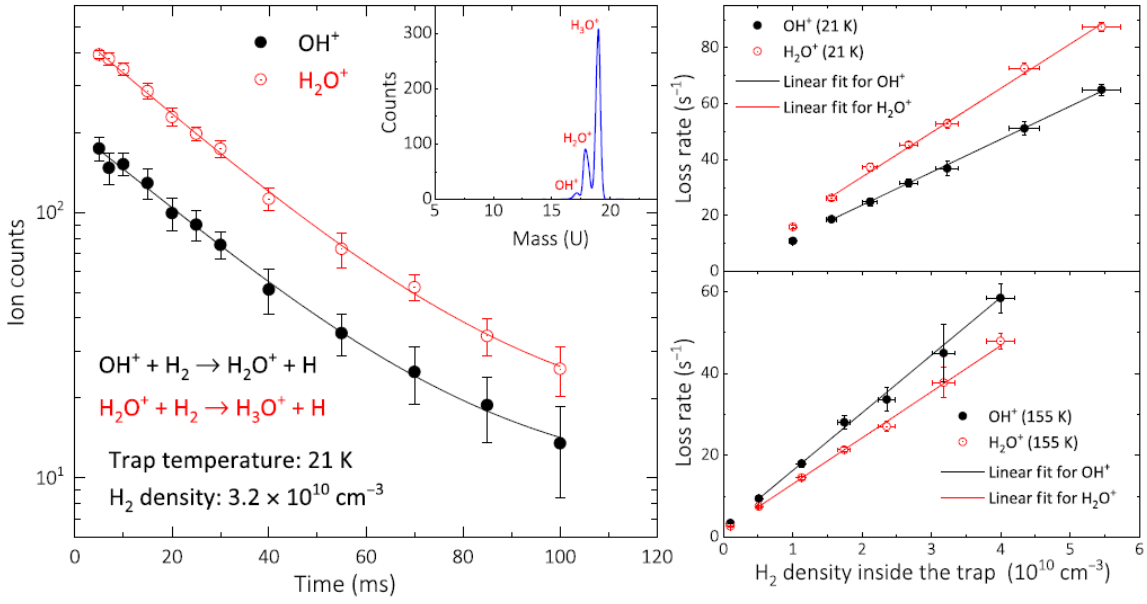

Figure 2.10: Exemplary ion counts of OH^+ and H_2O^+ as a function of storage time and loss rates versus H_2 density. (Left) Decay curves of OH^+ and H_2O^+ as observed in the 22-pole trap at 21 K with a H_2 number density of 3.2 × 10^{10} cm^{-3}. The inset shows a spectrum of a typical initial mass distribution produced by the ion source. (Right) Loss rates for OH^+ and H_2O^+ as a function of H_2 density at two different temperatures. The data points at the lowest

densities resulted from the residual H_2 in the trap, which varied with trap conditions and temperature. Those points, while fully consistent with the trend, were not included in the fit. From Sunil S. Kumar et al. 2018. [25]

Flowing Afterglow and ion trapping techniques use cryogenic cooling to obtain low temperatures, and therefore difficulties caused by condensation are encountered at the lowest temperatures (below~200 K) when using reactant gases other than H_2 or He[26], that makes the absolute reactant concentration difficult to determine.

Long time trapping technique leads to high sensitivity and long interaction times, allows one to determine very small rate coefficients at low temperatures, eg. for radiative association reactions. For example, the radiative association reaction between CH_3^+ and H_2 has been studied at 13 K by S. E. Barlow et al. 1984 using the ion trapping technique, where the rate coefficient is equal to $(1.8 \pm 0.3)\times10^{-13}$ cm^3 s^{-1}.[27]

2.2.4 Free jet

The free jet flow reactor is a technique used for the determination of ion/molecule reaction dynamics at unusually low temperatures. The free jet developed by Mark Smith was formed by a supersonic expansion of a gas mixture into a vacuum chamber, employing a pulsed nozzle. Using this technique, a very cold gas is produced: down to 1 K.[28] A free jet is a nonequilibrium medium. The density and temperature both drop with increasing distance from the nozzle (strong temperature and density gradient), this means that the determination of the exact temperature associated to the measurement of the rate coefficient is difficult.[26]

An example of an ion-neutral gas phase reaction using free jet technique, is the study made by L. K. Randeniya and M. A. Smith (1991). They measured the bimolecular rate coefficients for the reactions of N_2^+ ions with CH_4, O_2, and n-H_2 at temperatures below 15 K. N_2^+ ions were generated by Resonance-enhanced multiphoton ionization (REMPI). Reaction with CH_4 shows only a weak temperature dependence, the rate coefficient approaches to the Langevin capture rate at low energies. The rate coefficient for reaction O_2 increases rapidly when the temperature is decreased from 300 K and approaches a limiting value at low energies. The energy dependence of reaction with n-H_2 shows a minimum which resembles the reactions of NH_3^+ and $C_2H_2^+$ with H_2. [29]

2.2.5 Crossed Molecular beams

The crossed molecular beam (CMB) technique was demonstrated in 1953 by Taylor and Datz of Oak Ridge National Laboratory. Dudley Herschbach and Yuan T. Lee developed this technique, for which they were awarded the Nobel Prize in Chemistry in 1986. They refined the apparatus

and began probing gas-phase reactions in unprecedented detail. This method is particularly efficient in the case of reactions where product ions are distributed over a limited number of well-spaced energy levels. By inserting a skimmer into the supersonic zone of the free jet expansion, a molecular beam with a defined velocity is generated. The interaction between two molecular beams corresponds to the molecular crossed beams method. This technique enables one to study the gas phase reactions at different collision energies that can be accessed by varying the angle of collision.

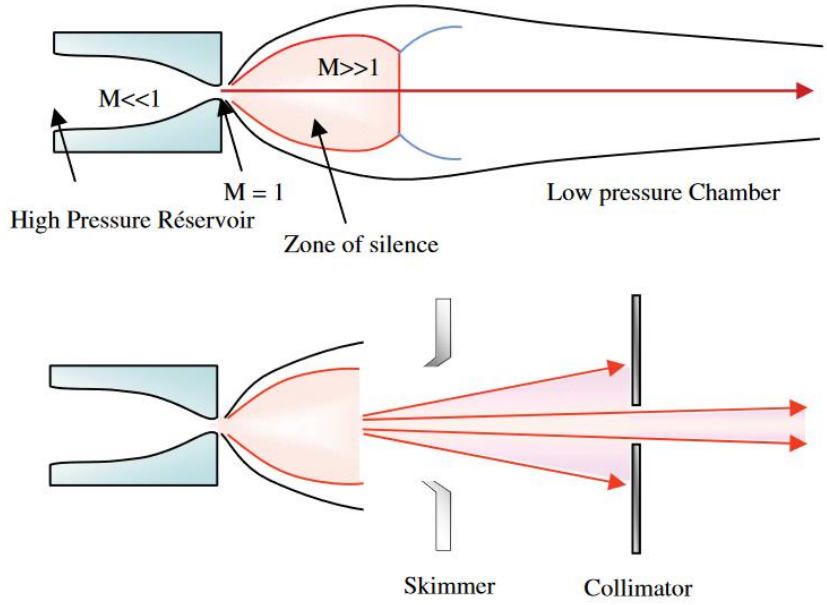

Figure 2.11 : Schematic views of free jet and molecular beam supersonic expansions. [30]

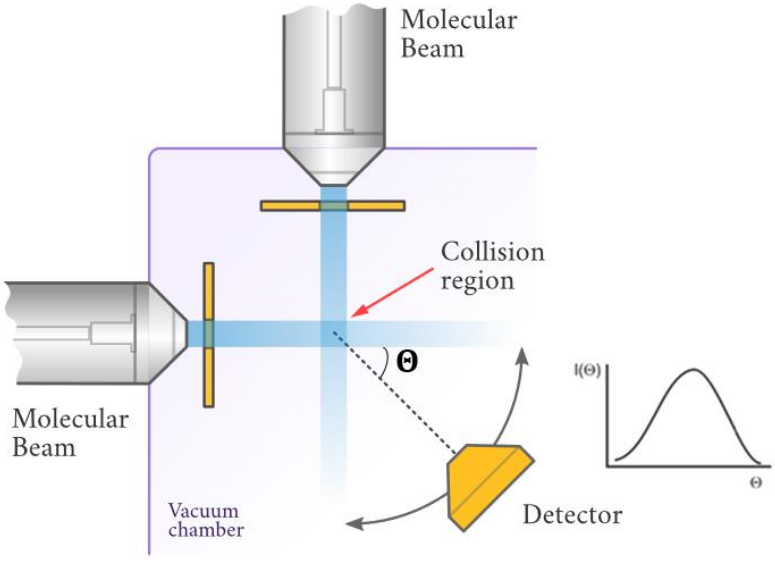

Figure 2.12: Schematic views of the crossed molecular beams technique. Adapted from chemistry LibreTexts site.[31]

For example, Friedrich et al. 1984, used the CMB technique to study the charge transfer reaction between N_2^+ ($X^2\Sigma_g$, v=0) ions with N_2 ($X^1\Sigma_g$, v=0) at room temperature, at two different collision energies (0.74 and 9.94 eV). They have demonstrated the existence of two distinct mechanisms for charge transfer in N_2^+/N_2 collisions at low energy. One of these is a long-range direct mechanism, while the second proceeds via a complex surviving several rotational periods, with extensive energy transfer. At higher energy, the direct mechanism is dominant, with little energy exchange.[32]

Despite that the crossed molecular beam technique enables experimentalists to determine the absolute integral cross-sections and the collision dynamics over appreciable interaction energies, especially at energies of astrophysical interest, it fails to find the rate coefficient in thermal equilibrium conditions. CMB technique encounters limitation at ions energies below a few eV.

2.2.6 CRESU technique

The CRESU technique is an efficient approach to study ion-neutral reactions at low temperatures. The CRESU technique and our experimental setup coupling a mass selective ion source to a CRESU chamber will be presented in details in chapter 3.

2.3 Conclusion

In this chapter, we have presented some capture models used to estimate the rate coefficient of chemical reactions and introduced the experimental techniques employed in the investigation of ion-neutral gas phase reactions at room and low temperatures. Experimental measurements of the rate coefficient and the branching ratios supported by theoretical calculations (ranging from empirical approaches to quantum-chemical calculations) are crucial to understand the chemistry and physics in the astrophysical environments. Experimental kinetic measurements are in particular used in the construction of photochemical models of astrophysical environments. The purpose of the theses models is to reproduce the abundance for the various observed chemical species in a wide range of environments ranging from dense molecular clouds,[33] diffuse interstellar medium to planetary settings such as Titan's atmosphere.[34]

References:

(1) Laidler, K. J. The Development of the Arrhenius Equation. J. Chem. Educ. **1984**, 61 (6), 494. https://doi.org/10.1021/ed061p494.

(2) Eichelberger, B. R.; Snow, T. P.; Bierbaum, V. M. Collision Rate Constants for Polarizable Ions. J Am Soc Mass Spectrom **2003**, 14 (5), 501–505. https://doi.org/10.1016/S1044-0305(03)00134-X.

(3) Langevin, M. Une Formule Fondamentale de Théorie Cinétique; 1905; Vol. 5, pp 245–288.

(4) Moran, T. F.; Hamill, W. H. Cross Sections of Ion—Permanent-Dipole Reactions by Mass Spectrometry. The Journal of Chemical Physics **1963**, 39 (6), 1413–1422. https://doi.org/10.1063/1.1734457.

(5) Su, T. Theory of Ion-Polar Molecule Collisions. Comparison with Experimental Charge Transfer Reactions of Rare Gas Ions to Geometric Isomers of Difluorobenzene and Dichloroethylene. J. Chem. Phys. **1973**, 58 (7), 3027. https://doi.org/10.1063/1.1679615.

(6) Su, T.; Su, E. C. F.; Bowers, M. T. Ion–Polar Molecule Collisions. Conservation of Angular Momentum in the Average Dipole Orientation Theory. The AADO Theory. The Journal of Chemical Physics **1978**, 69 (5), 2243–2250. https://doi.org/10.1063/1.436783.

(7) Mackay, G.; Betowski, L.; Payzant, J.; Schiff, H.; Bohme, D. Rate Constants at 297 0 K for Proton-Transfer Reactions with HCN and CH 3 CN. Comparisons with Classical Theories and Exothermicity. Journal of Physical Chemistry **1976**, 80 (26), 2919–2922.

(8) Chesnavich, W. J.; Su, T.; Bowers, M. T. Collisions in a Noncentral Field: A Variational and Trajectory Investigation of Ion–Dipole Capture. The Journal of Chemical Physics **1980**, 72 (4), 2641–2655. https://doi.org/10.1063/1.439409.

(9) Su, T.; Chesnavich, W. J. Parametrization of the Ion–Polar Molecule Collision Rate Constant by Trajectory Calculations. The Journal of Chemical Physics **1982**, 76 (10), 5183–5185. https://doi.org/10.1063/1.442828.

(10) Rankin, D. W. H. CRC Handbook of Chemistry and Physics, 89th Edition, Edited by David R. Lide. null **2009**, 15 (3), 223–224. https://doi.org/10.1080/08893110902764125.

(11) Smith, D.; Adams, N. G.; Alge, E. Isotope Exchange and Collisional Association in the Reactions of CH3+ and Its Deuterated Analogs with H2, HD, and D2. The Journal of Chemical Physics **1982**, 77 (3), 1261–1268. https://doi.org/10.1063/1.444002.

(12) Carles, S.; Adjali, F.; Monnerie, C.; Guillemin, J.-C.; Le Garrec, J.-L. Kinetic Studies at Room Temperature of the Cyanide Anion CN− with Cyanoacetylene (HC3N) Reaction. Icarus **2011**, 211 (1), 901–905. https://doi.org/10.1016/j.icarus.2010.08.019.

(13) Kotrík, T.; Dohnal, P.; Roučka, Š.; Jusko, P.; Plašil, R.; Glosík, J.; Johnsen, R. Collisional-Radiative Recombination Ar^{+} $+$ e $+$ e: Experimental Study at 77--180 K. Phys. Rev. A **2011**, 83 (3), 032720. https://doi.org/10.1103/PhysRevA.83.032720.

(14) Adams, N. G.; Smith, D.; Alge, E. Measurements of Dissociative Recombination Coefficients of H^+_3, HCO^+, N_2H^+, and CH^+_5 at 95 and 300 K Using the FALP Apparatus. The Journal of Chemical Physics **1984**, 81 (4), 1778–1784. https://doi.org/10.1063/1.447849.

(15) Adams, N. G.; Smith, D. The Selected Ion Flow Tube (SIFT); A Technique for Studying Ion-Neutral Reactions. International Journal of Mass Spectrometry and Ion Physics **1976**, 21 (3), 349–359. https://doi.org/10.1016/0020-7381(76)80133-7.

(16) Smith, D.; Adams, N. G. The Selected Ion Flow Tube (Sift): Studies of Ion-Neutral Reactions. In Advances in Atomic and Molecular Physics; Elsevier, 1988; Vol. 24, pp 1–49. https://doi.org/10.1016/S0065-2199(08)60229-8.

(17) Zymak, I.; Žabka, J.; Polášek, M.; Tran, T. D.; Španěl, P.; Smith, D. Experimental Study of the Reaction of O− Ions with CO2 Molecules with Different Ternary Gases at Temperatures Relevant to the Martian Ionosphere. Icarus **2021**, 354, 114057. https://doi.org/10.1016/j.icarus.2020.114057.

(18) Spesyvyi, A.; Smith, D.; Španěl, P. Selected Ion Flow-Drift Tube Mass Spectrometry: Quantification of Volatile Compounds in Air and Breath. Anal. Chem. **2015**, 87 (24), 12151–12160. https://doi.org/10.1021/acs.analchem.5b02994.

(19) Zakouril, P.; Glosik, J.; Skalsky, V.; Lindinger, W. Selected Ion Flow Drift Tube Studies of the Reactions of S+(4S) with CH4, C2H2, C2H4, and C3H8. J. Phys. Chem. **1995**, 99 (43), 15890–15898. https://doi.org/10.1021/j100043a030.

(20) Spesyvyi, A.; Spanel, P. Flow Drift Tube Study of Gas Phase Formation of Hydrated Hydronium. WDS'15 Proceedings of Contributed Papers **2015**.

(21) Cernuto, A.; Lopes, A.; Romanzin, C.; Cunha de Miranda, B.; Ascenzi, D.; Tosi, P.; Tonachini, G.; Maranzana, A.; Polášek, M.; Žabka, J.; Alcaraz, C. Effects of Collision Energy and Vibrational Excitation of CH3+ Cations on Its Reactivity with Hydrocarbons: But-2-Yne CH3CCCH3 as Reagent Partner. The Journal of Chemical Physics **2017**, 147 (15), 154302. https://doi.org/10.1063/1.4990514.

(22) Fathi, P. Synthesis of Complex Organics via Molecular Growth Mechanisms: Combined Experimental and Theoretical Studies on Ion-Neutral Reactions of C2H2N+ with Ubiquitous Hydrocarbons in Titan's Ionosphere. **2019**.

(23) Gerlich, D. State-Selected and State-to-State Ion-Molecule Reaction Dynamics. Part 1. Experiment. Advances in chemical physics series **1992**, 82, 1–176.

(24) Fanghänel, S.; Asvany, O.; Schlemmer, S. Optimization of RF Multipole Ion Trap Geometries. Journal of Molecular Spectroscopy **2017**, 332, 124–133. https://doi.org/10.1016/j.jms.2016.12.003.

(25) Kumar, S. S.; Grussie, F.; Suleimanov, Y. V.; Guo, H.; Kreckel, H. Low Temperature Rates for Key Steps of Interstellar Gas-Phase Water Formation. Sci. Adv. **2018**, 4 (6), eaar3417. https://doi.org/10.1126/sciadv.aar3417.

(26) Hawley, M.; Mazely, T. L.; Randeniya, L. K.; Smith, R. S.; Zeng, X. K.; Smith, M. A. A Free Jet Flow Reactor for Ion/Molecule Reaction Studies at Very Low Energies. International Journal of Mass Spectrometry and Ion Processes **1990**, 97 (1), 55–86. https://doi.org/10.1016/0168-1176(90)85040-9.

(27) Barlow, S. E.; Dunn, G. H.; Schauer, M. Radiative Association of C H 3 + and H 2 at 13 K. Phys. Rev. Lett. **1984**, 52 (11), 902–905. https://doi.org/10.1103/PhysRevLett.52.902.

(28) Hawley, M.; Smith, M. A. Charge-Transfer Chemistry of Ar+(2P,,2) and Kr+('P,,,) at Very Low Collision Energies. J. Phys. Chem. **1992**, 96 (6693–6697).

(29) Randeniya, L. K.; Smith, M. A. Gas Phase Reaction Rates of N^+_2 with CH_4, O_2, and n-H_2 at Very Low Temperatures. The Journal of Chemical Physics **1991**, 94 (1), 351–356. https://doi.org/10.1063/1.460349.

(30) Canosa, A. Gas Phase Reactive Collisions, Experimental Approach. EPJ Web of Conferences **2011**, 18, 02003. https://doi.org/10.1051/epjconf/20111802003.

(31) Reactive Collisions Can be Studied Using Crossed Molecular Beam Machin es https://chem.libretexts.org/@go/page/14567.

(32) Friedrich, B.; Howard, S. L.; Rockwood, A. L.; Trafton, W. E.; Wen-Hu, D.; Futrell, J. H. A Crossed Molecular Beam Study of the Reaction Dynamics of the Charge Transfer Reaction of N2+(X2Σg+, N= 0) with N2(X1Σg, N= 0) at Low and Intermediate Energies. International Journal of Mass Spectrometry and Ion Processes **1984**, 59 (2), 203–218. https://doi.org/10.1016/0168-1176(84)85095-8.

(33) Loison, J.-C.; Wakelam, V.; Gratier, P.; Hickson, K. M.; Bacmann, A.; Agùndez, M.; Marcelino, N.; Cernicharo, J.; Guzman, V.; Gerin, M.; Goicoechea, J. R.; Roueff, E.; Petit, F. L.; Pety, J.; Fuente, A.; Riviere-Marichalar, P. Oxygen Fractionation in Dense

Molecular Clouds. Monthly Notices of the Royal Astronomical Society **2019**, 485 (4), 5777–5789. https://doi.org/10.1093/mnras/stz560.

(34) Vuitton, V.; Yelle, R. V.; Klippenstein, S. J.; Hörst, S. M.; Lavvas, P. Simulating the Density of Organic Species in the Atmosphere of Titan with a Coupled Ion-Neutral Photochemical Model. Icarus **2019**, 324, 120–197. https://doi.org/10.1016/j.icarus.2018.06.013.

Chapter 3:

Experimental methodology: the CRESU-SIS machine

The CRESU technique (French acronym for “Cinétique de Réaction en Ecoulement Supersonique Uniforme” or “Reaction Kinetics in a Uniform Supersonic Flow”) developed in the 80’s by B. Rowe and J.-B. Marquette,[1] belongs to the family of flow reactors. The CRESU technique can generate cold (down to 6 K^2) uniform supersonic flows using a type of rocket engine nozzle, the Laval nozzle, giving the advantage of a wall-less flow reactor where no condensation occurs in the scrutinized medium. This method opened new horizons in the field of laboratory astrochemistry and chemical physics.

The CRESU-SIS device developed in Rennes (Figure 3.5) allows measuring the absolute rate coefficient and the branching ratios of targeted gas-phase ion-molecule reactions at various low temperatures.

3.1 The CRESU technique

The CRESU technique is based on the production of a uniform supersonic expansion of a buffer gas into a low-pressure (0.1 – 2 mbar) chamber through a Laval nozzle. The nozzle is designed by solving the nonlinear Navier–Stokes equations for viscous fluids. The optimally shaped convergent-divergent nozzle produces a flow at the exit which is at a constant Mach number (~ 5), the consequence being that the density, pressure, and the temperature at all points within the subsequent postnozzle flow are constant for tens of centimeters, which means a time scale of hundreds of microseconds. Some nozzles could generate uniform supersonic expansions with different temperature and pressure conditions, using binary mixtures or various buffer gases. The

experimental characterization of the uniformity length of supersonic flows is fundamental before application to chemical kinetics studies.

In order to achieve uniform flow conditions, the buffer gas flow rate can reach 100 slm (standard liter per minute) thus requiring substantial pumping capacity (up to 60 000 m^3 h^{-1}). The density of the flow is in order of 10^{15} to 10^{17} molecules cm^{-3}: the high density, i.e. the high number of collisions, ensures a local thermodynamical equilibrium (LTE) and rapid rotational relaxation of the molecular species (charged or neutral). These conditions allow us to measure the absolute rate coefficient and the branching ratios of molecular and atomic ions (cations and anions) with neutral reactants under the cold conditions found in astrophysical environments. The density of the flow is higher than the density in interstellar medium and planetary atmospheres, but this does not affect the kinetic study and branching ratios measurements in the case of bimolecular reactions. The neutral reactant is continuously injected in the supersonic flow with a controlled flow rate of a few sccm (standard cubic centimeters per minute) corresponding to a density of about 10^{12} molecule cm^{-3}.

Two dimensionless numbers are important for the characterization of the uniform supersonic flow: the Reynolds number, Re, and the Knudsen number K_n. The Reynolds number R_e characterizes the nature of the flow regime (laminar, transient, turbulent). It represents the relation between inertial forces and viscous forces. Viscous forces here are the actions of nozzle wall on the flow, and inertial forces are acquired by pressure differences of the fluid, converted into kinetic energy. Viscous forces are the origin of the appearance of the zone that surrounds the isentropic core of the flow, known as the boundary layers δ (see figure 3.1). The R_e number is defined by:

$$\mathrm{Re} = \frac{\rho u D}{\eta} \qquad \text{Eq. (3. 1)}$$

Where u is the velocity of the flow, D the characteristic length corresponding to the diameter of the exit of the nozzle, ρ is the density of the flow and η the dynamic viscosity.

The thickness of the boundary layer δ is directly related to Re by the following equation:

$$\frac{\delta}{D} = \frac{1}{\sqrt{\mathrm{Re}}} \qquad \text{Eq. (3. 2)}$$

The Reynolds number Re is a good indicator of the flow quality. If the Reynolds number is sufficiently high, the dissipating phenomena are negligible, and the boundary layer δ is smaller.

The Kundsen number is used to determine the flow regime in terms of flow continuity (continuous, rarefied). It is defined as:

$$K_n = \frac{\lambda}{L} \qquad \text{Eq. (3. 3)}$$

Where λ represents the mean free path of particles in the flow (μm). Otherwise, the Knudsen number can be expressed as a function of the Mach number, M, the Reynolds number Re, and of the adiabatic index of the γ gas by the von Kármán relation:

$$K_n = \frac{M}{Re}\sqrt{\frac{\gamma\pi}{2}} \qquad \text{Eq. (3. 4)}$$

Where M is the Mach number, (M=u/a; a is the speed of sound in the surrounding medium), γ is the ratio of the specific heat capacities (J mol^{-1} g^{-1}) at constant pressure and volume ($\gamma = C_p/C_v$).

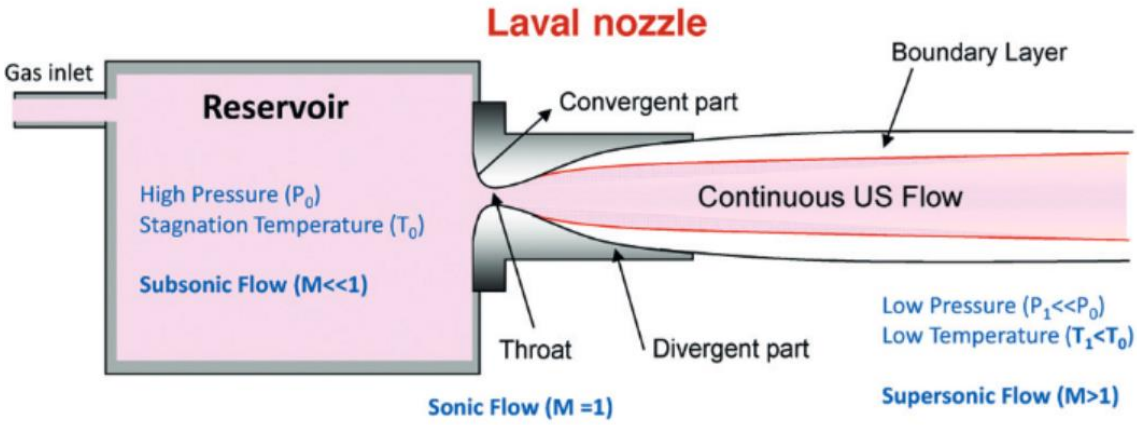

Figure 3.1: Main characteristics of the CRESU expansion.[3]

The flow pattern of a supersonic flow depends on the profile of the Lava1 nozzle (i.e. converging-diverging) which generates it. The flow temperature, T, and flow pressure, P, and the density, ρ, are expressed by the isentropic relationship:

$$\frac{T_0}{T} = 1 + M^2\frac{(\gamma-1)}{2} \qquad \text{Eq. (3. 5)}$$

$$\frac{P_0}{P} = (T_0/T)^{(\gamma/\gamma-1)} \qquad \text{Eq. (3. 6)}$$

$$\frac{\rho_0}{\rho} = (T_0/T)^{(1/\gamma-1)} \qquad \text{Eq. (3. 7)}$$

In equations 3.5-3.7, T_0, P_0, and ρ_0 are the temperature, pressure, and density in the stagnation region (reservoir), respectively, and T, p, and ρ are the temperature, pressure, and density in the gas beam, respectively.

The gas expansion through the de Laval nozzle converts the internal energy of the gas species into kinetic energy. For a compressible perfect gas with a constant specific heat capacity C_p and with a well-defined temperature, the energy conversion is driven by the following very simple equation:

$$C_pT+ u^2/2=C_pT_0 \qquad \text{Eq. (3. 8)}$$

where T_0 and T are the temperatures of the gas prior and after expansion respectively and u is the supersonic flow velocity.

By neglecting the effects related to the viscosity and by supposing that the expansion is adiabatic, the conservation of the mass across a section A is expressed by the Hugoniot relation[4]:

$$\frac{du}{u}(M^2-1) = \frac{dA}{A} \qquad \text{Eq. (3. 9)}$$

The characterization of the uniform supersonic flow in terms of pressure, temperature and density is performed using a Pitot Tube moving along the gas expansion. The Pitot tube is a 10 cm of 1/8 inch stainless steel tube mounted on a support capable of moving 7 cm in the y-axis, and 60 cm in x-axis. It provokes a perturbation and creates a shock-wave detached from this obstacle. From the pressure measured behind the shock wave, one can retrieve the Mach number of the flow and the flow pressure, density and temperature.[5] Figure 3.2 shows 2D profile and 1D characteristics of the He36 K Laval nozzle obtained using the Pitot tube. In terms of supersonic flow quality, this nozzle is one of the best available in the laboratory thanks to the size of the isentropic core (≈ 25 cm length and almost ≈ 2 cm diameter) and more than 195 μs of hydrodynamic time.

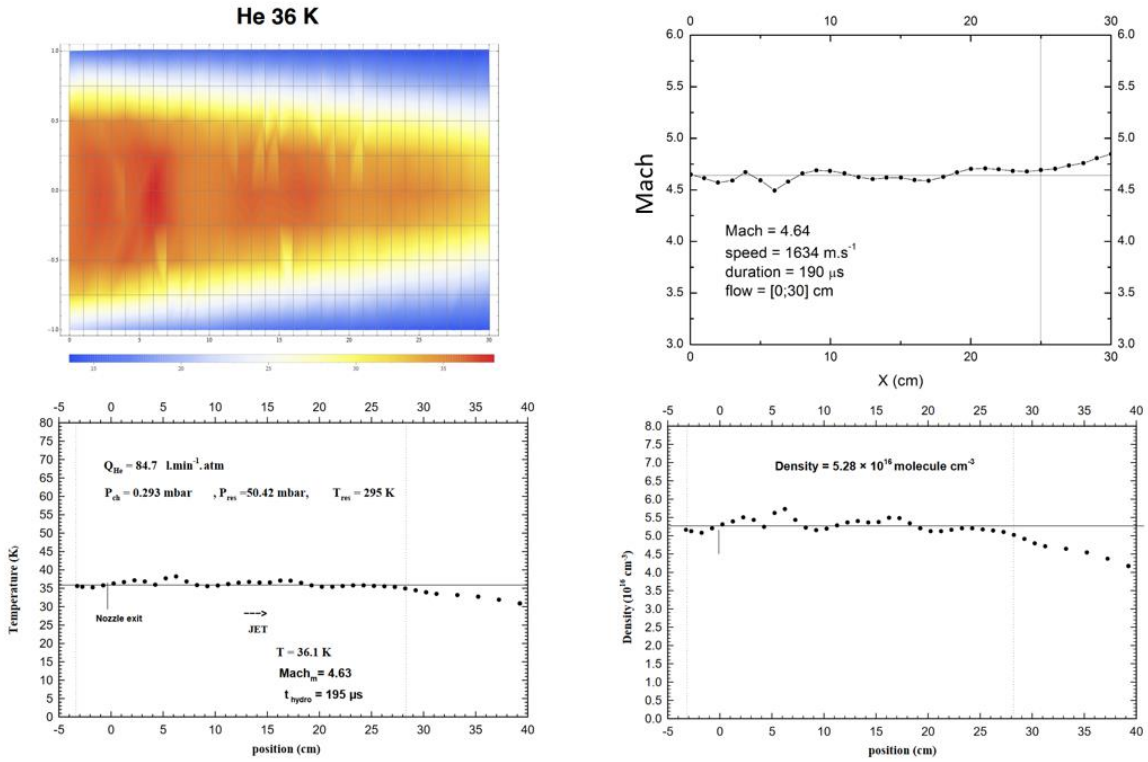

Figure 3.2: 2D profile and 1D characteristics of the He36 K Laval nozzle obtained using the Pitot tube.

According to the laws that govern the behavior of flows in a supersonic regime, the chamber pressure ($P_{chamber}$) should be equal to that at the exit of the Laval nozzle (P_{flow}). If it is not the case, the flow losses its uniformity. So, after the expansion of the gas throw the Laval nozzle, there are three possible scenarios: these cases are simulated by our colleague Abdessamad Benidar as shown in Figure 3.3.

The first case is when the pressure of the flow is inferior to that in the chamber ($P_{flow}<P_{chamber}$), the flow converges at the exit of the Laval nozzle (Figure 3.3 a). The second case is when the pressure of the flow in superior to that in the chamber ($P_{flow}>P_{chamber}$), the flow diverges near the exit of the Laval nozzle (Figure 3.3 b). The last scenario is when the pressure of the flow is equal to that in the chamber ($P_{flow=}P_{chamber}$), in this case we talk about a well-adapted case (Figure 3.3 c).

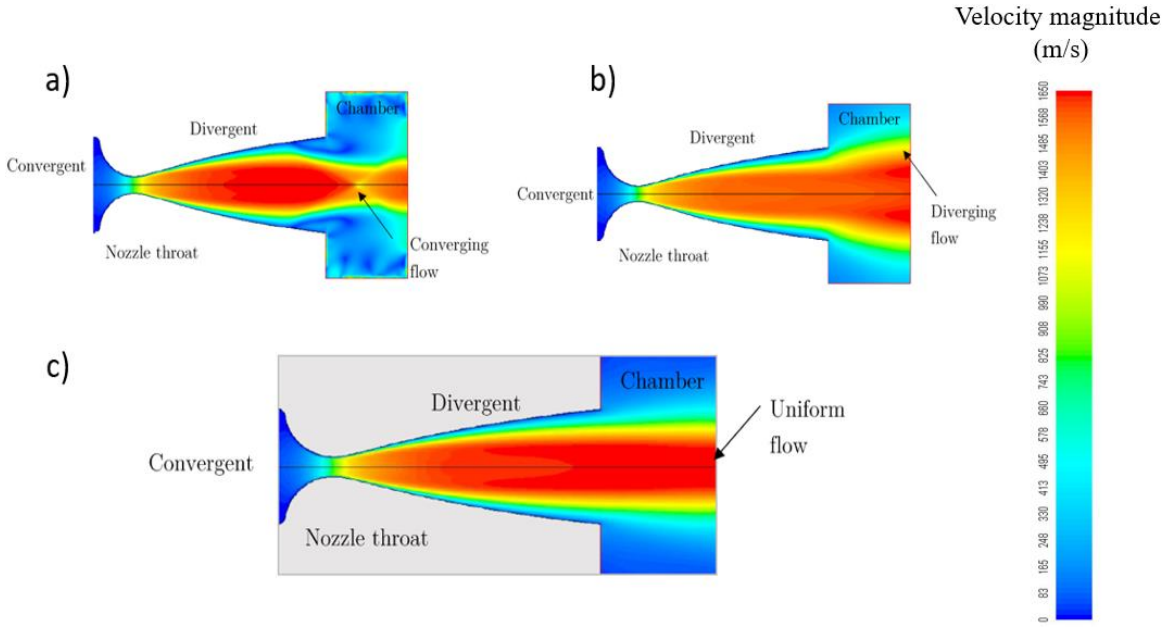

Figure 3.3: CFD simulations of the helium flow generated by a He36 K nozzle. Mach number map **a)** $P_{flow}<P_{chamber}$, **b)** $P_{flow}>P_{chamber}$, **c)** $P_{flow}=P_{chamber}$ ($P_{reservoir}$ = 50.31 mbar, $P_{chamber}$=0.292 mbar, $T_{reservoir}$= 293 K, $T_{chamber}$= 36 K, Q_{helium}= 88.8 slm.

In order to limit the high gas consumption required to generate high-quality USFs (Uniform Supersonic Flows), in the mid 1990's, M.A. Smith (University of Arizona, USA) and co-workers developed a pulsed version of the CRESU technique. A similar apparatus was constructed in the group of S. Leone at Berkeley (USA), using a pulsed Laval nozzle.[6] An example of reactions studied using a pulsed Laval nozzle expansion is the reaction of OH radicals with propene and isoprene, in the temperature range of 58-300 K, by Troe's group.[7] Another version of the pulsed CRESU was also developed in 2009 by Sébastien Morales and Bertrand Rowe[8] in the Astrophysics Laboratory group of Rennes 1 University, and later transferred to the department of Physical Chemistry of the University of Castilla-La Mancha (UCLM) in Ciudad Real in the group of E. Jiménez et al [9]. The apparatus was based on an aerodynamic chopper for gas phase reaction kinetic studies at ultra-low temperatures. This technique saves a factor of ~ 20 on the pumping capacity necessary to generate continuous uniform supersonic flows and thus to achieve lower temperatures and pressures, and reduces the requirement of gas consumption.

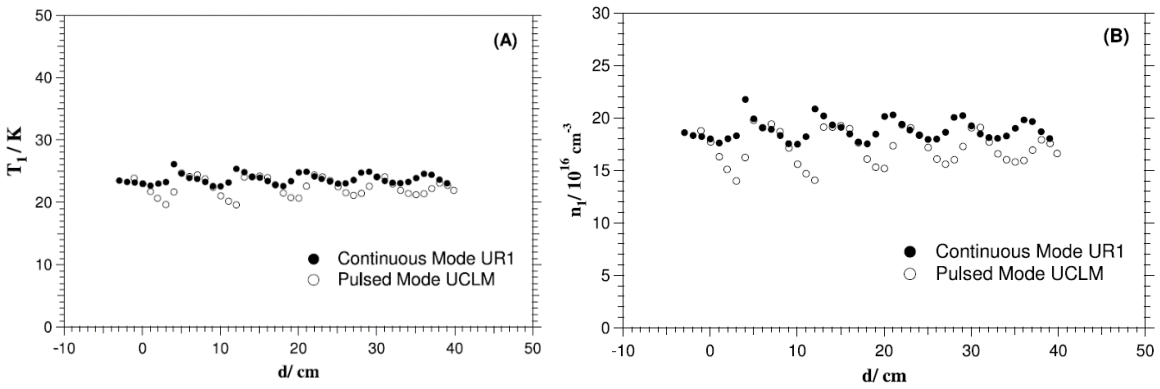

Figure 3.4: Spatial profiles of the gas temperature (A) and gas density (B) in the uniform supersonic flow in the pulsed and continuous modes. The averaged pressure in the jet was also obtained from Pitot measurements and was 0.54±0.08) millibars for the pulsed mode. From E. Jiménez et al. 2015 [9]

3.2 Selective Ion Source

The CRESU-SIS method combines the CRESU method with a mass-selective ion source. In the present set-up, the mass selective ion source is developed by Fasmatech (Greece), which is coupled to a CRESU chamber. The proof of concept of the CRESU-SIS experimental setup was published in 2019[10]. In that work, Rennes' group studied the reactivity of Ar^+ with C_2H_6, N_2O, and N_2. The reaction between O_2^+ ions with ethane C_2H_6 was also investigated. The results are in good agreement with previous measurements (FA, SIFT, CRESU, ICR) and empirical models.

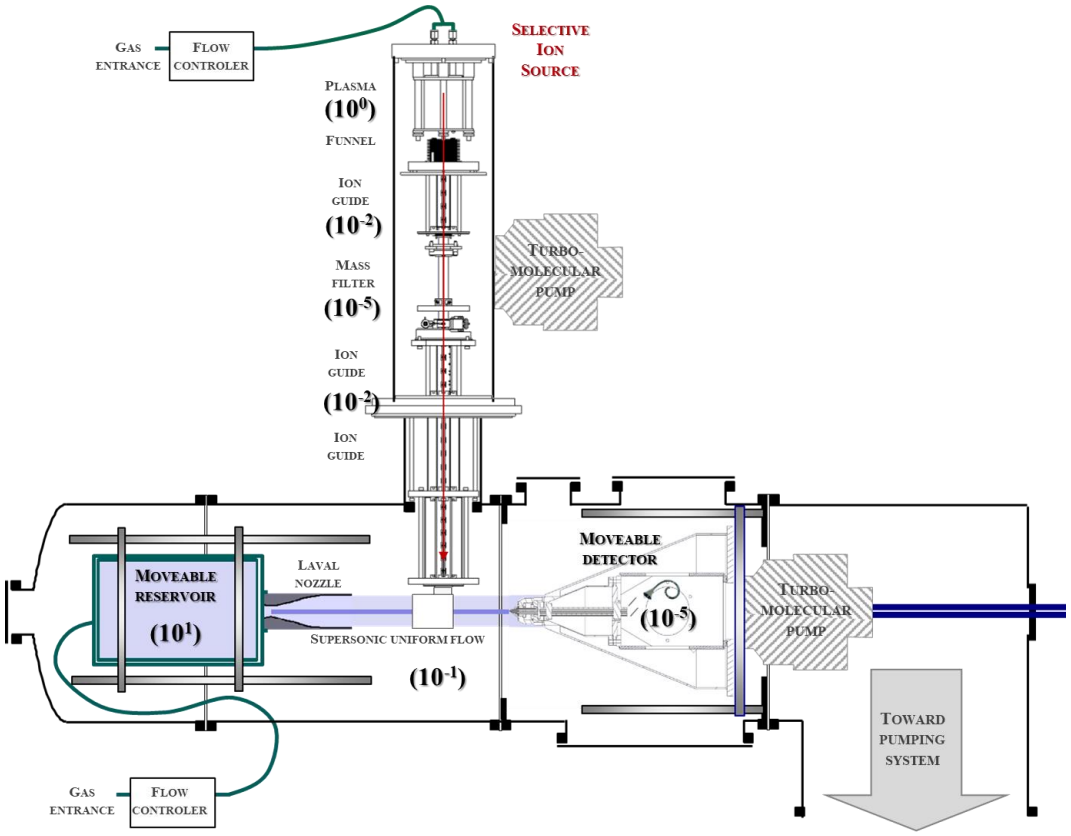

Figure 3.5: The CRESU reaction chamber incorporating the new mass-selective ion transfer line. A movable quadrupole mass spectrometer equipped with a skimmer/ hexapole ion guide combination is used for monitoring ions in the de Laval expansion. High-capacity root pumps (around 60000 m^3/h in helium) maintain the desired pressure (in order to 10^{-1} mbar) in the reaction chamber. The numbers in brackets are the pressure orders of magnitude in mbar unit.

3.2.1 Generation of ions

The ions are produced in a cold, stable, and dense plasma generated by a hollow cathode discharge (HCD) (P~2 mbar, $U_{discharge}$ ~395 V, $I_{discharge}$ ~950 mA) obtained with a continuous flow of helium (0.750 slm) and a small quantity of precursor gas (for example we inject 5 sccm of nitrogen N_2 to create N_2^+ ions). The typical conditions for the operation of the plasma source are summarized in table 3.1. The cathode is connected to a high-power supply, and the anode is held at ground potential. Because the plasma is globally neutral, the sum of negative charges is equal to the sum of positive charges. As most of negative charges are carried by electrons, we observe that the number of cations is one order of magnitude higher than the number of anions. The ions generated by the HCD are injected into an ion funnel which is driven by high-frequency low-amplitude RF waveforms (3.5 MHz).

Helium flow	Pressure	$U_{discharge}$	$I_{discharge}$	Precursor (targeted ion)	Precursor quantity
0.750 slm	~1.5 – 2 mbar	~ 395 V	~950 mA	N_2 (N_2^+) Ar (Ar^+) $ClCH_2CN$ (CH_2CN^+) CH_3Cl (CH_3^+) ...	few sccm

Table 3.1: Typical conditions for the operation of the plasma source. For each precursor, the target ion is indicated in brackets.

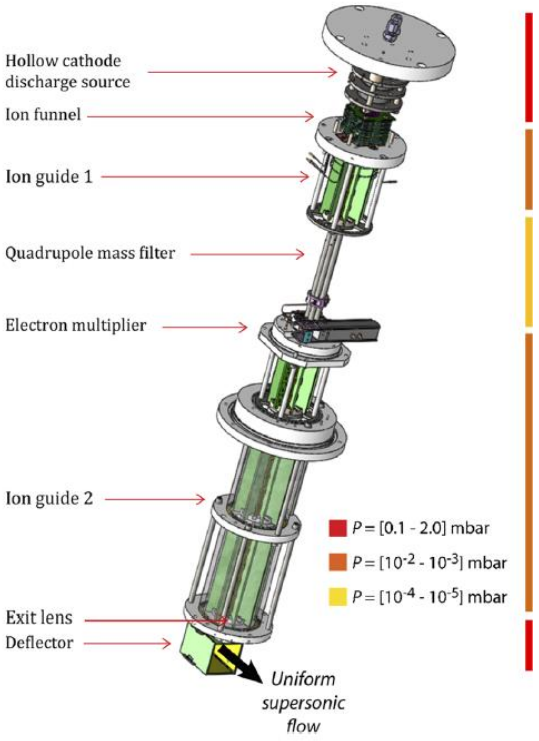

Figure 3.6: 3D CAD model of the ion optical line. The main components of the system are indicated. Pressure regions are also highlighted.[10]

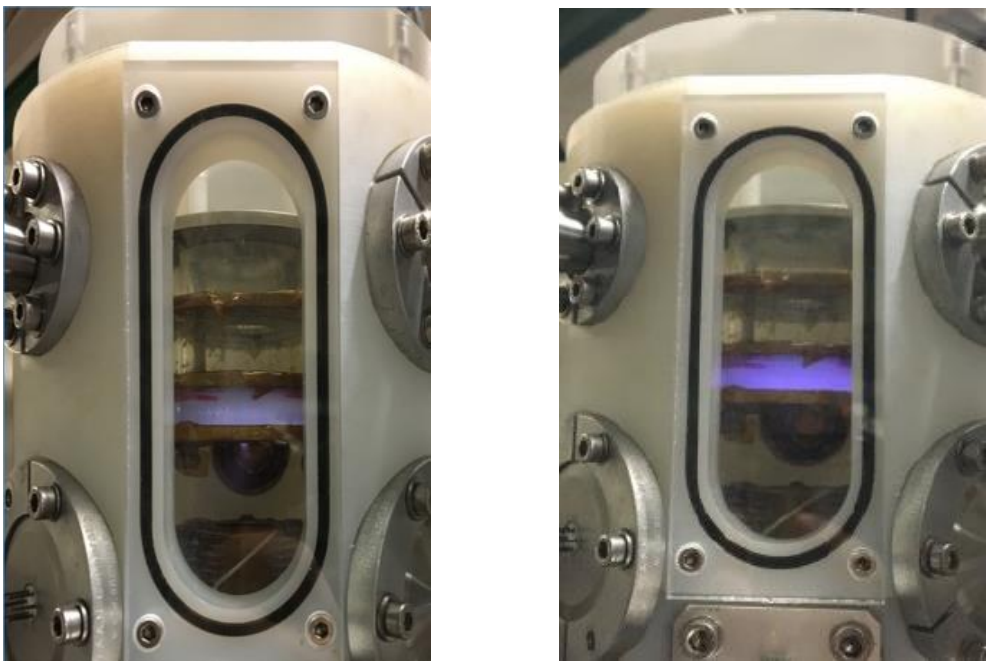

Figure 3.7: Ion source showing the plasma generated by the hollow cathode discharge in a He/O_2 (left) and Ar/O_2 (right) mixtures.

3.2.2 Mass-selective ion transfer line

The mass selection of the ions is provided by a radio frequency quadrupole mass filter (QMF) giving an output ion current of about 1 nA. Ions are introduced into the QMF with an optimal kinetic energy of 10 eV. The QMS is a device that can separate charged atoms or molecules according to their mass-to-charge ratio. Ionized molecules are accelerated (~ few eV) towards the quadrupole analyzer region where a combination of radio-frequency RF ($V_0 \cos(\omega t)$) and direct-current DC (U) fields are applied to cylindrical rods arranged along the axis of the ion beam. Ions entering a field experience a deflecting force, depending on the strength of the field and the mass-to-charge ratio of the ion. For given values of the RF and DC fields, only ions with a specific mass can pass longitudinally through the rods.

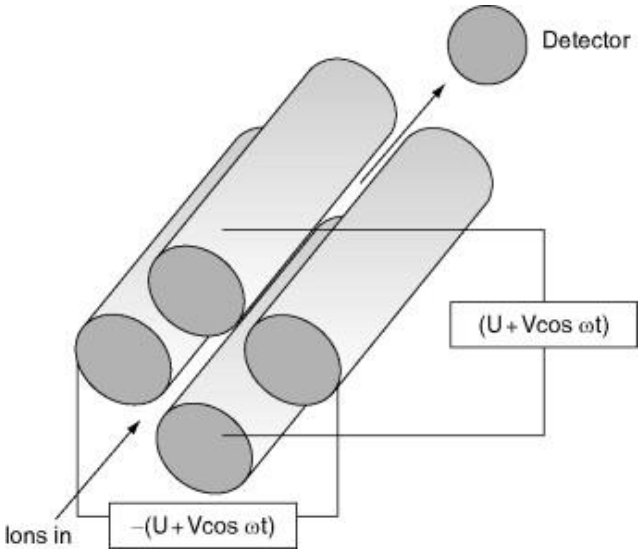

Figure 3.8: Schematic diagram of a quadrupole mass spectrometer.[11]

At the end of the QMF, there is an electron multiplier which allows two operating modes that were supported by fast switching electronics: off-axis detection (electron multiplier on) and on-axis transmission (electron multiplier off). The channeltron amplifies the ion signal by electron multiplication. The efficiency of the CEM depends on the average number of secondary electrons released by an incident ion. In detection mode, a mass spectrum can be generated without any filtering. In transmission mode, appropriate lens potentials are applied in order to ensure a good ion transmission into the ion guides. The resolution R which is equal to m/Δm (where m is the mass of the ion and Δm is the width of the peak) determines the ability to distinguish nearby peaks, it increases as the length of the rods and the mass of the ion increase.

Several quadrupoles ($P \approx 10^{-5}$ mbar) and octopoles ($P \approx 10^{-2}$ mbar) ion guides are used to transport ions from their production zone, through the selection mass filter and finally down to the uniform supersonic flow with a good transmission. Studies of Douglas and French (1992)[12] on the collisional focusing effects in RF quadrupoles show that, provided a low initial ion kinetic energy (1–30 eV), the ion transmission through a small aperture at the exit of a quadrupole increases as the pressure increases to reach a maximum near 10^{-2} mbar, which is very close to the pressure conditions of our octupole ion guides. In order to maximize the transmission and counteract collisional cooling, a weak DC gradient is applied across the segments of ion guides. All DC and RF potentials applied to the ion transfer line are controlled electronically through our own computer interface. We use two types of power supplies: bipolar dc power supply units (PSUs) that are employed for the transfer line, that can be operated in positive and negative ion modes, and a single RF PSU delivering a 3.5 MHz sinusoidal waveform is used to drive the funnel, the

ion guides, and the hexapole integrated upstream the detection QMS, while independent DC PSUs are employed to control all static potentials applied to the lens electrodes and to establish the axial DC gradients across the ion guides. Ions selected in the QMF are focused using a set of lenses through a differential pressure aperture into the octopole ion guide.

The final ion current at the bottom of the SIS is around 600 pA. The ions arrive at right angle compared to the neutral uniform supersonic flow axis requiring for the injection a deflector with adapted applied potentials (around +1 V and -30 V for radial and vertical axes respectively) which allows the alignment of ions trajectories with the supersonic flow towards the entrance of the detection system.

The selective ion source can work in positive and negative modes. Negative ions are detected at the end of the mass filter, and we have measured a quantity of ≈ 100 pA at the lens at the end of the selective ion source. To work in negative mode, we should invert the polarity of all applied potentials.

Figure 3.9 shows two mass spectra (recorded without m/q selection) registered at the level of the mass filter, in the case of creation of cations (positive mode) and creation of O^- and O_2^- anions (negative mode).

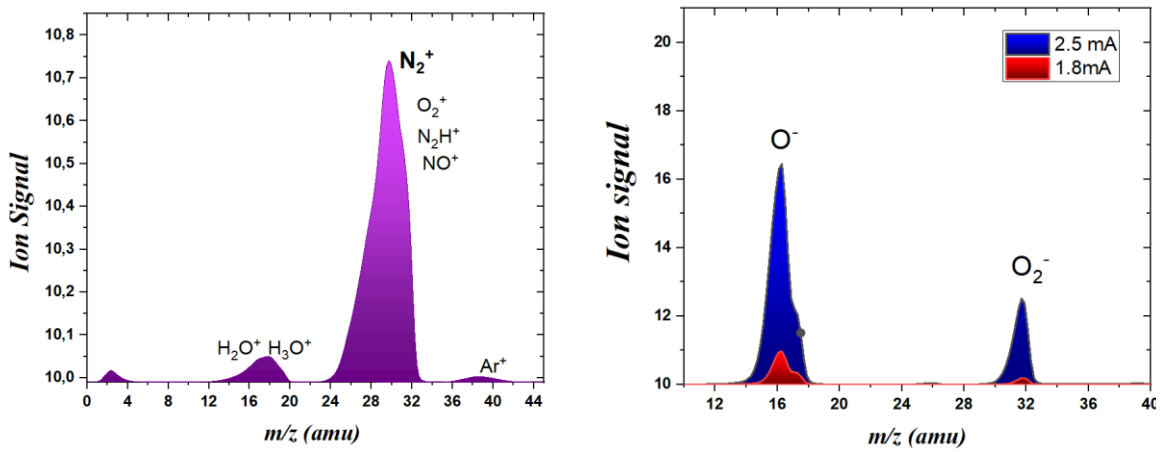

Figure 3.9: Mass spectra registered at the level of the mass filter of the Selective ion source working in positive mode (left) and negative mode (right). In positive mode, the plasma is generated by the HCD in a He/N_2 mixture, with Q_{He}= 0.750 slm, and Q_{N_2}= 5 sccm. For negative mode, the plasma is generated by the HCD in a He/O_2 mixture, with Q_{He}= 0.750 slm, and Q_{O_2}= 3 sccm.

The buffer gas of the CRESU chamber flows back into the ion source, due to the relative high pressure in the chamber (~mbar) comparing with the pressure in the quadrupole ion guide at the end of the selective ion source (~10^{-2} mbar). In order to study the effect of the nature of the

buffer gas on the ion transmission efficiency, Fasmatech performed some simulations ($C_2H_5^+$ ions in this case), considering two buffer gases predominantly used in our Laval nozzles: helium and the nitrogen. Simulations show that in the case of helium buffer gas, the transmission is more than 60%, but in the case of nitrogen buffer gas, the ion transmission was strongly inhibited (< 5%). The gas-dependent transmission could be explained by the higher collision cross-section of the molecular nitrogen N_2 (σ= 0.43 nm^2)[13] relative to the helium He (σ= 0.21 nm^2),[13] which lead to more ion-molecule collisions and scattering, and therefore lower transmission. [14] (Figure 3.10)

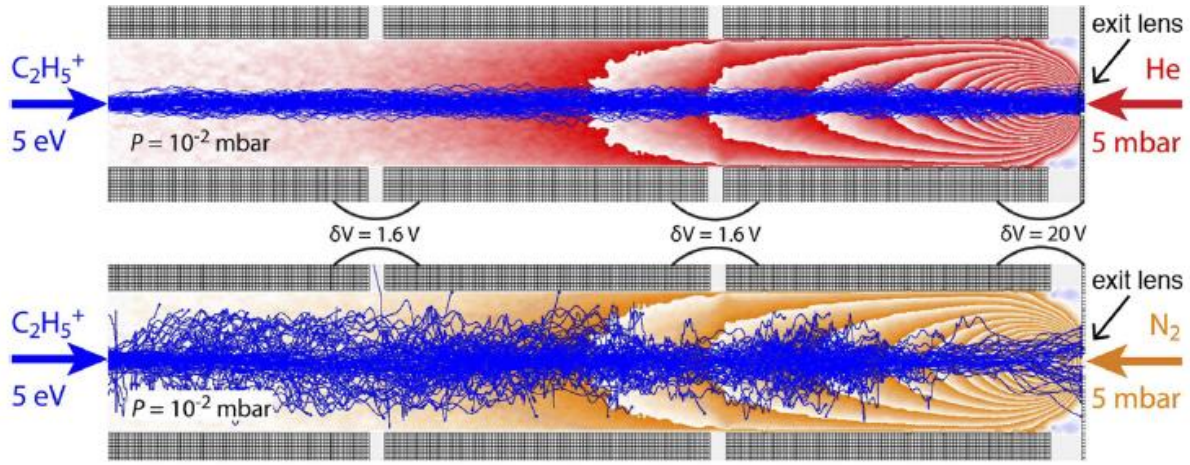

Figure 3.10: Simulated trajectories of $C_2H_5^+$ ions in the injection region (last three segments of ion guide 2/exit lens) superimposed on velocity contours of 50 m/s for He (red) and N_2 (orange) buffer gases with maximum axial and radial speeds of 620 m/s and 360 m/s, respectively.

3.3 Detection part

The monitoring of ions along the de Laval expansion is performed by a movable quadrupole mass spectrometer (QMS) housed in a differentially pumped chamber (P≈10^{-5} mbar). The detection chamber, mounted on a position-controlled translating stage, was recently modified to incorporate a rf hexapole ion guide combined with a molecular beam skimmer (orifice diameter D usually 0.8 mm) to enhance sampling efficiency of reactant and product ions. The skimmer was polarized by a few volts (~ -2 V for cations).

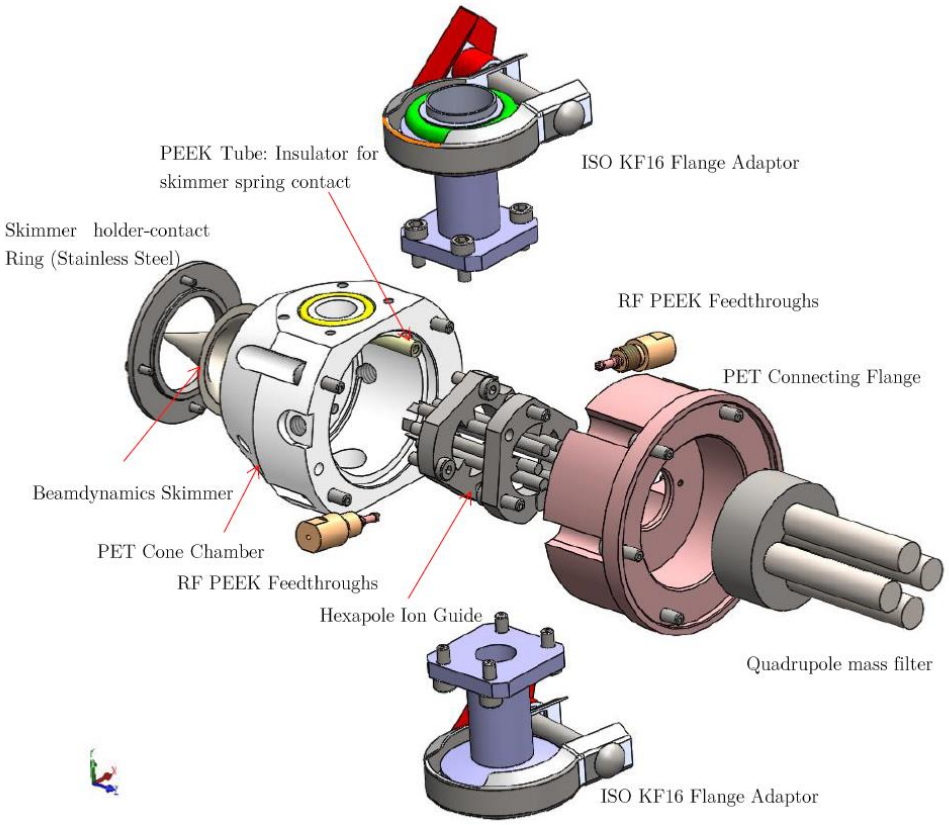

Figure 3.11: A schematic diagram of the different parts used to assemble the skimmer, the hexapole ion guide, and the quadrupole mass spectrometer [14]

In our case, the resolution of the QMS is typically 30 and the m/q range is 0-100 u. At the end of the QMS, a channel electron multiplier (also known as channeltron, CEM) is used to detect ionic species in the flow. In our experimental setup, we are using the Magnum 5901 CEM delivered by Photonis (gain ≈ 5×10^{7}) well adapted to operate at reltively high pressures (10^{-4} mbar).

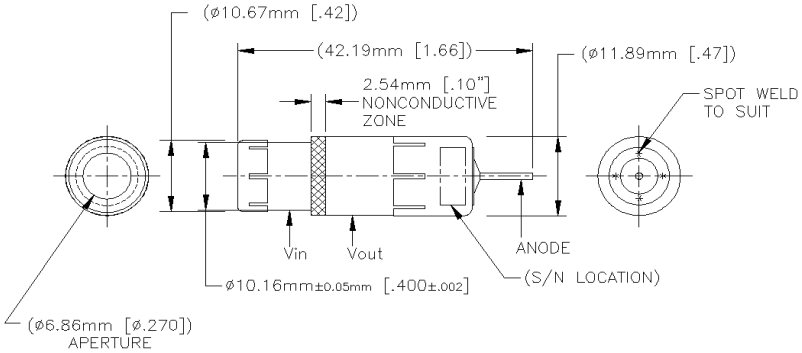

Figure 3.12: dimensions of Magnum 5901 CEM used to detect ions.

Ion trajectories, and therefore their detection in the USF are very sensitive to the voltages applied to the deflector. Applying adapted voltages on the deflector allowed for more than 95% of the selected ions to be drifted toward the skimmer. The measurements showed that, in the absence of neutral reactant, the ion signal must not vary greater than 5% along the flow, for a distance up to 20 cm (see for example the figure 4.3 in chapter 4) to provide adequate condition for kinetic measurements. We found that a change of ±5 V in the deflector potential leads to its complete disappearance of ion signal.

As an example, figure 3.13 shows a mass spectrum recorded in the flow by our movable QMS at 24 K.

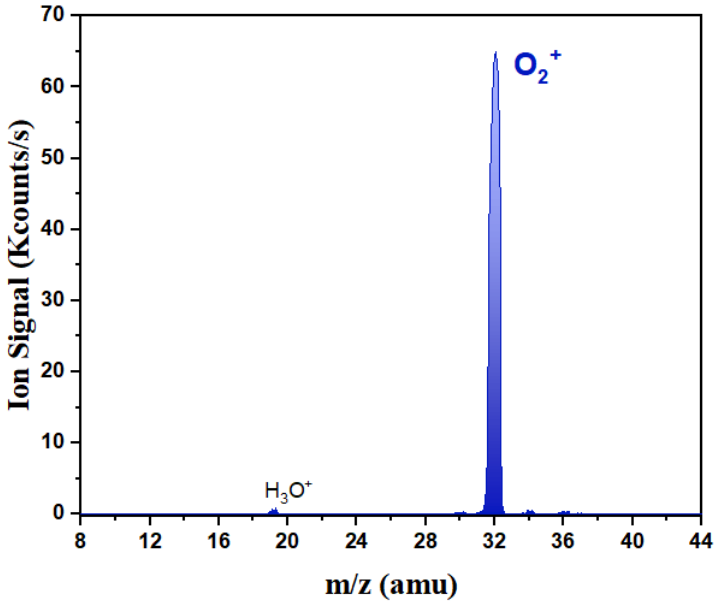

Figure 3.13: Mass spectrum registered in the flow (T= 24 K) after the selection of O_2^+ ions (m/z= 32 u) by the selective ion source.

The mass filter strongly reduces the transmission of other ions than the desired one produced in the source such as H_3O^+ by a factor of ~ 100.

3.4 Gas introduction

The buffer gas, the precursor, and the neutral reactant are introduced into the source and the reservoir of the CRESU chamber using mass flow controllers (Bronkhorst or MKS). These controllers are calibrated regularly in order to reduce the errors in the density of introduced gas. The neutral density should be known precisely to determine an absolute rate coefficient.

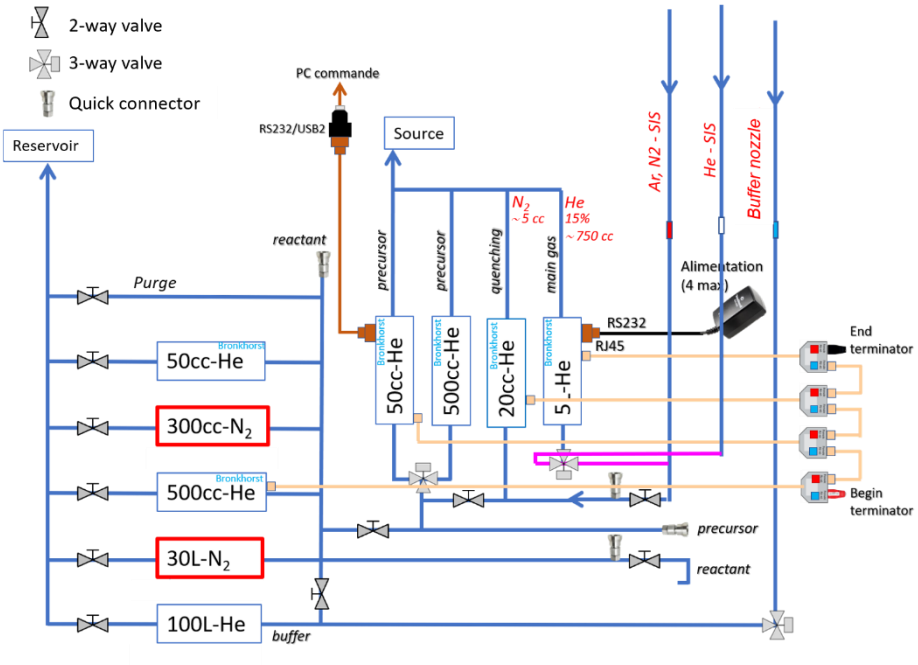

Figure 3.14: Map of controllers used to inject gas in the source and the reservoir of the CRESU chamber. [15]

The vibrational relaxation of molecular ions by neutrals is generally efficient because of the added electrostatic potential between the ions and neutrals.[16] As presented in the work of Baptiste Joalland et al.,[10] due to the high number of collisions, the Ar^+ ions are de-excited from ($^2P_{1/2}$) to ($^2P_{3/2}$) in the sub-microsecond time scale, directly in the dense plasma of the source, while for O_2^+ ions, the vibrational deactivation of O_2^+ (v = 1, 2) with different neutral partners is also achieved during their travel in the ionization source. In some cases, to ensure the quenching of exited ions, and to avoid their presence in the reaction zone, we inject a small quantity of a quencher gas in the source. The nature of the quencher gas depends on the studied ion.

3.5 The determination of the rate coefficient

Because of the constant flow velocity, the moveable detector allows to follow the time evolution of the ion signals for a hydrodynamic time τ_h of typically 150-200 µs. The slope of the evolution of ion signal with time at fixed neutral density corresponds to the pseudo-first order rate coefficient k_{1st} (the loss rate, s^{-1}), and the slope of the loss rate as a function of the neutral reactant density determines the rate coefficient of the collisional chemical reaction.

3.6 The temperature and the velocity of injected ions

One of the key aspects of the experimental scheme is to ensure the good thermalization of the injected ions, that itself allows the derivation of meaningful rate coefficients at a given flow temperature k(T).

In order to study the velocity and temperature of injected ions, our colleague Abdessamad Benidar did some simulations using COMSOL software of the injection of Ar^+ ions (in which all parameters needed to the simulations, such as collision cross sections, exists in the program database) of initial kinetic energy of 5 eV (similar ions energy used in the simulations of Fasmatech, section 3.2.2) are guided and confined by the octopole to be injected into the CRESU using the deflector. In these simulations, the uniform supersonic helium flow is defined with a temperature of 50 K, a speed of 1630 m/s with an isentropic core of 16 mm. The deflector is brought to a ddp of 28 V (U_{top}= -1; U_{bottom} = -29V). Figure 3.15 shows a simulation of the injection of Ar^+ ions in the CRESU's supersonic flow.

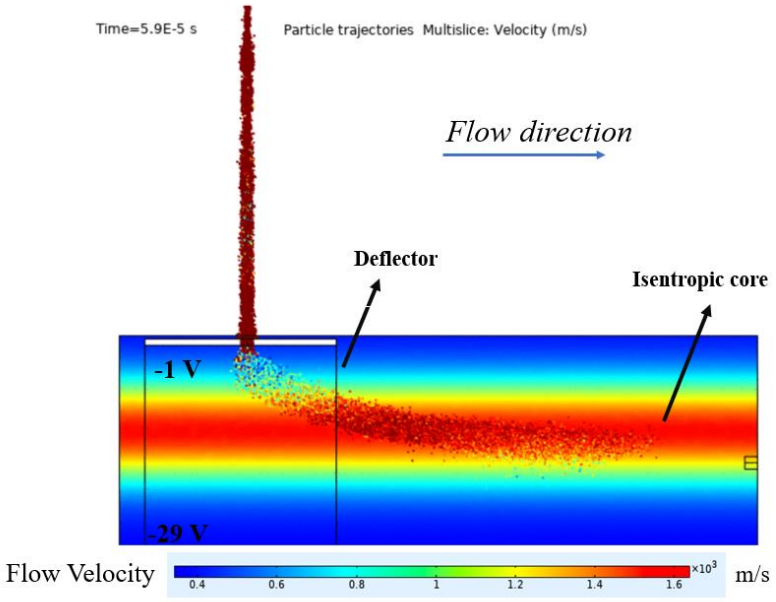

Figure 3.15: Velocity simulation showing the injection of Ar^+ ions in the CRESU helium flow (T= 50 K, n= 10.4 × 10^{16} molecule.cm^{-3}, isentropic core = 16 mm).

Simulations show that due to the high number of collisions with the buffer gas of the supersonic flow, the ions converge rapidly to the velocity of the flow, and they are not accelerated by the electric field generated by the deflector. (Figure 3.16)

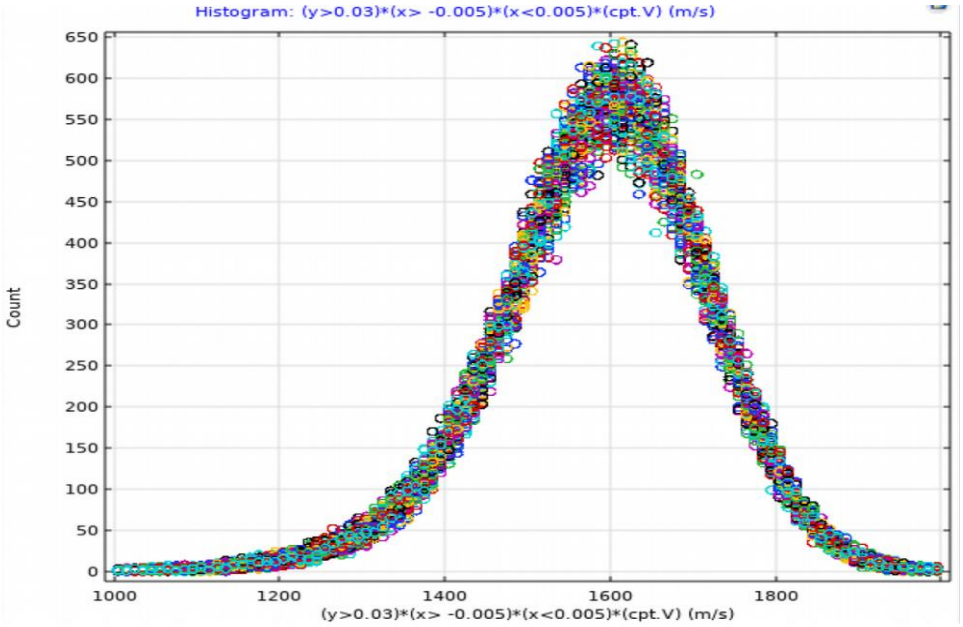

Figure 3.16: Temperature distribution of a group of Ar+ ions injected in the uniform supersonic flow at time between 80 μs and 100 μs.

The ions velocity can be expressed by the Maxwell-Boltzmann distribution:

$$f(v) = \left(\frac{2}{\pi}\right)^{1/2} \left(\frac{m}{k_B T}\right)^{3/2} v^2 \exp\left(-\frac{mv^2}{2k_B T}\right) \qquad \text{Eq. (3.10)}$$

This expression was used in order to deduce the temperature of the injected ions in the flow. Results show that at a distance 2 < x < 3 cm from the injection zone, the ions have a temperature ~ 58 K, and after few centimeters, their temperature decreases to reach the temperature of the cold flow ~50 K at a distance 7 < x < 8 cm. Usually, in our experiments, the first measurement of the ion signal is around 7 cm, so we can assume that the ions are "safely" injected in the flow, and they have temperature close to the temperature of the isentropic core, due to the high density of the flow (therefore high number of collisions between the ions and the buffer gas of the CRESU expansion).

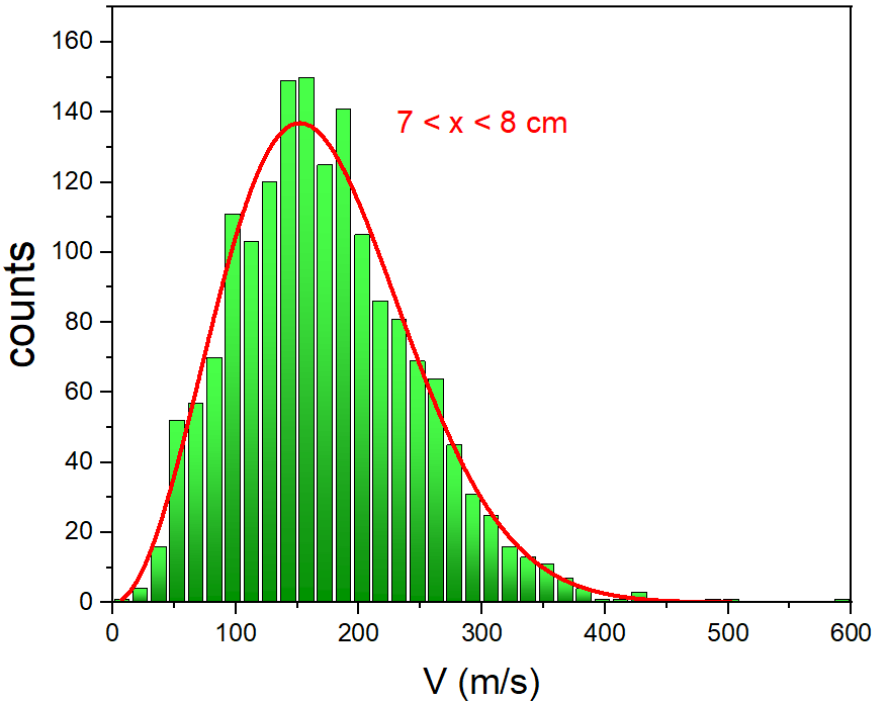

Figure 3.17: velocity distribution of the Ar^+ ions injected in the flow at a distance 7 < x < 8.

3.7 Conclusion

This chapter gave a brief overview of the CRESU technique, and described the CRESU-SIS experimental setup developed in Rennes 1 University.

The design of the ion transfer line, which takes advantage of the relatively high pressure in the reaction chamber and of the combination of quadrupolar and octopolar radio frequency field orders, makes possible to concurrently:

(i) Produce a great variety of positive and negative ions through its modular ion source.

(ii) Select the primary ion of interest for a given m/z ratio, that makes the measurements of the rate coefficient and the branching ratios more precise.

(iii) Maximize the ion transmission through large pressure gradients between the ionization source (~mbar), the quadrupole mass filter (~10^{-5} mbar), and the de Laval expansion (~mbar).

(iv) Ensure the prompt rovibrational thermalization of the mass-selected ions.

(v) Redirect the ion cloud along the propagation axis of the cold de Laval expansion readily.

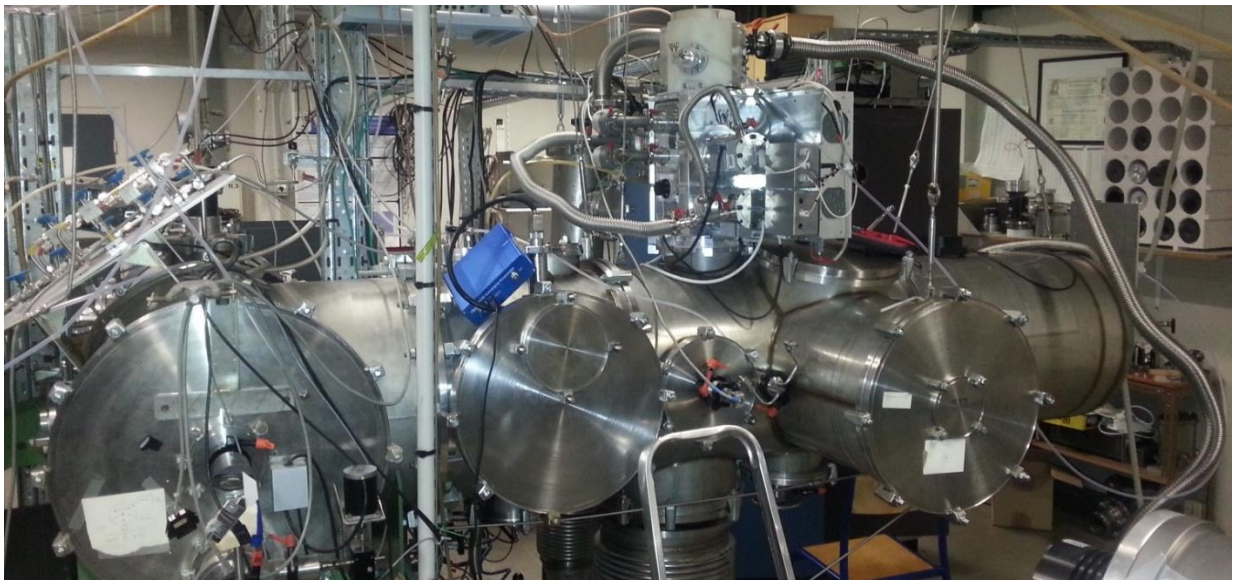

Figure 3.18: Image of the CRESU-SIS apparatus used in Rennes.

In the next chapter, the CRESU-SIS method will be applied to investigate the reactivity (kinetics and branching ratios) of the N_2^+ ions with propyne CH_3CCH and allene CH_2CCH_2 at low temperatures (down to 24 K).

References:

(1) Rowe, B. R.; Marquette, J. B. CRESU Studies of Ion/Molecule Reactions. International Journal of Mass Spectrometry and Ion Processes **1987**, 80, 239–254. https://doi.org/10.1016/0168-1176(87)87033-7.

(2) Berteloite, C.; Lara, M.; Bergeat, A.; Le Picard, S. D.; Dayou, F.; Hickson, K. M.; Canosa, A.; Naulin, C.; Launay, J.-M.; Sims, I. R.; Costes, M. Kinetics and Dynamics of the S (D 2 1) + H 2 → SH + H Reaction at Very Low Temperatures and Collision Energies. Phys. Rev. Lett. **2010**, 105 (20), 203201. https://doi.org/10.1103/PhysRevLett.105.203201.

(3) Potapov, A.; Canosa, A.; Jiménez, E.; Rowe, B. Uniform Supersonic Chemical Reactors: 30 Years of Astrochemical History and Future Challenges. Angewandte Chemie International Edition **2017**, 56 (30), 8618–8640. https://doi.org/10.1002/anie.201611240.

(4) Brun, R. Introduction to Reactive Gas Dynamics; OUP Oxford, 2009.

(5) Durif, O. Un Nouvel Instrument Pour Étudier La Cinétique et Les Rapports de Branchement Des Collisions Réactives Entre Espèces Neutres Dans Les Écoulements Supersoniques Uniformes. **2019**.

(6) S Lee; R Hoobler; S Leone. A Pulsed Laval Nozzle Apparatus With Laser Ionization Mass Spectroscopy for Direct Measurements of Rate Coefficients at Low Temperatures With Condensable Gases. **2000**, No. 71.

(7) Spangenberg, T.; Köhler, S.; Hansmann, B.; Wachsmuth, U.; Abel, B.; Smith, M. A. Low-Temperature Reactions of OH Radicals with Propene and Isoprene in Pulsed Laval Nozzle Expansions. J. Phys. Chem. A **2004**, 108 (37), 7527–7534. https://doi.org/10.1021/jp031228m.

(8) Morales, S. Le Hacheur Aérodynamique: Un Nouvel Instrument Dédié Aux Processus Réactionnels à Ultra-Basse Température. **2009**.

(9) Jiménez, E.; Ballesteros, B.; Canosa, A.; Townsend, T. M.; Maigler, F. J.; Napal, V.; Rowe, B. R.; Albaladejo, J. Development of a Pulsed Uniform Supersonic Gas Expansion System Based on an Aerodynamic Chopper for Gas Phase Reaction Kinetic Studies at Ultra-Low Temperatures. Review of Scientific Instruments **2015**, 86 (4), 045108. https://doi.org/10.1063/1.4918529.

(10) Joalland, B.; Jamal-Eddine, N.; Papanastasiou, D.; Lekkas, A.; Carles, S.; Biennier, L. A Mass-Selective Ion Transfer Line Coupled with a Uniform Supersonic Flow for Studying Ion–Molecule Reactions at Low Temperatures. J. Chem. Phys. **2019**, 150 (16), 164201. https://doi.org/10.1063/1.5086386.

(11) Mellon, F. A. MASS SPECTROMETRY | Principles and Instrumentation. In Encyclopedia of Food Sciences and Nutrition (Second Edition); Caballero, B., Ed.; Academic Press: Oxford, 2003; pp 3739–3749. https://doi.org/10.1016/B0-12-227055-X/00746-X.

(12) Douglas, D. J.; French, J. B. Collisional Focusing Effects in Radio Frequency Quadrupoles. J. Am. Soc. Mass Spectrom. **1992**, 3 (4), 398–408. https://doi.org/10.1016/1044-0305(92)87067-9.

(13) Collisional Cross Section https://chem.libretexts.org/@go/page/1403 (accessed 2021 -10 -15).

(14) Jamal Eddine, N. Reactivity of Molecular Anions at Low Temperature: Implications for the Chemistry of the Interstellar Medium Ant Titan's Atmosphere. **2017**.

(15) Credits to Basile Bataille, Physics Student at Rennes 1 University, during the Internship with Sophie Carles.

(16) Ferguson, E. E. Vibrational Quenching of Small Molecular Ions in Neutral Collisions. J. Phys. Chem. **1986**, 90 (5), 731–738. https://doi.org/10.1021/j100277a008.

Chapter 4:

Kinetics and Branching for the Reactions of N_2^+ with C_3H_4 Isomers at Low Temperatures and Implications for Titan's Atmosphere

Cyclopropenylidene C_3H_2 has recently been detected in Titan's atmosphere. One of the precursors of this carbene has been identified as the cyclopropenyl cation (c-$C_3H_3^+$) that can form C_3H_2 through dissociative recombination. This combined experimental/theoretical work explored the reactivity of N_2^+ ions with C_3H_4 isomers, namely propyne (CH_3CCH) and allene (CH_2CCH_2), as possible pathways to the formation of c-$C_3H_3^+$, the smallest aromatic species. For the first time, both reactions were investigated at low temperatures between 24 and 71 K. Rate coefficients, product identity, and branching ratios were measured within uniform supersonic flows combined with a newly developed mass-selective ion source and an improved detection scheme. The experimental results were complemented with coupled cluster ab initio calculations to enable the firm identification of the possible reaction paths and product isomers. The results show that the rate coefficients are large and their temperature dependence in remarkable agreement with capture models. The derived reaction rates and branching ratios have been included in a photochemical model of Titan's atmosphere. The results point to a secondary role of the $N_2^+ + C_3H_4$ reactive pathways in the formation of c-$C_3H_3^+$.

4.1 Introduction

The Cassini–Huygens mission to Titan, which explored Saturn's largest moon from 2004 to 2017, has revealed a fascinating and complex world that could provide a good analogue of Earth during its early history. Under irradiation from UV solar photons, bombardment from galactic cosmic rays and high energetic electrons from Saturn's magnetosphere, the dense atmosphere of Titan, dominated by nitrogen (N_2) and methane (CH_4), leads to the production of a wealth of organic species. Our knowledge of the atomic and molecular constituents of Titan's atmosphere, their spatial distribution and their temporal variations has also seen some significant progress through combined Earth-based and space-based observations and in situ measurements. The composition of the dense troposphere has been determined by the Cassini Gas Chromatography/Mass Spectrometer (GCMS) measurements.[1] For the stratosphere, advances have relied on ground-based mm-wave instruments (IRAM, ALMA,…)[2,3], infrared (IR) space observatories ISO[4] and Herschel[5], and the Composite Infrared Spectrometer (CIRS) embarked onboard Cassini[6]. The mesosphere has been characterized by the Cassini Visible Infrared Mapping Spectrometer (VIMS)[7] and Ultraviolet Imaging Spectrograph (UVIS)[8]. The much dilute high layer of the atmosphere, the thermosphere, has been solely investigated by the Ion Neutral Mass Spectrometer (INMS), which conducted mass spectrometric measurements of both ions and neutrals onboard Cassini.[9] In this particular region, a plethora of hydrocarbons [two-carbon acetylene (C_2H_2), ethylene (C_2H_4), and ethane (C_2H_6), the three-carbon propyne/allene (C_3H_4), propene (C_3H_6) and propane (C_3H_8), the four-carbon diacetylene (C_4H_2) and the six-carbon benzene (C_6H_6)] and nitriles [hydrogen cyanide (HCN) and hydrogen isocyanide (HNC), cyanoacetylene (HC_3N), acetonitrile (CH_3CN), acrylonitrile (CH_3CCN), propanenitrile (C_2H_5CN), cyanogen (C_2N_2)] have been detected.

The INMS mass spectra spanning the 0-100 u range show peaks arranged in clusters separated by 10 to 15 u that coincide with the sequential addition of hydrogenated carbon or nitrogen atoms. Noteworthy, a good correspondence is found between the ion and neutral spectra. However, due to the low resolution of the embarked mass spectrometer ($m/\Delta m$~100), and the absence of isomer identification inherent to the method, the assignment of the peaks cannot be self-sufficient and relies heavily on a good knowledge of the chemistry. The latest modeling study based on INMS measurements[10] puts forward key hydrocarbon ions such as CH_3^+, CH_5^+, $C_2H_5^+$, $C_3H_3^+$, $C_3H_5^+$, $C_4H_3^+$, $C_4H_5^+$, $C_6H_7^+$, $C_7H_7^+$, and nitriles such as $HCNH^+$.[11] Many other ions stay under the radar because of mass overlap; they include N_2^+ since $HCNH^+$ is the dominant species at m/z=28 u, and also N_2H^+ concealed by $C_2H_5^+$ (m/z=29 u). To assess their

presence, well-known reactions dominating their loss processes can be employed. The best tracer of N_2^+ is considered to be CH_3^+ as it can only be produced massively through the reaction of N_2^+ with the second most abundant species in the atmosphere, methane (CH_4).[12,13] The N_2^+ cation is of particular importance as it is considered as a primary ion along with N^+ and CH_4^+. These three cations are directly produced upon interaction of N_2 and CH_4 with solar photons and suprathermal photo- and secondary electrons.

Propyne CH_3CCH has been first uncovered in the Voyager IR spectrum of Titan in the 80's. A stratospheric abundance of C_3H_4 of 3×10^{-8} was determined for the mid-latitude region.[14] Further observations by ISO in 2003 led by Coustenis et al.[4] provided a disk average value of $1.2\square10^{\square8}$. During targeted flybys [15,16], Cassini/INMS measured the abundance of neutral C_3H_4 in the ionosphere and derived a mole fraction for propyne in the $2\square7\square10^{\square6}$ range. Propyne was also detected by the CIRS instrument through its 633 cm^{-1} emission feature[17] . Propadiene, also referred to as allene, CH_2CCH_2, an isomer of propyne, was unambiguously identified by the Texas Echelle Cross Echelle Spectrograph (TEXES) on the NASA Infrared Telescope Facility through its emission near 12 $\square$m with a measured volume mixing ratio of $6.9\square10^{\square10}$ at the altitude of 175 km[18]. CIRS measurements of propyne made at the same time indicate that the abundance ratio of propyne to propadiene is 8.2 at the same altitude. Propyne and propadiene constitute the first hydrocarbon isomer pair detected on Titan. Both isomers have been included in several photochemical models.[11,19,20] According to Dobrijevic et al.,[21] the main pathway for the formation of both isomers in the stratosphere is the associative reaction between hydrogen and propargyl radicals (C_3H_3):

$$C_3H_3 + H\ (+\ M) \rightarrow C_3H_4\ (+M) \qquad \text{Eq. (4.1)}$$

Below 200 km, the CH_2CCH_2 molecule can be produced additionally by the photodissociation of propene (C_3H_6).

In the ionosphere, C_3H_4 can be generated through the reaction of the CH radical with C_2H_4 and through the recombination of $C_3H_5^+$ with electrons:

$$C_3H_5^+ + e^- \rightarrow C_3H_4 + H \qquad \text{Eq. (4.2)}$$

The primary loss channel of C_3H_4 is photodissociation back to propargyl C_3H_3:

$$C_3H_4 + h\nu \rightarrow C_3H_3 + H \qquad \text{Eq. (4.3)}$$

Conversion from propadiene to propyne can take place through the reaction:

$$H + CH_2CCH_2 \rightarrow CH_3CCH + H \qquad \text{Eq. (4.4)}$$

The ion and neutral chemistry proposed above is however incomplete as major sources of uncertainty remain, besides the fact mentioned above that the INMS measurements cannot alone rule out isomers and lead to a firm identification of the alleged species. In particular, major sources of uncertainty come from the lack of information on product identity and branching as well as their temperature dependence (available data are often restricted to room temperature). While this is especially problematic for radical-neutral reactions, with only one study below 50 K reported so far[22], several techniques have been developed to measure the low-temperature kinetic rate coefficients as well as the products of ion-molecule reactions: crossed and merged molecular beams, ion traps and flow reactors. Cryogenic ion traps are for instance tailored to examine the reaction kinetics of ions over a wide dynamic range.[23] In practice however, condensation of the neutral co-reactants onto the walls of the chamber limits their use to light neutrals such as H_2 or He.[24] Uniform supersonic flows, which belong to the family of flow reactors, are well adapted to explore quantitatively the reactivity of ions with large neutral molecules[25–27] – it is one of the rare techniques to provide rate coefficients obtained under well-controlled thermalized conditions and over a wide range of low temperatures[28]. Here, we use a new approach, which combines a CRESU (Cinétique de Réaction en Ecoulement Supersonique Uniforme) reactor with a mass-selective ion source,[29] to measure for the first time the low-temperature rate coefficients and product branching of two key Titan's atmospheric reactions involving isomeric hydrocarbon targets: N_2^+ with propyne CH_3CCH and propadiene CH_2CCH_2 at 24, 36, 49 and 71.6 K. The experimental results are complemented with quantum chemical calculations to help identify the relevant products and chemical pathways.

4.2 Experiments

The low-temperature reaction of N_2^+ with C_3H_4 (propyne and allene) was investigated using a novel mass selective ion source (SIS) combined with a CRESU flow reactor. The CRESU-SIS device allows measuring absolute rate coefficients and the branching ratios of targeted gas-phase reactions at various low temperatures (down to 15 K). Details on this new approach can be found in chapter 3. The neutral cold and dense uniform supersonic flow is generated by the isentropic expansion of a continuous buffer gas (here helium or a mixture of helium and nitrogen) through a Laval nozzle. The density, the velocity and the temperature in the core of the supersonic flow are uniform over several tens of centimetres (See Table 4.1 for the

characteristics of the Laval nozzles used in this work). The supersonic flow, which can be viewed as a wall-less chemical reactor, can be inseminated with a small quantity of the studied ionic and neutral reactants allowing reactive collisions. The neutral reactants propyne and allene are commercially available from Air Liquide with purity higher than 96% and 98% respectively. These species are continuously injected in the supersonic flow with a controlled flow rate of a few sccm (standard cubic centimeter per minute) corresponding to a density of about 10^{12} molecule cm^{-3}.

In the present set-up, ions are produced in a plasma generated by a hollow cathode discharge (P~2 mbar, $U_{discharge}$ ~ 395 V, $I_{discharge}$ ~ 950 mA) obtained with a continuous flow of helium (0.750 slm) and a small quantity of nitrogen N_2 (5 sccm). The mass selection of the N_2^+ ions is provided by a radio frequency quadrupole mass filter giving an output ion current of about 1 nA. The final ion current at the bottom of the SIS is about 600 pA. According to Kato et al.[30] and Ferguson[31], the collisional vibrational relaxation coefficient of N_2^+(v =1) by N_2 is about 5-8×10^{-10} cm^3 $molecule^{-1}$ s^{-1}, meaning that the relaxation to the ground state is achieved in a few µs, i.e. directly in the plasma of the SIS start station. As a result, the N_2^+ ions are in their ground vibrational state before being injected into the uniform supersonic flow.

Nozzle	Buffer gas	T_{jet} (K)	Mach	τ	n (10^{16} molecule.cm^{-3})	$P_{chamber}$ (mbar)	flow rate (l/min)
He6K	He	24.1	5.84	196	18.3	0.630	93.4
He36K	He	36.1	4.63	195	5.28	0.293	84.7
Ar7K	He	49.1	3.87	150	10.4	0.770	67.0
Ar7K	He/N_2 (1:1)	57.0	4.08	158	6.91	0.550	20:20
Ar50K0.3	He	71.6	3.08	163	6.01	0.640	97.7

Table 4.1: Characteristics of the supersonic uniform flows determined from impact pressure measurements.

4.3 Results

4.3.1 Reaction Products Figure 1 shows two mass spectra recorded at 49 K after a reaction time of t = 50 µs and with a reactant density [C_3H_4] = 1.4×10^{12} molecule cm^{-3} for propyne and allene. For both reactions, the main ion product detected is $C_3H_3^+$, followed by $C_3H_2^+$ and $C_3H_4^+$ ions (respectively m/z=39, 38 and 40 u). In addition, the mass spectra

reveal traces of $C_3H_5^+$ (m/z=41 u) and C_3H^+ (m/z=37 u) as can be seen on the inset of Figure 1. Without any neutral reactant, ions other than N_2^+, namely N_2H^+ at m/z = 29 u, NO^+ at m/z = 30 u, O_2^+ at m/z = 32 u, H_2O^+ at m/z= 18 u, and H_3O^+ at m/z= 19 u, are also detected.

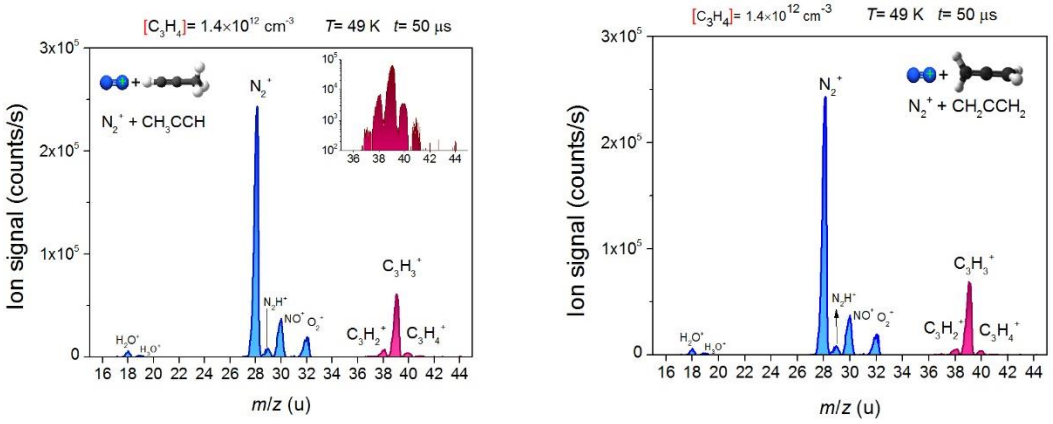

Figure 4.1: Mass spectra measured in a 49 K uniform supersonic flow inseminated by mass-selected N_2^+ cations in presence of CH_3CCH (A) and CH_2CCH_2 (B) neutral reactants at a density of 1.4 $\times 10^{12}$ molecule cm^{-3}. The ions are detected at a distance of 8 cm from the injection lens of the SIS, corresponding to a reaction time of 50 µs. The inset shows a close-up of the products in log scale.

These ions are the products of reactions of N_2^+ with impurities present in the neutral supersonic flow, unless they are not filtered out by the SIS due to the large bandpass of our quadrupole mass filter ($\Delta m/z$ = ±4 u). The reactions with impurities are considered as follows:

i. The $H_3O^+ + C_3H_4$ (propyne and allene) reactions have been studied in SIFT (Selected Ion Flow Tube) and FA-SIFDT (Flowing Afterglow - Selected Ion Flow Drift Tube) experiments at room temperature and the only observed exit channel for both reactions is $C_3H_5^+ + H_2O$ with reaction enthalpies ΔH = -0.83 and -0.87 eV and rate coefficients k = 1.7-1.8 and 1.4×10^{-9} cm^3 $molecule^{-1}$ s^{-1} for propyne and allene, respectively.[30,31]

ii. The $H_2O^+ + C_3H_4$ reaction is considered as a source of $C_3H_5^+$ and potentially $C_3H_4^+$ in line with the proton affinities of propyne (748 kJ/mol) and allene (775.3 kJ/mol) which are larger than the ones of OH (593.2 kJ/mol) and H_2O (691 kJ/mol).[32] The contribution of the $H_2O^+ + C_3H_4$ reaction to the BR of $C_3H_4^+$ is weak. As an illustration, the H_2O^+ ion signal drops by less than 5 % in the presence of neutral reactant with a density $[C_3H_4]$ of 6×10^{12} molecule cm^{-3}, meaning that H_2O^+ is not highly reactive with C_3H_4. In spite of its small contribution,

this effect is taken into account in the determination of the branching ratios of the N_2^+ + C_3H_4 reactions.

iii. According to Milligan et al., N_2H^+ reacts with C_3H_4 to form the $C_3H_5^+$ ion exclusively as it has been observed in FA-SIFDT experiments at 300 K [31]. The experimental rate coefficients are k = 1.5 and 1.4×10^{-9} cm^3 $molecule^{-1}$ s^{-1} and the corresponding reaction enthalpies are ΔH = -2.87 and -2.91 eV for propyne and allene, respectively.

iv. The NO^+ + C_3H_4 (propyne and allene) reactions have also been studied in SIFT experiments[30] at 298 K. Propyne only generates the $[C_3H_4{\square}NO]^+$ adduct with a rate coefficient of k = 6.3×10^{-11} cm^3 $molecule^{-1}$ s^{-1}, while the reaction with allene exhibits two exit channels corresponding to the $[C_3H_4{\square}NO]^+$ adduct (90%) and the $C_3H_3^+$ ion (10%). However, the rate coefficient k = 2.5×10^{-11} cm^3 $molecule^{-1}$ s^{-1} for the NO^+ + CH_2CCH_2 reaction is too low to be competitive here. The lack of a significant drop in the NO^+ signal at low temperatures (a few percent) and the absence of an ion signal at m/z=70 u allow to discard any interference from the NO^+ + C_3H_4 reactions.

v. Two SIFT experiments have been performed at room temperature to examine the O_2^+ + C_3H_4 (propyne and allene) reactions. Wilson et al. only observed the charge transfer reaction, i.e. $C_3H_4^+$ + O_2, with rate coefficients of k = 1.6 and 1.3×10^{-9} cm^3 $molecule^{-1}$ s^{-1} for propyne and allene respectively [30]. Dicker et al., also studied the O_2^+ + CH_2CCH_2 reaction and derived a rate coefficient k = 1.3×10^{-9} cm^3 $molecule^{-1}$ s^{-1}, but they observed three exit pathways: the charge transfer (94%), the $C_3H_3^+$ + HO_2 exit channel (4%) and the CH_2CO^+ + CH_2O one (2%) with calculated corresponding enthalpies ΔH = -2.39, -2.87 and -2.91 eV [34]. In the work of Wilson et al.[30], the presence of vibrationally excited O_2^+ ions was assumed. In the latter experiments of Decker et al.[34], this issue was considered and O_2 was added to quench the excited O_2^+ ions. This can explain the different results from the two SIFT experiments. Then, the $C_3H_4^+$ and $C_3H_3^+$ ions can also be formed by the O_2^+ + C_3H_4 reaction, this is considered in the branching ratio determination (see thereafter).

vi. For the C_3H^+ product, all the reaction enthalpies calculated in this work for the different exit channels of the N_2^+ + C_3H_4 reactions are positive (see Figure 2), suggesting that the observed C_3H^+ traces come from a secondary reaction between C_3H_4 and some impurities. These reactions do not affect the evolution of the N_2^+ density and therefore the derived rate coefficient of the studied reactions.

In order to qualitatively analyze the stoichiometry of the species observed in the mass spectra we performed a reduced theoretical analysis by calculating the enthalpies of formation and the corresponding relative reaction enthalpies by means of high level ab initio theories. The ab initio calculations were performed using the spin unrestricted coupled-cluster theory with single and double excitations (UCCSD) along with the augmented correlation-consistent valence double zeta (aug-cc-pVDZ) basis set. All calculations were carried out with the MOLPRO (version 2015.1) quantum chemistry software package[35,36]. The structure and energy properties of all molecular species were determined in their minimum configuration, i.e. following full geometry optimization. Various starting geometries were examined in order to find the structures and properties of the most stable $[N_2–C_3H_4]^+$ complexes. Harmonic vibrational frequency and normal mode calculations were performed to compute the zero-point vibrational energies (ZPVE) and the total enthalpies of formation. More details about the geometries and energies of the species are given in the Supplementary Material.

Figure 2 shows the schematic diagram of the relative reaction enthalpies for the observed hydrocarbon cations and a few other related ones. Since the experiments were carried out at various temperatures, the reaction enthalpies were calculated at 0 K only, i.e. taking into account the total electronic and zero point vibrational energies exclusively. Note that many more cyclic complexes exist but our analysis was limited to the two most stable $[N_2C_3H_4]^+$ ones.

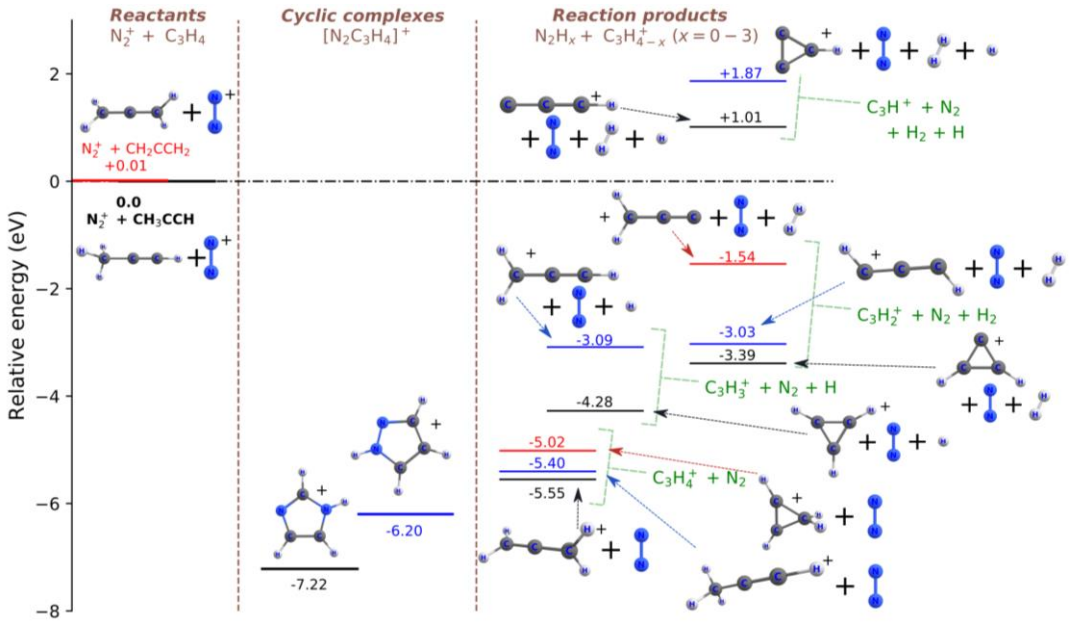

Figure 4.2: Schematic diagram of the $N_2^+ + CH_3CCH$ and $N_2^+ + CH_2CCH_2$ reaction enthalpies with the experimentally observed (or potential) formation channels of $C_3H_{4-x}^+$

(x = 0–3) ion products. The enthalpy of all species is calculated in the UCCSD/aug-cc-pVDZ framework, including ZPVE corrections. All energies are relative to separated N_2^+ and propyne (CH_3CCH) reactants.

Given the low temperatures of the experiments, the $N_2^+ + C_3H_4$ reactions can only form exoergic products i.e. $CH_2CCH_2^+$ and CH_3CCH^+ cations (pure charge transfer) as well as the different $C_3H_3^+$ and $C_3H_2^+$ isomers. According to our calculations the endoergic exit channels towards the C_3H^+ cations remain out of reach. As one can also see in Figure 2, the most exoergic $N_2C_3H_4^+$ species have a cyclic structure. The first of them (1H-imidazole cation) has a very large relative exoergicity of about -7.22 eV, while the second isomer (pyrazole cation) has a slightly higher relative enthalpy, with about -6.20 eV. Both of these cations are highly exoergic with respect to the reactants and the $C_3H_4^+$, $C_3H_3^+$ and $C_3H_2^+$ product formation channels. However, since the formation of these cyclic species implies strong re-orientations and multiple internuclear rearrangements which possibly involve many intermediate transition states, we expect that such $N_2C_3H_4^+$ complexes do not form effectively from the linear molecular reactants.

Charge transfer reactions (both dissociative and nondissociative), which lead to the formation of the observed $C_3H_4^+$, $C_3H_3^+$ and $C_3H_2^+$ products, most probably proceed via the formation of non-stable, quasi-bound complexes (i.e. complex with large intramolecular distance, in agreement with the capture theory), producing excited $C_3H_4^+$ cations preliminarily. These complexes are represented by close superposition of the colliding molecular species, where their bond lengths and angles are not distorted, but where the electron exchange from C_3H_4 towards N_2^+can effectively proceed, involving electronic transitions between multiple potential energy surfaces. This mechanism is supported by the Franck-Condon principle, according to which the electronic transitions proceed much faster than nuclear movements and rearrangements. If the primary cations are formed by conserving a large amount of internal energy, their dissociation proceeds according to a unimolecular decomposition scheme.

4.3.2 Rate coefficients. Kinetic data were obtained under pseudo-first order conditions, i.e. with a $[C_3H_4]$ neutral density in excess compared to the $[N_2^+]$ density. The loss rate of N_2^+ was determined by the evolution of the N_2^+ signal with time for a given neutral reactant density. The variation of the N_2^+ loss rates with the neutral reactant density gives the absolute

rate coefficient k(T) of the reaction at a fixed temperature, as illustrated in Figure 3 for N_2^+ + CH_2CCH_2 at 24 K. The results are summarized in Table 2.

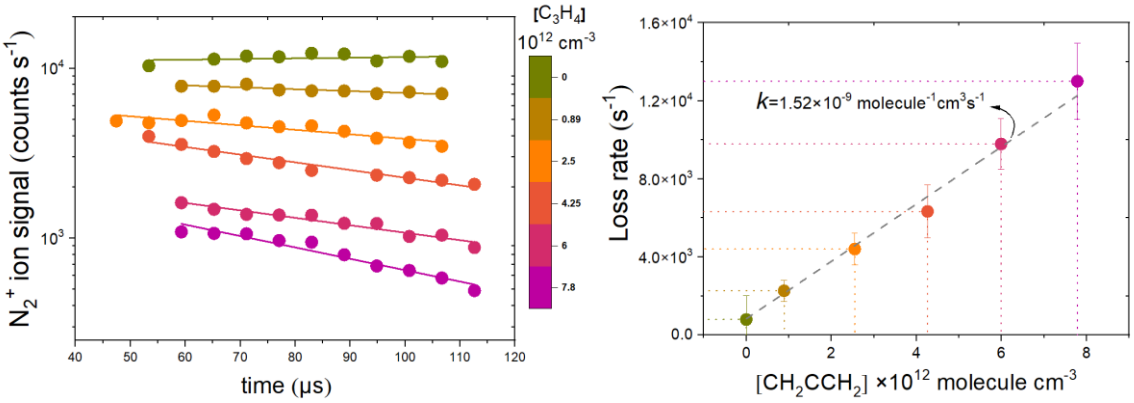

Figure 4.3: N_2^+ ion signal as a function of time for a range of neutral CH_2CCH_2 densities (left) and corresponding loss rates as a function of CH_2CCH_2 densities (right) at 24 K.

T (K)	24.1	36.1	49.1	57.0	71.6
N_2^+ + CH_3CCH	3.73 ± 0.41	3.4 ± 0.36	2.52 ± 0.34	2.39 ± 0.25	2.13 ± 0.21
N_2^+ + CH_2CCH_2	1.52 ±0.16		1.40 ±0.2		1.56 ±0.22

Table 2: Absolute rate coefficients k of the N_2^+ + CH_3CCH and N_2^+ + CH_2CCH_2 reactions measured with the CRESU-SIS device at different temperatures in $\times 10^{-9}$ cm^3 $molecule^{-1}$ s^{-1} unit. The uncertainties take into account statistical and systematic (10%) contributions.

For N_2^+ + CH_2CCH_2, the rate coefficients show a quasi-independence with temperature. The measured values are in good agreement with the Langevin value of $k_L=1.38\times10^{-9}$ cm^3 $molecule^{-1}$ s^{-1} estimated from $k_L=2\pi e\sqrt{\alpha/\mu}$, where e is the elementary charge, α the static dipole polarizability of the neutral molecule ($\alpha_{CH2CCH2}$= 5.69 $Å^3$ from Ref. [37]), and μ the reduced mass of ion-molecule system. For N_2^+ + CH_3CCH, the Langevin model is not suitable since the permanent dipole moment μ_D of the neutral reactant is not considered. For a polar neutral reactant, the Su and Chesnavich model[38] gives a rate coefficient $k_{SC} = K_{cap} \times k_L$ which is temperature dependent with $K_{cap} = 0.4767x + 0.6200$ when $x = \frac{\mu D}{\sqrt{2\alpha T k_B}} \geq 2$. Considering the dipole moment of propyne (μ_D=0.784 D)[39] and its polarizability

(α_{CH3CCH}= 5.55 Å^3)[40], we determined for all the temperatures a value of the x parameter greater than 2 for the studied N_2^+ + CH_3CCH reaction. Then the estimated values of the rate coefficients from the Su and Chesnavich model are k_{SC}=3.49, 3.01, 2.70, and 2.38×10^{-9} cm^3 molecule^{-1} s^{-1} at 24, 36, 49, and 71.6 K respectively. Figure 4, which displays the experimental values obtained in this work and the estimated values obtained from the simple capture models of Langevin and Su and Chesnavich, illustrates their remarkable agreement.

Several arguments concur to rule out termolecular processes for the N_2^+ + C_3H_4 reactions. First, no peak at m/z= 68 u, corresponding to the association product, is detected in the mass spectra. Second, the rate coefficient of the N_2^+ with CH_3CCH reaction is not affected by changing the buffer gas, i.e. pure helium at 49.1 K and helium-nitrogen mixture (1:1) at 57 K. Thirdly, an increase of the total density or a decrease of the temperature both lead to a rise of the rate coefficient in a termolecular process; yet the measured rate coefficients for propyne and allene follow closely the Su and Chesnavich and the Langevin models, respectively (see Figure 4), including between 24.1 K and 36.1 K where the total density is changed by more than 3-fold (18.3□10^{16} and 5.28□10^{16} molecule cm^{-3}, respectively). This set of observations strongly supports a bimolecular process only.

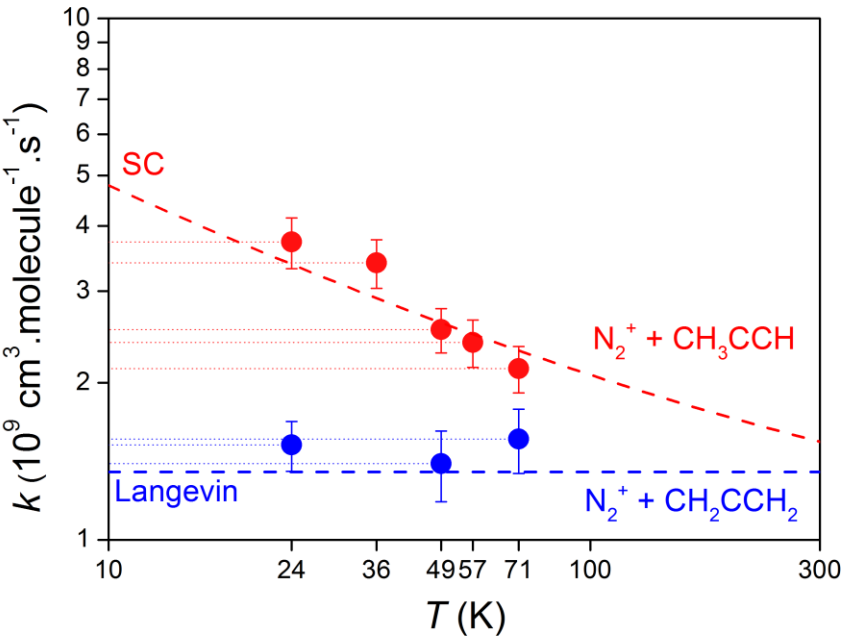

Figure 4.4: Comparison between the measured absolute rate coefficients k as a function of temperature for the N_2^+ with CH_3CCH (red filled circles) and CH_2CCH_2 (blue filled circles)

reactions and the Langevin (blue dashed line) and Su & Chesnavich (red dashed line) models.

4.3.3 Branching ratios The $C_3H_2^+$, $C_3H_3^+$ and $C_3H_4^+$ ions are clearly identified as the primary products of the N_2^+ + CH_3CCH / CH_2CCH_2 reactions. The enthalpies of the N_2^+ + C_3H_4 reactions producing C_3H^+ are positive and the formation of $C_3H_5^+$ is well explained by the reactions between N_2^+ with impurities. As mentioned above as well, the O_2^+ + C_3H_4 reaction represents however a small but non-negligible source (up to a few percent) of $C_3H_3^+$ and $C_3H_4^+$ ions, even if the initial abundance of N_2^+ ions is much higher—by a factor of 16—than the abundance of O_2^+. In order to determine accurate branching ratios for the N_2^+ + C_3H_4 reactions, we have also explored the low-temperature reactivity of O_2^+ with propyne and allene with our CRESU-SIS experimental setup—the results will be presented in detail in an upcoming publication. In this case, the detected products are $C_3H_3^+$, $C_3H_4^+$, and $C_2H_2O^+$ (with branching ratios $\alpha(T)$, $\beta(T)$, and $\chi(T)$, respectively), in agreement with Decker et al.'s observations for allene at 300 K. The small contributions of the O_2^+ + C_3H_4 reactions measured while studying the N_2^+ + CH_3CCH / CH_2CCH_2 reactions were eliminated by subtracting $\alpha(T)\times\Delta O_2^+$ and $\beta(T)\times\Delta O_2^+$ to each of the $C_3H_3^+$ and $C_3H_4^+$ integrated peaks, respectively, with ΔO_2^+ representing the decrease of the O_2^+ ion signal.

The apparent BRs for the three exit channels $C_3H_2^+$, $C_3H_3^+$ and $C_3H_4^+$, corrected to eliminate the contributions of the O_2^+ + C_3H_4 reactions, are shown in Figure 5 as a function of [C_3H_4] density in the case of propyne at 49 K. The values vary slightly and linearly with the [C_3H_4] density, due to secondary reactions of the primary ion products with C_3H_4. To limit the contribution of those reactions, the BRs were determined at short reaction times and by extrapolating their values for a null [C_3H_4] density = 0 (y-intercept of the linear fit).

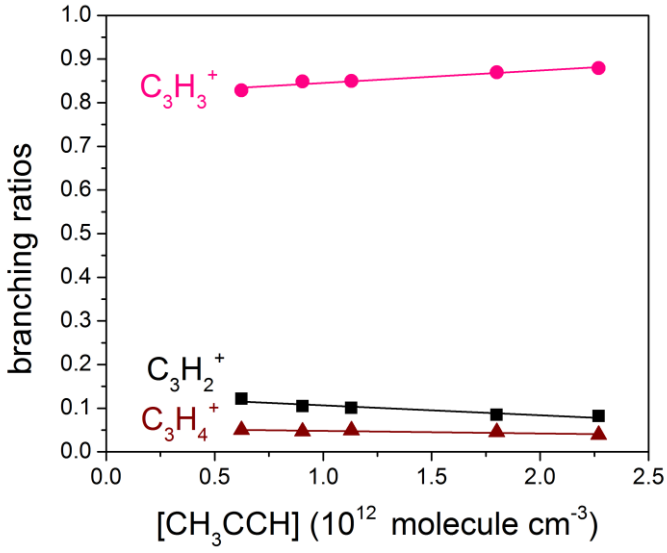

Figure 4.5: Evolution of the branching ratios (BRs) with the [CH_3CCH] density, measured at 49 K for a reaction time of 56 μs. The BRs are corrected to eliminate the contribution of the $O_2^+ + C_3H_4$ reaction.

The BRs of the studied reactions and their temperature dependence, obtained after correction for the $O_2^+ + C_3H_4$ reaction contributions and extrapolation to a null [C_3H_4] density, are shown in Figure 6 and summarized in Table 4. For both reactions, the BR of the main exit channel leading to $C_3H_3^+$ decreases as the temperature decreases, while no significant variation is observed for the other dissociative $C_3H_2^+$ exit channel. Hence, a small yet significant increase of the BR associated with the nondissociative charge transfer reaction leading to $C_3H_2^+$ is observed.

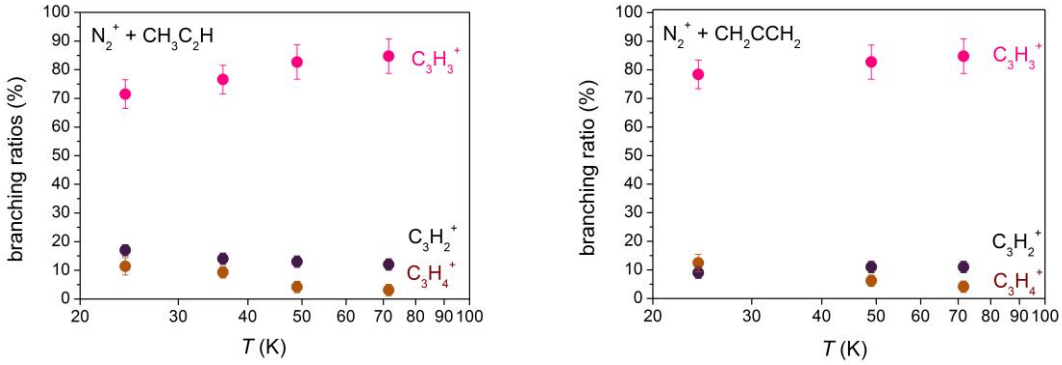

Figure 4.6: Temperature dependence of the branching ratios between the primary products of $N_2^+ + CH_3CCH$ (left) and $N_2^+ + CH_2CCH_2$ (right) reactions. The error bars were estimated by adding systematic (±0.02) and statistical (±5%) contributions.

	CH_3CCH				CH_2CCH_2			
T (K)	24.1	36.1	49.0	71.6	24.1	36.1	49.0	71.6
$C_3H_2^+$	0.17	0.14	0.13	0.12	0.09	-	0.11	0.11
$C_3H_3^+$	0.72	0.77	0.83	0.85	0.785	-	0.83	0.85
$C_3H_4^+$	0.11	0.09	0.04	0.03	0.125	-	0.06	0.04

Table 4.4: Branching ratios of the reactions of N_2^+ with the two C_3H_4 isomers at 24.1, 36.1, 49.0 and 71.6 K. These values take into account the natural isotopic abundance of carbon 13.

4.4. Discussion

4.4.1 Reaction dynamics To better understand the outcomes of the title reactions, we first invoke the reaction of Ar^+ with ethylene C_2H_4 studied in a flowing-afterglow apparatus by Tsuji et al. [41], as Ar^+ is only slightly more energetic than N_2^+ (recombination energy of 15.76 eV for Ar^+ versus 15.58 eV for N_2^+). The reported branching was 0.76:0.20:0.04 for $C_2H_2^+$:$C_2H_3^+$:$C_2H_4^+$. The $C_2H_2^+$:$C_2H_3^+$ ratio was found to increase further while increasing the internal energy of $C_2H_4^+$. From these measurements it was inferred that 95% of the CT excess energy is released into internal energy of the $C_2H_4^+$ ion before its decomposition. The authors concluded that the reaction proceeds via two competing mechanisms:

i. A near-resonant, dissociative CT occurring at long range without significant momentum transfer. This mechanism is dominant and leads to the formation of $C_2H_2^+$ and $C_2H_3^+$. It involves nonadiabatic transitions between charge states of $N_2^+ + C_2H_4$ and $N_2 + C_2H_4^+$, which populate some of the $C_2H_4^+$ excited electronic states.

ii. A nonresonant, nondissociative CT occurring via an “intimate collision” that enables significant momentum transfer. This mechanism is responsible for the $C_2H_4^+$ product, which

is formed with less internal energy when compared to dissociative CT and therefore cannot decompose.

In the case of reactions of N_2^+ with hydrocarbons, Gichuhi and Suits have measured the product branching for the reactions of N_2^+ with methane CH_4, acetylene C_2H_2, and ethylene C_2H_4 at 40 K using a modified velocity map imaging apparatus.[42] The reaction with acetylene was found to form only $C_2H_2^+$ via nondissociative CT, while the reaction products for the reaction with ethylene led to the formation of $C_2H_2^+$ and $C_2H_3^+$ whereas no $C_2H_4^+$ was observed, suggesting that this reaction proceeds only via the near-resonant dissociative mechanism. Interestingly, the branching of 0.76:0.24 is remarkably close to the one measured for the $Ar^+ + C_2H_4$ reaction.

In light of these previous results, the two CT mechanisms (dissociative and nondissociative) are likely responsible for the outcomes of the reactions studied here, although a careful mapping of the potential energy surfaces of the $N_2^+ + C_3H_4$ system would be necessary to fully validate this assumption. The measured rate coefficients, which are all collisional, indeed suggest that these fast reactions take place at long range via CT. The CT can deposit more than 5 eV of internal energy in the $C_3H_4^+$ precursor (based on the NIST Chemistry WebBook, the CT between N_2^+ and propyne releases 5.22 eV; the CT between N_2^+ and allene releases 5.89 eV). $C_3H_4^+$ can then undergo rapid internal conversion to the ground state and possibly rearrange before the cleavage of C-H bonds occurs. The potential energy diagram of $C_3H_4^+$, adapted from Mebel and Bandrauk [43], is shown in Figure 7. The lowest-energy dissociation channel leads to cyclopropenyl c-$C_3H_3^+$ + H, with an energy of 1.68 eV and a transition state (TS) at 1.87 eV above $CH_2CCH_2^+$, i.e. about one third of the total excess energy. This pathway implies the rearrangement of $CH_2CCH_2^+$ and CH_3CCH^+ into c-$C_3H_4^+$ prior dissociation. The pathway leading to l-$C_3H_3^+$ + H is barrierless and the exit channel lies 2.84 eV above $CH_2CCH_2^+$—about one half of the available energy. At similar energies lie the two lowest-energy H_2 loss channels, namely CH_3CCH^+ □ $HCCCH^+ + H_2$ (2.79 eV, TS at 2.93 eV), and c-$C_3H_4^+$ □ c-$C_3H_2^+ + H_2$ (2.56 eV, no TS found). The only other exit channel energetically accessible after CT with N_2^+ is the loss of H_2 from $CH_2CCH_2^+$, (4.39 eV, no TS found) which requires more than two thirds of the excess energy to be funneled into.

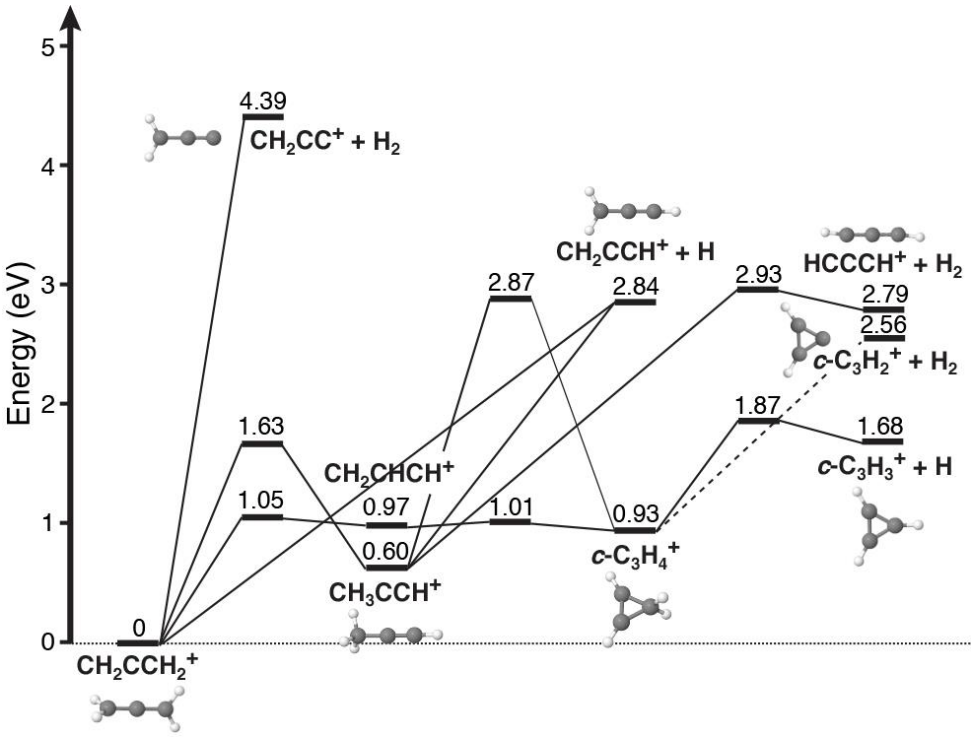

Figure 4.7: Potential energy diagram of the ground state of $C_3H_4^+$, adapted from Mebel and Bandrauk[43]. Energies were calculated at the CCSD(T)/cc-pVTZ//B3LYP/6-311G** level of theory and are shown relative to the global minimum, the allene cation $CH_2CCH_2^+$. All the dissociation channels accessible for the ion precursor after charge transfer with N_2^+, which can deposit up to 5.89 eV into $C_3H_4^+$, are reported. Note that no transition states were found for the H_2 loss channels from $CH_2CCH_2^+$ and c-$C_3H_4^+$—dashed lines connect these stationary points.

These energy considerations are fully in line with the measured branching ratios. Previous experimental work on the unimolecular decomposition of $CH_2CCH_2^+$ and CH_3CCH^+ have shown that the main isomer formed is cyclic $C_3H_3^+$,[44–46] corresponding to the lowest-energy dissociation channel on the $C_3H_4^+$ potential energy surface. Liu et al.[47] investigated theoretically the isomerization barrier to form c-$C_3H_3^+$ from linear propargylium H_2CCCH^+ at the QCISD(T)/6-311+G(d,p)//B3LYP/6-31G(d) level of theory. They reported a direct pathway with a 3.8 eV barrier and a pathway through TS – intermediate – TS with a 2.1 eV barrier, both well above the relative enthalpy of 1.1 eV. In case of an internally highly excited $C_3H_4^+$ cation, both cyclic and linear $C_3H_3^+$ isomers may form via unimolecular decomposition processes. The allene and propyne cations formed in electronic/vibronic

excited states via CT might not necessarily dissociate following the lowest energy pathway, as e.g. pointed out in a work on the photoabsorption and photoionization of propyne[46]. The examination of unimolecular decomposition process which has guided part of our analysis so far may provide some further hints. In the absence of quantitative determination of branching ratios between isomers from photoionization, one can turn to electron-impact ionization studies. Infrared spectroscopic measurements conducted by Brünken et al.[48] showed that electron-impact ionization of allene CH_2CCH_2 leads to the dominant production of the cyclic $C_3H_3^+$ isomer (81%) over the linear one (19%) and that the isomeric ratio is independent of the electron energy over the 14-70 eV range. Only a fraction of the energy of the colliding electron will effectively contribute to ionize and excite the molecule as most of it will be carried away with the electron itself after the encounter, since elastic electron scattering cross sections are typically orders of magnitude higher compared to the inelastic ones at such energies (see, e.g. Ref. [49]). The ionization process will take away the amount of energy corresponding to the adiabatic ionization potential of the target, allene, which is 9.7 eV and the remaining excess energy will be deposited as internal energy for the cations. Considering the electron energy range covered, one could expect that typically only a few of eV (see subsection 2.4 in Ref. [50]) ends up in internal energy of the molecular target. Then, although direct photoionization and electron-impact ionization differ, one can expect a similar trend, supporting the hypothesis of a cyclic product to dominate. According to the energy diagram, this should also hold in the case of propyne.

The formation of less prominent $C_3H_2^+$ is thought to occur directly from the CH_3CCH^+ structure—note that we observed slightly more $C_3H_2^+$ with propyne than with allene. The cyclic isomer of $C_3H_2^+$ is also accessible, possibly without a barrier, but both these channels are not expected to contribute significantly.

The temperature dependence of the branching ratios gives further insights into these two competing CT mechanisms. While it has been shown previously that the near-resonant dissociative CT is largely independent of collision energy,[51] the nondissociative CT mechanism is not. Here, the slight but consistent increase of the yield toward $C_3H_4^+$ with decreasing temperature, associated with nonresonant, nondissociative CT for both target hydrocarbons, simply reflects the greater probability to form a bound complex at low collision energy, even after the long-range CT deposited such internal energy into $C_3H_4^+$. Since the electron transfer processes are mainly driven by nonadiabatic couplings at long range, a quantitative explanation for this mechanism cannot be provided as the treatment of

such complex processes is out of the scope of the present work. However, we can expect that, at lower collision energies, the charge transfer mechanisms lead to $C_3H_4^+$ cations with less internal energy and higher kinetic energy, which can be observed in the mass spectra as well. At higher temperatures, the primary $C_3H_4^+$ cation is formed with more internal energy which may effectively initiate a unimolecular decomposition into smaller species. Respectively, higher branching ratios are expected for the $C_3H_3^+$ and $C_3H_2^+$ products with less amount of $C_3H_4^+$ in this case.

4.4.2 $C_3H_3^+$ in Titan's atmosphere Latest models coupling ion and neutral chemical networks [10,19], supported by Cassini observations, have simulated the vertical density profile of many ionized and neutral organics in Titan's atmosphere. In terms of mole fraction, ionized species concentrate in the ionosphere spanning the 700-1400 km altitude range, where ionic processes play a key part in the chemistry [19] and in the formation of heavy molecules acting as aerosol embryos [52]. The generative or destructive role of ions is however not restricted to charged species and can notably include the production of neutrals, in particular through dissociative recombination. At an altitude of 1000 km, the most abundant hydrocarbons ions are $C_2H_5^+$, $C_3H_3^+$, $C_3H_5^+$ followed by CH_5^+, $C_5H_5^+$ and $C_5H_7^+$ [53]. Among them, the $C_3H_3^+$ ion possesses two isomers, which cannot be observationally distinguished: the most energetically stable aromatic cyclopropenyl cation c-$C_3H_3^+$ and the linear propargyl cation l-$C_3H_3^+$. The major loss process of ionic aromatic species in Titan's atmosphere is commonly considered to be dissociative recombination. Recent photochemical models [11,48] confirm that (neutral) benzene is mainly generated in the thermosphere by ion chemistry and Loison et al. note that the large abundance of C_6H_6 in the upper atmosphere is not the result of efficient formation pathways, but instead is due to the fact that once generated, the aromatic ring is preserved from photodissociation in the upper atmosphere.[19] The major loss process for c-$C_3H_3^+$ in Titan's atmosphere was also formally identified as dissociative recombination, leading to the formation of c-C_3H_2 or c-C_3H [10]. In the work of McEwan et al. [55], the authors pointed to the probable presence c-C_3H_2 and encouraged its search. Two years ago, the smallest cyclic hydrocarbon cyclopropenylidene c-C_3H_2 was effectively discovered in Titan by Nixon et al. with the help of the Atacama Large Millimeter/sub-millimeter Array (ALMA) radiotelescope, hence confirming this prediction.[56]

4.4.3 Chemical reactivity of $C_3H_3^+$ The reactivity of the $C_3H_3^+$ cation was investigated in the mid-90's in the laboratory at room temperature by employing a low pressure ICR trap (□10^{-6} mbar) [55,57] and high-pressure SIFT methods (□ mbar) [55,58,59]. The linear isomer of

$C_3H_3^+$ appears to be significantly more reactive with hydrocarbons than the cyclic isomer of $C_3H_3^+$, due to a greater efficiency in forming a long-lived intermediate and also because the latter is more energetically stable. At high pressure or when the trapping time is long enough, this intermediate complex can be stabilized faster by collisions leading to larger rate coefficients such for the $C_3H_3^+ + CD_4$, C_2H_2 and C_2H_4 reactions where the ionic adduct have been observed. For instance, the reactions between l-$C_3H_3^+$ and several small hydrocarbons of interest for Titan as C_2H_2, C_2H_4, C_3H_4 (allene and propyne) and C_3H_6 were measured with rate coefficients around 10^{-9} cm^3 $molecule^{-1}$ s^{-1} in SIFT or ion trap experiments at room temperature, which is close to the Langevin rate constant. In summary, laboratory works evidenced the low chemical reactivity of the c-$C_3H_3^+$ ion, making it a terminal species of the chemical network.

4.4.4 Formation pathways of $C_3H_3^+$ in photochemical models The formation route of this carbocation is not completely secured. Recent photochemical models favor the ion – molecule reactions to form $C_3H_3^+$ because the radiative association of C_3H^+ with H_2 to form $C_3H_3^+$, a process which takes place in the interstellar cloud, presents a very low rate (below or around 10^{-12} cm^3 $molecule^{-1}$ s^{-1}). These ion – molecule reactions mainly lead to the formation of the most stable cyclic c-$C_3H_3^+$. In the work of Ali et al., a combination of calculations and experiments leads to the conclusion that under low temperature and pressure conditions of Titan's atmosphere, the hydrocarbon chemistry could play a fundamental role in the synthesis of organic compounds. The $CH_3^+ + C_2H_2$ or C_2H_4 reactions generate the $C_3H_5^+$ ion which is followed by monomolecular decomposition yielding the cyclopropenyl cation c-$C_3H_3^+$ [60]. In others recent models, key ion – molecule reactions involve the three most abundant ions, $C_2H_5^+$, $C_2H_4^+$ and CH_3^+ with a density of above 10 cm^{-3} (420, 120 and 31 cm^{-3} respectively at 1125 km) and neutral acetylene C_2H_2, one of the most abundant hydrocarbons with a peak molar fraction around 3.1×10^{-4} at 1077 km. These bimolecular reactions are:

$$C_2H_5^+ + C_2H_2 \rightarrow c\text{-}C_3H_3^+ + CH_4 \qquad \text{Eq. (4.5)}$$

$$C_2H_4^+ + C_2H_2 \rightarrow c\text{-}C_3H_3^+ + CH_3 \qquad \text{Eq. (4.6)}$$

$$CH_3^+ + C_2H_2 \rightarrow c\text{-}C_3H_3^+ + H_2 \qquad \text{Eq. (4.7)}$$

with rate coefficients (in cm^3 $molecule^{-1}$ s^{-1} units) of 6.84×10^{-11}, 6.47×10^{-10} for the reactions (5) and (6) in the Vuitton et al. [10] and Dobrijevic et al. [19] models and 2.88×10^{-10} for the reaction (7) in the Vuitton et al. work and 1.15×10^{-9} for the global reaction $CH_3^+ + C_2H_2$ in

the Dobrijevic et al. study. Despite the same molar fraction as C_2H_2, ethylene C_2H_4 (for which the INMS detection cannot be easily distinguished from that of C_2H_2 [15]) is not considered as a possible source of c-$C_3H_3^+$ through the $C_2H_5^+$, $C_2H_4^+$, $CH_3^+ + C_2H_4$ reactions. Indeed, at the exception of an ICR study of the $C_2H_4^+ + C_2H_4$ reaction for which the $C_3H_3^+$ product has been observed [61], the numerous theoretical and experimental studies all conclude that the $C_2H_4^+ + C_2H_4$ and $C_2H_5^+ + C_2H_4$ reactions do not form the $C_3H_3^+$ product [62]. In contrast, C_2H_4 can react with CH_3^+ to preferentially produce the c-$C_3H_3^+$ isomer through the monomolecular decomposition of $C_3H_5^+$ but this reaction is not a preferred pathway due to its low rate coefficient (the experimental value obtained by ICR measurements is 9.2×10^{-10} cm^3 $molecule^{-1}$ s^{-1}) and its branching ratio leading to the $C_3H_3^+$ formation (5%) [62]. At last, the fourth most abundant ion $C_2H_3^+$ with a density around 14 cm^{-3} at 1125 km[10], reacting with C_2H_2 or C_2H_4 doesn't form $C_3H_3^+$ [62].

4.4.5 $N_2^+ + C_3H_4$: a new pathway to form c-$C_3H_3^+$ in Titan's ionosphere? Among all the detected hydrocarbon species, the two isomers of C_3H_4 have been included in several photochemical models [10,18,19,63]. Their total abundance is comparable to C_2H_2 and surpasses the one of the other considered C_3 hydrocarbons. In the coupled ion-neutral photochemical model of Vuitton et al. [10], the abundances of propyne CH_3-C_2H and allene CH_2CCH_2 peak in the upper atmosphere with very similar calculated maximum mole fractions, e.g. of 1.5×10^{-5} and 1.8×10^{-5} cm^{-3} at 1075 km. Their combined contribution (3.3×10^{-5} molecule cm^{-3}) falls in between the uncorrected ($6.31\pm0.24\times10^{-6}$ molecule cm^{-3}) and corrected ($1.4\pm0.9\times10^{-4}$ molecule cm^{-3}) mole fractions from INMS [15,53]. Around the same altitude, from both Dobrijevic et al. [19] and Vuitton et al. [10] photochemical models, the N_2^+ abundance peaks at around 50 cm^{-3} (around 1100 km) for the first model and at 37 cm^{-3} (1125 km) for the second one which is the same order of magnitude as the CH_3^+ density. The concentration of this primitive photolysis product cannot however be directly established by mass spectrometry because of the overlap with $HCNH^+$ considered to be 40 times more abundant and in a lesser extent with $C_2H_4^+$.

Our work combining laboratory experiments and theoretical considerations (see the energetic landscape of the Figure 7) shows that the reaction of N_2^+ with both C_3H_4 isomers generates dominantly c-$C_3H_3^+$ ions over the low temperature range explored (T= 24 -71.6 K) and to a lesser extent the $C_3H_2^+$ and $C_3H_4^+$ cations. The nature of the $C_3H_2^+$ isomer remains elusive considering our incomplete understanding of the energetic landscape. However, given the low efficiency of the $C_3H_2^+$ and $C_3H_4^+$ exit channels, their inclusion in

the chemical network will affect only marginally the overall chemical setting. The story is not the same for the cyclopropenyl c-$C_3H_3^+$ cation. Its reaction enthalpy is lower than that of l-$C_3H_3^+$ by 1.19 eV, and these isomers are protected from isomerization with a significant barrier of at least 2.17 eV. [48] In a warmer environment, such as the one characterizing Titan's atmosphere above 800 km in which the gas temperature reaches 150 K, we can reasonably assume that the branching ratio into the c-$C_3H_3^+$ channel will be similar. Since the exoergicity is large, the additional energy corresponding to a temperature rise from 70 to 150 K should not allow populating much more levels. The branching ratio into $C_3H_3^+$ measured at 70 K of 0.85 can be then considered as a lower limit. Based on these premises and on the reported channel-specific reaction rate (see above) the reaction of N_2^+ with C_3H_4 isomers may participate in the production of c-$C_3H_3^+$.

To evaluate the possible contribution of this pathway to the formation of c-$C_3H_3^+$ we included the evaluated reaction rates within a photochemical model of Titan's atmosphere[64] that has been updated with the latest chemical network coupling ion and neutral chemistry from Vuitton et al. [10]. Our calculations suggest that the N_2^+ + CH_3C_2H/CH_2CCH_2 contribution has a secondary role compared to the dominant production terms from the reactions of $C_2H_4^+$ and $C_2H_5^+$ with acetylene (Figure 8). At the production peak near 1125 km, the cumulative contribution of the N_2^+ + C_3H_4 channels (dashed black line) is comparable to other secondary production pathways such as from reaction of CH_2^+ with C_2H_2 and CH_3^+ with C_2H_2, C_2H_4 and HC_3N. However, at its maximum contribution the N_2^+ pathway is ~40x lower than the total production rate (solid black line), while its column integrated contribution is about 2% of the total column production above 600 km.

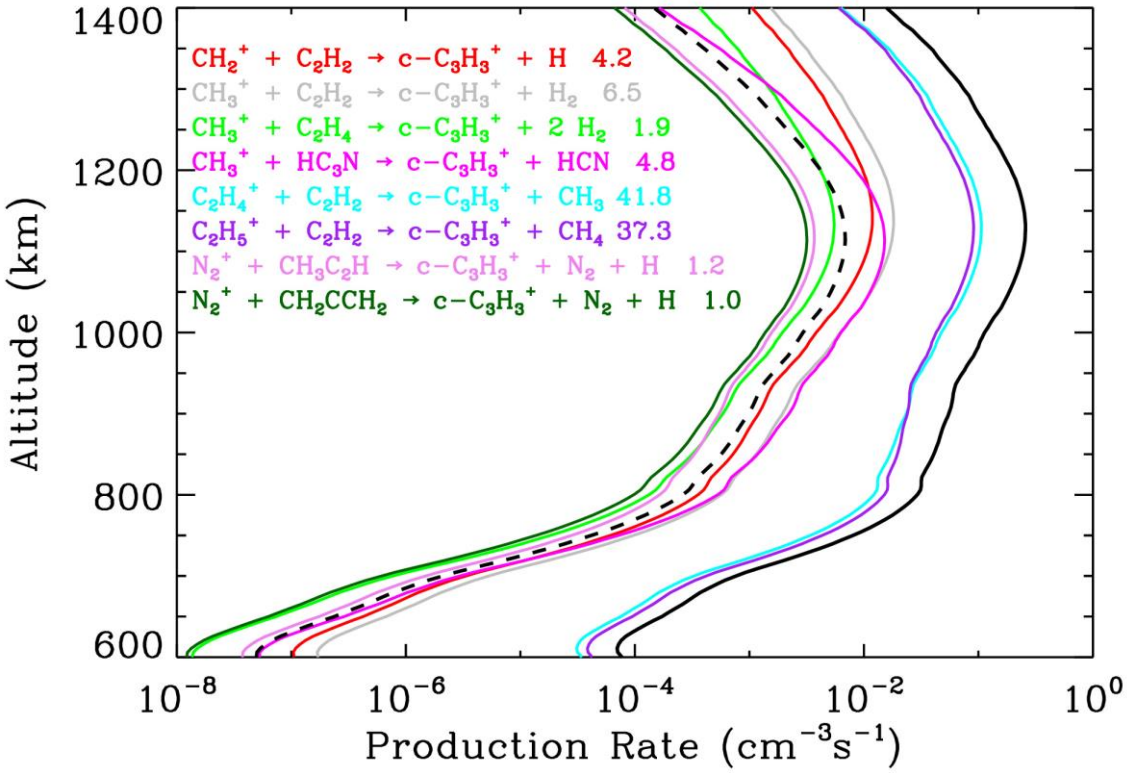

Figure 4.8: Contribution of different chemical pathways to the production of c-$C_3H_3^+$ in Titan's upper atmosphere. The indicated values represent the percentage contributions of each reaction to the total column production rate above 600 km.

4.5 Conclusion

The rate coefficients and the branching ratios for the reactions of N_2^+ with propyne (CH_3CCH) and allene (CH_2CCH_2) have been experimentally determined at 24, 36, 49 and 71.6 K using the CRESU-SIS apparatus. All measured rate coefficients are large, agreeing with the classical capture models of Langevin (for allene) and Su and Chesnavich (for propyne). Three primary products $C_3H_2^+$ (m/z=38 u), $C_3H_3^+$ (m/z=39 u), $C_3H_4^+$ (m/z=40 u), have been observed even if their isomers are indistinguishable in our present experimental setup. High-level ab initio calculations have been performed, which allowed to qualitatively analyze in many details the possible reaction pathways. Three exothermic exit pathways have been identified for the two studied reactions. The pure charge transfer is the most exothermic exit channel, while the two others correspond to dissociative charge transfer pathways leading to the $C_3H_3^+$ and $C_3H_2^+$ products. These three exit channels have been observed, the main one corresponding to the

$C_3H_3^+$ formation. The theoretical exploration of the pure charge transfer mechanism provides an explanation of the temperature dependence of the $C_3H_4^+$ ion formation. The theoretical analysis also helped in the interpretation of the differences in relative reaction probabilities.

Our results indicate that the reaction of N_2^+ with both isomers of C_3H_4 generates primarily the cyclic form of $C_3H_3^+$. The low-reactivity of this isomer makes its presence likely in Titan's atmosphere. Our evaluation on Titan's atmospheric photochemistry suggests that the contribution of this pathway to the formation of cyclic $C_3H_3^+$ is however of secondary importance relative to other pathways.

This work confirms the ability of the experimental approach (mass-selective ion source to inseminate uniform supersonic flows) in providing temperature-dependent branching ratios of bimolecular ion-molecule reactions. Future experiments will focus on the reactivity of key molecular ions for astrophysical environments such as CH_3^+ and whose neutral counterparts are not available off the shelf. Although the reaction rates and branching ratios are available for a large selection of ion-molecule reactions, mostly at room temperature, large discrepancies between reported values persist and temperature dependence studies remain rare.

References

(1) Niemann, H. B.; Atreya, S. K.; Bauer, S. J.; Carignan, G. R.; Demick, J. E.; Frost, R. L.; Gautier, D.; Haberman, J. A.; Harpold, D. N.; Hunten, D. M.; Israel, G.; Lunine, J. I.; Kasprzak, W. T.; Owen, T. C.; Paulkovich, M.; Raulin, F.; Raaen, E.; Way, S. H. The Abundances of Constituents of Titan's Atmosphere from the GCMS Instrument on the Huygens Probe. Nature **2005**, 438 (7069), 779–784.

(2) Thelen, A. E.; Nixon, C. A.; Chanover, N. J.; Cordiner, M. A.; Molter, E. M.; Teanby, N. A.; Irwin, P. G. J.; Serigano, J.; Charnley, S. B. Abundance Measurements of Titan's Stratospheric HCN, HC_3N, C_3H_4, and CH_3CN from ALMA Observations. Icarus **2019**, 319, 417–432. https://doi.org/10.1016/j.icarus.2018.09.023.

(3) Marten, A.; Hidayat, T.; Biraud, Y.; Moreno, R. New Millimeter Heterodyne Observations of Titan: Vertical Distributions of Nitriles HCN, HC_3N, CH_3CN, and the Isotopic Ratio $^{15}N/^{14}N$ in Its Atmosphere. Icarus **2002**, 158 (2), 532–544. https://doi.org/10.1006/icar.2002.6897.

(4) Coustenis, A.; Salama, A.; Schulz, B.; Ott, S.; Lellouch, E.; Encrenaz, T. h; Gautier, D.; Feuchtgruber, H. Titan's Atmosphere from ISO Mid-Infrared Spectroscopy. Icarus **2003**, 161 (2), 383–403. https://doi.org/10.1016/S0019-1035(02)00028-3.

(5) Rengel, M.; Sagawa, H.; Hartogh, P.; Lellouch, E.; Feuchtgruber, H.; Moreno, R.; Jarchow, C.; Courtin, R.; Cernicharo, J.; Lara, L. M. Herschel/PACS Spectroscopy of Trace Gases of the Stratosphere of Titan. A&A **2014**, 561, A4. https://doi.org/10.1051/0004-6361/201321945.

(6) Coustenis, A.; Achterberg, R. K.; Conrath, B. J.; Jennings, D. E.; Marten, A.; Gautier, D.; Nixon, C. A.; Flasar, F. M.; Teanby, N. A.; Bézard, B.; Samuelson, R. E.; Carlson, R. C.; Lellouch, E.; Bjoraker, G. L.; Romani, P. N.; Taylor, F. W.; Irwin, P. G. J.; Fouchet, T.; Hubert, A.; Orton, G. S.; Kunde, V. G.; Vinatier, S.; Mondellini, J.; Abbas, M. M.; Courtin, R. The Composition of Titan's Stratosphere from Cassini/CIRS Mid-Infrared Spectra. Icarus **2007**, 189 (1), 35–62. https://doi.org/10.1016/j.icarus.2006.12.022.

(7) Maltagliati, L.; Bézard, B.; Vinatier, S.; Hedman, M. M.; Lellouch, E.; Nicholson, P. D.; Sotin, C.; de Kok, R. J.; Sicardy, B. Titan's Atmosphere as Observed by Cassini/VIMS Solar Occultations: CH_4, CO and Evidence for C_2H_6 Absorption. Icarus **2015**, 248, 1–24. https://doi.org/10.1016/j.icarus.2014.10.004.

(8) Koskinen, T. T.; Yelle, R. V.; Snowden, D. S.; Lavvas, P.; Sandel, B. R.; Capalbo, F. J.; Benilan, Y.; West, R. A. The Mesosphere and Lower Thermosphere of Titan Revealed by Cassini/UVIS Stellar Occultations. Icarus **2011**, 216 (2), 507–534. https://doi.org/10.1016/j.icarus.2011.09.022.

(9) Waite, J. H.; Niemann, H.; Yelle, R. V.; Kasprzak, W. T.; Cravens, T. E.; Luhmann, J. G.; McNutt, R. L.; Ip, W.-H.; Gell, D.; De La Haye, V.; Müller-Wordag, I.; Magee, B.; Borggren, N.; Ledvina, S.; Fletcher, G.; Walter, E.; Miller, R.; Scherer, S.; Thorpe, R.; Xu, J.; Block, B.; Arnett, K. Ion Neutral Mass Spectrometer Results from the First Flyby of Titan. Science **2005**, 308 (5724), 982–986. https://doi.org/10.1126/science.1110652.

(10) Vuitton, V.; Yelle, R. V; Klippenstein, S. J.; Hörst, S. M.; Lavvas, P. Simulating the Density of Organic Species in the Atmosphere of Titan with a Coupled Ion-Neutral Photochemical Model. Icarus **2019**, 324, 120–197. https://doi.org/10.1016/j.icarus.2018.06.013.

(11) McEwan, M. J.; Anicich, V. G. Titan's Ion Chemistry: A Laboratory Perspective. Mass Spectrometry Reviews **2007**, 26 (2), 281–319. https://doi.org/10.1002/mas.20117.

(12) Dutuit, O.; Carrasco, N.; Thissen, R.; Vuitton, V.; Alcaraz, C.; Pernot, P.; Balucani, N.; Casavecchia, P.; Canosa, A.; Picard, S. L.; Loison, J.-C.; Herman, Z.; Zabka, J.; Ascenzi, D.; Tosi, P.; Franceschi, P.; Price, S. D.; Lavvas, P. Critical Review of N, N^+ , N_2^+, N^{++}, and N_2^{++} Main Production Processes and Reactions of Relevance to Titan's Atmosphere. ApJS **2013**, 204 (2), 20. https://doi.org/10.1088/0067-0049/204/2/20.

(13) Maguire, W. C.; Hanel, R. A.; Jennings, D. E.; Kunde, V. G.; Samuelson, R. E. C_3H_8 and C_3H_4 in Titan's Atmosphere. Nature **1981**, 292 (5825), 683–686. https://doi.org/10.1038/292683a0.

(14) Magee, B. A.; Waite, J. H.; Mandt, K. E.; Westlake, J.; Bell, J.; Gell, D. A. INMS-Derived Composition of Titan's Upper Atmosphere: Analysis Methods and Model Comparison. Planetary and Space Science **2009**, 57 (14), 1895–1916. https://doi.org/10.1016/j.pss.2009.06.016.

(15) Cui, J.; Yelle, R. V.; Vuitton, V.; Waite, J. H.; Kasprzak, W. T.; Gell, D. A.; Niemann, H. B.; Müller-Wodarg, I. C. F.; Borggren, N.; Fletcher, G. G.; Patrick, E. L.; Raaen, E.; Magee, B. A. Analysis of Titan's Neutral Upper Atmosphere from

Cassini Ion Neutral Mass Spectrometer Measurements. Icarus **2009**, 200 (2), 581–615. https://doi.org/10.1016/j.icarus.2008.12.005.

(16) Vinatier, S.; Bézard, B.; Nixon, C. A.; Mamoutkine, A.; Carlson, R. C.; Jennings, D. E.; Guandique, E. A.; Teanby, N. A.; Bjoraker, G. L.; Michael Flasar, F.; Kunde, V. G. Analysis of Cassini/CIRS Limb Spectra of Titan Acquired during the Nominal Mission: I. Hydrocarbons, Nitriles and CO_2 Vertical Mixing Ratio Profiles. Icarus **2010**, 205 (2), 559–570. https://doi.org/10.1016/j.icarus.2009.08.013.

(17) Lombardo, N. A.; Nixon, C. A.; Greathouse, T. K.; Bézard, B.; Jolly, A.; Vinatier, S.; Teanby, N. A.; Richter, M. J.; G Irwin, P. J.; Coustenis, A.; Flasar, F. M. Detection of Propadiene on Titan. ApJ **2019**, 881 (2), L33. https://doi.org/10.3847/2041-8213/ab3860.

(18) Li, C.; Zhang, X.; Gao, P.; Yung, Y. Vertical Distribution of C_3-Hydrocarbons in the Stratosphere of Titan. ApJ **2015**, 803 (2), L19. https://doi.org/10.1088/2041-8205/803/2/L19.

(19) Dobrijevic, M.; Loison, J. C.; Hickson, K. M.; Gronoff, G. 1D-Coupled Photochemical Model of Neutrals, Cations and Anions in the Atmosphere of Titan. Icarus **2016**, 268, 313–339. https://doi.org/10.1016/j.icarus.2015.12.045.

(20) Abeysekera, C.; Joalland, B.; Ariyasingha, N.; Zack, L. N.; Sims, I. R.; Field, R. W.; Suits, A. G. Product Branching in the Low Temperature Reaction of CN with Propyne by Chirped-Pulse Microwave Spectroscopy in a Uniform Supersonic Flow. J. Phys. Chem. Lett. **2015**, 6 (9), 1599–1604. https://doi.org/10.1021/acs.jpclett.5b00519.

(21) Gerlich, D. Ion-Neutral Collisions in a 22-Pole Trap at Very Low Energies. Physica Scripta **1995**, 1995 (T59), 256.

(22) Wester, R. Radiofrequency Multipole Traps: Tools for Spectroscopy and Dynamics of Cold Molecular Ions. J. Phys. B: At. Mol. Opt. Phys. **2009**, 42 (15), 154001. https://doi.org/10.1088/0953-4075/42/15/154001.

(23) Biennier, L.; Carles, S.; Cordier, D.; Guillemin, J.-C.; Le Picard, S. D.; Faure, A. Low Temperature Reaction Kinetics of CN^-+HC_3N and Implications for the Growth of Anions in Titan's Atmosphere. Icarus **2014**, 227, 123–131. https://doi.org/10.1016/j.icarus.2013.09.004.

(24) Bourgalais, J.; Jamal-Eddine, N.; Joalland, B.; Capron, M.; Balaganesh, M.; Guillemin, J.-C.; Le Picard, S. D.; Faure, A.; Carles, S.; Biennier, L. Elusive Anion

Growth in Titan's Atmosphere: Low Temperature Kinetics of the C_3N^- + HC_3N Reaction. Icarus **2016**, 271, 194–201. https://doi.org/10.1016/j.icarus.2016.02.003.

(25) Joalland, B.; Jamal-Eddine, N.; Kłos, J.; Lique, F.; Trolez, Y.; Guillemin, J.-C.; Carles, S.; Biennier, L. Low-Temperature Reactivity of C2n+1N– Anions with Polar Molecules. J. Phys. Chem. Lett. **2016**, 7 (15), 2957–2961. https://doi.org/10.1021/acs.jpclett.6b01191.

(26) Biennier, L.; Carles, S.; Lique, F.; Mitchell, J. B. Ion Chemistry in Uniform Supersonic Flows. In Uniform Supersonic Flows in Chemical Physics: Chemistry studied using the CRESU method close to Absolute Zero, B.R. Rowe, A. Canosa, D.E. Heard (Eds.); 2021.

(27) Joalland, B.; Jamal-Eddine, N.; Papanastasiou, D.; Lekkas, A.; Carles, S.; Biennier, L. A Mass-Selective Ion Transfer Line Coupled with a Uniform Supersonic Flow for Studying Ion–Molecule Reactions at Low Temperatures. J. Chem. Phys. **2019**, 150 (16), 164201. https://doi.org/10.1063/1.5086386.

(28) Kato, S.; Bierbaum, V. M.; Leone, S. R. Multiquantum Vibrational Deactivation of N_2^+(v) by Collisions with N_2 and O_2 at Thermal Energies. J. Phys. Chem. A **1998**, 102 (33), 6659–6667. https://doi.org/10.1021/jp981679k.

(29) Ferguson, E. E. Vibrational Quenching of Small Molecular Ions in Neutral Collisions. J. Phys. Chem. **1986**, 90 (5), 731–738. https://doi.org/10.1021/j100277a008.

(30) Wilson, P. F.; Freeman, C. G.; McEwan, M. J. Reactions of Small Hydrocarbons with H_3O^+, O_2^+ and NO^+ Ions. International Journal of Mass Spectrometry **2003**, 229 (3), 143–149. https://doi.org/10.1016/S1387-3806(03)00290-2.

(31) Milligan, D. B.; Wilson, P. F.; Freeman, C. G.; Meot-Ner, M.; McEwan, M. J. Dissociative Proton Transfer Reactions of H_3^+, N_2H^+, and H_3O^+ with Acyclic, Cyclic, and Aromatic Hydrocarbons and Nitrogen Compounds, and Astrochemical Implications. J. Phys. Chem. A **2002**, 106 (42), 9745–9755. https://doi.org/10.1021/jp014659i.

(32) NIST Chemistry WebBook, NIST Standard Reference Database Number 69; Linstrom, P. J., Mallard, W. G., Eds.; National Institute of Standards and Technology: Gaithersburg MD, 20899, 2005.

(33) KIDA. KInetic Database for Astrochemistry http://kida.obs.u-bordeaux1.fr/.

(34) Decker, B. K.; Adams, N. G.; Babcock, L. M. Gas-Phase Reactivity of $SO^{+}\cdot$: A Selected Ion Flow Tube Study11Dedicated to the Memory of Robert R. Squires.

International Journal of Mass Spectrometry **2000**, 195–196, 185–201. https://doi.org/10.1016/S1387-3806(99)00146-3.

(35) Werner, H. J.; Knowles, P. J.; Knizia, G.; Manby, F. R.; Schütz, M.; Celani, P.; Györffy, W.; Kats, D.; Korona, T.; Lindh, R. MOLPRO, Version 2015.1, a Package of Ab Initio Programs. University of Cardiff Chemistry Consultants (UC3): Cardiff, Wales, UK **2015**.

(36) Werner, H. J.; Knowles, P. J.; Knizia, G.; Manby, F. R.; Schütz, M. WIREs Comput. Mol. Sci. 2, 242–253 (2012). version **2012**.

(37) Gray, C. G.; Gubbins, K. E. Theory of Molecular Fluids. Volume 1: Fundamentals; Clarendon Press: Oxford, 1984.

(38) Su, T.; Chesnavich, W. J. Parametrization of the Ion–Polar Molecule Collision Rate Constant by Trajectory Calculations. The Journal of Chemical Physics **1982**, 76 (10), 5183–5185. https://doi.org/10.1063/1.442828.

(39) Rankin, D. W. H. CRC Handbook of Chemistry and Physics, 89th Edition, Edited by David R. Lide. null **2009**, 15 (3), 223–224. https://doi.org/10.1080/08893110902764125.

(40) Gussoni, M.; Rui, M.; Zerbi, G. Electronic and Relaxation Contribution to Linear Molecular Polarizability. An Analysis of the Experimental Values. Journal of Molecular Structure **1998**, 447 (3), 163–215. https://doi.org/10.1016/S0022-2860(97)00292-5.

(41) Tsuji, M.; Kouno, H.; Matsumura, K.; Funatsu, T.; Nishimura, Y.; Obase, H.; Kugishima, H.; Yoshida, K. Dissociative Charge-transfer Reactions of Ar^+ with Simple Aliphatic Hydrocarbons at Thermal Energy. The Journal of Chemical Physics **1993**, 98 (3), 2011–2022. https://doi.org/10.1063/1.464234.

(42) Gichuhi, W. K.; Suits, A. G. Primary Branching Ratios for the Low-Temperature Reaction of State-Prepared N_2^+ with CH_4, C_2H_2, and C_2H_4. J. Phys. Chem. A **2011**, 115 (25), 7105–7111. https://doi.org/10.1021/jp112427r.

(43) Mebel, A. M.; Bandrauk, A. D. Theoretical Study of Unimolecular Decomposition of Allene Cations. J. Chem. Phys. **2008**, 129 (22), 224311. https://doi.org/10.1063/1.3037204.

(44) Parr, A. C.; Jason, A. J.; Stockbauer, R. Photoionization and Threshold Photoelectron-Photoion Coincidence Study of Allene from Onset to 20 EV. International Journal of Mass Spectrometry and Ion Physics **1978**, 26 (1), 23–38. https://doi.org/10.1016/0020-7381(78)80002-3.

(45) Parr, A. C.; Jason, A. J.; Stockbauer, R.; McCulloh, K. E. Photoionization and Threshold Photoelectron—Photoion Coincidence Study of Propyne from Onset to 20 eV. International Journal of Mass Spectrometry and Ion Physics **1979**, 30 (3), 319–330. https://doi.org/10.1016/0020-7381(79)83009-0.

(46) Ho, G. H.; Lin, M. S.; Wang, Y. L.; Chang, T. W. Photoabsorption and Photoionization of Propyne. J. Chem. Phys. **1998**, 109 (14), 5868–5879. https://doi.org/10.1063/1.477209.

(47) Liu, G.; Li, Z.; Ding, Y.; Fu, Q.; Huang, X.; Sun, C.; Tang, A. Water-Assisted Isomerization from Linear Propargylium (H2CCCH+) to Cyclopropenylium (c-$C_3H_3^+$). J. Phys. Chem. A **2002**, 106 (43), 10415–10422. https://doi.org/10.1021/jp0212085.

(48) Marimuthu, A. N.; Sundelin, D.; Thorwirth, S.; Redlich, B.; Geppert, W. D.; Brünken, S. Laboratory Gas-Phase Vibrational Spectra of $[C_3H_3]^+$ Isomers and Isotopologues by IRPD Spectroscopy. Journal of Molecular Spectroscopy **2020**, 374, 111377. https://doi.org/10.1016/j.jms.2020.111377.

(49) Możejko, P.; Ptasińska-Denga, E.; Domaracka, A.; Szmytkowski, C. Absolute Total Cross-Section Measurements for Electron Collisions with Tetrahydrofuran. Phys. Rev. A **2006**, 74 (1), 012708. https://doi.org/10.1103/PhysRevA.74.012708.

(50) Gross, J. H. Principles of Ionization and Ion Dissociation. In Mass Spectrometry: A Textbook; Gross, J. H., Ed.; Springer International Publishing: Cham, 2017; pp 29–84. https://doi.org/10.1007/978-3-319-54398-7_2.

(51) Masson, A. J.; Birkinshaw, K.; Henchman, M. J. Collision Mechanism of a Dissociative Charge-Transfer Reaction at Low Energy. J. Chem. Phys. **1969**, 50 (9), 4112–4114. https://doi.org/10.1063/1.1671676.

(52) Lavvas, P.; Yelle, R. V.; Koskinen, T.; Bazin, A.; Vuitton, V.; Vigren, E.; Galand, M.; Wellbrock, A.; Coates, A. J.; Wahlund, J.-E.; Crary, F. J.; Snowden, D. Aerosol Growth in Titan's Ionosphere. Proc. Natl. Acad. Sci. U.S.A. **2013**, 110 (8), 2729–2734. https://doi.org/10.1073/pnas.1217059110.

(53) Waite, J. H., Jr.; Young, D. T.; Cravens, T. E.; Coates, A. J.; Crary, F. J.; Magee, B.; Westlake, J. The Process of Tholin Formation in Titan's Upper Atmosphere. Science **2007**, 316 (5826), 870–875. https://doi.org/10.1126/science.1139727.

(54) Loison, J. C.; Dobrijevic, M.; Hickson, K. M. The Photochemical Production of Aromatics in the Atmosphere of Titan. Icarus **2019**, 329, 55–71. https://doi.org/10.1016/j.icarus.2019.03.024.

(55) McEwan, M. J.; McConnell, C. L.; Freeman, C. G.; Anicich, V. G. Reactions of Isomeric $C_3H_3^+$ Ions: A Combined Low Pressure-High Pressure Study. J. Phys. Chem. **1994**, 98 (19), 5068–5073. https://doi.org/10.1021/j100070a021.

(56) Nixon, C. A.; Thelen, A. E.; Cordiner, M. A.; Kisiel, Z.; Charnley, S. B.; Molter, E. M.; Serigano, J.; Irwin, P. G. J.; Teanby, N. A.; Kuan, Y.-J. Detection of Cyclopropenylidene on Titan with ALMA. AJ **2020**, 160 (5), 205. https://doi.org/10.3847/1538-3881/abb679.

(57) Smyth, K. C.; Lias, S. G.; Ausloos, P. The Ion-Molecule Chemistry of $C_3H_3^+$ and the Implications for Soot Formation. Combustion Science and Technology **1982**, 28 (3–4), 147–154. https://doi.org/10.1080/00102208208952550.

(58) Prodnuk, S. D.; Grocert, S.; Bierbaum, V. M.; DePuy, C. H. Gas-Phase Reactions of $C_3H_n^+$ Ions. Organic Mass Spectrometry **1992**, 27 (4), 416–422. https://doi.org/10.1002/oms.1210270411.

(59) Smith, D.; Adams, N. G. Cyclic and Linear Isomers of $C_3H_2^+$ and $C_3H_3^+$: The $C_3H^+ + H_2$ Reaction. International Journal of Mass Spectrometry and Ion Processes **1987**, 76 (3), 307–317. https://doi.org/10.1016/0168-1176(87)83035-5.

(60) Ali, A.; Sittler, E. C.; Chornay, D.; Rowe, B. R.; Puzzarini, C. Organic Chemistry in Titan′s Upper Atmosphere and Its Astrobiological Consequences: I. Views towards Cassini Plasma Spectrometer (CAPS) and Ion Neutral Mass Spectrometer (INMS) Experiments in Space. Planetary and Space Science **2015**, 109–110, 46–63. https://doi.org/10.1016/j.pss.2015.01.015.

(61) O'Malley, R. M.; Jennings, K. R. Ion Cyclotron Resonance Mass Spectra of Fluoroalkenes I. Ion—Molecule Reactions of Ethylene and Vinyl Fluoride. International Journal of Mass Spectrometry and Ion Physics **1969**, 2 (6), 441–455. https://doi.org/10.1016/0020-7381(69)80042-2.

(62) Anicich, V. G. An Index of the Literature for Bimolecular Gas Phase Cation-Molecule Reaction Kinetics. JPL Publication 03-19 **2003**, 1–1194.

(63) Hébrard, E.; Dobrijevic, M.; Loison, J. C.; Bergeat, A.; Hickson, K. M.; Caralp, F. Photochemistry of C_3H_p Hydrocarbons in Titan's Stratosphere Revisited. A&A **2013**, 552, A132. https://doi.org/10.1051/0004-6361/201220686.

(64) Lavvas, P. P.; Coustenis, A.; Vardavas, I. M. Coupling Photochemistry with Haze Formation in Titan's Atmosphere, Part I: Model Description. Planetary and Space Science **2008**, 56 (1), 27–66. https://doi.org/10.1016/j.pss.2007.05.026.

(65) Ausloos, P.; Lias, S. G. Discrimination of $C_3H_3^+$ Structures on the Basis of Chemical Reactivity. J. Am. Chem. Soc. **1981**, 103 (21), 6505–6507. https://doi.org/10.1021/ja00411a045.

Chapter 5:
Reactivity of Ar^+ ions with C_2H_4 and CH_4 at low temperatures

This chapter presents the results obtained on the investigation of the reactivity of Ar^+ ions with methane and ethene at low temperatures using the CRESU-SIS experimental setup. In the first section we discuss the reaction of Ar^+ ions with ethene at 18.7 and 71.6 K. We present the kinetic experimental results, the branching ratios between the product exit channels and the ab-initio calculations that were performed to explain the experimental measurements. The rate coefficients and the products distribution are also measured for the reaction of Ar^+ ions with methane at 18.7 and 71.6 K, this will be presented in details in the second section.

5.1 Introduction

Alongside the astrophysical importance of ion-neutral reactions, such studies give also some insight into the reaction mechanisms, particularly, the charge transfer process which has been studied in various contexts for a long time.[1] The reactivity of Ar^+ ions with hydrocarbons has been the object of numerous investigations including saturated (CH_4, C_2H_6, C_3H_8, C_4H_{10}…) and unsaturated species (C_2H_2,C_2H_4, c-C_6H_6…) mainly driven by plasma physics applications.[2] Most of the studies have been performed at room temperature. Noteworthy, some discrepancies remain between studies regarding the branching into the various exit channels.

In Titan's atmosphere, the neutral argon ^{40}Ar has been detected by the Ion Neutral Mass Spectrometer on the Cassini orbiter.[3,4] According to WH Ip [5] and G. J. Molina-Cuberos et al.,[6] the neutral argon can be ionized in the lower ionosphere (from 1 and 400 km) by the absorption of galactic cosmic rays to form Ar^+ . [7,8]

Neutral argon has a high ionization potential (15.759 eV), comparable to N_2 (15.581 eV), so its production from solar photon ionization is expected to be small. At low altitudes the dense atmosphere reduces the penetration of photons. However, the ionization by hot suprathermal electrons and by galactic cosmic rays could contribute at altitudes below the photo-ionization peak, near 700 km and 60 km respectively.[9]

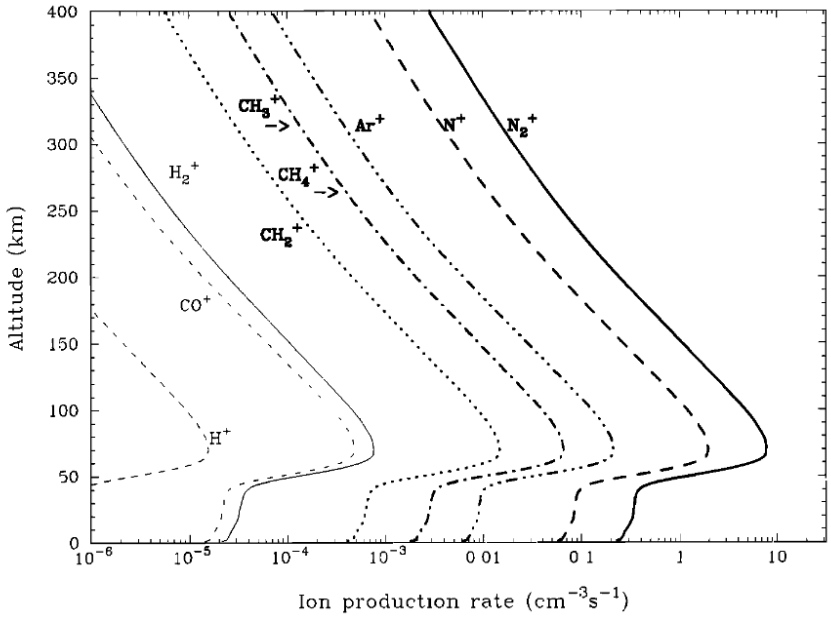

Figure 5.1: Ionization production rate profiles due to the absorption of galactic cosmic rays in Titan's atmosphere. From G. J. Molina-Cuberos et al.[7]

Both hydrocarbons, C_2H_4 and CH_4, are detected in situ at high altitude by the INMS instrument operating in neutral mode [10] and at distance by the Cassini Composite Infrared Spectrometer (CIRS) in the middle and upper stratosphere (altitudes from 45 to 250 km). [11]

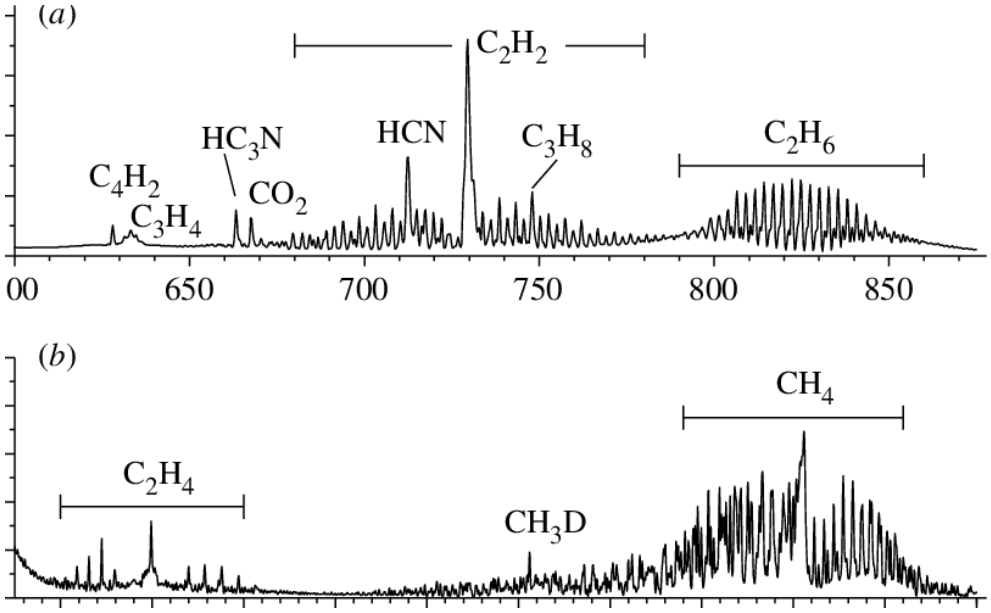

Figure 5.2: Synthetic spectrum of Titan in the mid-IR at CIRS maximum spectral resolution (0.5 cm) showing the vast array of emission features from trace species in the stratosphere.[11]

Farther from us, Ar^+ ions may play some role in the chemistry of the diffuse interstellar medium. The Ar^+ ions can be produced in the ISM via the reaction:

$$Ar + H_2^+ \rightarrow H_2 + Ar^+ \qquad \text{Eq. (5.1)}$$

or by cosmic ray ionization

$$Ar + CR \rightarrow Ar^+ + e^- + CR \qquad \text{Eq. (5.2)}$$

and then react with H_2 to form ArH^+,

$$Ar^+ + H_2 \rightarrow ArH^+ + H \qquad \text{Eq. (5.3)}$$

which is detected in the diffuse interstellar medium.[12] According to Schilke et al., ArH^+ could be a good tracer of atomic hydrogen. To that end, it is important to understand well the chemical network of Ar^+, a species which plays a key role in the production of ArH^+.

Besides the astrophysical importance of this work, the main object of this chapter is to understand the chemical mechanisms that occur in ion-neutral reactions, specifically charge transfer that can be, because of its quantum nature, a temperature-dependent process.

5.2 Reactivity of Ar^+ ions with C_2H_4

5.2.1 Previous measurements

The rate coefficient and the branching ratios of the $Ar^+ + C_2H_4$ were measured at room temperature using the Flowing Afterglow technique (FA) by M. Tsuji et al. in 1992,[13] where

$C_2H_2^+$, $C_2H_3^+$ and $C_2H_4^+$ were identified as primary ionic products. All these reactions pathways are exoergic. The authors of this study suggested the presence of two CT (Charge Transfer) mechanisms in the Ar^+/C_2H_4 reaction. One is a dominant near-resonant dissociative CT leading to $C_2H_3^+$ and $C_2H_2^+$, and the other is a minor non-resonant, nondissociative CT leading to the appearance of $C_2H_4^+$. Another study was performed earlier at room temperature by J. L. Franklin et al. (1961)[14] using the MS technique, with the detection of $C_2H_2^+$ and $C_2H_3^+$ ions as products. They suggested in that work that the formation of $C_2H_4^+$ by charge exchange with any of the rare gas ions is quite exothermic, and all of ethylene ions ($C_2H_4^+$) break down into smaller fragments. These previous results are summarized in table 5.1. To our knowledge the Ar^+/C_2H_4 reaction was not investigated at low temperatures below 300 K.

$Ar^+ + C_2H_4$ study	**Rate coefficient ($cm^3\ s^{-1}$)**	**Ionic products**
Masaharu Tsuji et al. (1992)	$1.10 \times 10^{-9} \pm 20$	$C_2H_4^+$ (0.04) $C_2H_3^+$ (0.76) $C_2H_2^+$ (0.20)
J. L. Franklin et al. (1961)	$1.10 \times 10^{-9} \pm 10$	$C_2H_3^+$ (0.87) $C_2H_2^+$ (0.13)

Table 5.1: Rate coefficients and branching ratios for the Ar^+/C_2H_4 reaction obtained by the studies of FA and MS techniques at room temperature.

5.2.2 Experimental results

The CRESU-SIS experimental setup is used to measure the rate coefficient and the branching ratios for the $Ar^+ + C_2H_4$ reaction at 18.7 and 71.6 K. This technique is described in details in chapter 3, and only the results are presented in this chapter. The characteristics of the Ar50K0.3 Laval nozzle that generates the flow at 71.6 K are shown in chapter 4, table 4.1, and those for the He20K nozzle are presented in Table 5.2.

Nozzle	**buffer gas**	**T_{jet} (K)**	**Mach**	**τ (µs)**	***n*** **(10^{16} molecule.cm^{-3})**	**$P_{chamber}$ (mbar)**	**flow rate (l/min)**
He20K	He	18.7	6.6	120	3 .7	0.11	45.7

Table 5.2: Characteristics of the supersonic uniform flow generated by the He20K nozzle determined from impact pressure measurements.

The Ar^+ ions (m/z= 40 u) are generated by the hollow cathode discharge source with a He (0.750 slm) /Ar (3 sccm) mixture. After the injection of the neutral reactant in the uniform supersonic flow, we observe four primary products for the $Ar^+ + C_2H_4$ reaction: $C_2H_2^+$ (m/z= 26 u), $C_2H_3^+$(m/z= 27 u), $C_2H_4^+$ (m/z= 28 u) and ArH^+ (m/z= 41 u), with $C_2H_3^+$ being the major product (see figure 5.4). In the spectrum recorded in the absence of C_2H_4 neutral reactant (figure 5.3), we observe a very small quantity of ArH^+ at m/z= 41 u, which is injected in the flow from the ion source. In order to verify that the ArH^+ ion is also a primary product for the $Ar^+ + C_2H_4$ reaction, we fixed the QMS at a distance = 7 cm from the deflector, and by comparing the ion signal at m/z= 41 u before and after the injection of C_2H_4, we remarked an increase in the ArH^+ ion counts. Primary products are identified by their time evolution at low initial neutral reactant densities. The branching ratio of each primary product is determined by the intersect with the y-axis. All these pathways are exothermic, the details of the energetic study are discussed in section 5.2.3. The branching ratios of these products changes between 18.7 and 71.6 K, in the goal of understanding this variation, an ab-initio calculation was performed (section 5.2.3).

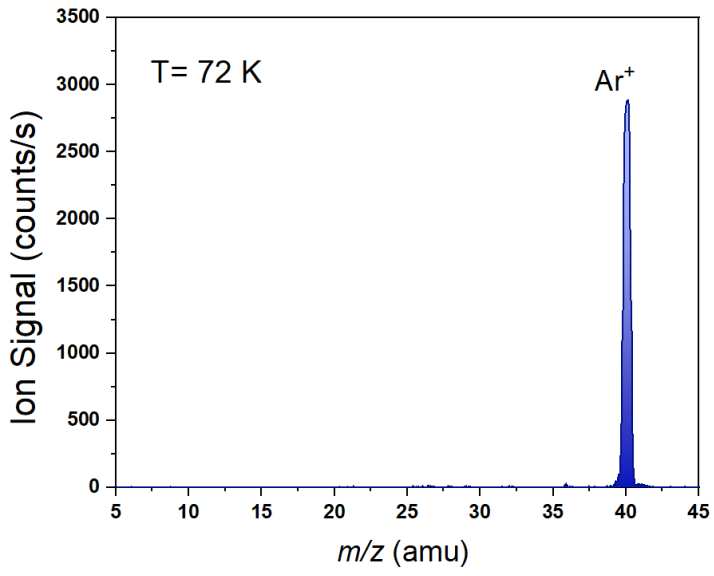

Figure 5.3: Mass spectrum recorded in the uniform supersonic flow in the absence of neutral reactant and at the temperature T= 72 K, the QMS is positioned at 7 cm from the injection zone (t~ 50 µs).

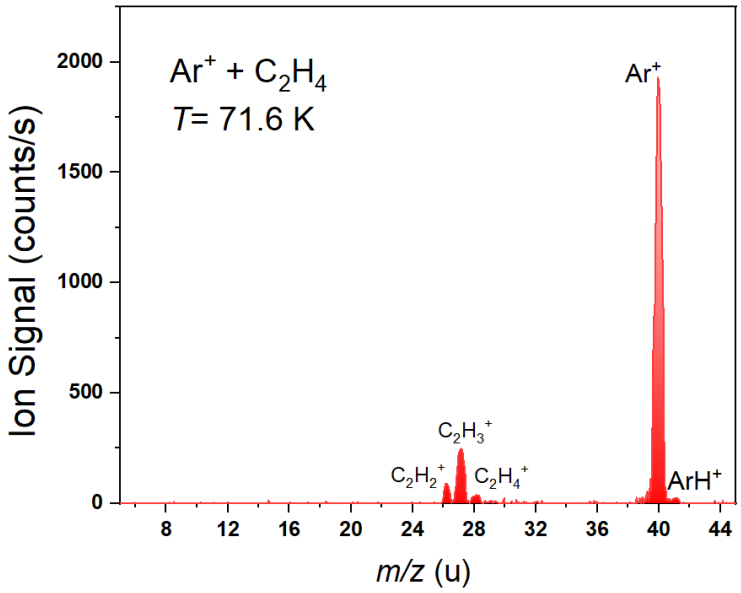

Figure 5.4: Mass spectrum recorded in the uniform supersonic flow in the presence of neutral reactant. T= 72 K, $[C_2H_4]$ = 2.9 × 10^{12} molecule/cm^3, reaction time ~ 65 µs.

5.2.2.1 Kinetic studies

The Kinetic measurements were obtained under pseudo-first order conditions by measuring the loss rates of the mass-selected ions for various concentrations of neutral co-reactant set in excess. Figure 5.5 illustrates the time evolution of the Ar^+ ion signal and its loss rate variation with the $[C_2H_4]$ density for the $Ar^+ + C_2H_4$ reaction at 18.7 and 71.6 K. The values of absolute rate coefficients k(T) at 18.7 and 71.6 K are (1.06 ± 0.13) ×10^{-9} cm^3 s^{-1} and (1.13 ± 0.15) ×10^{-9} cm^3 s^{-1} respectively. The uncertainties take into account statistical and systematic (10%) contributions. Our values are close to the values calculated by Langevin model (described in chapter 2), k_L = 1.2 ×10^{-9} cm^3 s^{-1}. The rate coefficient remains constant over the temperature range, and this is not surprising because the ethene molecule is a non-polar molecule, and the rate coefficient follows the Langevin model. Figure 5.6 shows our measured values of the rate coefficient and comparison with previous measurements and Langevin model. The relatively high value of the rate coefficient at 300 K give an argument on the bimolecularity of the $Ar^+ + C_2H_4$ reaction.

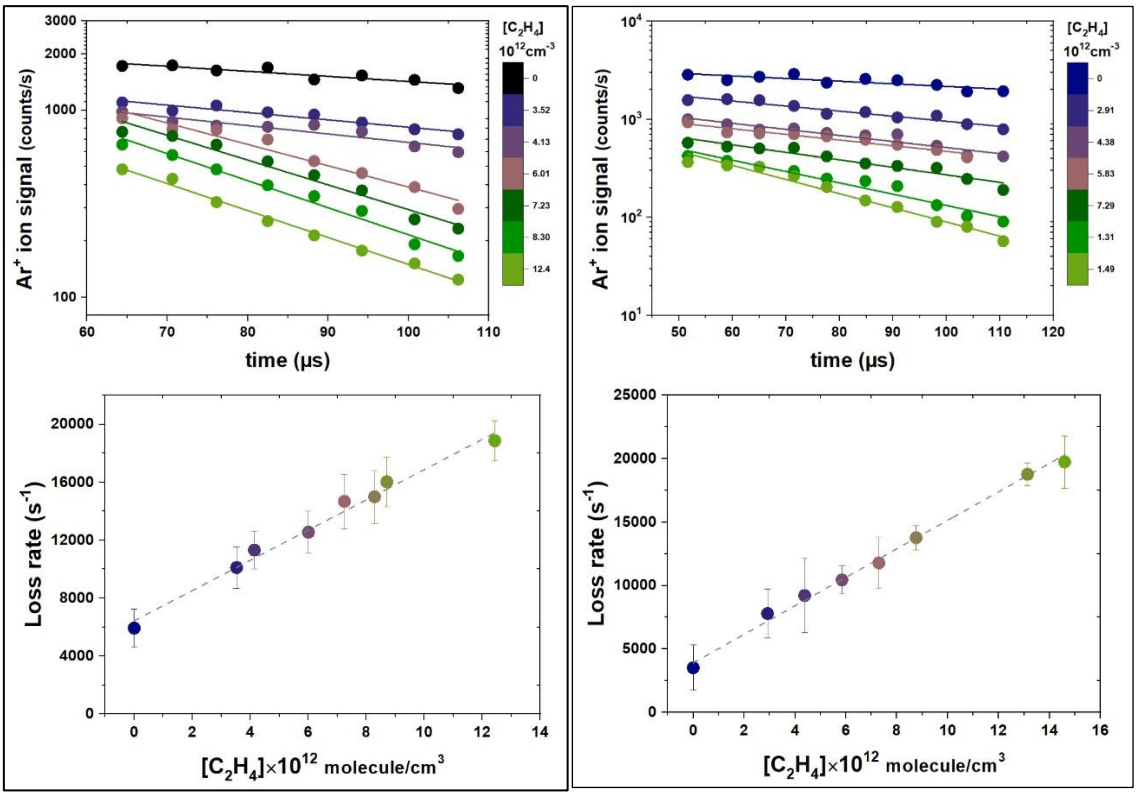

Figure 5.5: Ar^+ ion signal as a function of time for a range of neutral C_2H_4 densities and corresponding loss rates as a function of C_2H_4 densities at 18.7 K (left) and 71.6 K (right).

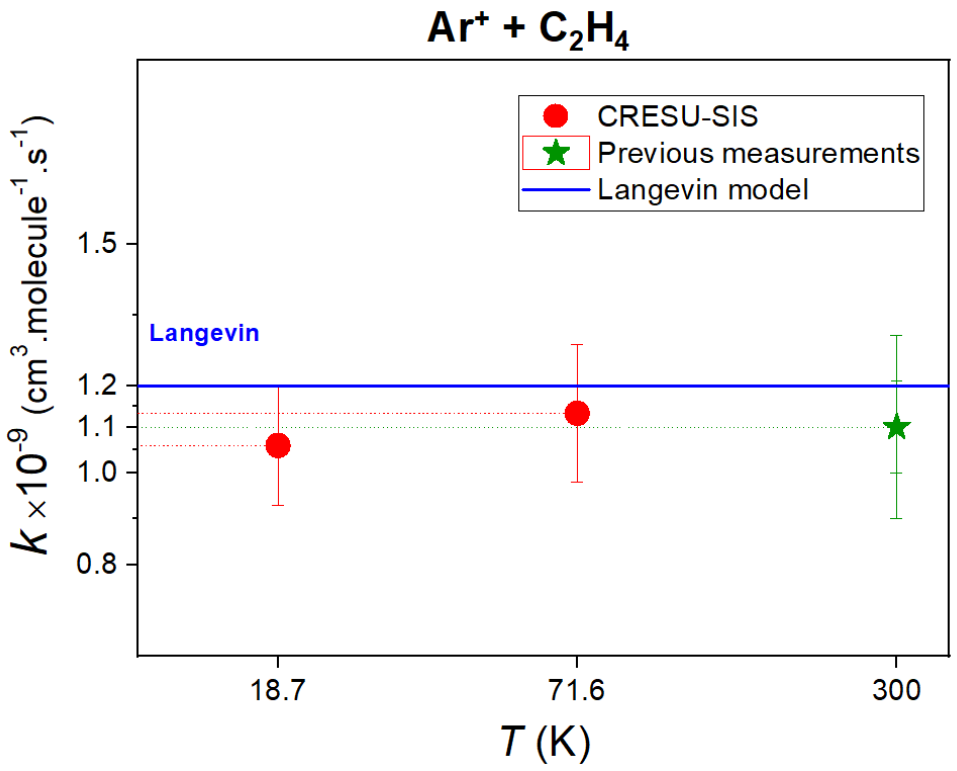

Figure 5.6: Values of the rate coefficient as a function of the temperature for the $Ar^+ + C_2H_4$ reaction measured by CRESU-SIS experimental setup and comparison with previous measurements and Langevin model.

5.2.2.2 Branching ratios

The branching ratios of ionic products measured by our CRESU-SIS experimental setup at low temperatures differ from those measured at room temperature. The charge transfer product, $C_2H_4^+$, increases to reach 22 % at 18.7 K, while this product doesn't appear in the measurements of J.L Franklin et al. (1962), and only in small quantity (4%) in the measurements of Tsuji et al. (1992) at room temperature. In previous measurements, the authors suggested that the dissociative CT product dissociates into smaller fragments. These mechanisms are endothermic, according to B. Joalland et al. with few eV.[15] At low temperature, the dissociation of $C_2H_4^+$ is not allowed. This can be the reason of the detection of an important quantity of $C_2H_4^+$ ions at low temperatures in our experiments. In the other hand, we don't observe a variation in the branching ratios of $C_2H_2^+$ and ArH^+ ions. The branching ratios of primary products detected in our study at low temperatures are summarized in table 5.3.

CRESU-SIS measurements				
Primary products of the $Ar^+ + C_2H_4$ reaction				
	$C_2H_4^+$	**$C_2H_3^+$**	**$C_2H_2^+$**	**ArH^+**
T= 18.7 K	0.22 ± 0.03	0.58 ± 0.05	0.16 ± 0.02	0.04 ± 0.02
T= 71.6 K	0.10 ± 0.02	0.68 ± 0.05	0.19 ± 0.03	0.03 ± 0.02

Table 5.3: Branching ratios for the products of the $Ar^+ + C_2H_4$ reaction recorded at 18.7 and 71.6 K using the CRESU-SIS experimental setup. The error bars were estimated by adding systematic (±0.02) and statistical (±5%) contributions.

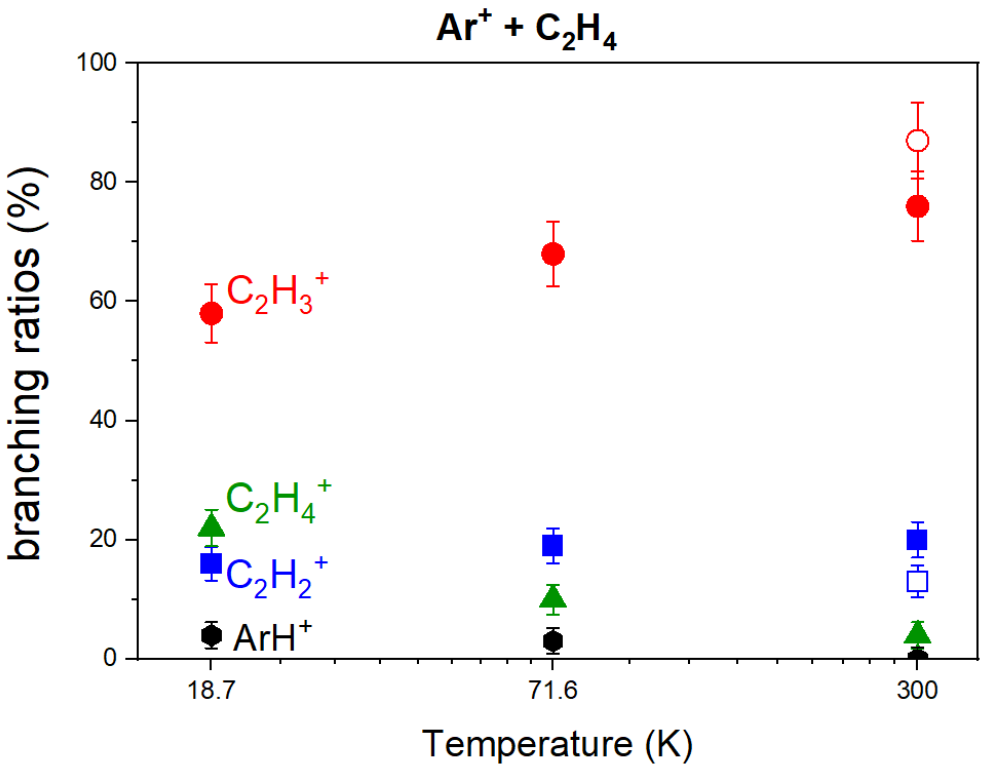

Figure 5.7: Branching ratios of the $Ar^+ + C_2H_4$ reaction measured at 18 and 72 K by CRESU-SIS technique and comparison with the measurements at room temperature by Tsuji et al. (full symbols) and J.L Franklin et al. (open symbols)

In order to gain more insight into the exit channels of the $Ar^+ + C_2H_4$ reaction, and to understand the variation of branching ratios at low temperatures, specifically the increase in the branching ratio of the CT product, our colleague Sandor Demes made some ab-initio calculations. These results are presented in the next section.

5.2.3 Ab-initio calculations

In order to study the collision of Ar^+ cation with ethylene, high-level ab initio calculations were performed. The spin unrestricted (open-shell) coupled cluster theory was used with single and double excitations and triple corrections (UCCSD(T)) along with the augmented correlation-consistent valence triple zeta (aug-cc-pVTZ) basis set. All calculations were done with the MOLPRO (version 2015.1) quantum chemistry software package.[16,17] The goal of the study is to find the enthalpies of formations for the reactants, the possible reaction products, including several intermediate complexes (ICs). From the calculated quantities it is possible to compute the corresponding reaction enthalpies. The structure and characteristics of all neutral and ionic species were found following full geometry optimization calculations. Harmonic vibrational

frequency and normal mode calculations were performed to compute the zero-point vibrational energy (ZPVE) corrections.

In order to examine the quality of our ab initio calculations, in Table 5.2 we compared our theoretical ionization potentials with the experimental values listed in the NIST database.[18] As one can see there is a very good overall agreement (1-3%) between the compared data, except for the C_2H• radical. It is worth to mention however that C_2H^+ was not observed in the experiments, and the theoretical calculations show, that all the reactions which lead to the formation of this cation are endothermic.

Molecule	**Calculated Ionization potential (eV)**	**Experimental ionization potential[18] (eV)**
C_2H_4	10.496	10.5138 ± 0.0006
C_2H_3•	8.460	8.59 ± 0.03
C_2H_2	11.090	11.41 ± 0.01
C_2H•	14.098	11.61 ± 0.07
Ar	15.614	15.759 ± 0.001

Table 5.4: Ionization potentials of the possible fragment species from $Ar^+ + C_2H_4$ reaction.

Based on the results of the performed ab initio calculations we have provided a qualitative analysis of the possible reaction pathways. The analysis of reaction enthalpies shows that the $C_2H_4^+$, $C_2H_3^+$, $C_2H_2^+$ and ArH^+ cations should be the primary products of the $Ar^+ + C_2H_4$ reaction due their negative (exothermic) enthalpy of formation. The results of reaction enthalpy calculations for the exothermic products are shown in Table 5.5. First, we can see that the most exothermic channel is the pure charge-exchange process: $C_2H_4 + Ar^+ \rightarrow C_2H_4^+ + Ar$. As we have also shown in our previous work (chapter 4), such a reaction can only proceed via crossings between multiple electronic states. This interstate crossing has a strong quantum-mechanical character, which is mainly determined by the non-adiabatic couplings between the particular states. These properties make the pure charge-exchange reactions more favorable at lower temperatures. Since in this type of reactions strong intermolecular motions and rearrangements are not likely to occur, the $C_2H_4 + Ar^+ \rightarrow C_2H_4^+ + Ar$ reaction proceeds without the formation of intermediate complexes. All other reaction products resulting from the studied reaction are characterized by hydrogen exchange process, and effectively proceeds via formation of intermediate complexes (according to capture theory)[19]. We found a highly

exothermic van der Waals-type $[Ar + C_2H_4]^+$ intermediate complex (see Figure 5.8) with a relative enthalpy of -6.6 eV (with respect to the reactants). This complex thus could be attributed as an intermediate complex towards the formation of $C_2H_3^+$, $C_2H_2^+$ and ArH^+ cations from $C_2H_4 + Ar^+$ reaction. Since the structure of this complex is not very distorted (the bond lengths and angles for C_2H_4 within the complex is very close to those of in the stable ethylene monomer), its formation can be very efficient without crossing reaction barriers (i.e. transition states).

Reactants	**Reaction products**	**Enthalpy change ΔH (eV)**
$C_2H_4 + Ar^+$	**$C_2H_4^+$** + Ar	-5.175
	$C_2H_2^+$ (lin) + H_2 + Ar	-2.833
	$C_2H_3^+$ +Ar + H•	-2.316
	C_2H_3 + **ArH^+**	-1.272
	C_2H_2(iso)$^+$ + H_2 + Ar	-0.851

Table 5.5: Product formation channels with the corresponding enthalpies calculated for the $Ar^+ + C_2H_4$ reaction at 0 K. "Iso" describes the $C_2H_2^+$ ion isomer where the two H-atoms are in the same side, and "lin" in the case of its repartition on the two molecule sides.

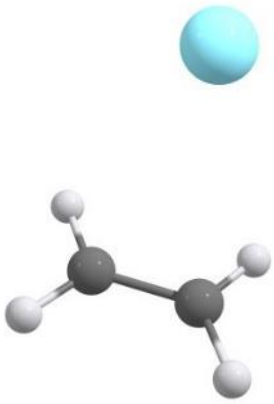

Figure 5.8: The structure of the van der Waals-type $[Ar + C_2H_4]^+$ intermediate complex in the $Ar^+ + C_2H_4$ reaction.

From the intermediate complex the formation of the final reaction products can be effective. The reaction which leads to formation of $C_2H_2^+$ (lin) along with H_2 can be the most favorable exit channel for the first glance, since it is the most exothermic (about -2,833 eV). However, if we analyze its geometry we can see that the formation of this cation is probably not feasible

along with a molecular hydrogen product. If we analyze its formation together with two H-atoms (i.e. the $C_2H_4 + Ar^+ \rightarrow C_2H_2^+(lin) + H + H + Ar$ process), we found an endothermic reaction enthalpy (about +1.652 eV). As a consequence, the most favorable dissociative charge-exchange reaction is probably the $Ar^+ + C_2H_4 \rightarrow C_2H_3^+ + Ar + H\bullet$ reaction with -2.316 eV reaction enthalpy, and the production of $C_2H_2(iso)^+$ cations can be less efficient (with enthalpy of -0.851 eV). This is in a good agreement with the experimental branching ratios. As we mentioned earlier, according to our ab initio results, all the possible reactions which lead to C_2H^+ production are endothermic.

It is worth to emphasize again that the mechanism of the pure charge exchange reaction, which leads to the formation of the parent cations ($C_2H_4^+$), principally differs from all others, since it is only possible through non-adiabatic dynamics, which has a strict quantum-mechanical nature. At low temperatures, when the collision is slower, the quantum-mechanical effects are more important and the non-adiabatic processes are more effective.[20] This is also in a good accordance with the experimentally observed temperature dependence of the branching ratios in case of $C_2H_4^+$ ion formation.

5.3 Reactivity of Ar^+ ions with methane

In addition to the reaction of Ar^+ ions with ethene, we have studied the reactivity of this ion with methane at 18.7 and 71.6 K using our CRESU-SIS technique. The branching ratios and the rate coefficient of the $Ar^+ + CH_4$ reaction were studied previously by FJFR (Free Jet Flow Reactor) at 10-20 K by Hawley et al.[21] In addition, the rate coefficient of this reaction was measured at 23, 36 and 71 K by Thomas Speck et al. (2001) using the CRESU technique.[22] Furthermore, this reaction was explored at room and high temperatures (700 K) using different techniques (SIFT, ICR, FA, Drift Tube…). In all of these measurements, the major ionic products are CH_2^+ and CH_3^+. Otherwise, the charge transfer product CH_4^+ is detected in many studies of the $Ar^+ + CH_4$ reaction at room temperature (FA, SIFT, MS..).[23,2]

5.3.1 Kinetic study

The rate coefficient of the $Ar^+ + CH_4$ reaction has been measured at 18.7 and 71.6 K. We obtain values of $k = (1.07 \pm 0.26) \times 10^{-9}$ cm^3 s^{-1} and $(1.10 \pm 0.30) \times 10^{-9}$ cm^3 s^{-1} for the rate coefficients at 18.7 and 71.6 K respectively. The variation of the loss rate, or the pseudo first order k_{1st}, is shown in figure 5.9, the rate coefficient corresponds to the slope of the variation of k_{1st} as function of the density of neutral reactant. The measured rate coefficients are very close to that calculated using the Langevin model, $k_L = 1.12 \times 10^{-9}$ cm^3 s^{-1}. The rate coefficient follows the

Langevin model over a large temperature range, due to the absence of dipole moment of the neutral reactant (CH_4). Figure 5.10 shows the rate coefficient of the $Ar^+ + CH_4$ reaction over the 10-20 K temperature range between (obtained by FJFR technique) and at 700 K (using the DT technique by Chatham et al.[24]). For the value at 300 K, it exists different measurements, we have chosen the most recent value measured by M. Tsuji et al. in 1993 employing the FA technique.

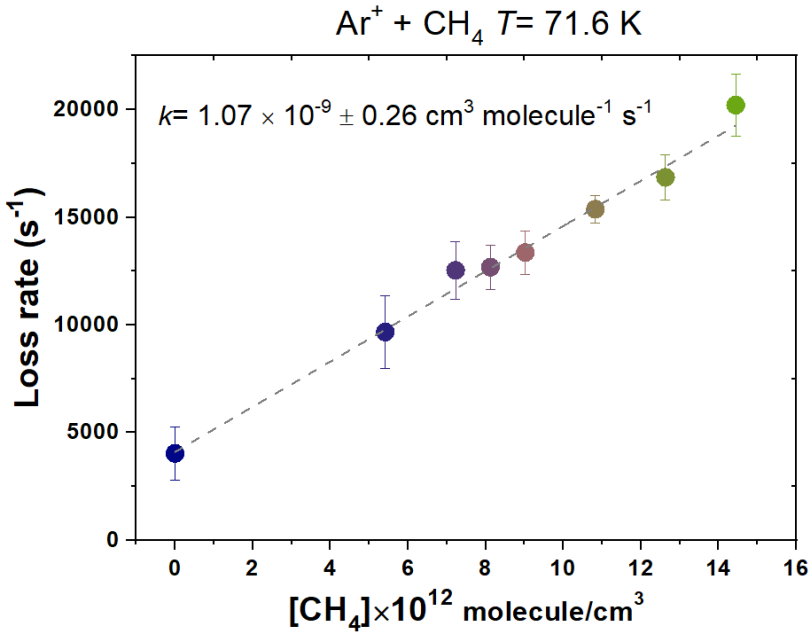

Figure 5.9: Loss rate of the Ar^+/CH_4 reaction as a function of the density of CH_4, T= 71.6 K.

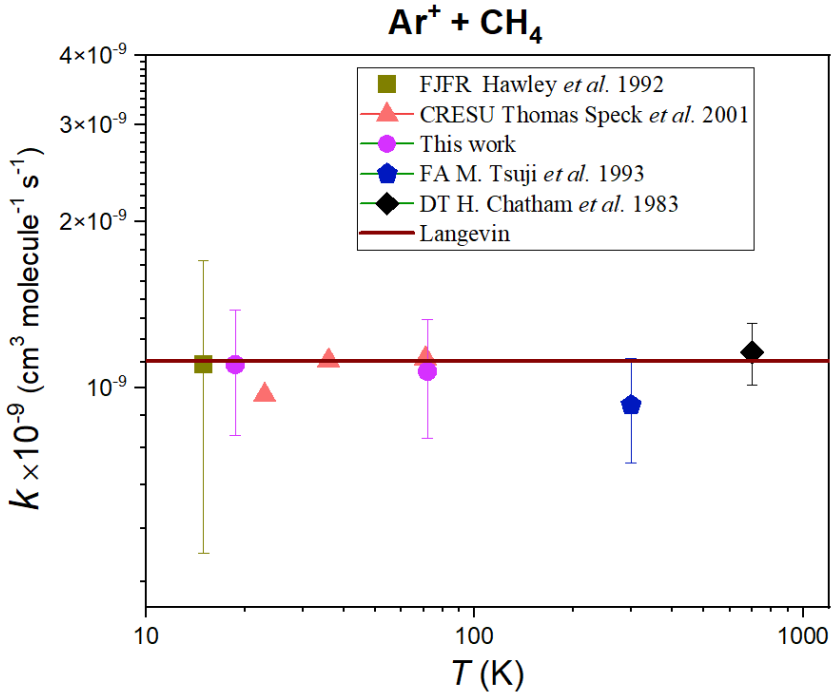

Figure 5.10: Rate coefficient of the Ar^+/CH_4 reaction obtained using the CRESU-SIS technique at 18.7 and 71.6 K and comparison with previous measurements.

5.3.2 Branching ratios

In our measurements for the $Ar^+ + CH_4$ reaction, we detected two primary products: CH_2^+ (m/z= 14 u) and CH_3^+ (m/z= 15 u). Despite an exothermic CT pathway for this reaction (ΔH= - 3.1 eV), the CH_4^+ ion is not detected as product. An hypothesis that could explain this observation is the presence of an energetic barrier. The branching ratios measured using the CRESU-SIS technique and comparison with those obtained at 10-20 K using FJFR are summarized in table 5.4. We don't observe an important variation in the branching ratios of the $Ar^+ + CH_4$ reaction at low temperatures, since the charge transfer product is not observed here.

Ar^+/CH_4		**Branching ratios**	
	T	**CH_2^+ (m/z= 14 u)**	**CH_3^+ (m/z= 15 u)**
This work: CRESU-SIS	71.6 K	0.22 ± 0.03	0.78 ± 0.06
This work: CRESU-SIS	18.7 K	0.21 ± 0.03	0.79 ± 0.06
FJFR by Hawley et al. (1992)	10-20 K	0.20	0.80

Table 5.6: Branching ratios of the $Ar^+ + CH_4$ reaction obtained at 18.7 and 71.6 K by CRESU-SIS technique and comparison with the measurements of Hawley et al. (1992) at 10-20 K.[21] The error bars were estimated by adding systematic (±0.02) and statistical (±5%) contributions.

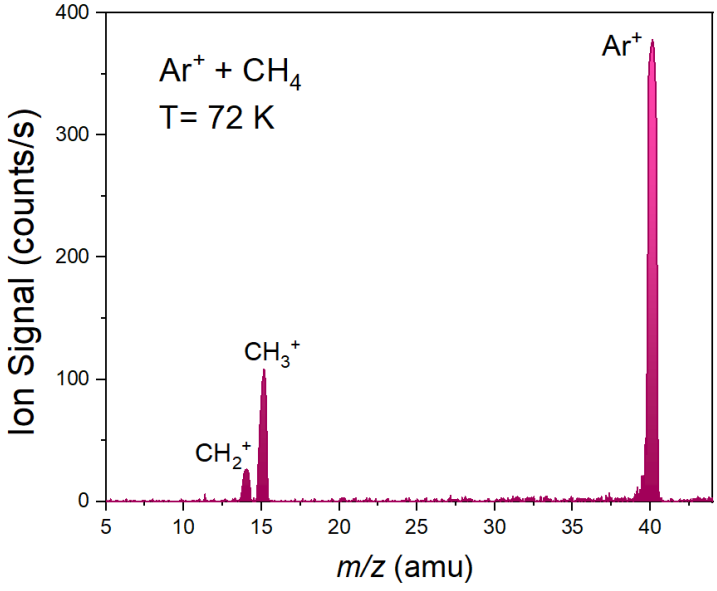

Figure 5.11: Mass spectrum registered in the uniform supersonic flow in the presence of neutral reactant. T= 71.6 K, $[CH_4] = 5.6 \times 10^{12}$ molecule/cm^3, reaction time ~ 65 µs.

5.4 Conclusion

In this chapter we have presented the results of the $Ar^+ + CH_4$ and $Ar^+ + C_2H_4$ reactions obtained at low temperatures by the CRESU-SIS experimental setup. The kinetic measurements are in good agreement with the values estimated by the Langevin model. For the branching ratios, in the case of the $Ar^+ + C_2H_4$ reaction, the results show that the branching into the charge transfer channel ($C_2H_4^+$) increases at low temperature (the branching ratio reaches 22 % at 18.7 K). It is explained by quantum nature of the process, which is getting more importance at low temperatures. For the reaction with CH_4, the charge transfer product is not detected. In this case the branching ratios of the products (CH_2^+ and CH_3^+) remain constant over the temperature explored. These results provide a strong incentive to investigate the CT mechanisms. The direct implications of these results for astrophysical environments are not presented, and need more efforts to be completed.

References:

(1) Dennerl, K. Charge Transfer Reactions. Space Sci Rev **2010**, 157 (1–4), 57–91. https://doi.org/10.1007/s11214-010-9720-5.

(2) Anicich, V. G. An Index of the Literature for Bimolecular Gas Phase Cation-Molecule Reaction Kinetics. JPL-Publication-03-19 **2003**, No. November, 1194.

(3) Yelle, R. V.; Cui, J.; Müller-Wodarg, I. C. F. Methane Escape from Titan's Atmosphere. J. Geophys. Res. **2008**, 113 (E10), E10003. https://doi.org/10.1029/2007JE003031.

(4) Waite, J. H. Ion Neutral Mass Spectrometer Results from the First Flyby of Titan. Science **2005**, 308 (5724), 982–986. https://doi.org/10.1126/science.1110652.

(5) Ip, W.-H. Titan's Upper Ionosphere. The Astrophysical journal **1990**, 362, 354–363.

(6) Molina-Cuberos, G. J.; López-Moreno, J. J.; Rodrigo, R.; Lara, L. M. Chemistry of the Galactic Cosmic Ray Induced Ionosphere of Titan. J. Geophys. Res. **1999**, 104 (E9), 21997–22024. https://doi.org/10.1029/1998JE001001.

(7) Molina-Cuberos, G. J.; López-Moreno, J. J.; Rodrigo, R.; Lara, L. M.; O'Brien, K. Ionization by Cosmic Rays of the Atmosphere of Titan. Planetary and Space Science **1999**, 47 (10–11), 1347–1354. https://doi.org/10.1016/S0032-0633(99)00056-2.

(8) Capone, L. A.; Dubach, J.; Prasad, S. S.; Whitten, R. C. Galactic Cosmic Rays and N2 Dissociation on Titan. Icarus **1983**, 55 (1), 73–82. https://doi.org/10.1016/0019-1035(83)90051-9.

(9) Private Discussion with Panayotis Lavvas, Groupe de Spectrométrie Moléculaire et Atmosphérique UMR CNRS 7331, Université de Reims Champagne-Ardenne, 51687 Reims, France.

(10) Vuitton, V.; Yelle, R. V.; McEwan, M. J. Ion Chemistry and N-Containing Molecules in Titan's Upper Atmosphere. Icarus **2007**, 191 (2), 722–742. https://doi.org/10.1016/j.icarus.2007.06.023.

(11) Teanby, N. A.; Irwin, P. G. J.; de Kok, R.; Nixon, C. A. Dynamical Implications of Seasonal and Spatial Variations in Titan's Stratospheric Composition. Phil. Trans. R. Soc. A. **2009**, 367 (1889), 697–711. https://doi.org/10.1098/rsta.2008.0164.

(12) Schilke, P.; Neufeld, D. A.; Müller, H. S. P.; Comito, C.; Bergin, E. A.; Lis, D. C.; Gerin, M.; Black, J. H.; Wolfire, M.; Indriolo, N.; Pearson, J. C.; Menten, K. M.; Winkel, B.; Sánchez-Monge, Á.; Möller, T.; Godard, B.; Falgarone, E. Ubiquitous Argonium (ArH^+) in the Diffuse Interstellar Medium: A Molecular Tracer of Almost Purely Atomic Gas. A&A **2014**, 566, A29. https://doi.org/10.1051/0004-6361/201423727.

(13) Tsuji, M.; Kouno, H.; Matsumura, K.; Funatsu, T.; Nishimura, Y.; Obase, H.; Kugishima, H.; Yoshida, K. Dissociative Charge-transfer Reactions of Ar^+ with Simple Aliphatic Hydrocarbons at Thermal Energy. The Journal of Chemical Physics **1993**, 98 (3), 2011–2022. https://doi.org/10.1063/1.464234.

(14) Franklin, J.; Field, F. Reactions of Gaseous Ions. IX. Charge Exchange Reactions of Rare Gas Ions with Ethylene. Journal of the American Chemical Society **1961**, 83 (17), 3555–3559.

(15) Joalland, B.; Mori, T.; Martínez, T. J.; Suits, A. G. Photochemical Dynamics of Ethylene Cation $C_2H_4^+$. J. Phys. Chem. Lett. **2014**, 5 (8), 1467–1471. https://doi.org/10.1021/jz500352x.

(16) Werner, H. J.; Knowles, P. J.; Knizia, G.; Manby, F. R.; Schütz, M.; Celani, P.; Györffy, W.; Kats, D.; Korona, T.; Lindh, R. MOLPRO, Version 2015.1, a Package of Ab Initio Programs. University of Cardiff Chemistry Consultants (UC3): Cardiff, Wales, UK **2015**.

(17) Werner, H.; Knowles, P. J.; Knizia, G.; Manby, F. R.; Schütz, M. Molpro: A General-purpose Quantum Chemistry Program Package. Wiley Interdisciplinary Reviews: Computational Molecular Science **2012**, 2 (2), 242–253.

(18) Lias, S.; Bartmess, J.; Liebman, J.; Holmes, J.; Levin, R.; Mallard, W. Ion Energetics Data in NIST Chemistry WebBook, NIST Standard Reference Database Number 69. National Institute of Standards and Technology, Gaithersburg MD **2018**, 20899.

(19) Ridge, D. P. Capture Collision Theory. In Structure/Reactivity and Thermochemistry of Ions; Springer, 1987; pp 1–13.

(20) Bircher, M. P.; Liberatore, E.; Browning, N. J.; Brickel, S.; Hofmann, C.; Patoz, A.; Unke, O. T.; Zimmermann, T.; Chergui, M.; Hamm, P. Nonadiabatic Effects in Electronic and Nuclear Dynamics. Structural Dynamics **2017**, 4 (6), 61510.

(21) Hawley, M.; Smith, M. A. Charge-Transfer Chemistry of Ar+(2P,,2) and Kr+('P,,,) at Very Low Collision Energies. J. Phys. Chem. **1992**, 96 (6693–6697).

(22) Speck, T.; Mostefaoui, T. I.; Travers, D.; Rowe, B. R. Pulsed Injection of Ions into the CRESU Experiment. International Journal of Mass Spectrometry **2001**, 208 (1–3), 73–80. https://doi.org/10.1016/S1387-3806(01)00383-9.

(23) Shul, R. J.; Passarella, R.; Yang, X. L.; Keesee, R. G.; Castleman, A. W. Studies of the Energy Dependence of Reactions of Ar^+ and Ar^+_2 with CH_4 and CS_2. The Journal of Chemical Physics **1987**, 87 (3), 1630–1636. https://doi.org/10.1063/1.453224.

(24) Chatham, H.; Hils, D.; Robertson, R.; Gallagher, A. C. Reactions of He^+, Ne^+, and Ar^+ with CH_4, C_2H_6, SiH_4, and Si_2H_6. The Journal of Chemical Physics **1983**, 79 (3), 1301–1311. https://doi.org/10.1063/1.445884.

Chapter 6:

Kinetic study and branching ratios for the reactions of CH_2CN^+ with C_2H_4 and C_2H_6 at 49 K

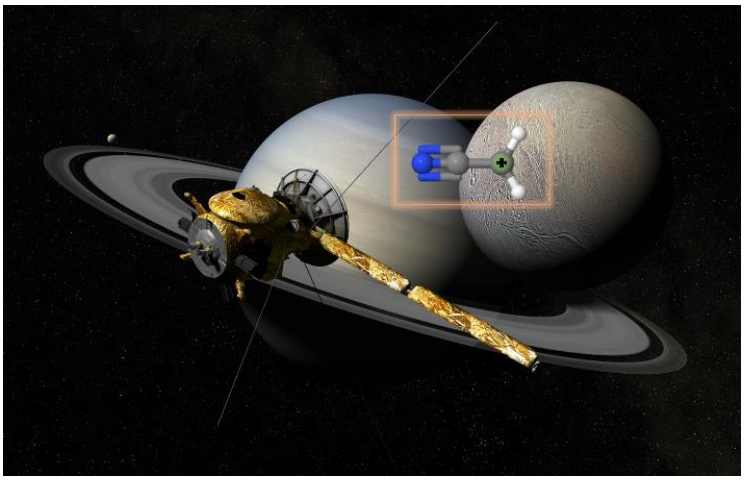

6.1 Introduction

According to NASA, Titan is one of the most earth-like worlds found by far.[1] An exo-moon baring such features attracts scientists to explore its atmosphere. The chemistry in Titan's atmosphere is one of the most complex known in the Solar System, and leads to the formation of solid organic aerosols responsible for Titan's brownish color. Nitrile ions are very abundant in Titan's ionosphere, and contribute to this chemistry. For instance, the $HCNH^+$ ion is the major species between 900 and 1200 km. In the stratosphere, a proton transfer reaction can occur between $HCNH^+$ and less abundant species such as C_4H_2, HC_3N and CH_3CN. At low altitudes, where three-body ion-molecule association reactions are favored by the lower temperatures (up to ~ 70 K) and higher densities (~ 1.5 bar),[2] the nitriles ions contribute to the

formation of more complex organic-nitrogen molecules. The saturated (e.g hydrogen cyanide H–CN) and unsaturated nitriles (e.g propiolonitrile HC_3N) are both detected by Voyager-1 infrared observations and by the Ion Neutral Mass Spectrometer (INMS) on the Cassini spacecraft.[3,4] These species can be formed by neutral-neutral reactions of CN radicals with unsaturated hydrocarbons. Formation of cluster ions can also take place there. For instance, $HCNH^+$ ions can associate with C_2H_2 to sequentially generate $HCNH^+ \cdot C_2H_2$ and $HCNH^+ \cdot (C_2H_2)_2$ ion clusters. The latter species can be destroyed by electronic recombination, producing complex organic-nitrogen species, such as CH_3CH_2CN, CH_2CHCN and HCCCN.[5] Furthermore, the peak at m/z=40 u is detected by the INMS. For this peak, model calculations predict a density of 2.3 cm^{-3} for the $C_2H_2N^+$ ion (including all isomers) and 0.93 cm^{-3} for the $C_3H_4^+$ ion in the ionosphere.[4] The main formation pathway for the CH_2CN^+ (m/z = 40 u) ion in Titan's atmosphere is the reaction between CH_2^+ and HCN: [6,7]

$$CH_2^+ + HCN \rightarrow CH_2CN^+ + H \qquad \text{Eq. (6.1)}$$

In addition, CH_2CN^+ can be formed by ionization of acetonitrile (CH_3CN) through ultraviolet (UV) radiation or highly energy electron impact.

$$CH_3CN + h\boldsymbol{\nu} \rightarrow CH_2CN^+ + H \qquad \text{Eq. (6.2)}$$

$$CH_3CN + e^- \rightarrow CH_2CN^+ + H + 2e^- \qquad \text{Eq. (6.3)}$$

Since acetonitrile is one of the most abundant nitrogen-containing species with a fractional abundance of about 1.51×10^{-6} at 1025 km above Titan's surface [8], such a production route of CH_2CN^+ could be efficient in this environment. In addition, CH_2CN^+ could emerge from the ionization of the CH_2CN radical that has been proposed to form in the reaction of N (^2D) atoms with ethene (C_2H_4), or N (^4S) with ethynyl C_2H_3.[9]

$$N\ (^2D) + C_2H_4 \rightarrow CH_2CN \qquad \text{Eq. (6.4)}$$

$$N\ (^2S) + C_2H_3 \rightarrow CH_2CN + H \qquad \text{Eq. (6.5)}$$

The CH_2CN^+ ions could also directly be produced in Titan's atmosphere by the reaction between N^+ (^1D) or N^+ (^3P) and C_2H_4.[3]

$$N^+\ (^1D) + C_2H_4 \rightarrow CH_2CN^+ \qquad \text{Eq. (6.6)}$$

$$N^+\ (^1P) + C_2H_4 \rightarrow CH_2CN^+ \qquad \text{Eq. (6.7)}$$

In addition, the reaction of acetonitrile with N_2^+ (one of the primary ionization products in Titan's ionosphere) preferably forms CH_2CN^+. This reaction was studied by Wilson K. Gichuhi and Arthur G. Suits (2012), and the results show the production of two primary ionic products:

CH_2CN^+ (ΔH= -1.19 eV,) and CH_3CN^+ (ΔH= - 3.38 eV), with branching ratios equal to 0.86 ± 0.01 and 0.14 ± 0.01 respectively.[10]

$$N_2^+ + CH_3CN \rightarrow CH_2CN^+ + H + N_2 \qquad \text{Eq. (6.8)}$$

It exists four isomers for CH_2CN^+ (figure 6.1): one cyclic c-$CHCHN^+$ (the most stable isomer), and three linear ones (CH_2CN^+, CH_2NC^+, $HCCNH^+$).[11] In this work, we investigated the reactivity of the CH_2CN^+ cation with ethylene ($H_2C{=}CH_2$) and ethane ($H_3C{-}CH_3$) in the gas phase at 49 K. Regarding to the kinetic studies, the rate coefficient of CH_2CN^+ with neutral hydrocarbons reactions has not been studied before, even at room temperature ; an additional incentive to investigate its reactivity.

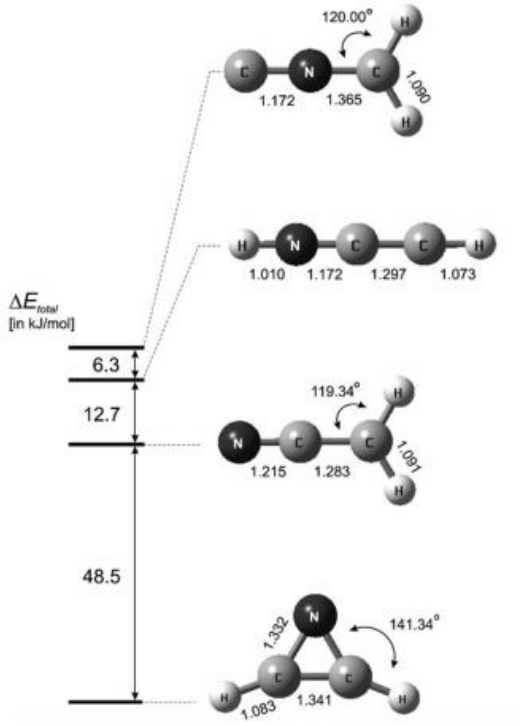

Figure 6.1: Isomers of CH_2CN^+ ion[11]

6.2 Experimental results

The reaction of $C_2H_2N^+$ with C_2H_6 and C_2H_4 was investigated using the CRESU-SIS technique. The detailed description of our experimental setup is presented in chapter 3. Experimentally, the ionization of acetonitrile by electronic impact (EI) can lead to the production of all $C_2H_2N^+$ isomers, since the EI ionization by 70 eV electrons leads to the formation of $C_2H_2N^+$ ions with an internal energy above the threshold of interconversion between linear and cyclic isomers.[12–14] The cyclic isomer can be produced by using methylisonitrile and 1-H-1,2,3-triazole as precursors. By contrast, the use of iodoacetonitrile (ICH_2CN) or chloroacetonitrile ($ClCH_2CN$) as precursors preferably produces the linear isomer CH_2CN^+.[15] According to Gui-xia Liu et

al.,[16] the linear-cyclic isomerization of $C_3H_3^+$ ion is endothermic with ~ 3.8 eV. By analogy with isoelectronic $C_3H_3^+$ isomers, we can presume that the linear-cyclic isomerization of CH_2CN^+ is highly endoergic.

In our study, the CH_2CN^+ ions are generated by the hollow cathode discharge source in a Helium/Chloroacetonitrile mixture. In such a source, the targeted ions can be generated by CT with He^+, Penning ionization with He* or through impact with high energy electrons (high energy portion of the electron energy distribution function). HCD is considered as soft ionization technique, which means that the ionization products are less energetic comparing to those produced by electron impact.

The reactivity of the CH_2CN^+ ion with different hydrocarbons was investigated by Pantea Fathi in the group of Wolf Geppert at Stockholm University. In their study, the CH_2CN^+ ion was produced through an electron impact of Chloroacetonitrile at 70–100 eV.[15] By using the same precursor ($ClCH_2CN$), we can assume that the same linear isomer (CH_2CN^+) is generated in our experimental work. A mass spectrum measured at the exit of the mass filter of the selective ion source is depicted in figure 6.2, it shows the presence of H_2O^+, H_3O^+, N_2^+, O_2^+, $CHCN^+$, CH_2CN^+ ions.

The uniform supersonic flow (USF) is generated by expansion of helium gas through the Ar7K de Laval nozzle. The characteristics of the flow are shown in chapter 4. The CH_2CN^+ ions are thermalized to their ground vibrational state by numerous collisions with the helium buffer gas in the selective ion source before being injected in the supersonic uniform flow. [17]

A mass spectrum in absence of neutral reactant at a distance of 12 cm (distance from the deflector to the movable mass spectrometer, that corresponds to a reaction time t of 75 μs) is shown in figure 6.3.

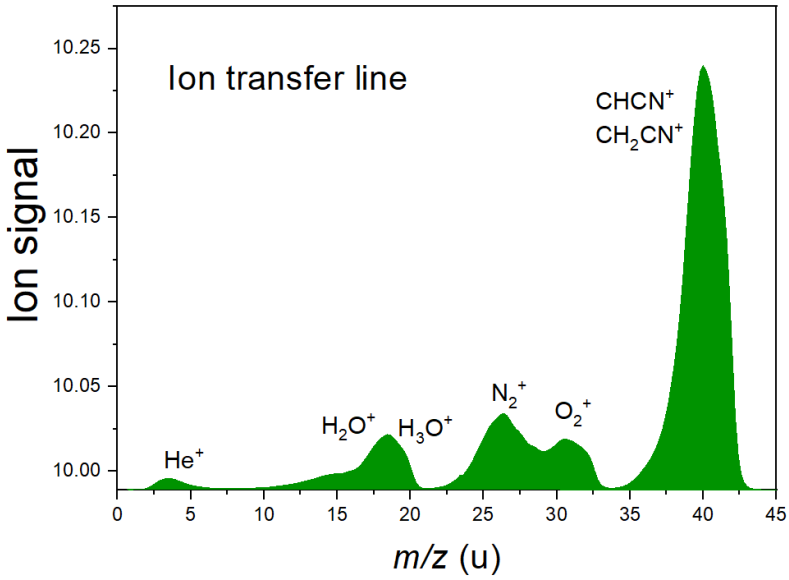

Figure 6.2: Mass spectrum recorded at the exit of the mass filter in the selective ion source. The plasma is generated by HCD of He/$ClCH_2CN$ mixture.

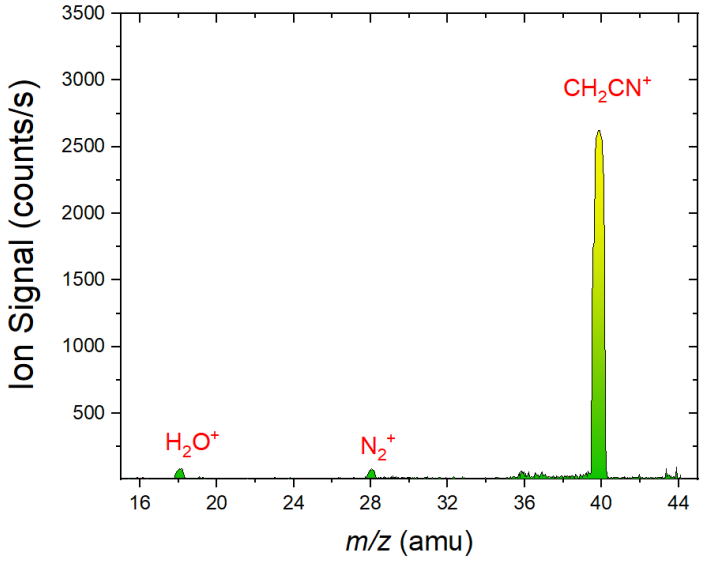

Figure 6.3: Mass spectrum of ionic species from the reaction of mass-selected $C_2H_2N^+$ recorded by CRESU-SIS at the distance of 12 cm in the absence of neutral reactant, T= 49 K.

6.2.1 Reaction of CH_2CN^+ with ethane C_2H_6

6.2.1.1 Reaction products and branching ratios

As an example, the figure 6.4 shows a mass spectrum recorded at the distance of 11 cm (t=68 µs) for a neutral reagent density of 9×10^{12} molecule.cm^{-3}. The reaction of CH_2CN^+ with C_2H_6 at 49 K shows the production of CH_3^+ (m/z= 15 u), $C_2H_3^+$ (m/z= 27 u), CNH_2^+(m/z= 28 u), $C_2H_5^+$ (m/z= 29 u), $C_3H_5^+$ (m/z= 41 u), $C_2H_4N^+$ (m/z= 42 u), $C_3H_7^+$ (m/z= 43 u) as primary products, and other secondary products that are presented in Table 6.1. The products at m/z=

26, 30, 44, 55, and 57 u, that are ascribed to $C_2H_2^+$, $C_2H_6^+$, $C_3H_8^+$, $C_4H_7^+$ and $C_4H_9^+$ ions respectively, cannot be produced directly via the $CH_2CN^+ + C_2H_6$ reaction at 49 K for energetic reasons (endoergic pathways). Latter species can be produced via secondary reactions or by side reactions between impurities and C_2H_6 (Table 6.1). The formation pathway of the HCN^+ ion (m/z= 27 u) is endothermic with ΔH= + 3.76 eV, this eliminates the possibility of the production of HCN^+ via $CH_2CN^+ + C_2H_6$ reaction in our study at low temperature. The peak at m/z= 28 u cannot be ascribed to $C_2H_4^+$ ion due to the same reason. The mass spectra recorded in the absence of neutral co-reactant show traces of $CHCN^+$ ion (m/z= 39 u), the corresponding ion signal doesn't change after the injection of C_2H_6, so we can assume that no primary or secondary products for the $CH_2CN^+ + C_2H_6$ reaction are observed at m/z= 39 u.

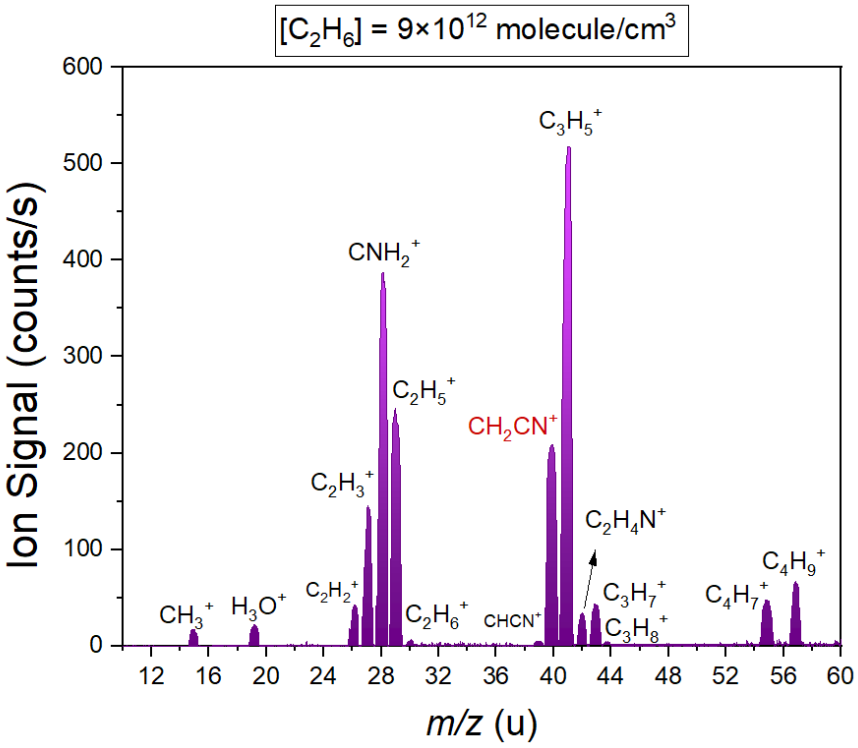

Figure 6.4: Mass spectra of ionic species from the reaction of mass-selected $C_2H_2N^+$ with C_2H_6 recorded by CRESU-SIS at t= 68 µs with $[C_2H_6] = 9\times10^{12}$ molecule.cm^{-3}. T= 49 K.

observed masses (u)	products	reactants	exit channel	ΔH (eV)	type
15	CH_3^+	$CH_2CN^+ + C_2H_6$	$CH_3^+ + CH_3CH_2CN$	-0.16±0.07	primary
26	$C_2H_2^+$	$N_2^+ + C_2H_6$	$C_2H_2^+ + 2H_2 + N_2$	-1.005	secondary
27	$C_2H_3^+$	$CH_2CN^+ + C_2H_6$	$C_2H_3^+ + C_2H_5N$	-0.22 ±0.16	primary
28	CNH_2^+	$CH_2CN^+ + C_2H_6$	$CNH_2^+ + C_3H_6$	-0.6	primary
29	$C_2H_5^+$	$CH_2CN^+ + C_2H_6$	$C_2H_5^+ + CH_3CN$	-1.94 ±0.08	primary
		$CH_2CN^+ + C_2H_6$	$C_2H_5^+ + CH_3NC$	-0.82 ±0.10	primary
		$CH_2CN^+ + C_2H_6$	$C_2H_5^+ + CH_2NCH$	-0.86 ±0.26	primary
30	$C_2H_6^+$	$N_2^+ + C_2H_6$	$C_2H_6^+ + N_2$	-4.05	secondary
41	$C_3H_5^+$	$CH_2CN^+ + C_2H_6$	$CH_2CHCH_2^+ + NHC + H_2$	-0.34 ±0.20	primary
		$CH_2CN^+ + C_2H_6$	$CH_2CHCH_2^+ + HNC + H_2$	-0.88 ±0.25	primary
		$CH_2CN^+ + C_2H_6$	$CH_2CCH_3^+ + CH_2NH + H_2$	-1.08 ±0.33	primary
42	$C_2H_4N^+$	$CH_2CN^+ + C_2H_6$	$CH_3CNH^+ + C_2H_4$	-2.95 ±0.06	primary
43	$C_3H_7^+$	$CH_2CN^+ + C_2H_6$	$CH_3CHCH_3^+ + HNC$	-2.34 ±0.09	primary
		$CH_2CN^+ + C_2H_6$	$CH_3CHCH_3^+ + HNC$	-1.46 ±0.09	primary
44	$C_3H_8^+$	$C_2H_6^+ + C_2H_6$	$C_3H_8^+ + CH_4$	-1.07	secondary
55	$C_4H_7^+$	$C_2H_2^+ + C_2H_6$	$C_4H_7^+ + H$	-1.778	secondary
57	$C_4H_9^+$	$C_2H_5^+ + C_2H_6$	$C_4H_9^+ + H_2$	-0.9974	secondary

Table 6.1: Possible products and enthalpy for each exit channel for the reaction of CH_2CN^+ with C_2H_6. Secondary reactions are highlighted in red.[14,18,19,20,21] In the case of presence of different isomers, the enthalpy of formation of the most stable isomer is considered in the calculations for the reaction enthalpies.

In order to deduce the branching ratios, it is preferable to work with low neutral reagent density, and at small reaction time. Under these conditions, the presence of secondary products is strongly reduced. That can be seen in the figure 6.5 which displays a mass spectrum recorded at t =56 μs and at a low reactant density $[C_2H_6] = 2\times10^{12}$ molecules cm^{-3}. In figure 6.6, we present the fraction of primary and secondary products at different neutral densities. By comparing the height of the peaks of the secondary products in figure 6.3 and 6.4, we can clearly see that the production of secondary species is more important at high neutral reactant density.

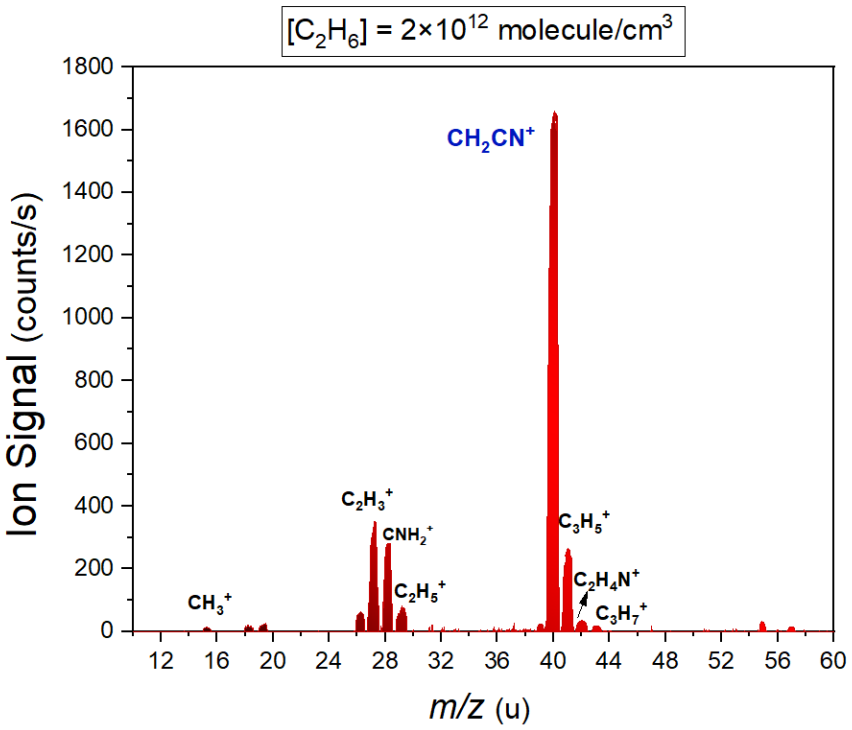

Figure 6.5: MS spectra of ionic species from the reaction of mass-selected $C_2H_2N^+$ with C_2H_6 recorded by CRESU-SIS at t= 56 µs and $[C_2H_6] = 2\times10^{12}$ molecule cm^{-3}. T= 49 K. Only the primary products are indicated on the graph.

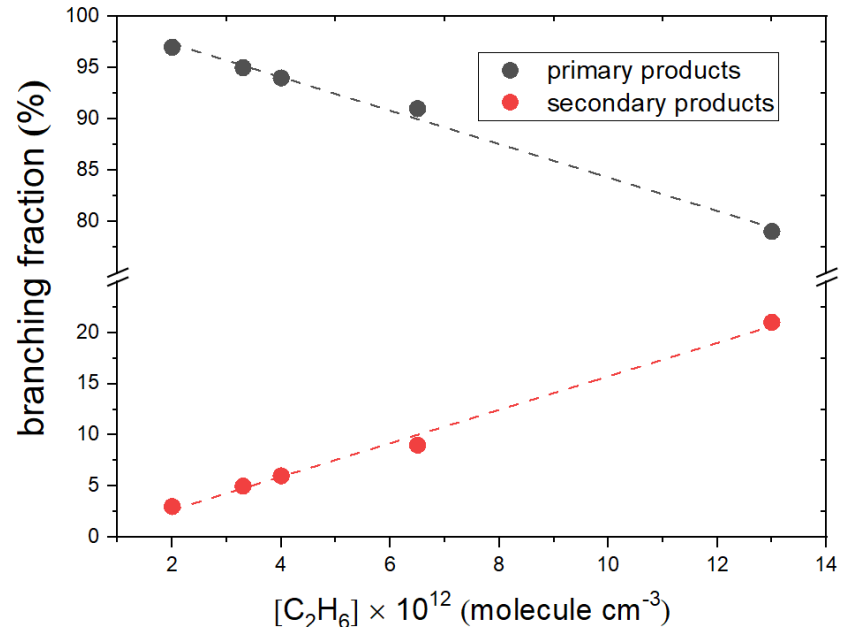

Figure 6.6: Sum of the ion signals of primary and secondary products at different neutral densities. Dashed lines correspond to linear fits.

In the literature we identify that the $C_2H_2^+ + C_2H_6$ and $C_2H_5^+ + C_2H_6$ secondary reactions are the origin of the production of $C_4H_7^+$ and $C_4H_9^+$ ions[20,22] that appear with large peaks at m/z= 55 and 57 u respectively (see figure 6.3). We examined the variation of the normalized ion signals of $C_4H_7^+$, $C_2H_2^+$, $C_4H_9^+$ and $C_2H_5^+$ as a function of time (figure 6.7): the ion signal of

each of these species is divided by the total ion signal. Graphs show that the fractions of $C_4H_9^+$ and $C_4H_7^+$ decrease with time, and $C_2H_5^+$ and $C_2H_2^+$ increase. This correlation supports the role of the $C_2H_2^+ + C_2H_6$ and $C_2H_5^+ + C_2H_6$ reactions in the production of the $C_4H_7^+$ and $C_4H_9^+$ ions.

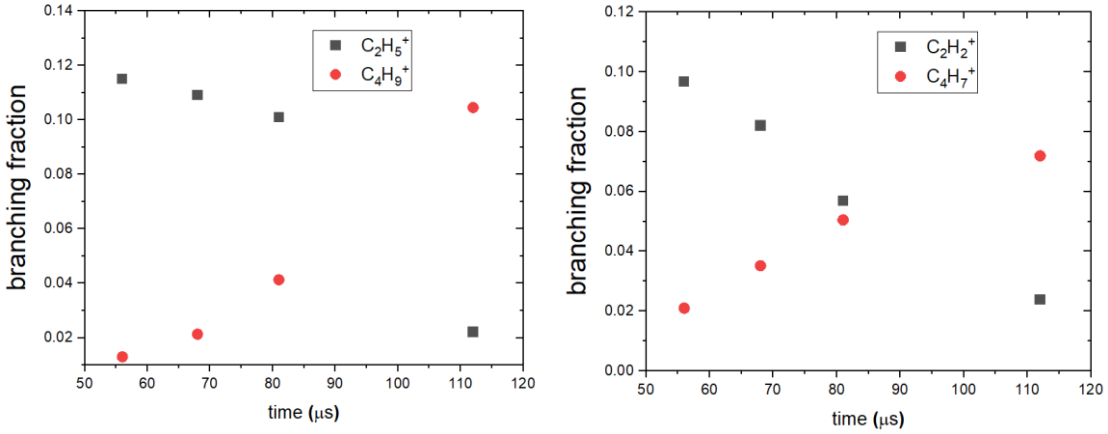

Figure 6.7: variation of fractions of $C_4H_9^+$/ $C_2H_5^+$ and $C_4H_7^+$/ $C_2H_2^+$ with reaction time. $[C_2H_6] = 9\times10^{12}$ molecule/cm^3. Points represent the normalized ion signal.

The $CH_2CN^+ + C_2H_6$ reaction has been studied with the guided ion beam GIB-MS technique by Pantea Fathi et al.[14] at different collision energies between 0.19 and 4 eV. A mass spectrum recorded GIB-MS at a collision energy $E_{CM} \sim 0.19$ eV (T~ 2204 K) in the centre of mass frame at pressure of $\sim10^{-5}$ mbar in the reaction cell is shown in figure 6.8. The branching ratios measured by CRESU-SIS at 49 K of primary products and comparison with results determined by GIB-MS are presented in Table 6.2.

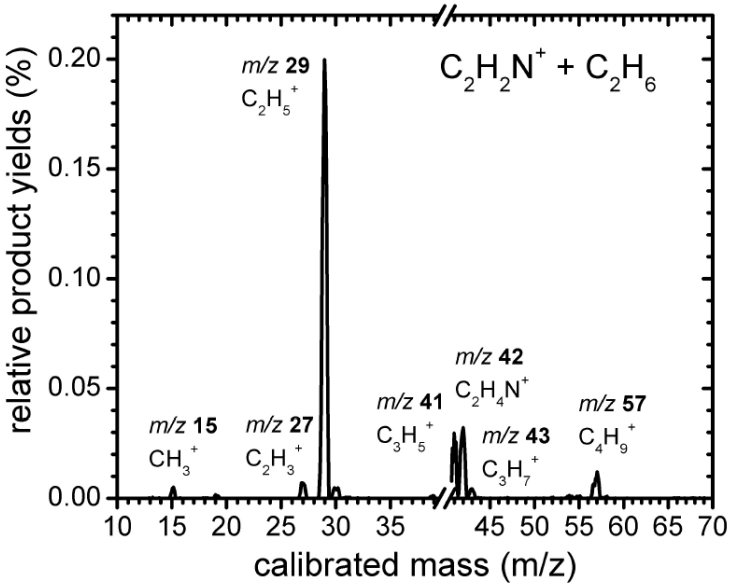

Figure 6.8: Product ion mass spectrum of the $C_2H_2N^+/C_2H_6$ reaction obtained from the GIB-MS at $P_{C_2H_6} \approx 10^{-5}$ mbar and collision energy $E_{CM} \sim 0.19$ eV in the center of mass frame. From Fathi et al. [14]

m/z (u)	product	BR CRESU-SIS, T=49 K	BR GIB, E_{CM} ~ 0.19 eV
15	CH_3^+	0.02 ± 0.02	0.02
27	$C_2H_3^+$	0.32 ± 0.04	0.02
28	CH_2N^+	0.26 ± 0.03	-
29	$C_2H_5^+$	0.06 ± 0.02	0.73
41	$C_3H_5^+$	0.26 ± 0.03	0.09
42	$C_2H_4N^+$	0.05 ± 0.02	0.10
43	$C_3H_7^+$	0.02 ± 0.02	0.02

Table 6.2: Comparison between branching ratios of primary products detected by CRESU-SIS at 49 K and reaction time t = 56 µs, and GIB-MS at E_{CM} ~ 0.19 eV. In our measurements, the error bars were estimated by adding systematic (±0.02) and statistical (±5%) contributions.

By comparing the branching ratios registered by our CRESU-SIS technique at 49 K and those by GIB-MS at E_{CM} ~ 0.19 eV (T~ 2204 K), we observe:

i. A lower production of $C_2H_5^+$ at low temperature (T=49 K). This can be interpreted by the absence of five pathways leading to the production of $C_2H_5^+$ in the GIB-MS studies at E_{CM} ~ 0.19 eV (T~ 2204 K).[14] Two of these channels are endothermic ($CH_2CN^+ + C_2H_6 \rightarrow C_2H_5^+ + CH_2NCH$, and $CH_2CN^+ + C_2H_6 \rightarrow C_2H_5^+ +$ c-NHCHCH) with ΔH= + 0.40 eV and 1.52 eV respectively. In our study at low temperature, the endothermic pathways are not allowed. This can be the reason behind the production of a major quantity of $C_2H_5^+$ in the GIB-MS experiments. Another hypothesis is that in the GIB-MS experiments, the density of the neutral reactant C_2H_6 is sufficiently high so that to promote the production of $C_2H_5^+$ ions by the following secondary reaction: $C_2H_3^+ + C_2H_6$, that leads to the formation of $C_2H_5^+$ as a major product.[23]

ii. The peak at m/z= 27 u that corresponds to the $C_2H_3^+$ ion increases from 2 % in the GIB-MS study to 32 % in our low temperature measurements. The same behavior is observed for the $C_3H_5^+$ ion, where the branching ratio increases from 9 % at a 0.19 eV collision energy (T~ 2204 K) to 26 % at 49 K. The prominent decrease in the BR of $C_2H_5^+$ ion leads to the increase of the branching ratios of $C_2H_3^+$ and $C_3H_5^+$ ionic products at 49 K.

iii. The peak at m/z= 28 u that corresponds to the $HCNH^+$ ion is not detected in the mass spectrum recorded with the GIB-MS technique at T~ 2204 K, in contrast, in our experiments at 49 K this peak is registered with a branching ratio equal to 28 %. The observation of an important quantity of this ion in our measurements at 49 K points to

a remarkable change in the reactivity of CH_2CN^+ ion with C_2H_6 at low temperature, i.e. low collision energy (~ 0.045 eV). To clear up this fact, an additional experimental study at different low temperatures is desirable. The production of $HCNH^+$ from the CH_2CN^+ + C_2H_6 reaction offers an additional pathway to generate this cation in Titan's atmosphere. $HCNH^+$ is detected by the INMS and CAPS instruments,[24,25] and photochemical models predict a very high density of 4.6×10^2 molecule cm^{-3}.[4] The $HCNH^+$ ion is considered to be highly reactive. It can react with C_2H_2 and C_2H_4 to form the $C_3H_4N^+$ and $C_3H_6N^+$ adducts respectively.[26]

6.2.1.2 Kinetic study

The measured rate coefficient of CH_2CN^+ with C_2H_6 reaction at 49 K is 0.92×10^{-9} molecule^{-1} cm^3 s^{-1}, that is in good agreement with the Langevin model[27] that has been used for the estimation of the rate coefficient of the ion-molecule reactions. In this case, α = 4.25 $Å^3$ (referring to Kenneth J.Miller, Additivity Methods in Molecular Polarizability)[28], μ= 17.14 u leading to a Langevin value of $k_L=1.16\times10^{-9}$ molecule^{-1} cm^3 s^{-1}.

The measurement of the loss rate (pseudo first order k_{1st}) corresponds to the slope of the variation of the quantity of CH_2CN^+ ions as a function of time. The rate coefficient corresponds to the slope of the variation of k_{1st} as a function of the density of the neutral reactant.

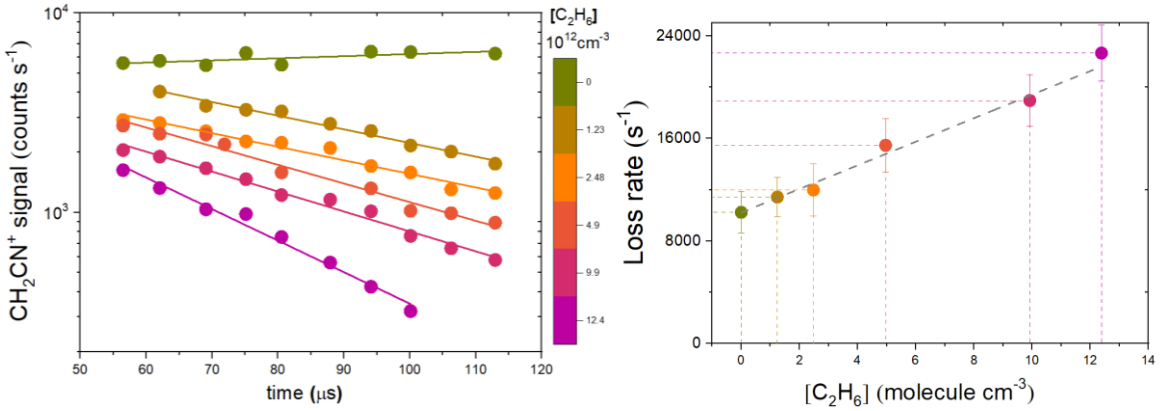

Figure 6.9: CH_2CN^+ ion signal at 49 K as a function of time for a range of C_2H_6 concentration (left) and corresponding loss rates as a function of C_2H_6 density (right), the slope of which determines the rate coefficient of the CH_2CN^+ + C_2H_6 reaction at 49 K.

6.2.2 Reaction of CH_2CN^+ ions with ethene C_2H_4

6.2.2.1 Reaction products and branching ratios

As an example, the figure 6.10 shows a mass spectrum recorded at the distance of 11 cm (t=68 µs) for a neutral reagent density of 3.14×10^{13} molecule.cm^{-3}. The reaction between CH_2CN^+ and C_2H_4 produces CH_3^+ (m/z= 15 u), $C_2H_3^+$ (m/z= 27 u), CH_2N^+ (m/z= 28 u), $C_3H_3^+$ (m/z= 39 u), $C_3H_5^+$ (m/z= 41 u), $C_2H_4N^+$ (m/z= 42 u), $C_3H_4N^+$ (m/z= 52 u), $C_4H_4N^+$ (m/z= 66 u), and $C_4H_4NH^+$ (m/z= 67 u) as primary products, and $C_2H_2^+$, $C_2H_5^+$, $C_4H_5^+$, $C_4H_7^+$, $C_3H_6N^+$, $C_4H_9^+$, $C_5H_5^+$, $C_5H_9^+$ as secondary products at m/z= 26, 29, 53, 55, 56, 57, 65 and 69 u respectively. Later species cannot be ascribed as primary products for the $CH_2CN^+ + C_2H_4$ reaction at 49 K due to an energetic reason (endoergic pathways) and then are produced by secondary or side reactions (see figure 6.10 and table 6.3)

observed masses (u)	products	reactants	exit channel	ΔH (eV)	type
15	CH_3^+	$CH_2CN^+ + C_2H_4$	$CH_3^+ + C_3H_3N$	-0.31 ±0.08	primary
26	$C_2H_2^+$	$N_2^+ + C_2H_4$	$C_2H_2^+ + 2H_2 + N_2$	-2.4149	secondary
27	$C_2H_3^+$	$CH_2CN^+ + C_2H_4$	$C_2H_3^+ + CH_3CN$	-1.12 ±0.09	primary
		$CH_2CN^+ + C_2H_4$	$C_2H_3^+ + CH_3NC$	-0.10 0.11	primary
28	$HCNH^+$	$CH_2CN^+ + C_2H_4$	$HCNH^+ + C_3H_4$	-0.42	primary
29	$C_2H_5^+$	$C_2H_3^+ + C_2H_4$	$C_2H_5^+ + C_2H_2$	-0.43 ±0.07	secondary
39	CH_2CCH^+	$CH_2CN^+ + C_2H_4$	$CH_2CCH^+ + HNCH_2$	-0.36 ±0.09	primary
41	$C_3H_5^+$	$CH_2CN^+ + C_2H_4$	$CH_2CHCH_2^+ + HCN$	-2.29 ±0.25	primary
	$C_3H_5^+$	$CH_2CN^+ + C_2H_4$	$CH_2CHCH_2^+ + HNC$	-1.75 ±0.20	primary
42	$C_2H_4N^+$	$CH_2CN^+ + C_2H_4$	$CH_3CNH^+ + C_2H_2$	-2.54 ±0.07	primary
52	$C_3H_4N^+$	$CH_2CN^+ + C_2H_4$	$C_3H_4N^+ + CH_4$	-2.48 ±0.06	primary
53	$C_4H_5^+$	$C_2H_2^+ + C_2H_4$	$C_4H_5^+ + H$	-0.817	secondary
55	$C_4H_7^+$	$C_2H_5^+ + C_2H_4$	$C_4H_7^+ + H_2$	-0.18	secondary
56	$C_2H_5NCH^+$	$HCNH^+ + C_2H_4$	$C_2H_5NCH^+$	-3.6 ±0.1	secondary
57	$C_4H_9^+$	$C_2H_5^+ + C_2H_4$	$C_4H_9^+$	-2.16	secondary
65	$C_5H_5^+$	$cycC_3H_3^+ + C_2H_4$	$C_5H_5^+ + H_2$	-0.62	secondary
66	$C_4H_4N^+$	$CH_2CN^+ + C_2H_4$	$C_4H_4N^+ + H_2$	NA	primary
67	$C_4H_4NH^+$	$CH_2CN^+ + C_2H_4$	$C_4H_4NH^+ + H$	-1.50 ±0.07	primary
69	$C_5H_9^+$	$C_3H_5^+ + C_2H_4$	$C_5H_9^+ + photon$	-1.88	secondary

Table 6.3: Possible products and enthalpy for each exit channels for the reaction of CH_2CN^+ with C_2H_4. Secondary reactions are highlighted in red. [18,19,20,21,15]

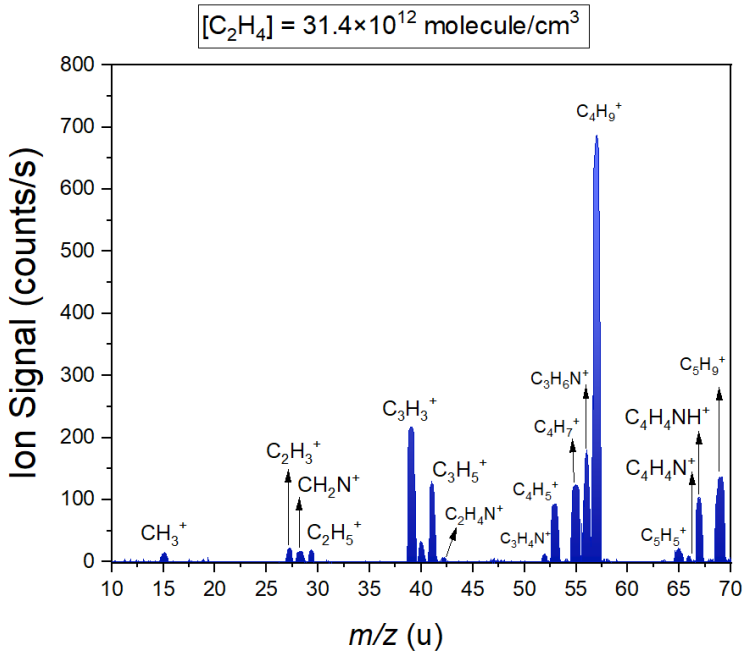

Figure 6.10: Mass spectrum of ionic species from the reaction of mass-selected $C_2H_2N^+$ with C_2H_4 recorded by CRESU-SIS at t =68 µs, $[C_2H_4]$ = 31.4×10^{12} molecule/cm^3. T= 49 K.

By comparing the mass spectra presented in figures 6.10 and 6.11 we observe that the secondary products are more and more important at high neutral reagent density, so in order to deduce the branching ratios of primary products we inject a small quantity of neutral reagent.

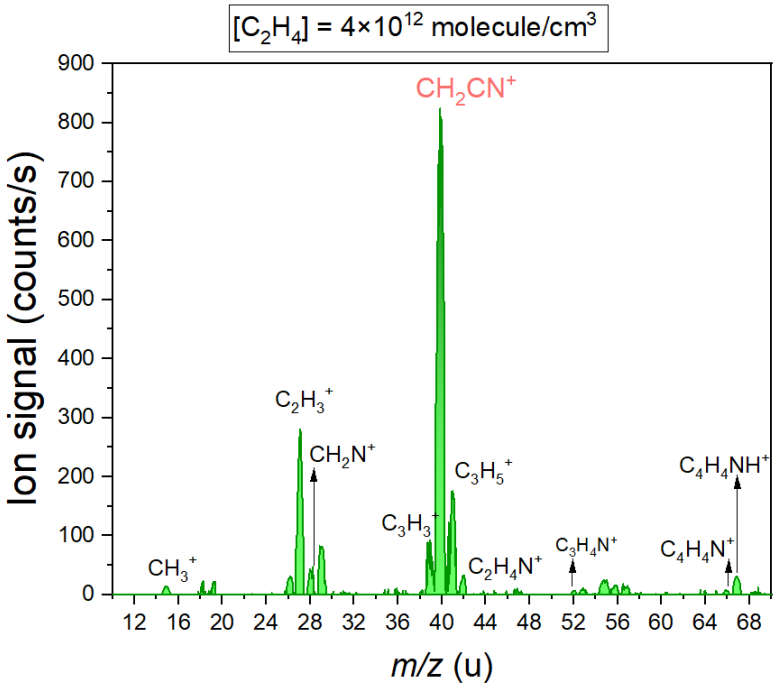

Figure 6.11: MS spectra of ionic species from the reaction of mass-selected $C_2H_2N^+$ with C_2H_4 recorded by CRESU-SIS at t= 68 µs (distance of 11 cm), T= 49 K, and $[C_2H_4]$ = 4×10^{12} molecule.cm^{-3} Only the primary products are labelled in the figure.

Figure 6.12 presents the variation of primary and secondary products with the C_2H_4 density, the graph shows that the primary products react once formed with C_2H_4 to generate secondary species.

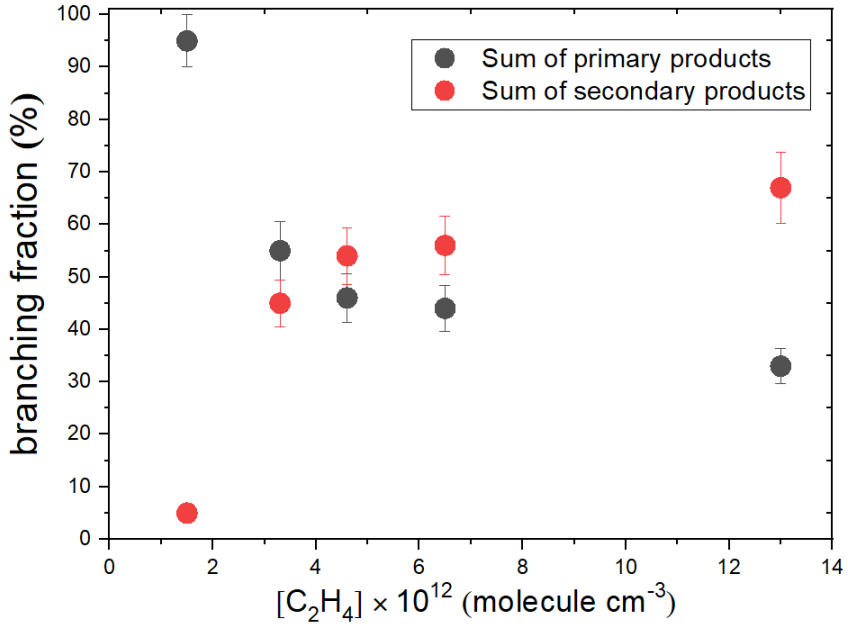

Figure 6.12: Sum of the ion signals of primary and secondary products at different C_2H_4 densities. T= 49 K, reaction time t= 68 μs.

The $CH_2CN^+ + C_2H_4$ reaction was studied with the guided ion beam method by Pantea Fathi et al.[15]. A mass spectrum recorded with GIB-MS at a collision energy E_{CM} ~ 0.64 eV (T~ 7427 K) in the centre of mass frame at pressure of ~10^{-5} mbar in the reaction cell is displayed on Fig. 6.13. The branching ratios measured by CRESU-SIS at 49 K of primary products and comparison with results recorded by GIB-MS are presented in table 6.4.

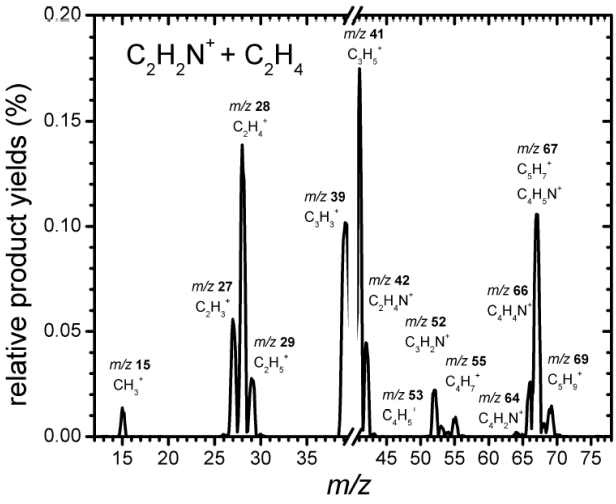

Figure 6.13: The product ion mass spectrum registered by GIB-MS associated with the $C_2H_2N^+/C_2H_4$ reaction at $P(C_2H_4) = 1.1 \times 10^{-5}$ mbar and measured at the collision energy E_{CM} ~ 0 .64 eV in the center of mass frame.[15]

	CRESU-SIS T= 49 K		GIB-MS E_{CM} ~ 0 .64 eV	
m/z (u)	product	BR	product	BR
15	CH_3^+	0.02 ± 0.02	CH_3^+	0.01
27	$C_2H_3^+$	0.39 ± 0.04	$C_2H_3^+$	0.09
28	CH_2N^+	0.08 ± 0.02	$C_2H_4^+$	0.20
39	$C_3H_3^+$	0.14 ± 0.03	$C_3H_3^+$	0.15
41	$C_3H_5^+$	0.25 ± 0.03	$C_3H_5^+$	0.25
42	$C_2H_4N^+$	0.05 ± 0.02	$C_2H_4N^+$	0.06
52	$C_3H_4N^+$	0.01 ± 0.02	$C_3H_4N^+$	0.02
66	$C_4H_4N^+$	0.01 ± 0.02	$C_4H_4N^+$	0.03
67	$C_4H_4NH^+$	0.05 ± 0.02	$C_4H_4NH^+$	0.16

Table 6.4: Comparison between branching ratios of primary products detected by CRESU-SIS at 49 K (left) and GIB-MS at collision energy E_{CM} ~ 0.64 eV (T~7427 K) (right). In our measurements, the error bars were estimated by adding systematic (±0.02) and statistical (±5%) contributions.

By comparing the branching ratios registered by our CRESU-SIS experimental setup and those by GIB-MS, we observe:

i. The peak at m/z = 28 u is ascribed mainly to the $C_2H_4^+$ ion (CT product) in the GIB-MS experiments, with an additional contribution of $HCNH^+$ ion. But the charge transfer channel is endothermic with 0.28 eV, that is not allowed in our study at low temperature. By calculating the heat of reaction $CH_2CN^+ + C_2H_4 \rightarrow HCNH^+ + C_3H_4$ we found that this reaction is exothermic with ΔH= - 0.42 eV. So, we can assume that the m/z = 28 u corresponds only to the $HCNH^+$ product in our experiments at low temperature. This can explain the decrease in the branching ratio of the m/z= 28 u product seen between the GIB-MS results at a collision energy E_{CM} ~ 0.64 eV (T~7427 K) and our CRESU measurements at 49 K.

ii. For the vinyl product ($C_2H_3^+$, m/z= 27 u), we observe an important increase in the branching ratio of this ion in our measurements at low temperature (from 9% to 39 %). The peak at m/z= 27 u cannot be ascribed to the HCN^+ ion due to energetic considerations: the $CH_2CN^+ + C_2H_4 \rightarrow HCN^+ + C_3H_4$ pathway is endothermic with ΔH= + 2.42 eV. A hypothesis that can explain the decrease of the branching ratio of the $C_2H_3^+$

ion in the GIB-MS measurements is that in this study the secondary reactions are important due to the relative high density of the neutral co-reactant (~ 10^{13} cm^{-3}): $C_2H_3^+$ ions react with the neutral reactant to form $C_2H_5^+$, where the latter reacts again with C_2H_4 to form $C_4H_7^+$ ions at m/z= 55 u. This can be confirmed by the large peaks at 29 and 55 u observed by the mass spectrum registered in the GIB-MS technique at E_{CM} ~ 0.64 eV (T~7427 K). The appearance of the $C_2H_3^+$ ions in a remarkable quantity at low temperature draws attention since this ion is detected in the Titan's atmosphere by the INMS with a calculated density = 5 molecule/cm^3.[4] These results show an additional pathway for the production of $C_2H_3^+$ ion in Titan's atmosphere.

6.2.2.1: Kinetic study

The measured rate coefficient of the reaction of CH_2CN^+ with C_2H_4 at 49 K is 0.85×10^{-9} $molecule^{-1}$ cm^3 s^{-1}, that is in good agreement with Langevin empirical model that equal to 1.19×10^{-9} $molecule^{-1}$ cm^3 s^{-1}. The figure 6.14 shows the variation of the CH_2CN^+ ion signal with time at different neutral reactant densities and the corresponding loss rate coefficient for the $CH_2CN^+ + C_2H_4$ reaction at 49 K.

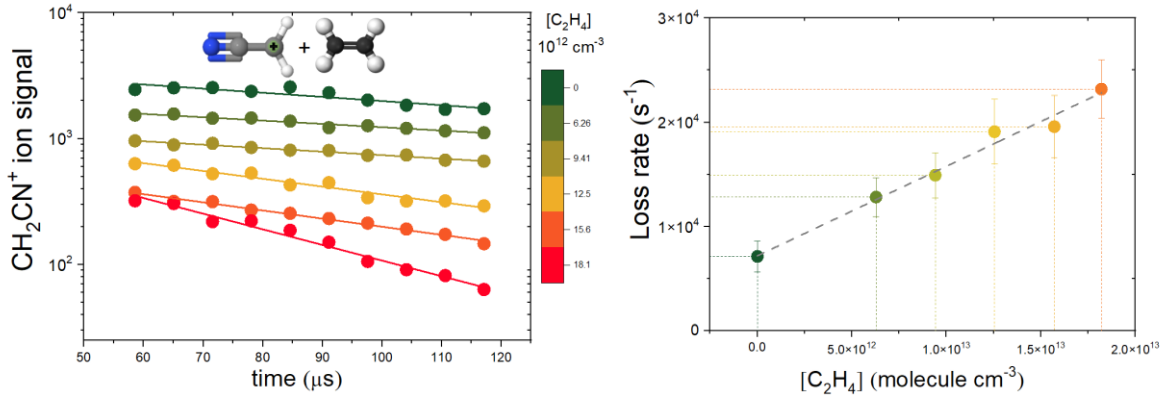

Figure 6.14: CH_2CN^+ ion signal at 49 K as a function of time for a range of ethylene densities (left) and corresponding loss rates as a function of C_2H_4 density (right), the slope of which determines the rate coefficient of the $CH_2CN^+ + C_2H_4$ reaction.

6.3 Conclusion

The reactivity of CH_2CN^+ ion with ethane C_2H_6 and ethylene C_2H_4 was investigated using CRESU-SIS method at 49 K. Experimental measurements of the rate coefficients are in good agreement with the empirical Langevin model, and this is not surprising due to the absence of a dipole moment for the neutral reactant molecules (C_2H_4 and C_2H_6). For the reaction with C_2H_6: CH_3^+, $C_2H_3^+$, CNH_2^+, $C_2H_5^+$, $C_3H_5^+$, $C_2H_4N^+$, $C_3H_7^+$ ions are identified as primary products at m/z= 15, 27, 28, 29, 41, 42 and 43 u respectively. Similarly, for the reaction with C_2H_4, CH_3^+,

$C_2H_3^+$, CH_2N^+, $C_3H_3^+$, $C_3H_5^+$, $C_2H_4N^+$, $C_3H_4N^+$, $C_4H_4N^+$ and $C_4H_4NH^+$ are the primary products at m/z= 15, 27, 28, 39, 41, 42, 52, 66 and 67 u respectively. The products isomers are indistinguishable in our experimental setup. These processes are of relevance for the generation of long chain species and ionic nitriles that may be of interest for the chemistry of Titan's ionosphere. The measurements with our CRESU-SIS experimental setup show a remarkable variation of the branching ratios of primary products comparing to those registered by GIB-MS technique at a collision energies $E_{CM} \sim 0.19$ eV and 0.64 eV for the reactions with C_2H_4 and C_2H_6 respectively.

References:

(1) Lorenz, R. D.; Leary, J. C.; Lockwood, M. K.; Waite, J. H. Titan Explorer: A NASA Flagship Mission Concept. AIP Conference Proceedings **2008**, 969 (1), 380–387. https://doi.org/10.1063/1.2844991.

(2) Fulchignoni, M.; Ferri, F.; Angrilli, F.; Ball, A. J.; Bar-Nun, A.; Barucci, M. A.; Bettanini, C.; Bianchini, G.; Borucki, W.; Colombatti, G.; Coradini, M.; Coustenis, A.; Debei, S.; Falkner, P.; Fanti, G.; Flamini, E.; Gaborit, V.; Grard, R.; Hamelin, M.; Harri, A. M.; Hathi, B.; Jernej, I.; Leese, M. R.; Lehto, A.; Lion Stoppato, P. F.; López-Moreno, J. J.; Mäkinen, T.; McDonnell, J. A. M.; McKay, C. P.; Molina-Cuberos, G.; Neubauer, F. M.; Pirronello, V.; Rodrigo, R.; Saggin, B.; Schwingenschuh, K.; Seiff, A.; Simões, F.; Svedhem, H.; Tokano, T.; Towner, M. C.; Trautner, R.; Withers, P.; Zarnecki, J. C. In Situ Measurements of the Physical Characteristics of Titan's Environment. Nature **2005**, 438 (7069), 785–791. https://doi.org/10.1038/nature04314.

(3) Monks, P. S.; Romani, P. N.; Nesbitt, F. L.; Scanlon, M.; Stief, L. J. The Kinetics of the Formation of Nitrile Compounds in the Atmospheres of Titan and Neptune. Journal of Geophysical Research: Planets **1993**, 98 (E9), 17115–17122. https://doi.org/10.1029/93JE01789.

(4) Vuitton, V.; Yelle, R. V; McEwan, M. J. Ion Chemistry and N-Containing Molecules in Titan's Upper Atmosphere. Icarus **2007**, 191 (2), 722–742. https://doi.org/10.1016/j.icarus.2007.06.023.

(5) Molina-Cuberos, G. J.; Schwingenschuh, K.; López-Moreno, J. J.; Rodrigo, R.; Lara, L. M.; Anicich, V. Nitriles Produced by Ion Chemistry in the Lower Ionosphere of Titan: PRODUCTION OF NITRILES IN TITAN. J.-Geophys.-Res. **2002**, 107 (E11), 9-1-9–11. https://doi.org/10.1029/2000JE001480.

(6) McEwan, M. J.; Anicich, V. G. Titan's Ion Chemistry: A Laboratory Perspective. Mass Spectrom. Rev. **2007**, 26 (2), 281–319. https://doi.org/10.1002/mas.20117.

(7) Anicich, V. G.; Huntress, W. T., Jr. A Survey of Bimolecular Ion-Molecule Reactions for Use in Modeling the Chemistry of Planetary Atmospheres, Cometary Comae, and Interstellar Clouds. ApJS **1986**, 62, 553. https://doi.org/10.1086/191151.

(8) Richard, M. S.; Cravens, T. E.; Wylie, C.; Webb, D.; Chediak, Q.; Perryman, R.; Mandt, K.; Westlake, J.; Waite Jr., J. H.; Robertson, I.; Magee, B. A.; Edberg, N. J. T. An Empirical Approach to Modeling Ion Production Rates in Titan's Ionosphere I: Ion

Production Rates on the Dayside and Globally. Journal of Geophysical Research: Space Physics **2015**, 120 (2), 1264–1280. https://doi.org/10.1002/2013JA019706.

(9) Dutuit, O.; Carrasco, N.; Thissen, R.; Vuitton, V.; Alcaraz, C.; Pernot, P.; Balucani, N.; Casavecchia, P.; Canosa, A.; Picard, S. Le; Loison, J. C.; Herman, Z.; Zabka, J.; Ascenzi, D.; Tosi, P.; Franceschi, P.; Price, S. D.; Lavvas, P. Critical Review of N, N+, N2+, N ++, and N2++ Main Production Processes and Reactions of Relevance to Titan's Atmosphere. Astrophysical Journal, Supplement Series **2013**, 204 (2). https://doi.org/10.1088/0067-0049/204/2/20.

(10) Gichuhi, W. K.; Suits, A. G. Low-Temperature Branching Ratios for the Reaction of State-Prepared N2+ with Acetonitrile. The Journal of Physical Chemistry A **2012**, 116 (3), 938–942. https://doi.org/10.1021/jp207096c.

(11) Frankowski, M.; Sun, Z.; Smith-Gicklhorn, A. M. Unraveling the Possible Isomers of CH4CN+ and CH2CN+ through FT-IR Matrix-Isolation Spectroscopy of Mass-Selected Ions and DFT Theory. Phys. Chem. Chem. Phys. **2005**, 7 (5), 797–805. https://doi.org/10.1039/B415412F.

(12) Holmes, J. L.; Mayer, P. M. A Combined Mass Spectrometric and Thermochemical Examination of the C2,H2,N Family of Cations and Radicals. J. Phys. Chem. **1995**, 99 (4), 1366–1370. https://doi.org/10.1021/j100004a042.

(13) Wincel, H.; Fokkens, R. H.; Nibbering, N. M. M. On the Rearrangement of the Cyanomethyl Cation Derived from Gaseous Acetonitrile. International Journal of Mass Spectrometry and Ion Processes **1990**, 96 (3), 321–330. https://doi.org/10.1016/0168-1176(90)85132-L.

(14) Fathi, P.; Geppert, W. D.; Ascenzi, D. Experimental and Theoretical Investigations of the Ion-Neutral Reaction of C2H2N+ with C2H6 and Implications on Chain Elongation Processes in Titan's Atmosphere. International Journal of Mass Spectrometry **2016**, 411, 1–13. https://doi.org/10.1016/j.ijms.2016.10.003.

(15) Fathi, P. Insights on Molecular Growth Pathways in Titan's Ionosphere through Combined Experimental and Theoretical Studies of the C2H2N+ + C2H4 Ion-Neutral Reaction. International Journal of Mass Spectrometry.

(16) Liu, G.; Li, Z.; Ding, Y.; Fu, Q.; Huang, X.; Sun, C.; Tang, A. Water-Assisted Isomerization from Linear Propargylium (H_2CCCH^+) to Cyclopropenylium ($c\text{-}C_3H_3^+$). J. Phys. Chem. A **2002**, 106 (43), 10415–10422. https://doi.org/10.1021/jp0212085.

(17) Fathi, P. Synthesis of Complex Organics via Molecular Growth Mechanisms: Combined Experimental and Theoretical Studies on Ion-Neutral Reactions of C2H2N+ with Ubiquitous Hydrocarbons in Titan's Ionosphere. **2019**.

(18) Wakelam, V.; Herbst, E.; Loison, J. C.; Smith, I. W. M.; Chandrasekaran, V.; Pavone, B.; Adams, N. G.; Bacchus-Montabonel, M. C.; Bergeat, A.; Béroff, K.; Bierbaum, V. M.; Chabot, M.; Dalgarno, A.; Van Dishoeck, E. F.; Faure, A.; Geppert, W. D.; Gerlich, D.; Galli, D.; Hébrard, E.; Hersant, F.; Hickson, K. M.; Honvault, P.; Klippenstein, S. J.; Le Picard, S.; Nyman, G.; Pernot, P.; Schlemmer, S.; Selsis, F.; Sims, I. R.; Talbi, D.; Tennyson, J.; Troe, J.; Wester, R.; Wiesenfeld, L. A Kinetic Database for Astrochemistry (KIDA). Astrophysical Journal, Supplement Series **2012**, 199 (1). https://doi.org/10.1088/0067-0049/199/1/21.

(19) P.J. Linstrom and W.G. Mallard, Eds. NIST Chemistry WebBook, NIST Standard Reference Database Number 69, National Institute of Standards and Technology,; Gaithersburg MD. https://doi.org/10.18434/T4D303.

(20) Anicich, V. G. An Index of the Literature for Bimolecular Gas Phase Cation-Molecule Reaction Kinetics. JPL-Publication-03-19 **2003**, No. November, 1194.

(21) Lias, S. G.; Liebman, J. F.; Levin, R. D. Evaluated Gas Phase Basicities and Proton Affinities of Molecules; Heats of Formation of Protonated Molecules. Journal of Physical and Chemical Reference Data **1984**, 13 (3), 695–808. https://doi.org/10.1063/1.555719.

(22) Hickson, K. M.; Wakelam, V.; Loison, J.-C. Methylacetylene (CH3CCH) and Propene (C3H6) Formation in Cold Dense Clouds: A Case of Dust Grain Chemistry. Molecular Astrophysics **2016**, 3–4, 1–9. https://doi.org/10.1016/j.molap.2016.03.001.

(23) Heslin, E. J.; Harrison, A. G. Bimolecular Reactions of Trapped Ions. IV. Reactions in Gaseous Ethane and Mixtures with C,H, and CD,'. 5.

(24) Cravens, T. E.; Robertson, I. P.; Waite Jr., J. H.; Yelle, R. V.; Kasprzak, W. T.; Keller, C. N.; Ledvina, S. A.; Niemann, H. B.; Luhmann, J. G.; McNutt, R. L.; Ip, W.-H.; De La Haye, V.; Mueller-Wodarg, I.; Wahlund, J.-E.; Anicich, V. G.; Vuitton, V. Composition of Titan's Ionosphere. Geophysical Research Letters **2006**, 33 (7). https://doi.org/10.1029/2005GL025575.

(25) Crary, F.; Young, D.; Baragiola, R.; Barraclough, B.; Berthelier, J.; Blanc, M.; Bouhram, M.; Coates, A.; Hartle, R.; Hill, T. Dynamics and Composition of Plasma at Titan. Science **2005**.

(26) Milligan, D. B.; Freeman, C. G.; Maclagan, R. G. A. R.; McEwan, M. J.; Wilson, P. F.; Anicich, V. G. Termolecular Ion-Molecule Reactions in Titan's Atmosphere. II: The

Structure of the Association Adducts of $HCNH^+$ with C_2H_2 and C_2H_4. J. Am. Soc. Mass Spectrom. **2001**, 12 (5), 557–564. https://doi.org/10.1016/S1044-0305(01)00215-X.

(27) Eichelberger, B. R.; Snow, T. P.; Bierbaum, V. M. Collision Rate Constants for Polarizable Ions. Journal of the American Society for Mass Spectrometry **2003**, 14 (5), 501–505. https://doi.org/10.1016/S1044-0305(03)00134-X.

(28) Miller, K. J. Additivity Methods in Molecular Polarizability. Journal of the American Chemical Society **1990**, 112 (23), 8533–8542. https://doi.org/10.1021/ja00179a044.

Conclusion and perspectives:

Ions are ubiquitous in space and contribute to the chemistry of astrophysical environments. These ions are detected at distance mostly employing radiotelescopes, or in situ by space probes that aim to explore the planets and their moons in the solar system (i.e. Cassini-Huygens mission). Among all the ionic processes (such as photoionization, electron attachment…), ion-neutral reactions play a crucial role in the formation and growth of ionic species.

Laboratory astrophysics for elementary reactions seeks to provide two types of information: the measurements of the rate coefficients k and the determination of the product distribution (the branching ratios between the different exit channels). The standard method for the study of ion-neutral reactions (also neutral-neutral reactions) at low temperatures is based on the cryogenic collision cooling of a gas. This method is restricted by the condensation of the neutral reactants on the walls of the system, that limits the reliability of the results, and the temperature range. The CRESU technique generates a cold (down to 6 K) uniform supersonic flow giving the advantage of a wall-less experiment where no condensation occurs in the scrutinized medium. The second advantage is the LTE due to the high density which allows us to consider a determined unique temperature for the reaction.

Using our CRESU-SIS technique, that couples a mass selective ion source to a CRESU chamber, we have investigated the reactivity of N_2^+ ions with C_3H_4 isomers (propyne and allene) at low temperatures (from 71.6 to 24 K). These species are detected in Titan's atmosphere. In collaboration with Sandor Demes and François Lique, an ab-initio calculation was performed in order to understand the variation of the branching ratios of the products. The aromatic cyclopropenyl cation c-$C_3H_3^+$ ion was observed as major product. An increase in the branching ratio of $C_3H_4^+$ was observed at low temperatures, this can be explained by the quantum nature of the pure charge transfer (CT) mechanism, which proceeds via crossings between multiple electronic states since it is only possible through non-adiabatic dynamics, and it is more important at low temperatures. The measured rate coefficients show an overall good agreement with empirical models. For the reaction with propyne, the rate coefficient increases from $(2.13 \pm 0.21) \times 10^{-9}$ at 24 K to $(3.73 \pm 0.41) \times 10^{-9}$ cm^3 $molecule^{-1}$ s^{-1} at 71.6 K, and seems to follow the Su and Chesnavich model that takes into account the dipole moment and the reaction temperature. In the case of the reaction with allene, the rate coefficient remains

constant over the temperature examined, with values close to that estimated by Langevin model, and this is not surprising due to the absence of the dipole moment of the neutral collision partner. The formation of c-$C_3H_3^+$ ion by the reaction of N_2^+ with C_3H_4 was included onto a photochemical model of Titan's atmosphere. Results show that this new pathway plays a secondary role relative to the dominant production terms of c-$C_3H_3^+$ from the reactions of $C_2H_4^+$ and $C_2H_5^+$ with acetylene.

The reactivity of Ar^+ ions with C_2H_4 and CH_4 was also investigated at 18.7 and 71.6 K. For the $Ar^+ + C_2H_4$ reaction, four primary products were detected: $C_2H_2^+$, $C_2H_3^+$, $C_2H_4^+$ and ArH^+. The pure CT product was observed in important quantities in our measurements with a branching ratio increasing from 10 % at 71.6 K to 22 % at 18.7 K. This reaction was also studied at room temperature using FA and MS techniques, where the pure CT product ($C_2H_4^+$) is only observed with a BR of 4 % in the FA measurements. In these studies, the authors suggest that the $C_2H_4^+$ product breaks down into smaller fragments. The fragmentation mechanism of $C_2H_4^+$ leading to $C_2H_2^+$ and $C_2H_3^+$ is endothermic and it is not allowed at low temperatures. This can explain the detection of $C_2H_4^+$ in our measurements using the CRESU-SIS technique. Similarly to the case of the $N_2^+ + C_3H_4$ reaction, the increase in the branching ratio of the pure CT product can be explained by the fact that this mechanism has a strict quantum-mechanical nature. For the $Ar^+ + CH_4$ reaction, CH_2^+ and CH_3^+ ions were detected as primary products. The pure charge transfer product CH_4^+ was not observed. In this case, we don't observe a variation in the branching ratios in our measurements at 18.7 and 71.6 K and comparing to the previous study using free jet technique at 10-20 K. Concerning the rate coefficients, for the reactions of Ar^+ with C_2H_4 and CH_4, our measurements give values close to those estimated by Langevin model due to the absence of dipole moment of neutral molecules. The direct implications of these results for the astrophysical environments are not presented and need more efforts to be completed.

To provide insights on the molecular growth mechanisms leading to large carbon and nitrogen-bearing species in Titan's ionosphere, in the last chapter, the experimental findings (kinetic study and products distribution) corresponding to the reaction of CH_2CN^+ ion with C_2H_4 and C_2H_6 at 49 K were presented. Our measurements of the branching ratios have been compared to those recorded by the GIB-MS technique at different collision energies. A remarkable difference was observed. For the $CH_2CN^+ + C_2H_6$ reaction, our results show the production of CH_2N^+ with a branching ratio equals to 26 %, while this product was not observed in the measurements using GIB technique. This result gives an additional formation pathway for the

most abundant ion in Titan's atmosphere ($HCNH^+$). An important increase in the branching ratio of the $C_2H_3^+$ ion was also noticed in our studies for the reactions with C_2H_6 and C_2H_4.

Recently, we have started the investigation of the reactivity of CH_3^+ ion with propyne, allene, ethene and methane at 18.7 and 71.6 K. The results show the production of ionic species of increasing size, with a remarkable variation in the branching ratios with the temperature. Many additional studies are desirable. In particular, we plan to extend the study of the reactivity of CH_2CN^+ ion with other hydrocarbons (CH_4 and C_2H_2) and at different low temperatures.

The successful investigation of the reactivity of cation-molecule reactions validated our approach. We are now in position to address more challenging objectives and target anion-molecule reactions. For example, we aim to study the reactivity of molecular anions such as $C_xH^-$and C_x^- which are identified in astrophysical environments (e.g. C_2H^- + HC_3N). One of the difficulties encountered in experiments with anions is their generation.

Using our CRESU-SIS technique, we would like also to focus our work on the first stages of nucleation induced by ions, specifically to explore how the injection of ions into the USF can accelerate the nucleation process from precursors such as HC_3N or CH_3CN. The high abundance of hydrocarbons and nitriles in the lower Titan's atmosphere could lead to the formation of aerosols by nucleation, especially polar species.

There is still a number of experimental challenges to carry out these studies. For example, it is necessary to update our plasma source in order to have a stable reliable source of negative ions, which are more difficult to produce than positive ions.

Despite that our mass selective ion source makes possible to produce ions at sufficient quantity to measure the rate coefficient and the branching ratios with high precision, the bandpass of the quadrupole mass filter remains large, allowing some ions to pass and complicate the ion spectrum (in some cases), one of the challenges is to reduce this bandpass by replacing the rods of the quadrupole mass filter with longer rods, in order to have only the ion under study in the USF.

Another aspect to be improved is the helium consumption by the Laval nozzles in our laboratory usually used for ion-molecule reaction studies (the flow rate can reach 100 L/min). Considering the increase of the helium price, a proposition is to use the nozzles with nitrogen buffer gas. But this reduces the ion transmission from the selective ion source into the USF (as shown in chapter 3). A solution in this case is to update the end of the SIS by adding an "aerodynamic

cushion" at ~ 1 mbar with helium gas, which avoids the nitrogen gas of the flow to back into the source, and at the same time maintains the good ion transmission.

En français:

Les ions sont omniprésents dans l'espace et contribuent à la chimie des environnements astrophysiques. Ces ions sont détectés à distance particulièrement à l'aide de radiotélescopes, ou in situ par des sondes spatiales qui visent à explorer les planètes et leurs lunes dans le système solaire (par exemple la mission Cassini-Huygens). Parmi tous les processus ioniques (tels que la photoionisation, l'attachement des électrons…), les réactions ion neutres jouent un rôle crucial dans la formation et la croissance des espèces ioniques. L'astrophysique de laboratoire pour les réactions élémentaires cherche à fournir deux types d'informations : les mesures des coefficients de vitesse k et la détermination de la distribution des produits (les rapports de branchement entre les différentes voies de sortie).

La méthode standard pour l'étude des réactions ion neutres (également des réactions neutres-neutres) à basse température est basée sur le refroidissement par collision cryogénique d'un gaz. Cette méthode est contrainte par la condensation des réactifs neutres sur les parois du système, qui limite la fiabilité des résultats, et la plage de température. La technique CRESU génère un flux supersonique uniforme froid (jusqu'à 6 K) offrant l'avantage d'une expérience sans paroi où aucune condensation ne se produit dans le milieu scruté. Le deuxième avantage est le LTE dû à la densité élevée qui permet de considérer une température unique déterminée pour la réaction.

En utilisant notre technique CRESU-SIS, qui couple une source d'ions sélective en masse à une chambre CRESU, nous avons étudié la réactivité des ions N_2^+ avec les isomères C_3H_4 (propyne et allène) à basse température (de 71,6 à 24 K). Ces espèces sont détectées dans l'atmosphère de Titan. En collaboration avec Sandor Demes et François Lique, un calcul ab-initio a été réalisé afin de comprendre la variation des taux de branchement des produits. L'ion c-C_3H_3 + du cation cyclopropényle aromatique a été observé comme produit principal. Une augmentation du rapport de ramification du C_3H_4 + a été observée à basse température, cela peut s'expliquer par la nature quantique du mécanisme de transfert de charge pur (CT), qui procède par croisements entre plusieurs états électroniques puisqu'il n'est possible que par une dynamique non adiabatique, et il est plus important à basse température. Les coefficients de taux mesurés montrent un bon accord global avec les modèles empiriques. Pour la réaction avec le propyne,

le coefficient de vitesse passe de (2,13 ± 0,21) × 10-9 à 24 K à (3,73 ± 0,41) × 10^{-9} cm^3 $molécule^{-1}$ s^{-1} à 71,6 K, et semble suivre les Su et Modèle de Chesnavich prenant en compte le moment dipolaire et la température de réaction. Dans le cas de la réaction avec l'allène, le coefficient de vitesse reste constant sur la température examinée, avec des valeurs proches de celle estimée par le modèle de Langevin, et cela n'est pas surprenant en raison de l'absence du moment dipolaire du partenaire de collision neutre. La formation d'ions c-$C_3H_3^+$ par la réaction de N_2^+ avec C_3H_4 a été incluse dans un modèle photochimique de l'atmosphère de Titan. Les résultats montrent que cette nouvelle voie joue un rôle secondaire par rapport aux termes dominants de production de c-$C_3H_3^+$ à partir des réactions de $C_2H_4^+$ et $C_2H_5^+$ avec l'acétylène. La réactivité des ions Ar^+ avec C_2H_4 et CH_4 a également été étudiée à 18,7 et 71,6 K. Pour la réaction Ar^+ + C_2H_4, quatre produits primaires ont été détectés : $C_2H_2^+$, $C_2H_3^+$, $C_2H_4^+$ et ArH^+. Le produit CT pur a été observé en quantités importantes dans nos mesures avec un rapport de ramification passant de 10 % à 71,6 K à 22 % à 18,7 K. Cette réaction a également été étudiée à température ambiante en utilisant les techniques FA et MS, où le produit CT pur ($C_2H_4^+$) n'est observé qu'avec un BR de 4 % dans les mesures FA. Dans ces études, les auteurs suggèrent que le produit C2H4 + se décompose en fragments plus petits. Le mécanisme de fragmentation de $C_2H_4^+$ conduisant à $C_2H_2^+$ et $C_2H_3^+$ est endothermique et n'est pas autorisé à basse température. Ceci peut expliquer la détection de $C_2H_4^+$ dans nos mesures avec la technique CRESU-SIS. Comme dans le cas de la réaction N_2^+ + C_3H_4, l'augmentation du rapport de ramification du produit CT pur peut s'expliquer par le fait que ce mécanisme est de nature mécanique quantique stricte. Pour la réaction Ar^+ + CH_4, les ions CH_2^+ et CH_3^+ ont été détectés comme produits primaires. Le produit de transfert de charge pur CH4+ n'a pas été observé. Dans ce cas, nous n'observons pas de variation des rapports de branchement dans nos mesures à 18,7 et 71,6 K et par rapport à l'étude précédente utilisant la technique du jet libre à 10-20 K. Concernant les coefficients de vitesse, pour les réactions de Ar^+ avec C_2H_4 et CH_4, nos mesures donnent des valeurs proches de celles estimées par le modèle de Langevin du fait de l'absence de moment dipolaire des molécules neutres. Les implications directes de ces résultats pour les environnements astrophysiques ne sont pas présentées et nécessitent plus d'efforts pour être complétées.

Pour fournir des informations sur les mécanismes de croissance moléculaire conduisant à de grandes espèces carbonées et azotées dans l'ionosphère de Titan, dans le dernier chapitre, les résultats expérimentaux (étude cinétique et distribution des produits) correspondant à la réaction de l'ion CH_2CN+ avec C_2H_4 et C_2H_6 à 49 K ont été présentés. Nos mesures des rapports

de branchement ont été comparées à celles enregistrées par la technique GIB-MS à différentes énergies de collision. Une différence remarquable a été observée. Pour la réaction CH_2CN^+ + C_2H_6, nos résultats montrent la production de CH_2N^+ avec un taux de ramification égal à 26%, alors que ce produit n'a pas été observé dans les mesures utilisant la technique GIB. Ce résultat donne une voie de formation supplémentaire pour l'ion le plus abondant dans l'atmosphère de Titan ($HCNH^+$). Une augmentation importante du rapport de ramification de l'ion $C_2H_3^+$ a également été remarquée dans nos études pour les réactions avec C_2H_6 et C_2H_4. Récemment, nous avons commencé l'étude de la réactivité de l'ion CH_3^+ avec le propyne, l'allène, l'éthène et le méthane à 18,7 et 71,6 K. Les résultats montrent la production d'espèces ioniques de taille croissante, avec une variation remarquable des rapports de ramification avec la température.

De nombreuses études complémentaires sont souhaitables. En particulier, nous prévoyons d'étendre l'étude de la réactivité de l'ion CH_2CN^+ avec d'autres hydrocarbures (CH_4 et C_2H_2) et à différentes basses températures.

L'étude réussie de la réactivité des réactions cation-molécule a validé notre approche. Nous sommes maintenant en mesure d'aborder des objectifs plus ambitieux et de cibler des réactions anion-molécule. Par exemple, nous visons à étudier la réactivité d'anions moléculaires tels que C_xH^- et C_x^- qui sont identifiés dans des environnements astrophysiques (par exemple C_2H- + HC_3N).

Une des difficultés rencontrées dans les expériences avec les anions est leur génération. En utilisant notre technique CRESU-SIS, nous aimerions également concentrer nos travaux sur les premières étapes de la nucléation induite par les ions, en particulier pour explorer comment l'injection d'ions dans l'USF peut accélérer le processus de nucléation à partir de précurseurs tels que HC_3N ou CH_3CN. La forte abondance d'hydrocarbures et de nitriles dans l'atmosphère inférieure de Titan pourrait conduire à la formation d'aérosols par nucléation, en particulier d'espèces polaires.

Il reste encore un certain nombre de défis expérimentaux pour mener à bien ces études. Par exemple, il est nécessaire de mettre à jour notre source de plasma afin d'avoir une source stable et fiable d'ions négatifs, qui sont plus difficiles à produire que les ions positifs.

Malgré le fait que notre source d'ions sélective en masse permet de produire des ions en quantité suffisante pour mesurer le coefficient de vitesse et les rapports de ramification avec une grande précision, la bande passante du filtre de masse quadripolaire reste importante, permettant à certains ions de passer et de compliquer le spectre ionique (en certains cas), l'un des enjeux est

de réduire cette bande passante en remplaçant les tiges du filtre de masse quadripolaire par des tiges plus longues, afin de n'avoir que l'ion à l'étude dans l'USF. Un autre aspect à améliorer est la consommation d'hélium par les tuyères de Laval de notre laboratoire habituellement utilisées pour les études de réaction ion-molécule (le débit peut atteindre 100 L/min). Compte tenu de l'augmentation du prix de l'hélium, une proposition est d'utiliser des tuyères fonctionnantes avec un mélange hélium/azote. Mais cela réduit la transmission d'ions de la source d'ions sélective dans l'USF (comme indiqué au chapitre 3). Une solution dans ce cas est d'ajouter un "fenêtre aérodynamique" à ~ 1 mbar avec de l'hélium gazeux, ce qui évite à l'azote gazeux du flux de remonter dans la source, et en même temps maintient la bonne transmission ionique.

UNIVERSITÉ DE RENNES 1

Titre : Réactions ion-molécule à basse température avec des écoulements supersoniques uniformes et investigations sur la chimie des environnements astrophysiques

Mots clés : CRESU, astrophysique de laboratoire, collisions réactives, processus ioniques, chimie du milieu interstellaire, atmosphère de Titan

Résumé : La compréhension des mécanismes régissant la formation des molécules organiques complexes dans le milieu interstellaire et les atmosphères planétaires froides repose notamment sur l'exploration de processus ioniques en conditions extrêmes. Le dispositif expérimental CRESU-SIS, développé pour étudier les réactions ion-neutres en phase gazeuse à basse températures, est en mesure de répondre à ce défi. Cet instrument unique, qui combine une source d'ions sélective (SIS) au réacteur CRESU qui génère un écoulement supersonique uniforme de très basse température, permet de mesurer les coefficients de vitesse de réactions entre des ions et des molécules neutres et de déterminer les rapports de branchement entre les différentes voies de sortie. La réactivité des ions N_2^+, Ar^+, et CH_2CN^+ avec des hydrocarbures (e.g CH_4, C_2H_4…) a été étudiée expérimentalement et analysée à l'aide de calculs quantiques. La réaction entre N_2^+ et les isomères linéaires de C_3H_4 (allene et propyne) a été incluse dans un modèle photochimique pour l'atmosphère de Titan.

Title: Ion-molecule reactions at low temperature with uniform supersonic flows and insights into the chemistry of astrophysical environments

Keywords: CRESU, laboratory astrophysics, reactive collisions, ionic processes, chemistry of the interstellar medium, Titan's atmosphere

Abstract: Understanding the mechanisms governing the formation of complex organic molecules in the interstellar medium and cold planetary atmospheres relies in particular on the exploration of ionic processes under extreme conditions. The CRESU-SIS experimental setup, developed to study ion-neutral reactions in the gas phase at low temperatures, is able to meet this challenge. This unique instrument, which combines a selective ion source (SIS) with the CRESU reactor which generates a uniform supersonic flow at very low temperature, makes it possible to measure the rate coefficients of the reactions between ions and neutral molecules and to determine the branching ratios between the different exit channels. The reactivity of N_2^+, Ar^+, and CH_2CN^+ ions with hydrocarbons (e.g CH_4, C_2H_4 ...) has been studied experimentally and analyzed using quantum calculations. The reaction between N_2^+ and the linear isomers of C_3H_4 (allene and propyne) has been included into a photochemical model for the atmosphere of Titan.